VNIVERSITAT DE VALÈNCIA

Departamento de Física Aplicada y Electromagnetismo, Facultad de Física

Programa de Doctorado en Física

Preparation and characterisation of optical and optoelectronic devices based in two-dimensional semiconductors

Daniel Andrés Penares

Bajo la supervisión de

Prof. Dr. Juan Francisco Sánchez Royo

Noviembre 2019

Author

Daniel Andres-Penares

Supervisor

Prof. Dr. Juan Francisco Sánchez-Royo

VNIVERSITAT DE VALÈNCIA **Departament de Física Aplicada i Elecromagnetisme**

Juan Francisco Sánchez Royo, catedrático del Departamento de Física Aplicada y Electromagnetismo

Certifica:

Que la presente memoria **"Preparation and characterisation of optical and optoelectronic devices based in two-dimensional semiconductors"** ha sido realizada bajo su dirección en el Departamento de Física Aplicada y Electromagnetismo de la Universidad de Valencia por **Daniel Andrés Penares**, y constituye su Tesis para optar al grado de Doctor en Física por la Universidad de Valencia (RD99/2011).

Y para que así conste, en cumplimiento de la legislación vigente, presenta en el Departamento de Física Aplicada y Electromagnetismo de la Universidad de Valencia la referida Tesis Doctoral, y firma el presente certificado.

Valencia, a 4 de noviembre de 2019,

Juan Francisco Sánchez Royo

Campus de Burjassot-Paterna
C/ Dr. Moliner, 50
46100 Burjassot (València)
telf. **963543307**
fax **963544775**
www.uv.es/fisapl
dep.fisica.aplicada@uv.es

Esta tesis doctoral ha sido realizada gracias al soporte de las siguientes ayudas predoctorales:

- Oferta pública de una plaza de investigador en formación con contrato laboral temporal. Proyecto: «Nanotecnología y nanomateriales para fotónica y optoelectrónica (NANOFOT), CPI-15-276. Programa Prometeu per a grups d'investigació d'Excel · lència de la Conselleria d'Educació, Cultura i Esport» (GVPROMETEOII2014- 059).
- Ayuda para la contratación de personal investigador de carácter predoctoral ACIF/2016/385 de la Conselleria de Educación de la Generalitat Valenciana
- Ayuda para la formación de personal investigador de carácter predoctoral "Atracció de Talent" UV-INV-PREDOC17F1-539274 de la Universidad de Valencia, dentro de la cual se obtuvo una ayuda para estancias de personal investigación en formación durante 4 meses en 2018

VNIVERSITAT DE VALÈNCIA

~~The best is the enemy of the good~~

~~Voltaire~~

The good is the worst enemy of the best

Someone from CMSJdR

Contents

Acknowledgments (Agradecimientos)

Querría empezar diciendo que en esta sección me voy a permitir el lujo de escribirla de seguido, sin corregirla ni una sola vez. ¿Por pereza? Para nada. Creo que así es la única forma de que las siguientes lineas sean realmente naturales y sinceras, que evite que me corrija, que me autocensure, que me corte o que suene artificial tras depurar demasiadas frases. Unos agradecimientos más caóticos quizá, pero los prefiero al natural, que es como pienso que deberían ser porque al fin y al cabo, así es como son.

A mis 26 años (27 cuando la defienda, pero 26 mientras escribo estas líneas), intentar comprimir los agradecimientos de 4 años en algo manejable es una quimera, lo tengo clarísimo. 4 años de tesis, los mismos casi que de carrera y máster... Contando que los primeros 18 años para todo el mundo son como años de prueba, de trasteo y de simplemente crecer, estos 4 últimos años son básicamente media vida de persona consciente, de formación humana y profesional, donde las personas con las que me he cruzado han marcado mi vida tanto a nivel científico como, más importante, a nivel personal. Eso no se remarca lo suficiente: los últimos 9 años de universidad y tesis han sido, sin duda, los más importantes a nivel de formación personal. Y la tesis, esa segunda mitad, de madurez real, han afianzado quién y cómo iba a ser. Así que intentaré ser breve para que esta sección no ocupe más que un capítulo como tal. No prometo nada.

Por dónde empezar esta larga lista de agradecimientos es muy fácil. Al fin y al cabo, esta no es mi tesis doctoral, es nuestra tesis, tan mía como de mi tutor, Juan Francisco Sánchez Royo. Yo lo tuve muy claro cuando allá por tercero de carrera fui a hablar contigo (¡y lo escribo así directamente porque seguramente seas uno de los pocos que lea realmente estas líneas de entre los aquí mencionados!). A mi ya me interesaba el departamento en general, ya iba apuntando hacia este campo... pero como ya te he dicho alguna que otra vez, una charla de las que se daban los jueves durante la carrera fue lo que sin duda hizo click en la decisión de “quiero hacer el

TFG con él". Yo no he visto aún una persona que transmita tanta pasión e ilusión en lo que hace. Y en estos 4 años de tesis (+2 de TFG y TFM, que se dice pronto) no ha habido momento en el que esa ilusión haya decaído ni un poco, sino todo lo contrario. Porque al final todos los conocimientos a nivel científico como tal que he aprendido contigo no quedan en nada al lado de que esa actitud y emoción en lo que hacemos haya pasado a formar parte de mi también. Tener a alguien que te ayude en el día a día, en cada proyecto, en cada gestión, a lo largo de tantos años, del que aprender que cualquier detalle es mejorable, que te haga dar lo mejor de ti es de agradecer sin duda, pero que además de todo eso proyecte y transmita tanta ilusión por ello no tiene precio. Y la mejor forma que tengo de demostrarlo es que allá donde vaya espero estar a la altura y que piensen "¿de dónde viene este chico?", se topen con alguna de las páginas de la UV que redirijan a la tuya y entonces vean de quién sale todo. Por todo eso, gracias.

No puedo sino seguir por toda la gente con la que he trabajado en estos años. Todas esas personas del Departamento de Física Aplicada y Electromagnetismo y más concretamente, del Instituto de Ciencia de Materiales de la Universidad de Valencia y la Unidad de Dispositivos y Materiales Optoelectrónicos, con quienes más he compartido momentos. Al final es una pequeña gran familia con la que colaborar es tan cómodo como se verá reflejado a lo largo de la tesis con tantas personas que me han ayudado en los distintos proyectos que se desarrollan en ella. Ana Cros-Stotter, María Ángeles Yuste, Isaac Suárez-Álvarez, Rafael Abargues-López, Pedro Rodríguez-Cantó, Martina Delgado-Pinar, Miguel V. Andrés-Bou, Carlos Zapata-Rodríguez,... A todos ellos, gracias, por toda la ayuda en distintos momentos, en distintos proyectos, en infinitas burocracias, en discusiones científicas con las que realmente he aprendido ciencia de verdad. Mención especial merece Juan P. Martínez Pastor, cuyas enriquecedoras discusiones se ven reflejadas en todos y cada uno de los proyectos que en esta tesis se engloban, donde su despacho siempre abierto y tan cercano para cualquiera que lo necesite le da un toque de calidad (y realidad científica) a cualquier extraña explicación teórica que se me ocurriera de cualquier medida que le mostrara.

Quizá bajando un poco, pero tampoco mucho, o al menos de momento, el nivel "científico", está ese bloque de estudiantes de doctorado con los que he tenido la suerte de cruzarme en estos años. Desde los que ya estaban a los que dejo empezando su camino, compartir cafés, comidas, preocupaciones, cervezas y salseos han sido un motor increíble para el día a día. Olaia Álvarez-Bermúdez, Soledad

Roig-Sánchez, Antonio García-Barberá, Alberto Maulu, Mattia Signoretto, Mauro Brotons-Gisbert, Juan Navarro-Arenas, Rodolfo E. Canet-Albiach, Jaume Noguera-Gómez. Gracias a todos... y suerte a los que empezáis, sabéis cómo buscarme para cualquier cosa como antes estuvieron para mi!

In this paragraph it is necessary a language change, because I want to thank everyone I met during my stay in Edinburgh, to the members of the Quantum Photonics Lab of Heriot-Watt University. First, to Prof. Brian D. Gerardot, who gave me the oportunity to feel like a member of his research group and the new topics I learned. Second, to Mauro Brotons-Gisbert, again, who after welcoming me in our PhD office when I started in Valencia, welcomed me again during my stay in Edinburgh. And finally, to every member and amazing people I met there. Cristian, Sarah, Santosh, Raphäel, Daniel, Guillem, Zak, Markus, Hyeonjun and, later, Aidan, Micaela, Karen and Willeke. Thank you very much, because a stay in a new city, a new country could be hard, but with people like you it felt like home.

Pasando ya de lo más enfocado en la tesis doctoral a lo más puramente personal, me gustaría agradecer a los amigos de siempre, de donde vengo, los que estaban ahí desde que tengo memoria, a los de "se sale Dani a jugaaaar?". Después de todos estos años, aunque cada vez sea más difícil quedar, las fiestas del pueblo, Turbas o San Mateo no se los salta nadie. Por eso, lobos y lobas, WW, gracias a todos, hoy y desde que salía a jugar al parque de enfrente.

Y de los amigos de niñez a los que llegaron más tarde. El Colegio Mayor San Juan de Ribera ha marcado sin duda toda mi vida universitaria, y las amistades que aquí he conocido han influido más en mi formación a cualquier nivel de lo que podría haber encontrado en otro sitio. Y escribo "aquí", porque tras 5 años viviendo en el Colegio y otros 3 fuera, escribo estas líneas de nuevo viviendo unos meses entre sus muros. Y nada ha cambiado, solo las caras, pero no lo que es. Desde los directores con los que he vivido, todos los que trabajan allí y, cómo no, a los colegiales, antiguos y actuales, con los que viví y los que viven lo que vivimos en su momento, que son los que realmente forman el Colegio. Cómo no destacar al Consejo de Sabios. Si soy (cuando sea) presidente, director o CEO de algo importante, liberad la agenda, porque seréis sin duda mis almirantes, capataces, ministros, capitanes, compañeros y, como ya lo sois, hermanos, de cualquier cosa en la que esté metido. Grandes. Que no se nos olvide lo que dijo el chino que trabaja en El Frenazo.

Y no podía terminar de otra forma, cerrando como comenzaba. Empezaba diciendo

que ésta no es mi tesis, que es nuestra tesis, pero no solo nos pertenece a mi tutor y a mi. Desde que empecé la universidad no escuchaba un “a ver si apruebas” sino un “a ver si aprobamos”. Nunca hubo un “la siguiente beca la consigues”, sino un “la siguiente beca la conseguimos”. Y no era simplemente una forma de hablar, yo siempre lo he sentido así. Porque yo no conseguía nada solo, lo conseguíamos entre todos. La página de la UV yo me la he leído un par de veces cuando necesitaba alguna información, pero ellos lo hacían doscientas desde casa. Las resoluciones y convocatorias de becas, ni me imagino cuántas veces se las han leído. De tener pensada la maleta que se llevarían por si hace frío meses antes de que me tuviera que ir siquiera. Y, a día de hoy, sigue pasando, en cualquier detalle, en cualquier cosa, están ahí, con todo lo que tienen y un poco más. Como decían en el cole cuando era pequeño, que a mi me gustaba que si lo bueno es breve, dos veces bueno, no me extenderé en este agradecimiento, porque ni sabría hacerlo como merecen. Ellos no han hecho la tesis doctoral, pero me han hecho a mi mismo. Este párrafo es para mis padres, por los que soy quien soy, y para mi hermana, que me hace ser como querría ser para ella. Igual la frase no tiene ningún sentido, pero tiene todo el sentido del mundo para mi. Gracias, por todo. Ahora, vamos a por el postdoc, juntos.

Seguro que me dejo a mucha gente en estas líneas. Al final hacer como grupitos de gente a la que he conocido es lo más común, pero eso no quita que haya muchas personas individuales que sin duda han influido en mi, y ellos ya lo saben. A todos y cada uno de vosotros, los que menciono y a los que seguro me dejo, gracias.

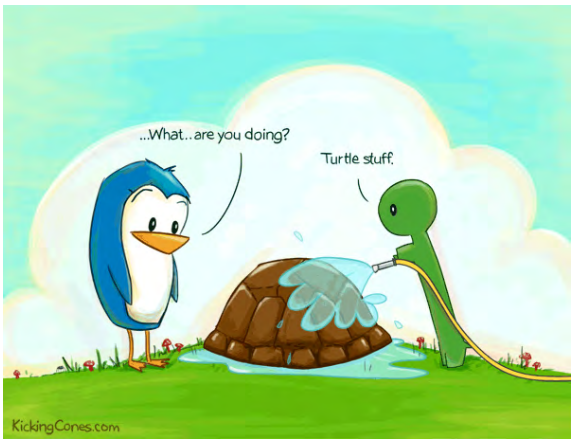

Figure 0.1: Hace años te prometí que la palabra "pingüino" aparecería en algo científico que escribiera. Aquí lo tienes, pichón. Drawing reproduced with the permission of Katrina, from KickingCones.com

Abstract

In the Materials Science field, two-dimensional materials have gained the scientific community attention in recent years. The change and the appearance of novel properties when their thickness is reduced to nanometric scale has special interest for its fundamental properties study for, from these base, the design and its implementation in devices. The wide variety of materials with the possibility of being exfoliated at the two-dimensional level opens the field to different applications, from optoelectronic devices, detection and sensing, energy storage, catalysis, medical applications and quantum information technologies, among others.

This thesis gathers results in both directions: a fundamental science level study in two-dimensional materials less explored by the scientific community and its implementation in optoelectronic devices focused on different applications.

In the first part, optical and electrical properties of the family of III - VI semiconductors, less explored and complementary in many properties to the well-known transition-metal dichalcogenides will be studied. The photoluminescence of Gallium Selenide will be analysed, where a shift in its luminescent emission of 120 meV is demonstrated experimentally when the thickness of GaSe slabs is reduced from the bulk to 8 nm, a result superior to that reported at the moment and consistent with that expected by calculations, with a shift from 2.02 eV in its bulk state up to 3.2 eV when the monolayer is obtained, from the visible spectra to the near ultraviolet according to first principles calculations. The oxidation mechanism of this material under normal conditions is also studied by techniques such as atomic force microscopy, optical contrast and X-ray photoelectron spectroscopy to understand the evolution in its degradation processes detected in two-dimensional GaSe samples. A second member of the III-VI semiconductor family has been studied in this thesis, Indium Selenide, a material whose optical properties are known to a greater extent, but whose electrical properties in its two-dimensional form have not been explored will be the focus of the study. This thesis demonstrates the usage of

multiterraced nanosheets of this material as heterojunctions without defects in its junction that behave as p - n heterojunctions, the basis of modern optoelectronics in devices such as transistors, photodetectors or photodiodes. Based on the change in its band structure when thickness is reduced, its behavior as a photodetector is studied through its I - V characteristics and a detailed study of the carrier recombination in the barrier generated by the change of prohibited band gap in the area where the thickness changes. In addition, for the modeling and design of electrical devices using this material, the dependance of the work function with the nanosheet thickness is studied by means of Kelvin probe force microscopy and first principles calculations, demonstrating that the work function of InSe slightly increases when the two-dimensional liimit is reached. Finally, as an application of this material in its two-dimensional form, its abilities for sensing of gases by means of the change in the photoluminescence of the samples exposed to different concentrations, times and gases is proposed and demonstrated. Thiols will be used due to their presence of the sulfide radical, present in different organic food and similar decays and trinitrotoluene as an example of gas present in bomb detection, among others.

After presenting the III -VI semiconductors, a second part of the thesis will focus on its experimental implementation in proto-devices to take advantage of or to optimise the properties described above, comparing the results in each case with monolayers of transition metal dichalcogenides such as Tungsten Selenide or Molybdenum Selenide. Specifically, we will try to take advantage of the recently demonstrated out-of-plane dipole nature of the Indium Selenide nanosheets, contrary to the transition metal dichalcogenides, which hampers its usage in the vertical excitation - vertical collection usual configuration in scientific studies. First, through the use of silicon oxide microspheres on the two-dimensional nanosheets, the extraction and collection of their photoluminescence will be optimised, both in the case of Indium Selenide and Tungsten Selenide. Besides, the behavior as an out-of-plane dipole will be demonstrated in the case of the Indium Selenide and the low energy contribution of the Tungsten Selenide photoluminescent emission associated with the charged exciton or trion due to the whispering gallery modes that occur in the microspheres. This technique offers an additional control to the photoluminescent emission of these materials depending on the diameter of the microspheres, both in an enhancement in its intensity and in the effective emission position peak collected for its implementation in a specific application.

After this, these two-dimensional materials will be studied in vertical heterostruc-

tures together with perovskite nanocrystals with visible photoluminescent emission, obtaining an enhancement in the photoluminescence collected in the case of Indium Selenide nanosheets compared to that obtained together with Molybdenum Selenide, where the photoluminescence detected is reduced by depositing a nanocrystalline perovskite on the exfoliated monolayers. The reason for this effect is the reabsorption by the Indium Selenide of what is emitted by the perovskite layer on top, due to the optimal arrangement of its out-of-plane dipole and the multidirectional emission of the perovskites, as opposed to the in-plane dipole of transition metal dichalcogenides, already optimal for vertical excitation and collection. These studies support are promising for the engineering of optoelectronic devices based on these two-dimensional heterostructures.

Finally in this second part, the possible integration of these two-dimensional materials into photonic devices is studied. In particular, the behavior of Indium Selenide nanosheets and Tungsten Selenide and Molybdenum Selenide monolayers on photonic waveguides is studied, allowing excitation and collection interchangeably in the horizontal and vertical directions to the exfoliation plane, in all possible configurations. After some essays steps with Indium Selenide, the implementation of the transition metal dichalcogenides in the photonic waveguides is studied in detail, obtaining experimental measurements in all guiding configurations, as well as their different behavior in its absorption and photoluminescent emission against polarised light in the waveguide.

In a third and final part of the thesis two two-dimensional materials not explored in the literature will be presented: Bismuth Sulfide and Molybdenum Oxide. In the case of Bismuth Sulfide, a semiconductor material is presented that, in addition to its anisotropy between the exfoliation plane and the vertical direction, presents an unusual optical and structural anisotropy within the plane, demonstrated by several optical techniques such as Raman spectroscopy, photoluminescence, optical contrast, differential reflectivity and transmittance. The application of such anisotropy in optical fibers as a Fabry-Perot cavity in its core is demonstrated, from which results its birefringence is obtained in comparison with other reported laminar materials. Finally, Molybdenum Oxide is presented as a two-dimensional insulating material, uncommon in the two-dimensional materials field, where hexagonal Boron Nitride is the only one considered. The exfoliability of Molybdenum Oxide and its advantages over hexagonal Boron Nitride are demonstrated: its absence of low temperature defects and its almost-zero nuclear spin compared to hexagonal Boron Nitride, which

hampers its usage in nuclear spintronics oriented devices. The usage of this new material as a two-dimensional insulator is demonstrated by the encapsulation of transition metal dichalcogenides monolayers within this material and studying its behavior at low temperature, from its single photon emitters behavior to the narrowing in the emission and absorption of the encapsulated semiconductor, obtained by photoluminescence and differential reflectivity at low temperature, respectively.

1 Introduction

This chapter will describe the framework in which this thesis is framed, from a brief description of the field state-of-the-art, as well as its growing interest applied in different fields and the importance and potential in its growth. Finally, it will describe the focus of the thesis and its objectives, as well as the different projects worked within it.

1.1 State-of-the-art: graphene, two-dimensional transition metal dichalcogenides and hBN

Within material science, nanomaterials is a field in its heyday, we are in an apogee where new studies around different nanomaterials and their properties are presented every day, obtaining newer and newer properties. The accumulted knowledge in this field has promoted that expansion and implementation of these nanomaterials at a commercial level. It is a field that experiences an exponential growth but that society incorporates in its day to day at an overwhelming pace.

In nanomaterials, at least one dimension is in the nanometric scale [68]. In this regime, the atoms or molecules that consitute the nanomaterial experience qualitative changes in their properties, which affect the final nanomaterial properties. In these configurations, size-effects properties become relevant. Effects such as quantum confinement, superparamagnetism or surface plasmon resonances take their place in these nanomaterials.

When we mention a material, in general, the three-dimensional (3D) or bulk material is considered. In a nanomaterial, if all its dimensions are restricted in the range of a few nanometers (not exceeding 500 nm as a general rule, considering after that the micrometric scale), they are usually called zero-dimensional (0D) materials. For

instance, nanoparticles or quantum dots belong to this family. Studies that completely cover the scientific spectrum, e.g. from its use for leading medical purposes [20, 25, 59, 34] or quantum technologies to be developed [19, 39, 52, 65] or as fundamental parts in daily applications, from body creams [38, 28] to televisions [43, 21], among others.

Two of the dimensions of the material are nanometric in a one-dimensional (1D) material, with nanowires at their maximum example. Like before, cutting-edge studies are deployed around these materials [5, 7] meanwhile they are completely embodied in our DNA [35], or any carbon nanotube racket tennis that we can purchase as examples of day-to-day 1D materials. And last but not least, if only one of its dimensions is considered nanometric, a two-dimensional (2D) or layered material is the object of study. Is in these 2D materials where this thesis is framed.

Perhaps one of the best examples chronologically of these dimensionality variety lies among the carbon materials. Carbon, in its 3D form, is graphite. It has been used since the 4th millenium BC [27], usually known as black lead or plumbago, and uses as a steel component [54], dry lubricant [53] or any pencil we use are not impressive nowadays.

However, in the past, the scientific community saw a potential in this material, with a structure which made possible its nanometric form. It was not until 1985 when fullerene, its 0D form, was obtained [70]. This fact suggested the 1D form existance, the carbon nanotubes, which 6 years later, in 1991, were first demostrated [16]. Although the 2D graphite (called graphene in a monolayer (ML) state) was the starting material to understand and theoretically form fullerenes and carbon nanotubes, it was the last obtained, when in 2004 A. Geim and K. Novoselov isolated a graphene ML sheet [322].

Graphene was the first 2D material obtained, by a simpler technique than previously proposed: graphite, from its bulk state, was exfoliated in MLs of graphene using commercial scotch tape. However, the simplicity of its obtaining method has not been what astonished the scientific community (creating its own field, that of 2D materials, one of the most cutting-edge and booming fields in the last years), but its amazing properties, completely different from those of its 3D state. The ML of graphene turned out to possess one of the highest thermal and electrical conductivities [26]. Besides, its mechanical properties, such as stiffness or strength, highlighted among similar materials, supporting very high strain prior to mechanical

failure [228], being able to be bent or wrinkled without damage.

However, in optoelectronics, its massless Dirac fermions band structure [238, 48] opened the study of this novel electrical properties, becoming the 2D quintessential conducting material. Many efforts were made to open a gap in this material by many techniques to use graphene as a 2D semiconductor for devices. From morphological manipulations through strain [64, 49, 31, 69, 46], shear [30], patterning graphene into nanoribbons [42] or periodic ripples [44], changing its chemistry through hydrogenation [33] or applying a perpendicular electric field [48], among others. But the specific conditions for this fact and its difficulty opened the gate wide open for other 2D materials to complement graphene, in these cases, already intrinsically semiconductors in their 3D form.

2D Transition Metal Dichalchogenides (TMDs) such as Molybdenum Sulphide (MoS_2), Molybdenum Selenide ($MoSe_2$), Tungsten Sulphide (WS_2) and Tungsten Selenide (WSe_2) were obtained with similar techniques to graphene up to its 2D ML form and could be, after graphene, the most studied 2D materials. Among the several studies about this family of materials worth noting, due to the quantum confinement effects in the exfoliation plane, the indirect-to-direct transition in their band gap when the materials are exfoliated from their bulk state to their ML [316, 338] and their strong exciton binding energy, which makes them ideal for their excitonic physics study even at room temperature (RT). For the first time, intrinsically 2D semiconductor materials had been obtained for their application in optoelectronics. So after a 2D conductor and 2D semiconductors, hexagonal Boron Nitride (hBN) was obtained with similar techiques in its ML state. With a 5.97 eV band gap [71], filled the void as a 2D insulator.

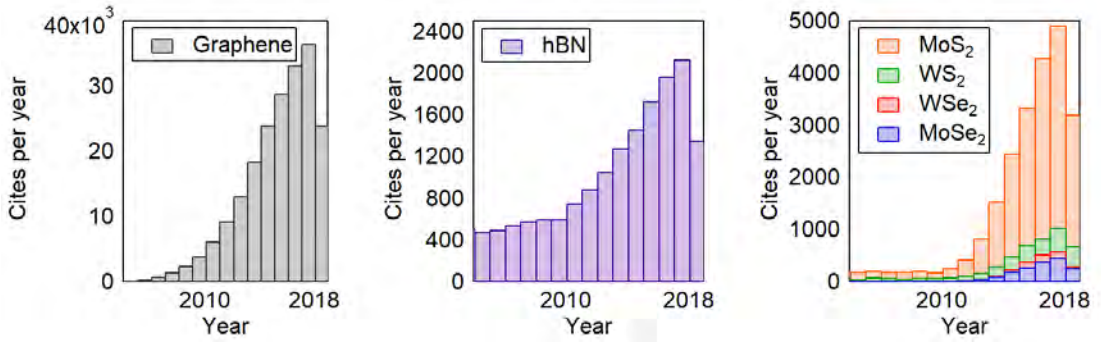

Figure 1.1: Cites per year in the last 15 years about 2D topics, data obtained from Web of Science, Fundación Española para la Ciencia y la Tecnología (FECYT).

These ideas not only boosted the interest about their basic properties among the scientific community, as observed in Figure 1.1, but also about applications of that interesting properties. Fields such as optoelectronic devices [50, 41, 29, 51], telecomunications [13, 23, 66], biosensing [110, 109, 102, 111] or medicine [67, 32, 58, 15] started to apply these studies to actual applications or devices. In some cases, 2D materials not only surpass the materials already used with better performance, but also complemented them enhancing or giving new capabilities.

The relevance of these 2D materials was not only achieved in already-fundamented fields, but creating or supporting fields where the other materials could not achieve, such as foldable wearable technologies [72, 11, 37, 9], valley- and spintronics [18, 24, 57, 60, 8], quantum technologies [1, 36, 17, 55] or superconductivity [45, 56] are a few examples.

The nanomaterials cited before are just examples of the most and first 2D materials studied. But just as we have the periodic table that collects all the elements, and those elements come together to form an large variety of materials, to keep attention to a few of these when describing the material science field in general is to be basically blinded. When we talk about 2D materials we have to think about all of them, the acquaintances and those that are to come, their properties and those that have not yet been discovered, the already proposed applications and the applications that will come. Therefore, the study of new 2D materials is needed.

The future of the 2D materials seems unimaginable, and the limit of their potential applications, unreachable. The number of materials that obtain new properties in their 2D state only increases every day, and the variety in these properties and their different combinations predicts a field that in the coming years will only grow exponentially, both in its understanding and in its implementation in different and new applications.

1.2 Objective of the thesis

In this context, this thesis focuses beyond the next premises:

- Among the different methods of preparing 2D materials, each with different advantages and disadvantages, all the samples studied will be prepared by micromechanical exfoliation (Subsection 2.1.1), a technique with which samples of great purity and quality are obtained in order to study its new properties.

- Less-explored 2D materials, their properties and their implementation in devices are main concerns in this thesis.
- In order to compare the less-explored 2D materials addressed, "classic" TMDs will be studied for comparison, obtaining new understanding in their properties too.
- This thesis has a great experimental weight, since the whole process will be addressed: from the preparation of different 2D materials, to its characterisation through different techniques, the study of their properties via different methods, to its implementation in devices for specific applications, concerning different fields, from sensing, to microresonators, perovskites, implementation in integrated optical waveguides, optical fibres... The inmersion of the 2D materials explored in different enviroments or fields, together with the study of its basic properties, raises a broad vision of its application in different fields, with the aim of opening new mixed-fields of study.

Therefore, among the III-VI semiconductors, Gallium Selenide (GaSe) and Indium Selenide (InSe) will be studied. First, their basic optical and electrical properties will be addressed, to finally include them among different devices to enhance or apply its properties on a specific matter.

Besides, new 2D materials barely explored with in-plane anisotropy such as Bismuth Sulphide (Bi_2S_3) as a semiconductor and Molybdenum Trioxide (MoO_3) as an insulator will be presented, studied and a device implementation will be proposed.

The completion of this doctoral thesis is part of the Low-dimensional materials (Lowdim) line of research within the Optoelectronic Materials and Devices Unit (UMDO) of the Institute of Materials Science of the University of Valencia (ICMUV). Besides, the last chapter has been developed in the Institute of Photonics and Quantum Sciences (IPaQS) of the Heriot-Watt University (Edinburgh, United Kingdom) during a 5-months stay.

1.3 Organisation of the chapters

This thesis starts briefly sketching the field state-of-the-art in which is framed, the 2D materials, and presenting the background of well-known 2D flagship materials

such as graphene, the TMDs or hBN, pointing out the several applicability fields and its potential (Chapter 1).

After that, the experimental techniques that have been addressed and employed through the different projects embraced during this thesis have been presented, achieving the whole process, from the preparation and characterisation of samples, through its study of various optical and electrical properties, to the implementation of these materials in devices and applications (Chapter 2).

One of the focuses of this thesis aims in less-explored semiconductors beyond the TMDs for optoelectronic applications: the III-VI semiconductors, where optical properties of GaSe and electrical properties of InSe will be studied (Chapter 3).

III-VI semiconductors exhibit not enough absorption or emission in some circunstances, so next Chapters explore techniques to overcome this issue, from the usage of microspherical resonators to tune the optical response of 2D materials (Chapter 4), to the development and characterisation of 2D InSe/perovskites hybrid heterostructures (Chapter 5), ending with an integrated-device-oriented study through their implementation in optical waveguides (Chapter 6). In all of them, even though the objective starts as enhancement to the III-VI semiconductors, have been reproduced for comparison with better-known semiconductors such as TMDs, reaching new understanding about their nature.

Finally, after three chapters where the anisotropy between the z direction and the x - y exfoliation plane becomes quite relevant, the non-frequent in-plane x - y anisotropy has been evaluated in two poorly unexplored 2D materials: Bi_2S_3 as a semiconductor (Chapter 7) and MoO_3 as an insulator (Chapter 8), concluding both proposing an application using nanosheets of the materials presented.

The thesis will end concluding the main results of the different projects involved and its future prospects (Chapter 9).

Bibliography

[1] M Koperski, K Nogajewski, A Arora, V Cherkez, P Mallet, J Veuillen, J Marcus, P Kossacki, and M Potemski. Single photon emitters in exfoliated WSe2 structures. *Nature Nanotechnology*, 10(6):503–506, 2015.

[2] Kin Fai Mak, Changgu Lee, James Hone, Jie Shan, and Tony F. Heinz. Atomically thin MoS2: A new direct-gap semiconductor. *Physical Review Letters*, 105(13):2–5, 2010.

[3] John R. Schaibley, Hongyi Yu, Genevieve Clark, Pasqual Rivera, Jason S. Ross, Kyle L. Seyler, Wang Yao, and Xiaodong Xu. Valleytronics in 2D materials. *Nature Reviews Materials*, 1(11), 2016.

[4] Sang Jin Kim, Kyoungjun Choi, Bora Lee, Yuna Kim, and Byung Hee Hong. Materials for Flexible, Stretchable Electronics: Graphene and 2D Materials. *Annual Review of Materials Research*, 45(1):63–84, 2015.

[5] Dominique Laroche, Daniël Bouman, David J. van Woerkom, Alex Proutski, Chaitanya Murthy, Dmitry I. Pikulin, Chetan Nayak, Ruben J.J. van Gulik, Jesper Nygård, Peter Krogstrup, Leo P. Kouwenhoven, and Attila Geresdi. Observation of the 4π-periodic Josephson effect in indium arsenide nanowires. *Nature Communications*, 10(1):1–7, 2019.

[6] K.S. Novoselov, A.K. Geim, S.V. Morozov, D. Jiang, Y. Zhang, S.V. Dubonos, I.V. Grigorieva, and A.A. Firsov. Electric Field Effect in Atomically Thin Carbon Films. *Science Reports*, 306(October):666–670, 2004.

[7] Chengzhou Zhu, Dan Du, and Yuehe Lin. Graphene and graphene-like 2D materials for optical biosensing and bioimaging: A review. *2D Materials*, 2(3), 2015.

[8] Thomas Mueller and Ermin Malic. Exciton physics and device application of two-dimensional transition metal dichalcogenide semiconductors. *npj 2D Materials and Applications*, (July):1–12, 2018.

[9] Jong-hyun Ahn and Byung Hee Hong. Things you could do with graphene Graphene for displays that bend Electrifying inks with 2D materials. *Nature Publishing Group*, 9(10):737–738, 2014.

[10] Oriol Lopez-Sanchez, Dominik Lembke, Metin Kayci, Aleksandra Radenovic,

and Andras Kis. Ultrasensitive photodetectors based on monolayer MoS2. *Nature Nanotechnology*, 8(7):497–501, 2013.

[11] Keun Soo Kim, Yue Zhao, Houk Jang, Sang Yoon Lee, Jong Min Kim, Kwang S Kim, Jong-hyun Ahn, Philip Kim, Jae-young Choi, and Byung Hee Hong. Large-scale pattern growth of graphene films for stretchable transparent electrodes. *Nature*, 457(7230):706–710, 2008.

[12] Kian Ping Loh, Qiaoliang Bao, Goki Eda, and Manish Chhowalla. Graphene oxide as a chemically tunable platform for optical applications. *Nature Publishing Group*, 2(12):1015–1024, 2010.

[13] Ming Liu, Xiaobo Yin, Erick Ulin-avila, Baisong Geng, Thomas Zentgraf, Long Ju, Feng Wang, and Xiang Zhang. A graphene-based broadband optical modulator. *Nature*, 474(7349):64–67, 2011.

[14] Di Xiao, Gui Bin Liu, Wanxiang Feng, Xiaodong Xu, and Wang Yao. Coupled spin and valley physics in monolayers of MoS 2 and other group-VI dichalcogenides. *Physical Review Letters*, 108(19):1–5, 2012.

[15] Wong Cheng, Kian Ping, and Chwee Teck. Biomaterials When stem cells meet graphene : Opportunities and challenges in regenerative medicine. *Biomaterials*, 155:236–250, 2018.

[16] Sumio Iljima. Helical microtubules of graphitic carbon. *Letters to Nature*, 354(November):56–58, 1991.

[17] Igor Aharonovich, Dirk Englund, and Milos Toth. Solid-state single-photon emitters. *Nature Publishing Group*, 10(10):631–641, 2016.

[18] A Morello and A S Dzurak. Spin-valley lifetimes in a silicon quantum dot with tunable valley splitting. *Nature Communications*, 4(May):1–8, 2013.

[19] Jingjing Xu and Ji Zheng. *Quantum Dots and Nanoclusters*. Elsevier Inc., 2019.

[20] Ebrahim Mostafavi, Pooneh Soltantabar, and Thomas J Webster. *Nanotechnology and picotechnology: A new arena for translational medicine*. Elsevier Inc., 2019.

[21] Liangrui He, Mi Fei, Jie Chen, Yunfei Tian, Yang Jiang, Yang Huang, Kai Xu, Juntao Hu, Zhi Zhao, Qiuhong Zhang, Haiyong Ni, and Lei Chen. Graphitic C3N4 quantum dots for next-generation QLED displays. *Materials Today*, 22(February):76–84, 2019.

[22] Andrea Splendiani, Liang Sun, Yuanbo Zhang, Tianshu Li, Jonghwan Kim, Chi Yung Chim, Giulia Galli, and Feng Wang. Emerging photoluminescence in monolayer MoS2. *Nano Letters*, 10(4):1271–1275, 2010.

[23] Seung Hoon Lee, Muhan Choi, Teun-teun Kim, Seungwoo Lee, Ming Liu, Xiaobo Yin, Hong Kyw Choi, Seung S Lee, Choon-gi Choi, Sung-yool Choi, Xiang Zhang, and Bumki Min. Switching terahertz waves with gate-controlled active graphene metamaterials. *Nature Materials*, 11(10):1–6, 2012.

[24] Aaron M Jones, Hongyi Yu, Jason S Ross, Philip Klement, Nirmal J Ghimire, Jiaqiang Yan, David G Mandrus, Wang Yao, and Xiaodong Xu. Spin - layer locking effects in optical orientation of exciton spin in bilayer WSe2. *Nature Physics*, 10(1):1–5, 2014.

[25] Recent Trends and Future Perspectives. *Nanotechnology in Modern Animal Biotechnology*. Springer, 2019.

[26] Alexander A Balandin, Suchismita Ghosh, Wenzhong Bao, Irene Calizo, Desalegne Teweldebrhan, Feng Miao, and Chun Ning Lau. Superior Thermal Conductivity of Single-Layer Graphene 2008. *Nano Letters*, 8(3):902 – 907, 2008.

[27] J Boardman, I E S Edwards, N G L Hammond, and E Sollberger. The Cambidge Ancient History Volume III. *Cambridge Histories Online*, III, 2008.

[28] Nirvesh Chaudhri, Girish C Soni, and S K Prajapati. Nanotechnology: An Advance Tool for Nano-cosmetics Preparation. *International Journal of Pharma Research and Review*, 4(April):28–40, 2015.

[29] Woong Choi, Mi Yeon Cho, Aniruddha Konar, Jong Hak Lee, Gi-beom Cha, Soon Cheol Hong, Sangsig Kim, Jeongyong Kim, Debdeep Jena, Jinsoo Joo, and Sunkook Kim. High-Detectivity Multilayer MoS2 Phototransistors with Spectral Response from Ultraviolet to Infrared. *Advanced Materials*, pages 5832–5836, 2012.

[30] Giulio Cocco, Emiliano Cadelano, Luciano Colombo, and Castro Neto. Gap opening in graphene by shear strain. *Physical Review B*, pages 1–4, 2010.

[31] Alessandro Cresti, Norbert Nemec, Blanca Biel, Gabriel Niebler, François Triozon, and Stephan Roche. Charge Transport in Disordered Graphene-Based Low Dimensional Materials. *Nano Res*, 1:361 – 394, 2008.

[32] Xili Ding, Haifeng Liu, and Yubo Fan. Graphene-Based Materials in Regenerative Medicine. *Advanced Healthcare Materials*, pages 1451–1468, 2015.

[33] D C Elias, R R Nair, T M G Mohiuddin, S V Morozov, P Blake, M P Halsall, A C Ferrari, D W Boukhvalov, M I Katsnelson, A K Geim, and K S Novoselov. Control of Graphene's Properties by Reversible Hydrogenation: Evidence for Graphane. *Science*, 610, 2009.

[34] Shiva Gholizadeh and Ghaleh Aziz. Application of nanomaterials in three - dimensional stem cell culture. *Journal of Cellular Biochemistry*, (November 2018):1–9, 2019.

[35] Qun Gu, Chuanding Cheng, and Ravikanth Gonela. DNA nanowire fabrication. *Topical Review*, pages 13–25, 2006.

[36] Yu-ming He, Genevieve Clark, John R Schaibley, Yu He, Ming-cheng Chen, Yu-jia Wei, Xing Ding, Qiang Zhang, Wang Yao, Xiaodong Xu, Chao-yang Lu, and Jian-wei Pan. Single quantum emitters in monolayer semiconductors. *Nature Nanotechnology*, (May):1–6, 2015.

[37] Woo Jin Hyun, O Ok Park, and Byung Doo Chin. Foldable Graphene Electronic Circuits Based on Paper Substrates. *Advanced Materials*, pages 4729–4734, 2013.

[38] Arturo A Keller, William Vosti, Hongtao Wang, and Anastasiya Lazareva. Release of engineered nanomaterials from personal care products throughout their life cycle. *J Nanopart Res*, 16:2489, 2014.

[39] Ferdinand F E Kohle, Joshua A Hinckley, Songying Li, Nikhil Dhawan, William P Katt, Jacob A Erstling, Ulrike Werner-zwanziger, Josef Zwanziger, Richard A Cerione, and Ulrich B Wiesner. Amorphous Quantum Nanomaterials. *Advanced Materials*, 1806993:1–9, 2018.

[40] Changgu Lee, Xiaoding Wei, Jeffrey W Kysar, and James Hone. Measurement of the elastic properties and intrinsic strength of monolayer Graphene. *Science*, 321(July):385–389, 2008.

[41] Hee Sung Lee, Sung-wook Min, Youn-gyung Chang, Min Kyu Park, Taewook Nam, Hyungjun Kim, Jae Hoon Kim, Sunmin Ryu, and Seongil Im. MoS2 Nanosheet Phototransistors with Thickness-Modulated Optical Energy Gap. *Nano Letters*, 12:3695 – 3700, 2012.

[42] Xiaolin Li, X Wang, L Zhang, S Lee, and H Dai. Chemically Derived, Ultrasmooth Graphene Nanoribbon Semiconductors. *Science*, 1229(2008), 2012.

[43] G Liu. United States Patent 10263220B2. *US Patent*, 2, 2019.

[44] I I Naumov and A M Bratkovsky. Gap opening in graphene by simple periodic inhomogeneous strain. *Physical Review B*, 245444(November):2–7, 2011.

[45] A H Castro Neto. Charge Density Wave , Superconductivity , and Anomalous Metallic Behavior in 2D Transition Metal Dichalcogenides. *Physical Review Letters*, pages 1–4, 2001.

[46] Zhen Hua Ni, Ting Yu, Yun Hao Lu, Ying Ying Wang, Yuan Ping Feng, and Ze Xiang Shen. Uniaxial Strain on Graphene : Raman. *ACS Nano*, 2(11):2301–2305, 2008.

[47] K S Novoselov, A K Geim, S V Morozov, D Jiang, M I Katsnelson, I V Grigorieva, and S V Dubonos. Two-dimensional gas of massless Dirac fermions in graphene. *Nature*, 438(November):197–200, 2005.

[48] Jeroen B Oostinga, Hubert B Heersche, Xinglan Liu, Alberto F Morpurgo, and Lieven M K Vandersypen. Gate-induced insulating state in bilayer graphene devices. *Nature Materials*, pages 151–157, 2007.

[49] Vitor M Pereira, A H Castro Neto, and N M R Peres. Tight-binding approach to uniaxial strain in graphene. *Physical Review B*, pages 1–8, 2009.

[50] Single-layer Mos Phototransistors. Single-Layer MoS2 Phototransistors. *ACS Nano*, (1):74–80, 2012.

[51] Andreas Pospischil, Marco M Furchi, and Thomas Mueller. Solar-energy conversion and light emission in an atomic monolayer p - n diode. *Nature Nanotechnology*, 9(March):257–261, 2014.

[52] Wei Ren, Gungun Lin, Christian Clarke, Jiajia Zhou, and Dayong Jin. Optical Nanomaterials and Enabling Technologies for High-Security-Level Anticounterfeiting. *Advanced Materials*, 1901430:1–15, 2019.

[53] S Shaji and V Radhakrishnan. An investigation on surface grinding using graphite as lubricant. *International Journal of Machine Tools and Manufacture*, 42:733–740, 2002.

[54] S N Singh, K E Blazek, T C I Tc, and T C Tc. Heat transfer and skin formation

in a continuous-casting mold as a function of steel carbon content. *Journal of Metals*, 17(October), 1974.

[55] Toan Trong Tran, Cameron Zachreson, Amanuel Michael Berhane, Kerem Bray, Russell Guy Sandstrom, Lu Hua Li, Takashi Taniguchi, Kenji Watanabe, Igor Aharonovich, and Milos Toth. Quantum Emission from Defects in Single-Crystalline Hexagonal Boron Nitride. *Physical Review Applied*, 034005:2–6, 2016.

[56] T Valla, A V Fedorov, P D Johnson, J Xue, K E Smith, and F J Disalvo. Charge-Density-Wave-Induced Modifications to the Quasiparticle Self-Energy in 2H-TaSe2. *Physical Review Letters*, pages 4759–4762, 2000.

[57] S A Wolf, D D Awschalom, R A Buhrman, J M Daughton, and S Von Molna. Spintronics: A Spin-Based Electronics Vision for the Future. *Science*, 294(November):1488–1496, 2001.

[58] Evan K Wujcik and Chelsea N Monty. Nanotechnology for implantable sensors: carbon nanotubes and graphene in medicine. *Nanomed Nanobiotechnol*, 5(June), 2013.

[59] Jun Yao, H Wang, M Chen, and M Yang. Recent advances in graphene-based nanomaterials : properties , toxicity and applications in chemistry , biology and medicine. *Microchimica Acta*, 2019.

[60] Hongyi Yu, Xiaodong Cui, Xiaodong Xu, and Wang Yao. Valley excitons in two-dimensional semiconductors. *National Science Review*, (December 2014):57–70, 2015.

[61] Beibei Zhan, Chen Li, Jun Yang, Gareth Jenkins, Wei Huang, and Xiaochen Dong. Graphene Field-Effect Transistor and Its Application for Electronic Sensing. *Small*, (20):4042–4065, 2014.

[62] Ming Zhou, Yueming Zhai, and Shaojun Dong. Electrochemical Sensing and Biosensing Platform Based on Chemically Reduced Graphene Oxide. *Anal. Chem.*, 81(14):5603–5613, 2009.

[63] Chengzhou Zhu and Shaojun Dong. Energetic Graphene-Based Electrochemical Analytical Devices in Nucleic Acid , Protein and Cancer Diagnostics and Detection. *Electroanalysis Review*, pages 14–29, 2014.

[64] V Meunier, A G Souza-Filho, E B Barros, and M S Dresselhaus. Physical

properties of low-dimensional sp 2 -based carbon nanostructures. *Reviews of Modern Physics*, 88(June):1–50, 2016.

[65] Lin Cheng, X G Zhao, W C Niu, C L Xu, Z Y Hou, and X Y Zhang. Application Technology of New Nanomaterials Electrochemical Sensors. *Acta Microscopica*, 28(3):586–595, 2019.

[66] A R Wright, X G Xu, J C Cao, and C Zhang. Strong nonlinear optical response of graphene in the terahertz regime. *Applied Physics Letters*, 072101(2009):1–4, 2012.

[67] Jun Yao, Yu Sun, Mei Yang, and Yixiang Duan. Chemistry, physics and biology of graphene-based nanomaterials: new horizons for sensing, imaging and medicine. *Journal of Materials Chemistry*, pages 14313–14329, 2012.

[68] The European Commission. Commission recommendation of 11 October 2011 on the definition of nanomaterial. *Official Journal of the European Union*, (June 2010):2010–2012, 2011.

[69] Seon-myeong Choi, Seung-hoon Jhi, and Young-woo Son. Effects of strain on electronic properties of graphene. *Physical Review B*, pages 23–26, 2010.

[70] H W Kroto, J R Heath, S C O'Brien, R F Curl, and R E Smalley. C60: Buckminsterfullerene. *Nature*, pages 62–63, 1985.

[71] C R Dean, A F Young, I Meric, C Lee, L Wang, S Sorgenfrei, K Watanabe, T Taniguchi, P Kim, K L Shepard, and J Hone. Boron nitride substrates for high-quality graphene electronics. *Nature Nanotechnology*, 5(August):0–4, 2010.

[72] Sukang Bae, Hyeongkeun Kim, Youngbin Lee, Xiangfan Xu, Jae-sung Park, Yi Zheng, Jayakumar Balakrishnan, Tian Lei, Hye Ri Kim, Young Il Song, Young-jin Kim, and Kwang S Kim. Roll-to-roll production of 30-inch graphene films for transparent electrodes. *Nature Nanotechnology*, 5(June):1–5, 2010.

2 Experimental techniques

In this chapter, a description of the experimental techniques employed in the different projects involved in the course of the thesis will be presented.

2.1 Sample preparation

The sample preparation methods from its bulk state to nanosheets and the transfer mechanisms to develop different devices will be described in this section.

2.1.1 Micromechanical exfoliation

In 2004, A. Geim and K. Novoselov [322] obtained for the first time via micromechanical exfoliation graphene nanosheets using a simple and, even today, one of the more effective techniques to obtain thin films up to MLs of exfoliable materials, obtaining high-quality nanosheets which conserve a defined and homogeneus crystalographic orientation. It is a top-down technique that exploits the laminar structure of the volumic material to be exfoliated and the difference in the strength between the weak interlayer van der Waals (vdW) bonds and the strong intralayer covalent bonds. By using this technique, a freshly cleaved bulk layered crystal is deposited on a scotch or adhesive tape and is gently peeled off several times in the tape, being folded repeatedly against itself. Due to the weaker vdW interlayer bonds, in each exfoliation the peeled off material separated from the bulk source will be thinner, obtaining eventually up to MLs of the original material. The more times the material is exfoliated, the nanosheets obtained will be thinner, at the cost of losing superficial size of the final nanosheets, so a compromise between this two effects is what is sought.

There is not a receipt for the ideal amount of times or pressure to apply in every exfoliation, it depends on the material exfoliated. Blue Nitto Tape has been used in

order to reduce as possible the amount of remaining adhesive residues in the final nanosheets exfoliated. Finally, once the material has been exfoliated on the tape, the last exfoliation will be performed between the tape and the target substrate to randomly transfer or re-exfoliate the nanosheets from the tape to the substrate.

Depending on the material, heating the target substrate during contact with the tape enhance the ratio of thinner nanosheets attached. A description of this process can be seen in Figure 2.1.

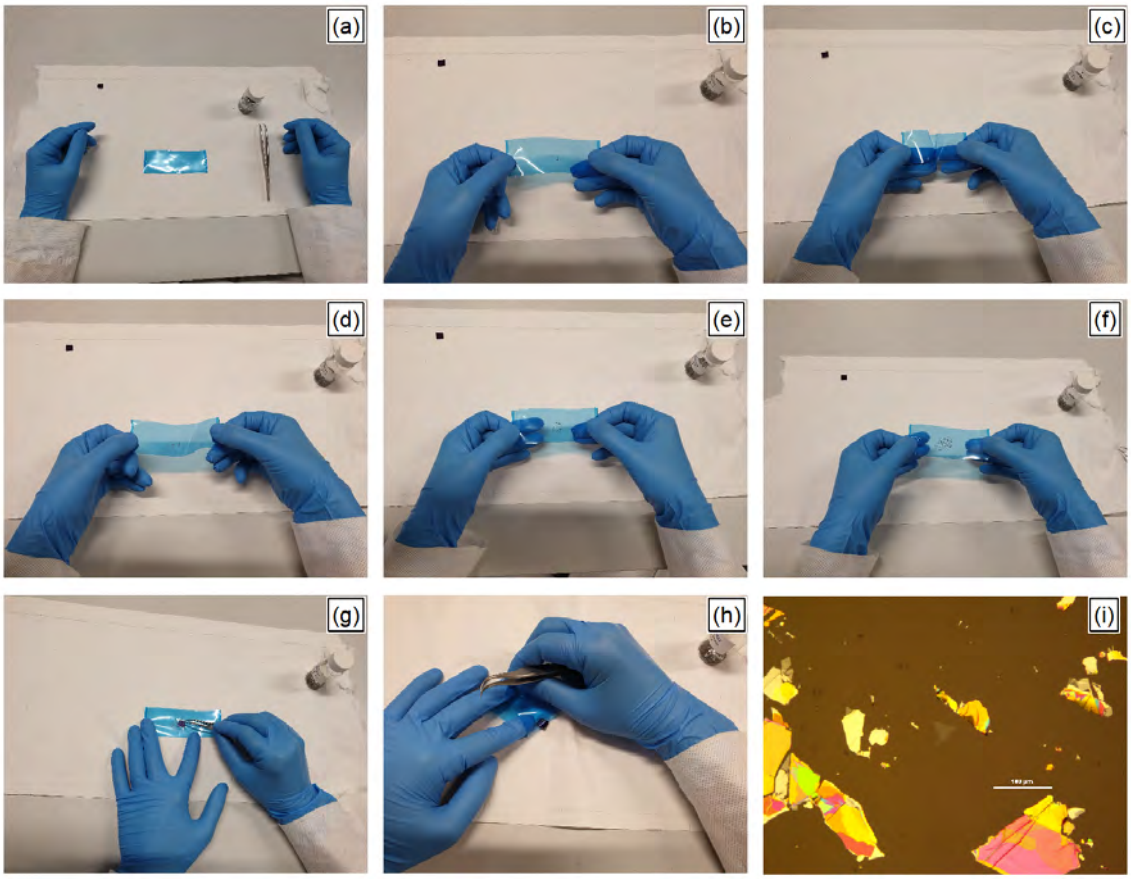

Figure 2.1: Micromechanical exfoliation: description from the bulk material to the nanosheets obtained in the target substrate.

This technique has been employed for the preparation of every material studied in this thesis (see Appendix A). Usually these steps have been performed in air, but depending the application it has been done in an Argon (Ar) enviroment in a glovebox to prevent sample degradation due to its interaction with to O_2 and H_2O in air.

2.1.2 Substrate preparation

Before the exfoliation of the material to be prepared, the target substrate must be chosen according to the specific application or study to be pursued. The substrate on which a 2D material is deposited greatly determines its properties given its surface-to-volume ratio [101, 349, 100, 98], so it can be used to enhance or hamper the desired future measurements. In this thesis, the most used substrates have been the following:

- Polydimethylsiloxane (PDMS) stamps: this substrate has been selected for its viscoelastic behavior and transparence, that makes it suitable for deterministic transfer techniques (see subsection 2.1.3.1). The PDMS stamp used in this thesis has been purchased from Gelpak (usually Gelfilm 4, since in this one better samples were obtained). The preparation consist, first, on cleaning a glass microscope slide in four x three steps: Thorlabs lens tissue cleaning with the solvent, ultrasonic 7 min bath in a solvent, air pump cleaning and 10 min heating at 130 °C, using, in this order, ethanol, acetone and isopropanol as solvents. After that, the desired stamp (usually, around 6 x 6 mm) is cut from the source polimer and, after detaching its two-sided plastic protection, transfer it to the cleaned glass slide.
- Silicon/Silicon Oxide (Si/SiO_2) substrates: if the exfoliated sample is going to be directly studied and does not need a specific deterministic transfer, usually the most employed substrate has been Si/SiO_2, with different SiO_2 thicknesses (90, 110, 285, 300 and 500 nm, in this thesis) considering its effect on the properties to be studied [87]. The preparation of these substrates starts with the wafer (purchased from Epak), from where they were cut using a diamond cutter (usually, 6 x 6 mm, but deppends on the application) from the Si side. After that, a similar cleaning procedure to that used in the previous glass microscope slides (four x three steps: Thorlabs lens tissue cleaning with the solvent, ultrasonic 7 min bath in a solvent, air pump cleaning and 10 min heating at 130 °C, using, in this order, ethanol, acetone and isopropanol as solvents) is needed before its usage.

Other substrates have been used as a direct target substrate after the micromechanical exfoliation, with similar preparation method as described before, such as:

- SiO_2 substrates for transmission measurements (Chapter 7).

- Indium Tin Oxide (ITO) substrates for Kelvin-Probe Force Microscopy (KPFM) measurements (Chapter 3).

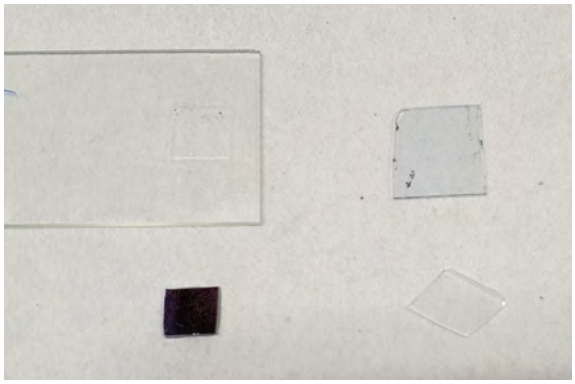

Figure 2.2: Substrates used through the thesis. From upper left to bottom right, PDMS stamp on glass slide, ITO, Si/SiO_2 (285nm) and SiO_2.

2.1.3 Deterministic transfer of two-dimensional nanosheets

In some projects, it is desired a deterministic transfer of the nanosheets exfoliated. The ability to transfer a nanosheet in any substrate with a micrometric precision allow the engineering of devices with different materials. As examples of the potential of these techniques, in this thesis they have been used to:

- Perform vertical heterostructures, stacking different nanosheets (Chapter 5 and Chapter 8).
- Their usage in precise treated substrate locations, such as:
  - Previously lithographed electrical contacts on a substrate (Chapter 3).
  - Optical waveguides patterned on a substrate (Chapter 6).
  - The core of a fibre (Chapter 7).

The next subsections describe the two techniques that allow this deterministic control on the nanosheets previously prepared.

2.1.3.1 All-dry viscoelastic transfer

Based on the technique described in [81] it is possible to control the position and orientation of a previously prepared nanosheet using a setup similar to that described in Figure 2.3.

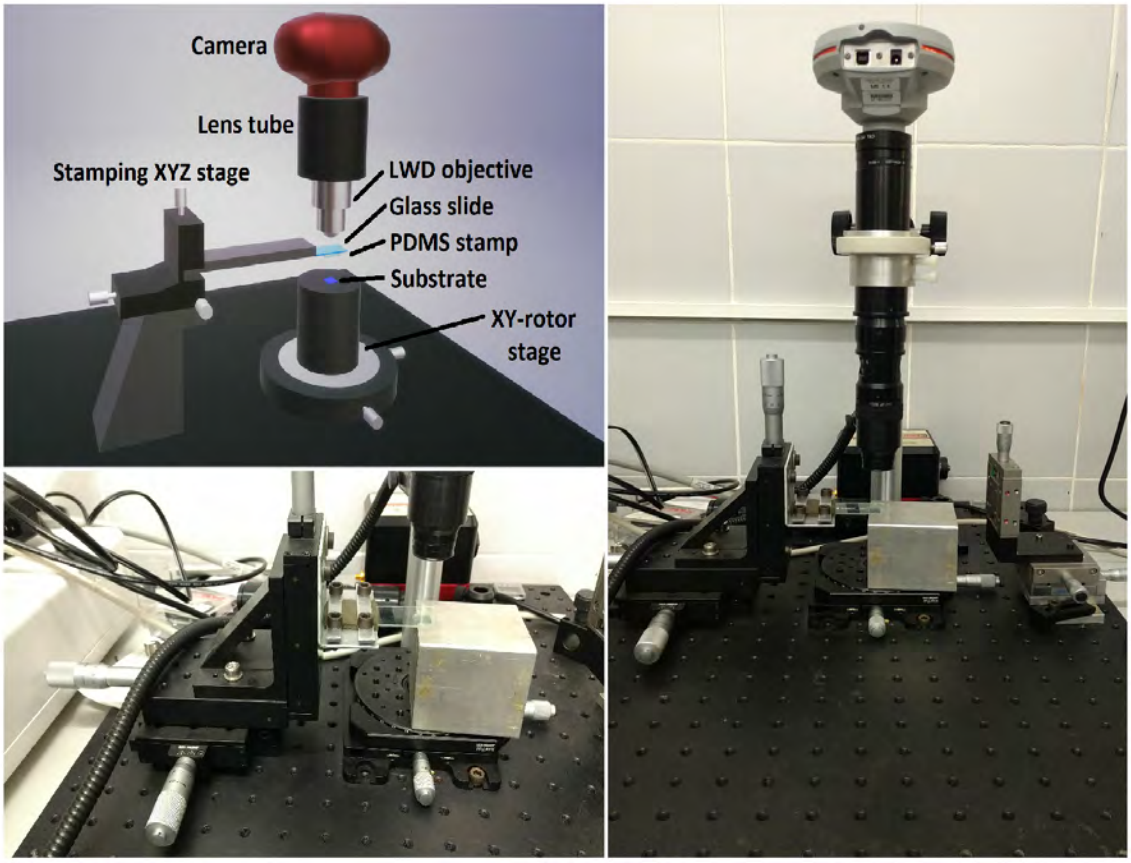

Figure 2.3: Setup for deterministic transfer of nanosheets. On the top left, schematic diagram of the main elements. On the right and bottom left, picture of the setup employed.

For that, the nanosheet must be exfoliated from the tape to a PDMS stamp, as described in previous lines and located via optical microscopy (Subsection 2.2.1). Facing down the nanosheet, the microscope slide is attached to a XYZ micromanipulator, so the nanosheet to be transfered can be located using the microscope above. Then, the target substrate is placed on a second micromanipulator (XY - rotor in the setup used) with a holder and attached (double-side tape or using vacuum through a hole underneath).

Due to the fact that both the glass slide and the PDMS stamp are transparent, it is possible to use the microscope above to focus down to the target substrate in order to align the precise position where the nanosheet is wanted to be transferred. Once they are aligned, the PDMS stamp micromanipulator is pressed down to get closer the nanosheet and the substrate. The microscope can change its vertical focus from the nanosheet to the target substrate and back during the approaching process

as needed, always keeping nanosheet and target location on the substrate aligned. Finally, the stamp with the nanosheet is pressed against the target substrate, which can be observed with a change in the optical contrast in the areas in contact. Once the nanosheet is in contact in the location desired, the stamp is peeled off gently using the PDMS stamp micromanipulator, being the nanosheet attached to the target substrate, detaching itself from the previous PDMS stamp. Pictures during the process can be seen in Figure 2.4.

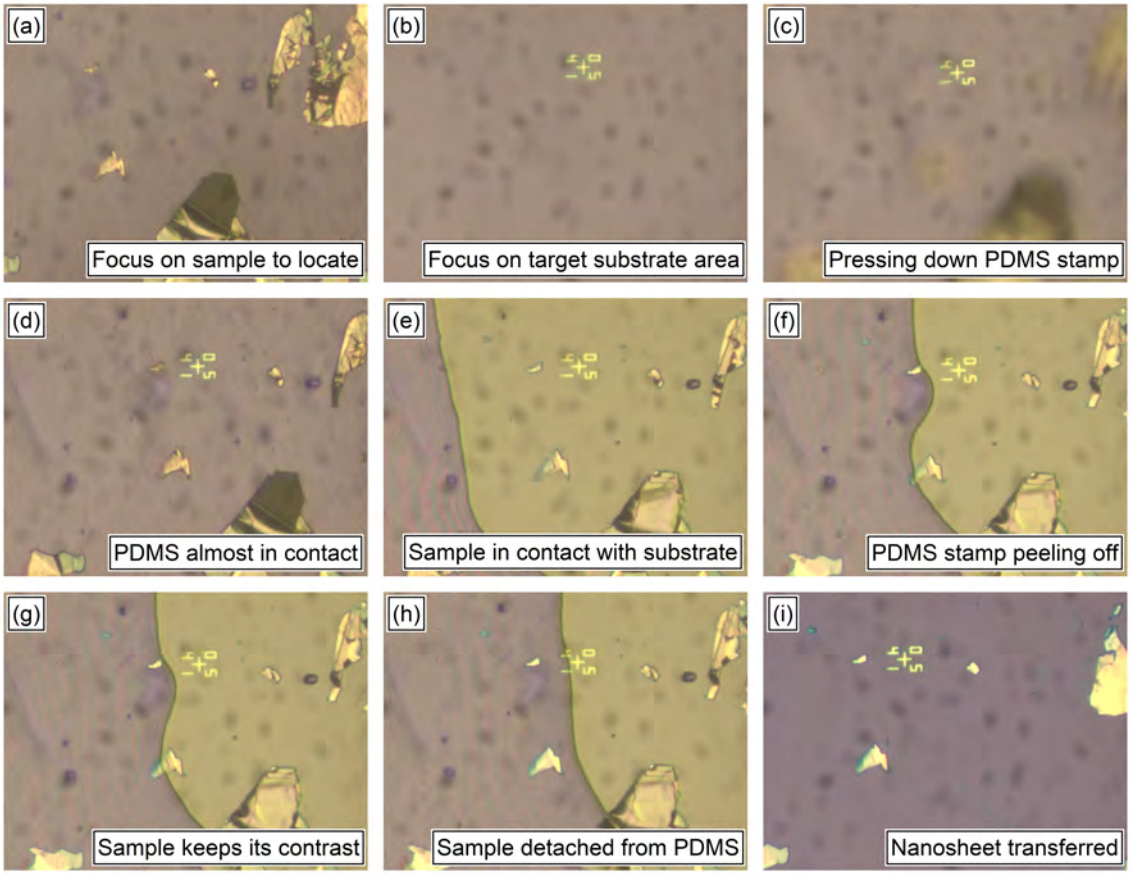

Figure 2.4: Pictures of the process transferring a nanosheet on a substrate.

Besides the XYZ position of the nanosheet and the XY position and orientation of the target substrate (using the micromanipulators), the tilt between the nanosheet and the substrate has huge impact on the transfer, which can be controlled adding a tilt stage on the XYZ stamp micromanipulator before the glass slide.

The ability to control which area of the PDMS stamp will touch the substrate first (and therefore, in the lift off process, will be the last area attached to the substrate) is

critical for some samples, due to the morphology of the nanosheets to be transferred or the appearance of air bubbles during the contact. Usually, in the lift off process, it is desired to detach first thicker samples, which use to drag thinner ones instead of the opposite, where the nanosheet can be broken or the thinner area re-attached to the PDMS. Besides, the amount of tilt will control the speed of contact. Finally, for some materials, a heater under the target substrate during the lift off can modify the viscosity of the PDMS, improving the transfer process.

It is the fastest and the highest transfer rate technique compared with other transfer techniques like the hot pick-up transfer (Subsection 2.1.3.2) or the wet transfer technique [86]. However, the top surface of the nanosheet transferred will have always been in contact with the PDMS, leaving possible residues if another nanosheet is transferred above (producing lower quality surfaces contact).

2.1.3.2 Hot pick-up transfer

This technique is described in [90]. If what was intended in the all-dry technique was to transfer a nanosheet from the PDMS stamp to the target substrate, in the hot pick-up transfer what is sought is the detaching of nanosheets from a substrate to a stamp. To do so, on the PDMS stamp can be attached a smaller 1 x 1 mm Polypropylene carbonate (PPC), due to the fact that this polymer has a glass-to-liquid temperature around 40 - 65 °C. Therefore, in contact with the nanosheet to detach from the substrate, it can be heated up, reaching its glass state, embracing the nanosheet. Then, cooling down to RT the polymer would solidify, being able to substract the nanosheet from the original substrate.

This process can be done as many times as nanosheets are needed, starting with the top one to, finally, deposit the whole stack of nanosheets detached from independent substrates to a final target substrate. With this technique, only the top surface of the top layer will be in contact with the polymer, leaving the remaining lattices cleaner, only having being in contact with the original substrate on one side (i.e., being clean as the substrate has been previously cleaned) and air on the other (the nanosheet can be exfoliated and stacked in an Ar enviroment, avoiding deterioration). This is, therefore, the best technique for vertical heterostructures where the interlattices between the nanosheets is sought to be the cleanest.

Hot pick-up transfer setup from the Institute of Photonics and Quantum Sciences (IPaQS) of the Heriot-Watt University (Edinburgh, United Kingdom) has been used

in Chapter 8, aiming for the cleanest interlayers possible for, among others, the detection of single-phonon emitters at low temperature (LT). The steps used in these heterostructures have been the following:

- Heat-up the substrate with the nanosheet to be picked-up at 110°C.
- Make contact between PPC and the nanosheet at that temperature. PPC becames fluid.
- Cool down the attached substrate - nanosheet - PPC structure until RT.
- Lift up the stack from the substrate, the nanosheet is snatched up.
- Repeat steps for each nanosheet. When two nanosheets are in contact, anneal at 110°C for 5 min to enhance its bonding.
- To release the whole stack, make contact with the target substrate, heat up at 110°C, anneal for 10 min and lift up.

Pictures of these steps can be watched in Figure 2.5, where a WSe_2 ML has been encapsulated between two MoO_3 nanosheets.

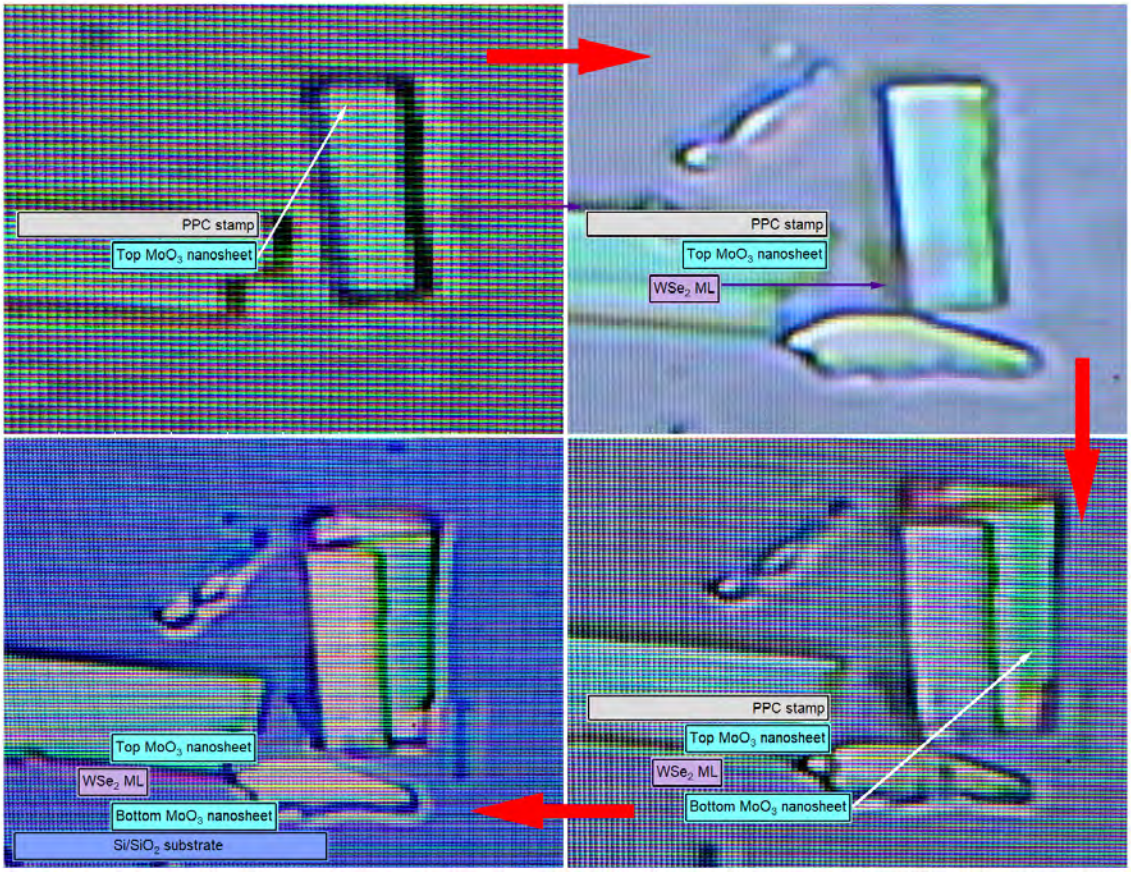

Figure 2.5: Hot pick-up transfer steps: pictures of the nanosheets lifted up and, finally, transferred on a substrate.

2.2 Optical characterisation

In this section, the optical characterisation techniques employed in the previously prepared samples and devices will be described.

2.2.1 Optical microscopy

The next step after the preparation of nanosheets in any substrate described before is its identification. The determination of the location and thickness of thin nanosheets is possible due to the natural optical contrast (OC) between the nanosheets and the substrate [322]. A change in the light phase through the nanosheet and the reflectivity variation between the substrate and the structure substrate/nanosheet

allow a reliable and fast thickness caracterisation method, as reported for graphene [83, 82], TMDs [89], hBN [80, 84] or III-VI semiconductors [87, 133, 208].

OC can be experimentally calculated using the optical microscopy pictures as

$$OC = \frac{R_{substrate} - R_{nanosheet}}{R_{substrate}}$$

being $R_{nanosheet}$ and $R_{substrate}$ the nanosheet/substrate structure and substrate reflectance, respectively.

The usage of band-pass filters capturing the pictures or the collection of the reflected light through a spectrometer improves this technique adding a wavelength dependance. It is usual when spectras are analysed to define the differential reflectivity (DR) as

$$DR = \frac{R_{nanosheet} - R_{substrate}}{R_{nanosheet}}$$

since improves the visualisation of the nanosheet absorption effect compared with OC [76].

Three different setups have been used to obtain OC or DR through the next chapters:

- A Nikon Eclipse LV150A optical microscope equipped with a Nikon DS-FI2 high-definition color camera (transmittance Red - Green - Blue (RGB) channels in Figure 2.6 for OC calculations in Chapter 3) for image acquisition from the laboratory ESA-VSC Consortium with different band-pass filters centred at visible wavelengths were used with full width at half maximums (FWHMs) of ~40 nm (Figure 2.6).
- A Zeiss Axio Scope.A1 microscope with an Axiocam ERc 5s camera.
- A Mightex white source with a 0.5 m focal length spectrometer and a nitrogen-cooled charge-coupled device with a measured spectral resolution of ~75 μeV at λ = 750 nm for an 1800 lines/mm grating in the Institute of Photonics and Quantum Sciences (IPaQS) of the Heriot-Watt University (Edinburgh, United Kingdom) for DR measurements in Chapters 7 and 8.

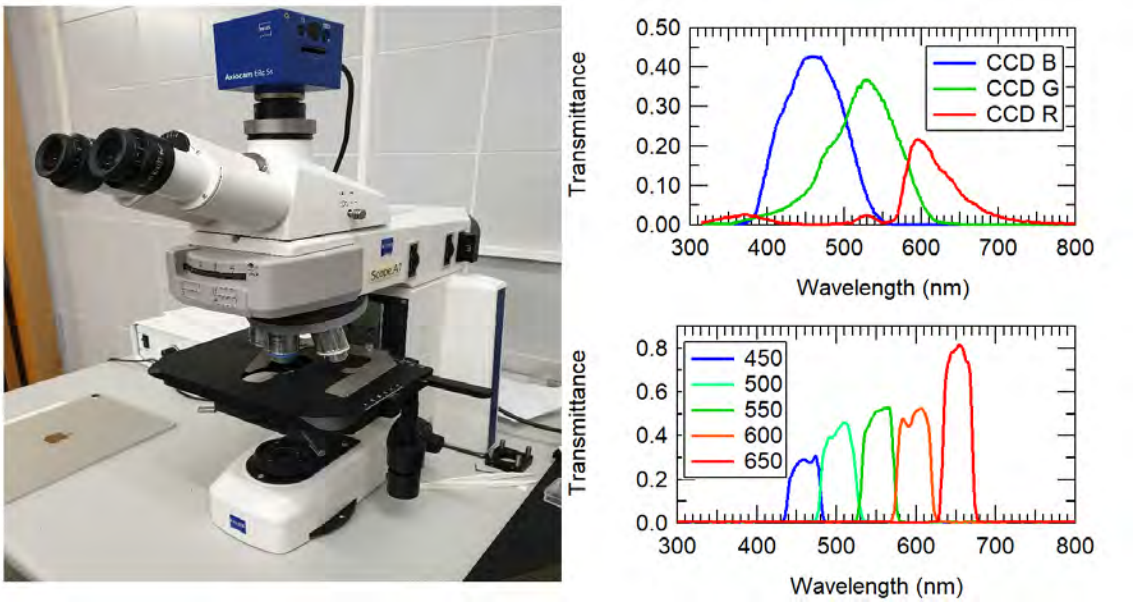

Figure 2.6: On the left, Zeiss microscope, generally used for the optical identification of the nanosheets exfoliated. On the right, charged-coupled device (CCD) channels (up) and band-pass filters (bottom) transmittances on the camera used for OC measurements.

OC has been used in every sample in this thesis in order to obtain its location and identification as ML, bilayer (BL), trilayer (TL) or thin nanosheets prior to its usage or further characterisation through other techniques. Specifically, OC has been analysed in Chapter 3 and Chapter 7, and DR in Chapter 7 and Chapter 8.

2.2.2 Transmission measurements

Transmission measurements have been used to study the light absorption in 2D materials. SiO_2 substrates, an Ocean Optics DH-2000 UV-VIS-NIR Lightsource, an Ocean Optics RedTide USB650 spectrometer and a Thorlabs camera for sample location in the first measurements and optical fibres optimised for 980 nm, a near IR source and an Optical Spectrum Analyser (OSA) lastly have been used in Chapter 7.

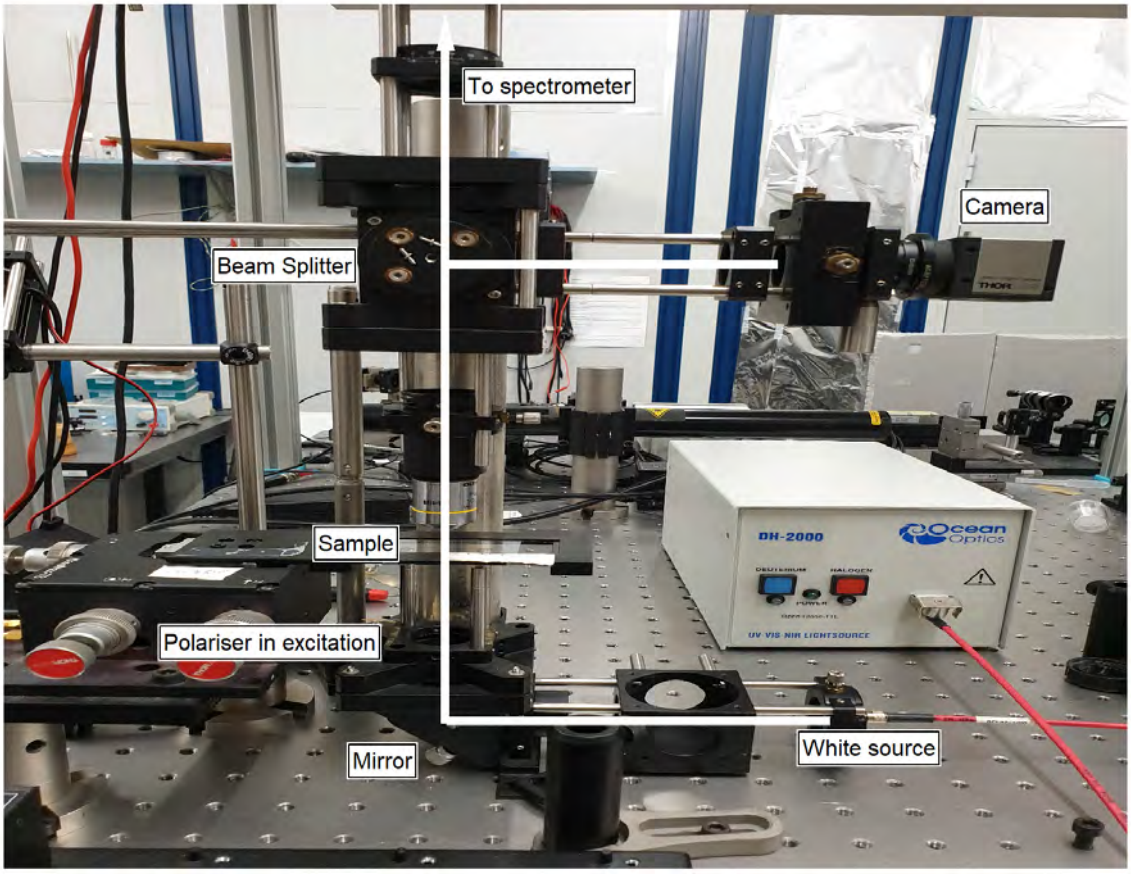

Figure 2.7: Transmission setup elements used in Chapter 7 to obtain the transmittance in Bi_2S_3 nanosheets.

2.2.3 Photoluminescence

Photoluminescence (PL) envolves any light emission process from any form of material produced after an incident radiation absorbed (hence the prefix *photo*, due to the photons exciting electrons to a higher energy level in a material). After the photoexcitation, relaxation processes involving the electrons and the holes in the material excited occur, where other photons of a different energy are radiated. The PL setups used through this thesis are described in the following lines:

- A Horiba Scientific Xplora μ-Raman system with 532 nm laser excitation from the Servei Central de Suport a la Investigació Experimental (SCSIE) in the University of Valencia have been utilised through many Chapters (3, 4, 5, 6, 7), either as a proper study technique or for the characterisation of TMDs or III-VIs thichness prior to their transfer for a future application. The excitation

optical beams were focused on the sample with a ~1μm^2 spot surface, with a power not exceeding 100μW to prevent overheating (Figure 2.8a).

- In Chapter 6 a multioriented PL in fibre setup have been employed, using a 532 nm and He-Ne (633 nm) excitation source and an Ocean Optics RedTide USB650 spectrometer. In this setup, in the horizontal direction the whole waveguide section have been excited/collected, and a ~200μm^2 collection and excitation vertical spot to cover the sample have been used (Figure 2.8b).
- In Chapter 8 a LT confocal μ-PL setup from the Institute of Photonics and Quantum Sciences (IPaQS) in the Heriot-Watt University, using a 532 nm Cobalt excitation with an objective lens (Numerical aperture (NA) of 0.82 yielding a diffraction limited focus of ~560 nm at λ = 750 nm) is used to spatially map the PL from the samples placed on automated nanopositioners in a T = 3.5 K closed-cycle cryostat. All spectra were acquired with a 0.5 m focal length spectrometer and a nitrogen-cooled charge-coupled device with a measured spectral resolution of ~75 μeV at λ = 750 nm for an 1800 lines/mm grating (Figure 2.8c).

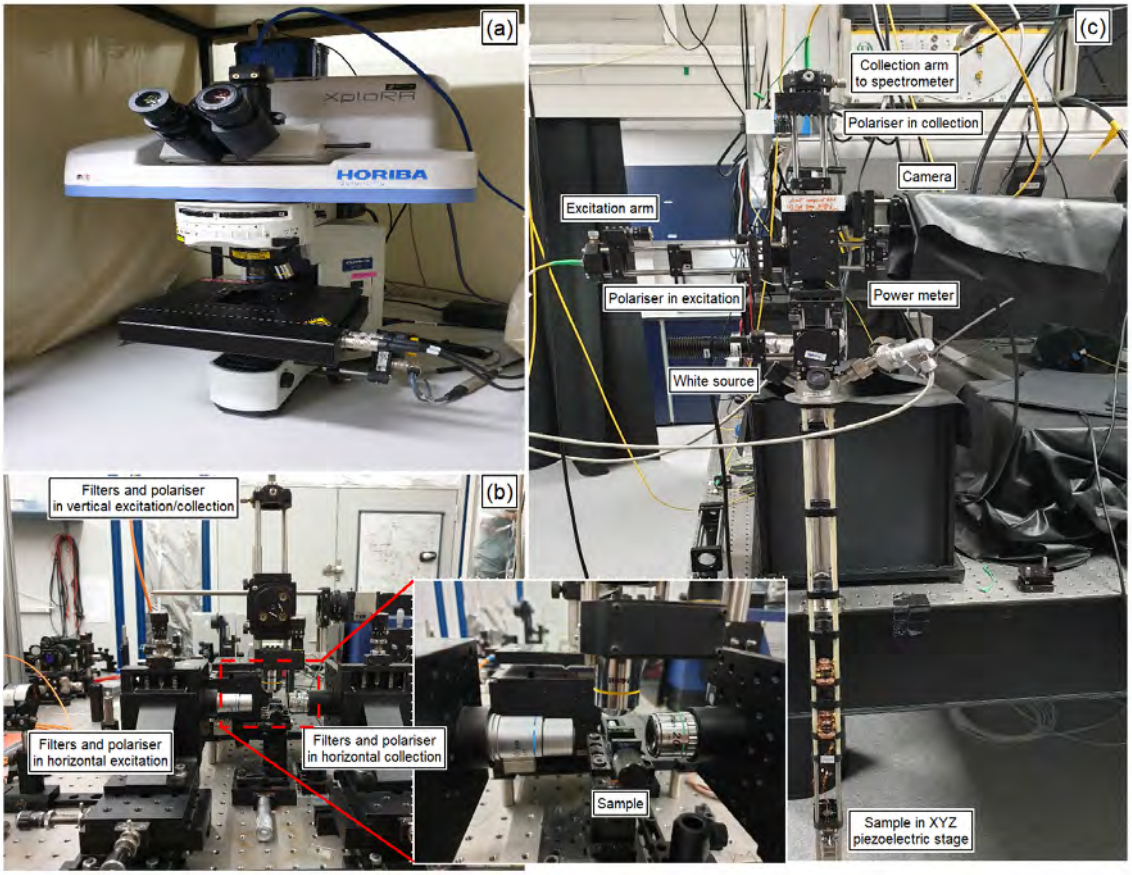

Figure 2.8: PL setups. Horiba Scientific Xplora μ-Raman system in the top - left (a), multi-oriented waveguide optical setup in the bottom - left (b) and hand-made LT confocal μ-PL setup on the right (c).

2.2.4 Raman spectroscopy

Raman spectroscopy is an spectroscopical technique used in several fields to study the low frequency modes in matter such as vibrational and rotational among others. It is based in inelastic dispersion phenomenoms, or Raman dispersion, in monocromatic light, generally a visible range laser, near infrared or near ultraviolet.

During this thesis it has been used in Chapter 7 in a Horiba Scientific Xplora μ-Raman system with 532 nm laser excitation, same setup used for PL in Subsection 2.2.3 (Figure 2.8a). The excitation optical beams were focused on the sample with a ~1μm^2 spot surface, with a power not exceeding 100μW to prevent overheating.

2.3 Electrical characterisation

The techniques employed through this thesis aiming to the study of the electrical properties of the materials addressed will be presented in this section.

2.3.1 I-V characterisation

The electrical behavior of a material can be determined studying the relation between the voltage and the current in which a material is exposed in different conditions. Even more, its behavior with and without a light excitation is relevant to this study as a photodetector.

In Chapter 3, a Keithley multimeter has been used to obtain the current - voltage (I - V) characteristics to measure the photocurrent generated using as contacts Au microgaps deposited via Karl Süss KG microplotter by Dr. Alberto Maulu and lithographied gold contacts on the nanosheets by Dr. Josep Canet-Ferrer using a white light source from Schott - Fostec. Finally, a confocal μ-PL setup (similar to the setup in Figure 2.8c) with a ~1μm^2 spot 405 nm laser have been used as excitation source, as seen in Figure 2.9, to measure the photocurrent generated in a previously deposited InSe staggered nanosheet.

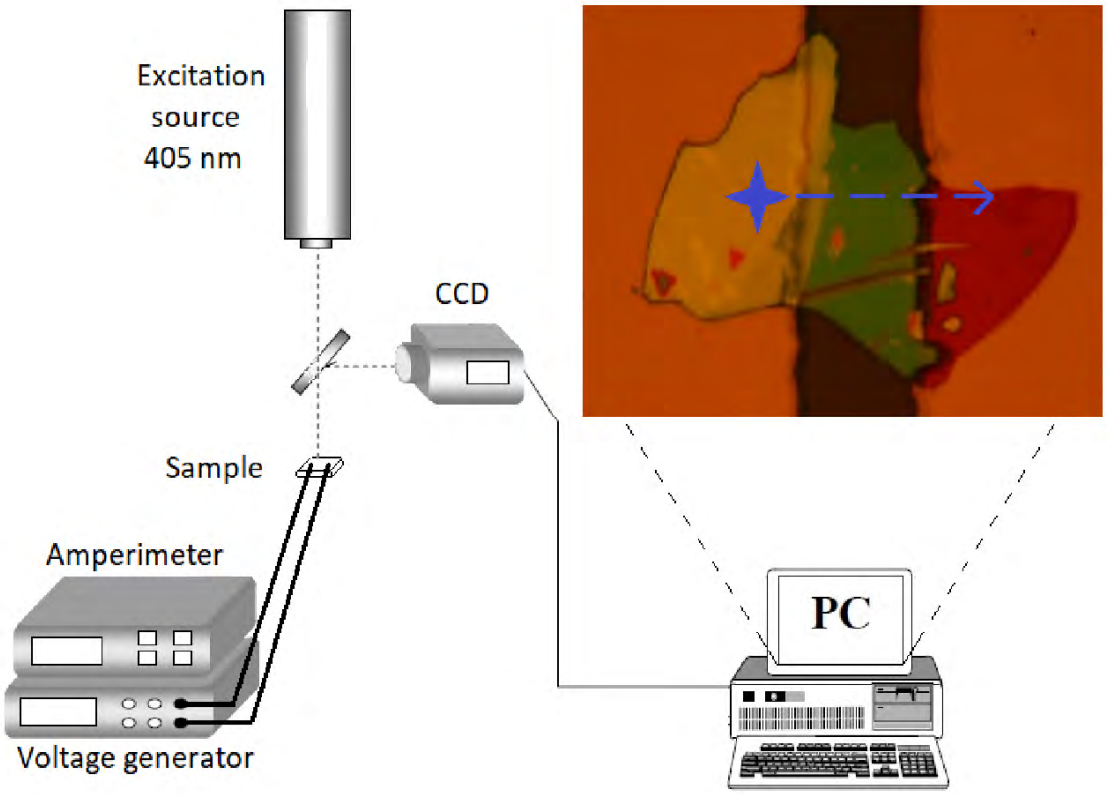

Figure 2.9: Confocal μ-PL setup used as excitation source for I - V characterisation.

2.3.2 Atomic Force Microscopy and Kelvin-Probe Microscopy

Even though OC, PL or Raman spectroscopy are techniques to characterise indirectly the nanosheets thicknesses, it can be directly measured via Atomic Force Microscopy (AFM). In order to understand its functioning, the elements which compose an AFM will be described in Figure 2.10.

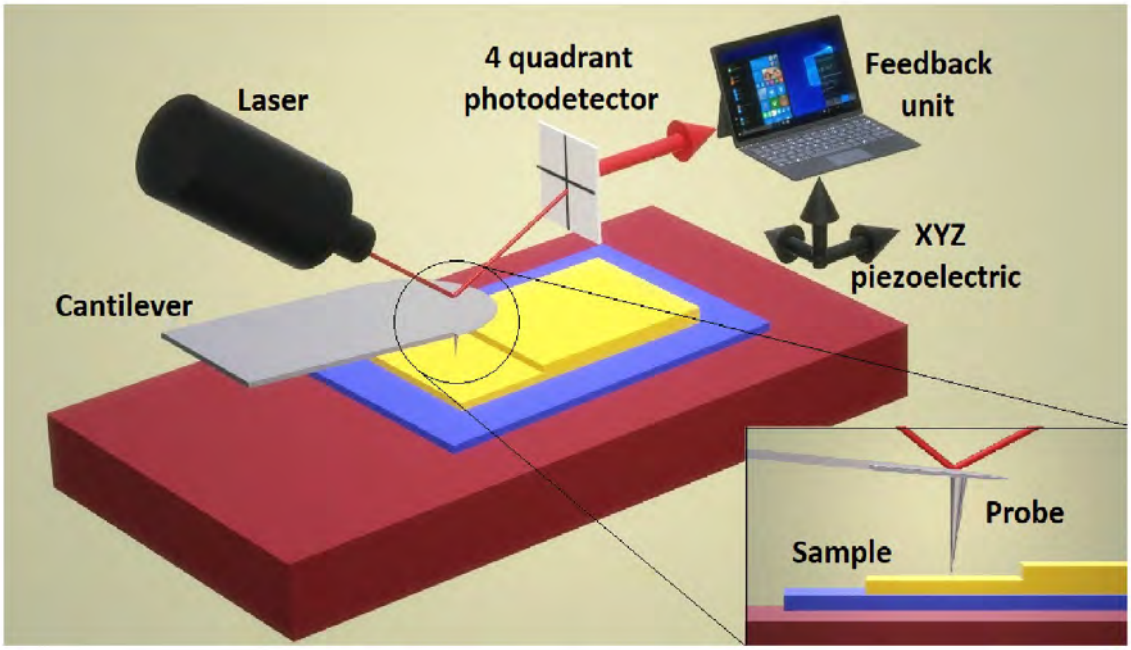

Figure 2.10: Schematic of the main elements in a AFM [88, 85, 75].

- Probe: it is a tip, Si in the setup used, that will go through the sample, separated a few nanometers away, and which will be affected by the electrostatic forces of the material, so that forces will appear on this tip depending on the proximity to the sample.
- Cantilever: it is a flexible lever that holds the tip, and due to the forces that appear on the tip, it flexes. It has a mirror that reflects the light that comes from a fixed laser, reaching a four-quadrant photodetector.
- Four-quadrant photodetector: the laser is reflected in the cantilever, initially detected in the center of the quadrants (it should be previously calibrated to be so). However, by changing the measuring point, the force can change by changing the distance to the nanosheet, and therefore the orientation of the cantilever mirror will change, which will reflect the laser to a different point from the center, detected by the photodetector.
- Data processing unit: this component will take the data given by the four-quadrant photodetector, applying a voltage to the piezoelectric that control the position of the sample so that the reflected laser beam returns to the center of the quadrants.
- Piezoelectrics: due to the small voltages they receive, these piezoelectrics

(three, one in each spatial direction) will move the sample. It should be noted the high nanometric precision of these movements, necessary for these measures. The piezoelectrics X and Y will sample the entire area to be studied while the piezoelectric Z will move in such a way that the reflected laser beam remains in the center. Therefore, by measuring how the sample is moved using the piezoelectric Z, the thickness of the sample would be characterised.

An AFM from Nanotec in contact mode will be used to obtain a nanometric precision thicknesses in Chapter 3 and Chapter 7.

Due to the conductance of the usual Si probes (usually metal-coated for this technique), and using a conductor substrate, it is possible to measure the current through a nanosheet applying a controlled voltage using substrate and probe as contacts. Kelvin-Probe Force Microscopy (KPFM) allow the study of the electrical properties in the nanosheets with the nanometrical precission of an AFM. The cantilever forms a capacitor with the surface which, when scanning the sample, opposite to usual AFM technique, is not piezoelectrically driven at its mechanical resting position although an alternating current (AC) voltage is applied, which will cause the cantilever to vibrate. A direct-current (DC) potential difference between the probe and the surface will be applied in order to minimise the frequency of vibration for every point scanned, obtaining a contact potential difference (V_{CPD}) map (Figure 2.11). V_{CPD} will be related with the work function of the materials in contact as

$$V_{CPD} = \phi_{probe} - \phi_{contact}$$

where ϕ_{probe} and $\phi_{contact}$ is the work function of the probe and the contact point, respectively. In order to characterise ϕ_{probe}, the reported substrate work function (ITO, [191, 193, 192]) has been employed, as

$$\phi_{probe} = V_{CPD(ITO)} + \phi_{ITO}$$

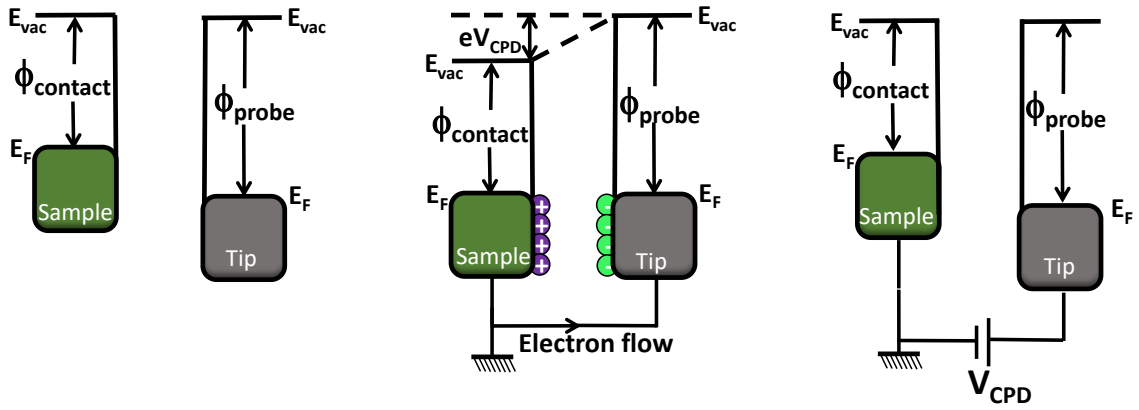

Figure 2.11: Electrical band alignment in a contact in KPFM.

This technique has been employed in Chapter 3 using the same Nanotec AFM setup as before. The data measured by KPFM has been analysed in collaboration with Dra. Ana Cros-Stotter.

2.3.3 X-ray photoelectron spectroscopy

X-ray photoelectron spectroscopy (XPS) is a technique which allow the study of the chemical composition and the atomic electronic states (therefore, the bonding state between the composing atoms) in the superficial layers of a sample. By measuring the kinetic energy and the number of electrons emitted by the sample when irradiated by X-rays, it can be obtained the bonding energy of the atoms excited.

In Chapter 3, XPS measurements have been performed in a Thermo VG Scientific ESCALAB-210 ultrahigh vacuum system (base pressure 10^{-10} mbar). The Mg K_α line (1253.6 eV) has been used as excitation source and the measurements have been taken over an area of 1 mm^2 of the Si/SiO_2 substrate on which nanoflakes were exfoliated. The C 1s peak (fixed to 285 eV) has been used as the binding energy reference.

2.4 Other techniques

2.4.1 Ellipsometry

Ellipsometry is an optical technique which allows the study of the dielectric properties (such as refractive indexes, absorption...) of thin films with a micrometric spacial resolution. It is based in reflectivity measurements and comparing the detected light (r_p) and the emitted (r_s), different properties like its composition, thickness, roughness, crystalline nature... can be obtained when the data is compared with a model.

In the configuration used, three different angles of incidence (AOI) have been measured to characterise the refractive indexes in the three XYZ directions in exfoliated nanosheets, through the analysis of the amplitude ratio upon reflection ($\tan\Psi$) and the phase shift (Δ), which depend on the reflectivity data measured as

$$\rho = \frac{r_p}{r_s} = \tan\Psi\, e^{i\Delta}$$

The ellipsometry measurements have been performed in the Institute of Photonics and Quantum Sciences (IPaQS) of the Heriot-Watt University (Edinburgh, United Kingdom) in an ellipsometer from Accurion in a Jacomex Glovebox. The model used in Chapter 8 to obtain the refractive indexes has been analysed and compared with the experimental data in collaboration with Dr. Mauro Brotons-Gisbert.

2.4.2 X-Ray Diffraction

X-Ray Diffraction (XRD) is a method to determine the atomic and molecular structure of a crystal using an incident X-Ray emission, which will diffract into specific directions. By measuring these angles and intensities, the crystallographic orientation of the atoms can be obtained.

The measurements and the analysis of the data to characterise the a and b cristallographic orientations on a bulk material has been performed in collaboration with Dra. María del Carmen Martínez Tomás in Chapter 7.

Bibliography

[73] K.S. Novoselov, A.K. Geim, S.V. Morozov, D. Jiang, Y. Zhang, S.V. Dubonos, I.V. Grigorieva, and A.A. Firsov. Electric Field Effect in Atomically Thin Carbon Films. *Science Reports*, 306(October):666–670, 2004.

[74] Chenhao Jin, Jonghwan Kim, Joonki Suh, Zhiwen Shi, Bin Chen, Xi Fan, Matthew Kam, Kenji Watanabe, Takashi Taniguchi, Sefaattin Tongay, Alex Zettl, Junqiao Wu, and Feng Wang. Interlayer electron-phonon coupling in WSe2/hBN heterostructures. *Nature Physics*, 13(2):127–131, 2017.

[75] N. J. Lee, J. W. Yoo, Y. J. Choi, C. J. Kang, D. Y. Jeon, D. C. Kim, S. Seo, and H. J. Chung. The interlayer screening effect of graphene sheets investigated by Kelvin probe force microscopy. *Applied Physics Letters*, 95(22), 2009.

[76] Yue Niu, Sergio Gonzalez-Abad, Riccardo Frisenda, Philipp Marauhn, Matthias Drüppel, Patricia Gant, Robert Schmidt, Najme Taghavi, David Barcons, Aday Molina-Mendoza, Steffen de Vasconcellos, Rudolf Bratschitsch, David Perez De Lara, Michael Rohlfing, and Andres Castellanos-Gomez. Thickness-Dependent Differential Reflectance Spectra of Monolayer and Few-Layer MoS2, MoSe2, WS2 and WSe2. *Nanomaterials*, 8(9):725, 2018.

[77] L. C. Gomes, S. S. Alexandre, H. Chacham, and R. W. Nunes. Stability of edges and extended defects on boron nitride and graphene monolayers: The role of chemical environment. *Journal of Physical Chemistry C*, 117(22):11770–11779, 2013.

[78] M. Brotons-Gisbert, J. F. Sánchez-Royo, and J. P. Martínez-Pastor. Thickness identification of atomically thin InSe nanoflakes on SiO2/Si substrates by optical contrast analysis. *Applied Surface Science*, 354:453–458, 2015.

[79] Ying ying Wang, Zhen hua Ni, Ting Yu, Ze Xiang Shen, Hao min Wang, Yi hong Wu, Wei Chen, and Andrew Thye Shen Wee. Raman Studies of Monolayer Graphene: The Substrate Effect. *Journal of Physical Chemistry C*, 112(29):10637–10640, 2008.

[80] Marie Krečmarová, Daniel Andres-Penares, Ladislav Fekete, Petr Ashcheulov, Alejandro Molina-Sánchez, Rodolfo Canet-Albiach, Ivan Gregora, Vincent Mortet, Juan P. Martínez-Pastor, and Juan F. Sánchez-Royo. Optical Contrast and Raman Spectroscopy Techniques Applied to Few-Layer 2D Hexagonal Boron Nitride. *Nanomaterials*, 9(7):1047, 2019.

[81] Andres Castellanos-Gomez, Michele Buscema, Rianda Molenaar, Vibhor Singh, Laurens Janssen, Herre S.J. Van Der Zant, and Gary A. Steele. Deterministic transfer of two-dimensional materials by all-dry viscoelastic stamping. *2D Materials*, 1(1), 2014.

[82] Inhwa Jung, Matthew Pelton, Richard Piner, Dmitriy A. Dikin, Sasha Stankovich, Supinda Watcharotone, Martina Hausner, and Rodney S. Ruoff. Simple approach for high-contrast optical imaging and characterization of graphene-based sheets. *Nano Letters*, 7(12):3569–3575, 2007.

[83] P. Blake, E. W. Hill, A. H. Castro Neto, K. S. Novoselov, D. Jiang, R. Yang, T. J. Booth, and A. K. Geim. Making graphene visible. *Applied Physics Letters*, 91(6), 2007.

[84] Dheeraj Golla, Kanokporn Chattrakun, Kenji Watanabe, Takashi Taniguchi, Brian J. Leroy, and Arvinder Sandhu. Optical thickness determination of hexagonal boron nitride flakes. *Applied Physics Letters*, 102(16):2011–2014, 2013.

[85] Ulrich Zerweck, Christian Loppacher, Tobias Otto, Stefan Grafström, and Lukas M. Eng. Accuracy and resolution limits of Kelvin probe force microscopy. *Physical Review B - Condensed Matter and Materials Physics*, 71(12):1–9, 2005.

[86] Ji Won Suk, Alexander Kitt, Carl W. Magnuson, Yufeng Hao, Samir Ahmed, Jinho An, Anna K. Swan, Bennett B. Goldberg, and Rodney S. Ruoff. Transfer of CVD-grown monolayer graphene onto arbitrary substrates. *ACS Nano*, 5(9):6916–6924, 2011.

[87] M Brotons-Gisbert, D Andres-Penares, J P Martínez-Pastor, A Cros, and J F Sánchez-Royo. Optical contrast of 2D InSe on SiO2/Si and transparent substrates using bandpass filters. *Nanotechnology*, 28(11), 2017.

[88] Wilhelm Melitz, Jian Shen, Andrew C. Kummel, and Sangyeob Lee. Kelvin probe force microscopy and its application. *Surface Science Reports*, 66(1):1–27, 2011.

[89] Gabino Rubio-Bollinger, Ruben Guerrero, David de Lara, Jorge Quereda, Luis Vaquero-Garzon, Nicolas Agraït, Rudolf Bratschitsch, and Andres Castellanos-Gomez. Enhanced Visibility of MoS2, MoSe2, WSe2 and Black-

Phosphorus: Making Optical Identification of 2D Semiconductors Easier. *Electronics*, 4(4):847–856, 2015.

[90] Filippo Pizzocchero, Lene Gammelgaard, Bjarke S. Jessen, José M. Caridad, Lei Wang, James Hone, Peter Bøggild, and Timothy J. Booth. The hot pick-up technique for batch assembly of van der Waals heterostructures. *Nature Communications*, 7(May), 2016.

[91] Joel I.Jan Wang, Yafang Yang, Yu An Chen, Kenji Watanabe, Takashi Taniguchi, Hugh O.H. Churchill, and Pablo Jarillo-Herrero. Electronic transport of encapsulated graphene and WSe2 devices fabricated by pick-up of prepatterned hBN. *Nano Letters*, 15(3):1898–1903, 2015.

[92] Y. Park, V. Choong, Y. Gao, B. R. Hsieh, and C. W. Tang. Work function of indium tin oxide transparent conductor measured by photoelectron spectroscopy. *Applied Physics Letters*, 68(19):2699–2701, 1996.

[93] M. M. Beerbom, B. Lägel, A. J. Cascio, B. V. Doran, and R. Schlaf. Direct comparison of photoemission spectroscopy and in situ Kelvin probe work function measurements on indium tin oxide films. *Journal of Electron Spectroscopy and Related Phenomena*, 152(1-2):12–17, 2006.

[94] J.S. Kim, B. Lagel, E. Moons, N. Johansson, I.D. Baikie, W.R. Salaneck, R.H. Friend, and F. Cacialli. Kelvin probe and ultraviolet photoemission measurements of indium tin oxide work function: a comparison. *Synthetic Metals*, 111:311–314, 2000.

3 III-VI semiconductors: optical and electrical properties

Following the current framework described in the field of 2D materials (Chapter 1), a less-explored family of 2D materials will be studied in detail in this chapter: the 2D materials based in III-VI semiconductors, with InSe and GaSe as its representatives.

3.1 Gallium Selenide

The results and comments described in this subchapter have been already published in "Quantum size confinement in gallium selenide nanosheets: band gap tunability versus stability limitation", Daniel Andres-Penares, Ana Cros, Juan P Martínez-Pastor and Juan F Sánchez-Royo, Nanotechnology, Volume 28, Number 17 (2017).

In this subsection, an updated view of this publication will be presented, with added supplementary information.

3.1.1 Introduction

Following the trend described in Chapter 1, other 2D semiconductors have started to attract the attention of the scientific community trying to overcome limitations of existing 2D semiconductors. 2D TMDs are direct bandgap, only, at the ML regime, so they have a limited application in optoelectronics. Black Phosphorous, with a direct band gap in the infrarred [373, 351], is a promising candidate for optoelectronics. However, it is unstable.

2D semiconductors based on III-VI materials, like InSe or GaSe, have demonstrated to be able to provide a wide optical bandgap window that can even reach the low-energy side of the visible spectrum. Following the path marked by 2D InSe, in

this chapter we study the prospects and limitations of 2D GaSe for optoelectronic applications.

Gallium selenide (GaSe), an indirect III-VI layered semiconductor with a ~2.02 eV band gap at RT [142], arises as one of the most promising candidates to extend even further the optical window of 2D materials with potential optoelectronic applications. This material gained interest in the past due to its non lineal optical properties [147, 131, 142]. Among the III-VI semiconductors, GaSe has been the first material reported as obtained in a 2D nanosheet regime. On one hand, the band gap of GaSe ML has been predicted increase by 1.2 eV with respect to that of bulk GaSe due to quantum confinement effects [214]. On the other hand, GaSe nanosheets have been already used as photodetectors with high responsivity and high external quantum efficiency [140], as high-performance field-effect transistors [145], and in hybrid heterostructures giving rise to photodetectors that combine a high gain with a fast photoresponse [249, 115]. Also, few layer GaSe may present potential applications for spin-polarization control [211], non-linear optics [127], and in optical microcavities [113]. Lately, its behavior as a saturable absorber for Q-switched [126] and mode-locked [122] laser has been demonstrated. These facts suggest that 2D GaSe may become a very versatile material for visible -or even ultraviolet- electronics and optoelectronics with tunable and optimised functionalities. Moreover, experimentally, it has been reported that the PL of GaSe nanosheets blueshifts only by 20 meV when the thickness of the nanosheet is reduced to a BL [140], a value that largely differs from the band-gap blueshift of 0.7 eV expected for a BL of GaSe by first-principles calculations [214].

Besides of the particular question presented above about the magnitude of the tunability range of the band gap of GaSe nanosheets, there is a general requirement that any 2D material must satisfy for the development of related devices, which is precisely to guarantee a relatively high structural stability under ambient conditions [146]. The stability of bulk GaSe has been studied in the past [139, 116], showing a well-established temperature-dependent oxidation diagram. Around RT (below 400 K), bulk-GaSe oxidation mostly produces elemental Se and Ga_2O_3, whereas above 400 K the simultaneous formation of Ga_2Se_3 and Ga_2O_3 takes place. At higher temperatures, Ga_2Se_3 tends to disappear in GaSe, favouring the formation of Ga_2O_3 as the main oxidation product. Oxidation processes appear also to deeply affect to the luminescent response of relatively thick GaSe nanosheets [118, 99], which hampers the further development of 2D GaSe optoelectronic devices. In fact, freshly prepared

bulk-like GaSe nanosheets show a clear PL peak centered at the energy position expected for bulk GaSe, but the intensity of the PL signal quenches as the exposition time in air increases [118, 99]. Oxidation processes taking place in bulk-like GaSe nanosheets at RT have been studied by Raman, PL, Auger, and XPS [118], revealing that oxidation of bulk-like GaSe nanosheets proceeds as in bulk GaSe, i.e., through the formation of Se and Ga_2O_3. Nevertheless, an additional and clear Raman signature coming from Ga_2Se_3 was also noted in these nanosheets [118] that suggests an oxidation process slightly different from that demonstrated in bulk material at RT [139, 116].

In this subchapter, a tuning of the optical band gap of 120 meV from bulk to 8 nm thick in freshly exfoliated GaSe nanosheets is demonstrated, by means of μ-PL and AFM. In this range of thicknesses, the obtained nanosheet-thickness dependence of the optical band gap can be estimated by the quantum size confinement of carriers in a quantum well of infinite barriers within the effective mass approximation. Second, it is evidenced that GaSe nanosheets exposed to air experience a strong oxidation process that exhibits a deep impact on their morphology and structural composition. Such oxidation process is clearly responsible for the quenching of the exciton PL of freshly-prepared GaSe nanosheets thinner than 8 nm. Morphologically, oxidation introduces strain that promotes the formation of nanospikes at the surface whose height increases as the thickness of the nanosheet does. Structurally, XPS results reveal that, in few layer nanosheets, the incorporated oxygen progressively replaces Se giving rise mostly to Ga_2O_3, an oxidation diagram that differs from that observed for bulk GaSe and bulk-like GaSe nanosheets under ambient conditions. The oxidation effects is thus introducing a strong limitation in the investigation of basic optical properties in few-layer GaSe, which can be reason why any remarkable band gap increase have been reported before. Present results allow understand oxidation effects in few layer GaSe nanosheets that should be prevented before their incorporation in future applications and devices.

3.1.2 Photoluminescence measurements

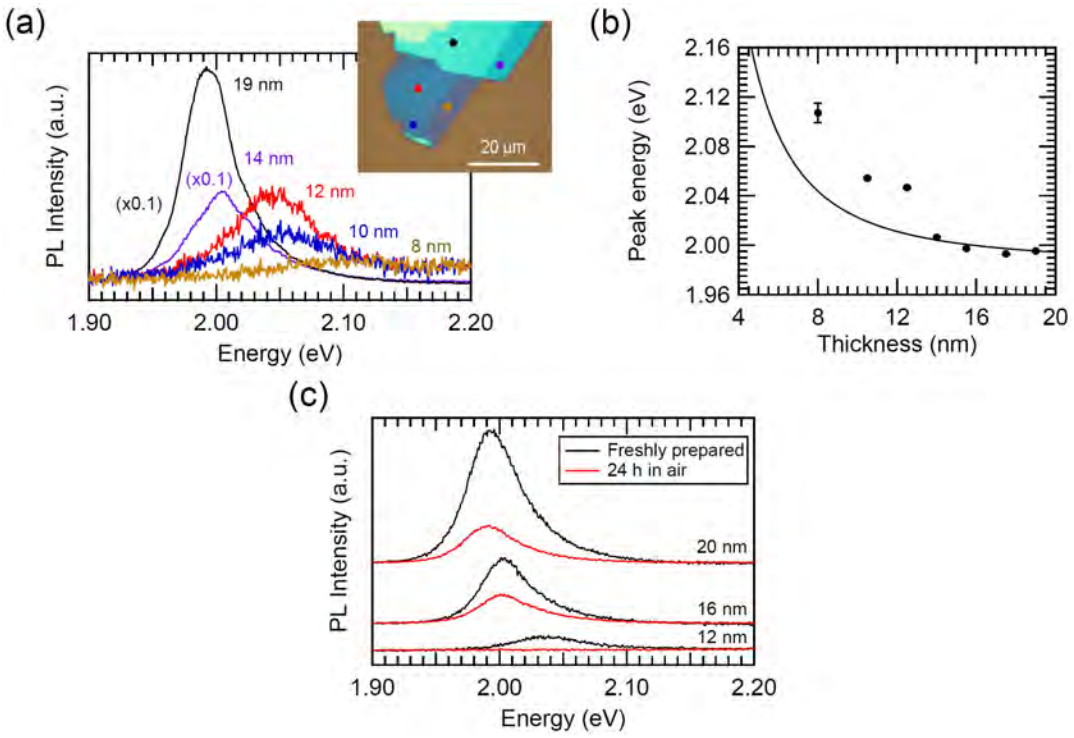

Figure 3.1: (a) µ-PL spectra acquired in different points of a multi-terrace GaSe nanosheet freshly exfoliated on a Si/SiO_2 substrate. The optical image of the nanosheet is shown at the top, in which measurement points have been indicated by filled circles whose color corresponds to that of the spectrum shown in the main figure. The thickness of each terrace is indicated on the corresponding µ-PL spectrum acquired. (b) Nanosheet-thickness dependence of the PL-peak maximum of the spectra shown in (a). Solid line corresponds to the thickness dependence of the exciton optical transition expected by using a simple model of a square quantum well potential of infinite height. (c) µ-PL spectra acquired in GaSe nanosheets just after exfoliation and after 24 h exposed to ambient conditions.

From bulk GaSe monocrystals (see Appendix A), atomically thin GaSe samples were micromechanically exfoliated on Si/SiO_2 (300nm) substrates (Subsection 2.1.1). The luminescent response of atomically thin GaSe nanosheets has been studied by µ-PL (using the Horiba Xplora described in Subsection 2.2.3). Figure 3.1a shows the µ-PL spectra acquired in selected points of a freshly exfoliated nanosheet (shown at the inset of Figure 3.1a) corresponding to terraces of a particular thickness, as determined by AFM (for more details, see Subsection 2.3.2). In the thickest nanosheets the maximum of the PL signal appears at 1.99 eV, as would be expected

for exciton recombination in bulk GaSe. As the thickness of the nanosheet decreases, the PL signal shifts to higher energies and decreases in intensity, similarly to that observed in other III-VI layered semiconductors as InSe [125, 208, 334].

It should be noticed here that, although few layer GaSe nanosheets were obtained by micromechanical exfoliation, the PL intensity of these thinner than 8 nm is strongly quenched and unmeasurable within our experimental signal-to-noise ratio. From results shown in Figure 3.1a it appears that the maximum of the PL-peak measured at each particular terrace of the nanosheet runs from 1.99 eV, in nearly bulk terraces, to 2.11 eV, in 8 nm thick ones (Figure 3.1b). These results are clearly in contrast with previous observations reporting a blueshift of the maximum of the PL-peak of only 20 meV when the thickness of the nanosheet is reduced to a BL (2 nm thick) [140]. The blueshift of the PL peak evidenced in Figures 3.1a and b can be attributable to quantum-size confinement effects on the optical band gap of GaSe nanosheets due to the natural quantum-well determined by a few layer GaSe sheet.

In order to check this hypothesis, the thickness dependence of the energy of the exciton optical transition (E_{exc}^{2D}) has been analysed in terms of a square quantum well potential of infinite barriers, given by

$$E_{exc}^{2D}(d) = E_g^{bulk} - E_{exc}^{bulk} + \frac{\pi^2\hbar^2}{2dm_{\|c}}$$

where $E_g^{bulk} = 2.0$eV and $E_{exc}^{bulk} = 19.2$meV are the direct band gap energy and exciton binding energy in bulk GaSe at RT [142], respectively, d is the quantum well thickness, and $m_{\|c} = (m_{e\|c}^{-1} + m_{h\|c}^{-1})^{-1} = 0.10m_0$ is the exciton reduced mass, as obtained from reported values of the electron ($m_{e\|c} = 0.26m_0$) and hole ($m_{h\|c} = 0.17m_0$) effective masses along the c-axis [142].

This simple model, although a constant exciton binding energy has been assumed, reproduces very well the thickness dependence of the exciton energy, E_{exc}^{2D}, obtained experimentally (Figure 3.1b), indicating that, in line with that observed in other 2D semiconductors [338, 125, 334], the band gap of GaSe nanosheets can be effectively tuned by quantum-size confinement effects. These results are relevant for further development of band gap tunable optoelectronic devices based on 2D GaSe.

However, to achieve this purpose, the nature of potential oxidation processes taking place in atomically thin GaSe nanosheets must be studied in detail and their stability under ambient conditions guaranteed, mostly taking into account results already reported for bulk GaSe [139, 116] and bulk-like GaSe nanosheets [118, 99]

revealing strong oxidation effects. Indeed, atomically thin nanosheets appear also to experience strong oxidation. In fact, apart from the lack of PL signal mentioned above for freshly prepared nanosheets thinner than 8 nm, it is observed that, already after 24 h exposed to air, the intensity of the PL signal of relatively thick nanosheets strongly diminishes and even becomes effectively quenched for 12 nm thick ones, as shown in Figure 3.1c. More subtle oxidation effects can be observed to occur even at early states of oxidation: Although a good agreement has been found between the experimental and calculated thickness dependence of E_{exc}^{2D} (Figure 3.1b), a small thickness-offset of 2 nm seems to exist between them. This small thickness offset can be due to oxidation effects at the nanometric scale, since AFM measurements were carried out in unavoidably oxidised samples and consequently slightly thicker than as prepared.

In this context, it would be interesting, for basic and technological purposes, to clarify whether oxidation of GaSe nanosheets occurs in a layer-by-layer fashion, as it has been observed in WSe_2 nanosheets [148], which would imply that controlled oxidation may be used to create nanosheets of a selected effective thickness. In this case, it may be expected a progressive blueshift of the PL-response of GaSe nanosheets to occur as the ambient exposition time increases, since a layer-by-layer reduction of the effective GaSe thickness would enhance quantum confinement effects on the exciton optical transition.

3.1.3 Oxidation processes in two-dimensional GaSe

As mentioned above, the PL intensity of GaSe nanosheets appears to progressively decrease as the exposition time increases without any appreciable blueshift of the main PL peak (Figure 3.1c). These facts indicate that strong oxidation processes homogeneously occur inside the atomically thin GaSe nanosheets, which tend to introduce a large density of defects inside GaSe nanosheets that enhance non-radiative recombination processes.

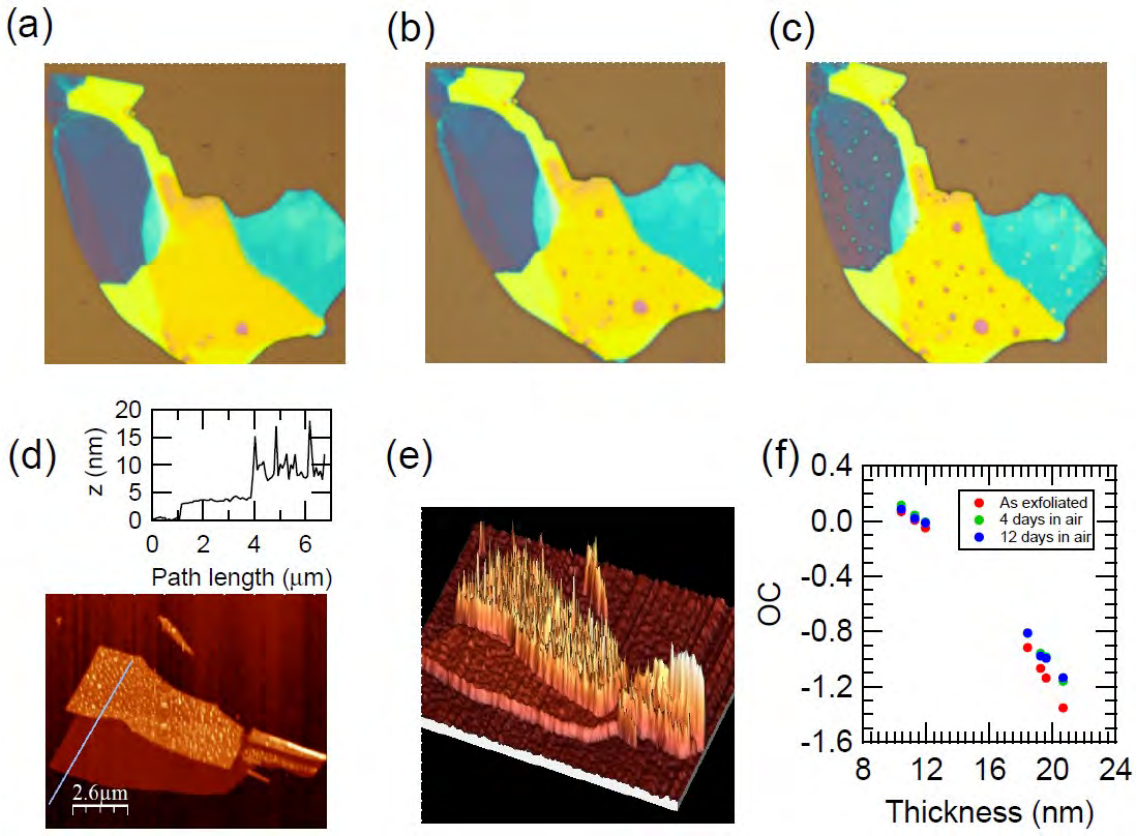

Figure 3.2: (a) Optical images of a selected GaSe nanosheet acquired just after exfoliation on a Si/SiO_2 substrate and after (b) 4 days and (c) 12 days in ambient conditions. (d) AFM image of a GaSe nanosheet and thickness profile (upper plot) along the path indicated on the image by a white line. (e) Three-dimensional perspective of the AFM image of the nanosheet shown in (d), revealing a high density of nano-spikes on the thickest terrace of the nanosheet. (f) Optical contrast values measured in the green channel from selected areas of homogeneous thickness of the GaSe nanosheet shown in (a)-(c).

The oxidation process evidenced above has deep effects on morphological and structural properties of GaSe nanosheets exposed to ambient conditions, as observed in optical (Figures 3.2a and c) and AFM (Figures 3.2d and e) images. The presence of randomly distributed spots can be optically detected to emerge on the nanosheet surface, as it has been already reported [118]. It can be noticed that such oxidation spots do not act as seeds for further local oxidation, but their density increases with the exposition time to air. AFM images of Figures 3.2d and e are representative of our observations in more than 10 samples of thickness ranging from few nanometers to bulk-like.

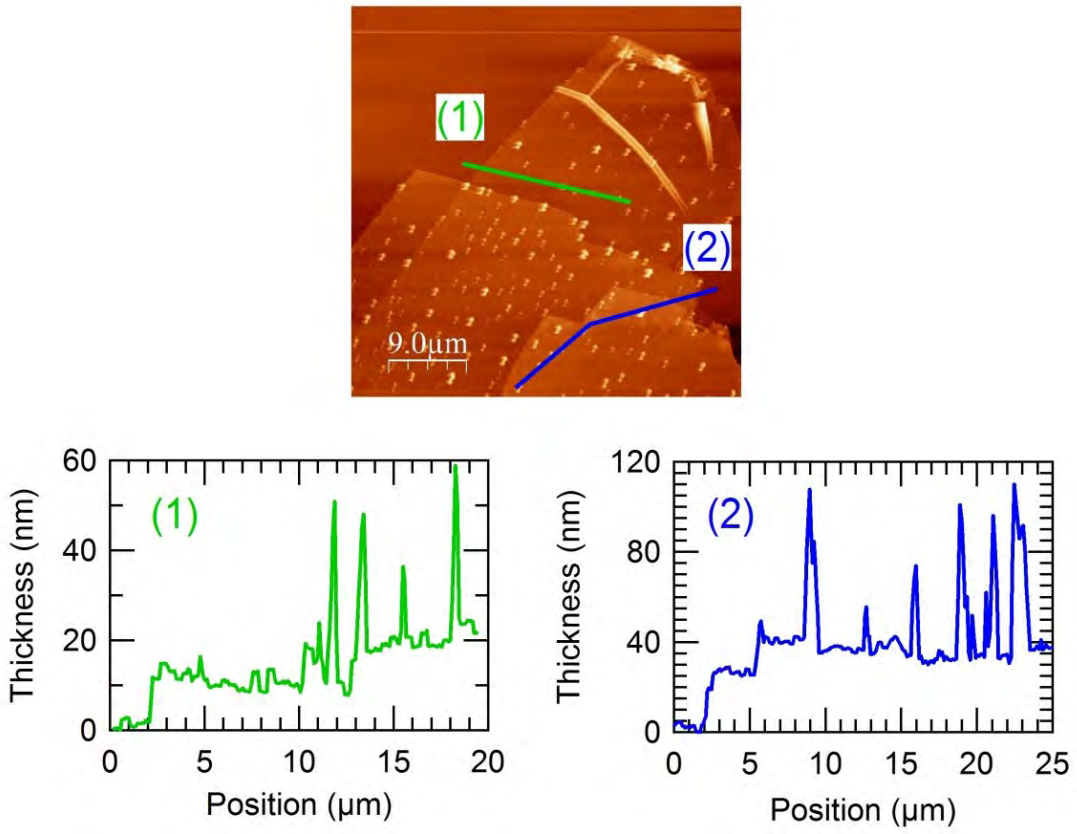

Figure 3.3: AFM image of an aged GaSe nanosheet with terraces of different thickness. Notice the presence of nanospikes spread over the whole sample, these appearing as brilliant spots. At the bottom, two different thickness profiles are shown, these corresponding to the paths (1) and (2) indicated on the AFM image by solid lines. Paths (1) and (2) probe terraces of the nanosheet with a thickness of 10-20 nm and 30-40 nm, respectively. In the 10-20 nm thick terrace, nanospikes reach heights of even 40 nm, whereas they reach heights of even 70 nm in the 30-40 nm thick terrace.

They reveal that surface spots observed by optical microscope arise from nanospikes originated by surface oxidation. Furthermore, the height of these spikes appears to depend on the thickness of the nanosheet: they introduce a surface roughness of around 5 nm in an atomically thin nanosheet 7 nm thick (Figure 3.2d), although the nanospikes can reach values as high as 70 nm in 40 nm thick bulk-like nanosheets (Figure 3.3). Thinnest nanosheets present a higher surface-to-volume ratio and, consequently, a lower internal resistance to structural modifications produced by the oxidation process than the thickest ones. Therefore, the observation of: (i) nanospikes whose height depends on the nanosheet thickness and (ii) optical spots

related to the nanospikes which do not act as seeds for further local oxidation; suggest that strong local structural relaxation processes take place which are associated to the strain introduced by the nanosheet oxidation.

Morphologically, the appearance of the spikes due to surface oxidation is expected to deeply modify the OC of GaSe nanosheets, as evaluated as described in Subsection 2.2.1. In fact, optical dark spots related to spikes are observed on relatively thick nanosheets (the yellow ones in Figures 3.2a and c), whereas they are optically detected as clear spots on thinner nanosheets (blue ones in Figures 3.2a and c). Indeed, this observation shall be related to modifications of the light interference pattern that makes visible GaSe nanosheets on Si/SiO_2 substrates, but may indicate that the validity of standard OC methods, which have been extensively used as a fast tool to accurately estimate the thickness of a large variety of 2D materials [133, 123], can be put into question to accurately estimate the thickness of GaSe nanosheets. To illustrate the effects of oxidation on the OC of GaSe nanosheets, it is shown in Figure 3.2f the OC in the green channel [133] extracted from images acquired in GaSe nanosheets under different ambient exposition times (Figures 3.2a and c). From these results, it appears that GaSe oxidation processes tend to increase OC (negative) values of nanosheets, especially for the thicker ones. This effect can be attributable to an enhancement of light scattering due the increase of surface roughness, at the same time that reduces the effective light reflectance of the nanosheets with a high oxidation degree.

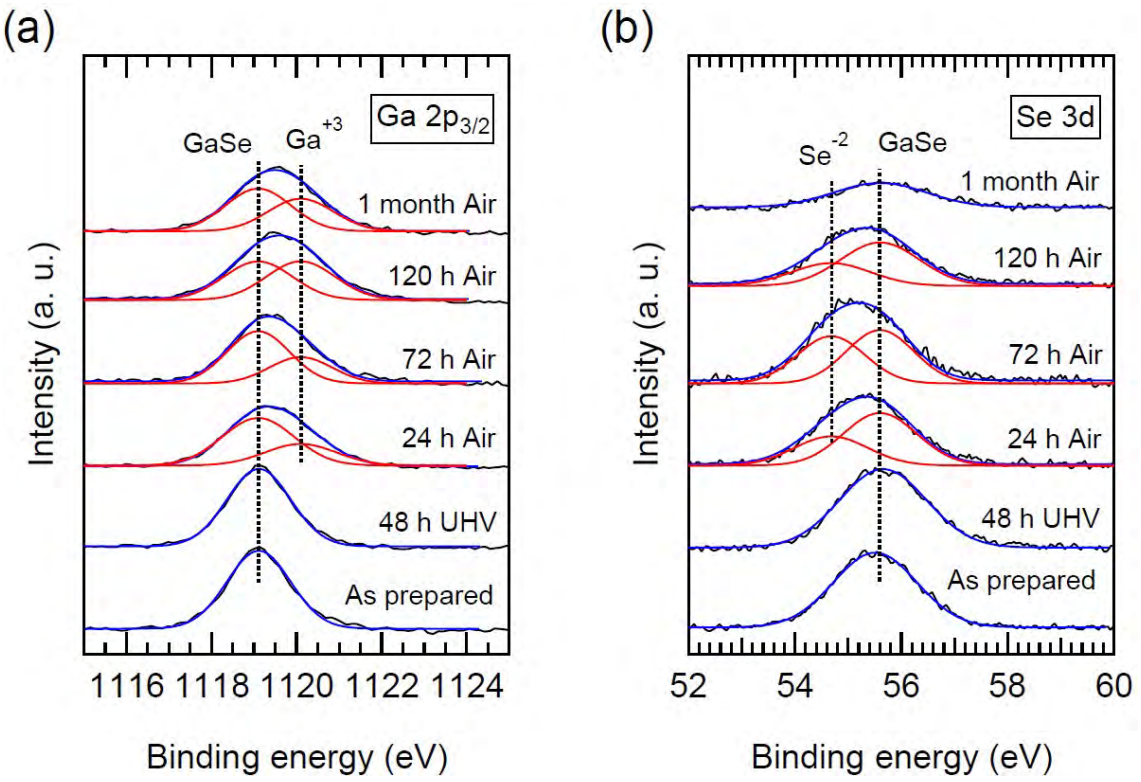

Figure 3.4: XPS spectra of the (a) Ga $2p_{3/2}$ and (b) Se 3d core levels acquired in GaSe nanosheets exfoliated on Si/SiO_2 substrates, as a function of the ambient exposition time of the sample previous to each measurement (which has been indicated on each corresponding spectrum). Blue curves are the result of fitting of the experimental spectra, by considering two Gaussian peaks (red curves). The position of each Gaussian peak has been indicated by vertical dashed lines.

Results mentioned above clearly establish the strong influence of oxidation on the structural, morphological, optical, and luminescent properties of atomically thin GaSe nanosheets. In the following, it is approached the question of the nature of oxidation reactions taking place in these nanosheets under ambient exposition. To this purpose, XPS measurements have been performed on a Si/SiO_2 substrate sustaining a high density of few-nanometers thick GaSe nanosheets.

Figure 3.4 shows XPS spectra measured in GaSe nanoflakes under different exposition time to ambient conditions. GaSe nanosheets appear to remain stable under vacuum, since the Se 3d and Ga 2p peaks exhibit no change in shape neither additional peaks have been detected after few days in vacuum. However, early exposition to air already produces an asymmetric broadening of the Ga 2p and Se 3d core-level peaks towards higher and lower binding energies, respectively, which tends to be

enhanced as the exposition time to air increases. Gaussian deconvolution of the Ga 2p and Se 3d peaks allows resolving two additional core-level components which emerge and develop, due to ambient exposition, at the high and low energy side of the Ga 2p and Se 3d peaks attributable to GaSe, respectively. The reacted Ga 2p core-level component, which emerges at energies +1.0 eV far from that of GaSe, can be attributed to Ga atoms with a Ga^{+3} oxidation state, whereas the reacted Se 2p component, emerging at -0.90 eV far from that of GaSe, can be originated by the presence of Se atoms with a Se^{-2} oxidation state. These results point out to the formation of Ga_2Se_3-like at the surface of the GaSe nanosheets after ambient exposition, in agreement with that observed in bulk GaSe [116] and GaSe nanosheets [118].

However, it seems not to be the main product of the oxidation of the GaSe nanosheets, since the Se^{-2}/Ga^{+3} atomic ratio, as extracted from XPS, appears to reach values significantly lower than that expected for nominal Ga_2Se_3. In fact, the Se^{-2}/Ga^{+3} ratio only seems to reach values as high as 0.15 for samples exposed up to three days in air, which suggests that most of the Ga^{+3} originated by the nanosheet oxidation adopts a Ga_2O_3 structure in atomically thin GaSe nanosheets. Moreover, a larger exposition time appears to reduce the Se^{-2}/Ga^{+3} atomic ratio in the nanoflakes.

All these facts suggest an oxidation diagram in which GaSe nanosheets exposed to air tend to experience a structural modification of their surface in which oxygen progressively replaces Se giving rise mostly to Ga_2O_3. Replaced Se appears transitorily to adopt a Ga_2Se_3-like configuration, but further oxidation seems to reduce the presence of Ga_2Se_3 in favour of Ga_2O_3. In contrast to previous works [118], traces from amorphous Se were not detected by XPS, which suggests that residual Se becomes finally desorbed from the nanosheets. Collaterally, the formation of the Ga_2O_3 overlayer seems to prevent further oxidation of the deepest part of the thickest GaSe nanosheets, as revealed by XPS for nanosheets exposed up to one month in air. These results suggest an oxidation process scheme that seems to differ from that observed in bulk and bulk-like GaSe nanosheets.

At RT, oxidation of bulk GaSe mostly produces elemental Se and Ga_2O_3 [139, 116]. However, oxidation of bulk-like nanosheets appears to produce [121], also, Ga_2Se_3, i.e., a product that would be obtained by oxidation of bulk GaSe at temperatures over 400 K [139, 116]. As discussed above, oxidation of atomically thin nanosheets produces, mainly, Ga_2O_3, with a residual presence of Ga_2Se_3 that diminishes as the

oxidation time increases. Oxidation processes observed here to occur in atomically thin GaSe nanosheets at RT appear better corresponding to what is observed in bulk GaSe at temperatures higher than 400 K [139, 116]. All these facts clearly indicate that decreasing the thickness of GaSe plays a similar role, from the point of view of the oxidation, to the increase of the oxidation temperature, which can be readily understood by considering that the surface-to-volume ratio increases by reducing the thickness of GaSe nanosheets and consequently enhances oxidation effectiveness, as increasing temperature does.

3.1.4 Conclusions

Results reported here demonstrate that the optical band gap band of atomically thin GaSe can be tuned by 120 meV from bulk to 8 nm thick nanosheet due to quantum confinement effects and suggest that even higher optical band gap blueshifts can be obtained in thinner nanosheets. Recent publications obtained a shift up to 2.42 eV in a BL [410]. Atomically thin GaSe nanosheets are, however, unstable under ambient conditions. Our results reveal the nature of the oxidation reactions taking place in atomically thin GaSe nanosheets that should be prevented before their incorporation in future applications and devices. These oxidation reactions differ from these occurring in bulk or bulk-like GaSe nanosheets and have a deep effect on the structural, optical, and luminescent properties of GaSe nanosheets. Oxygen progressively replaces Se giving rise to Ga_2O_3, with a residual presence of Ga_2Se_3 at the surface that diminishes in favour of Ga_2O_3 at long ambient exposition times.

Structurally, oxidation produces the emergence of sharp nanospikes at the nanosheet surface and introduces a large density of defects that strongly limit the luminescent response of the nanosheet, especially of these thinner than 8 nm. These results are relevant for the design and development of photonic/optoelectronic devices based on a two-dimensional semiconductor that is one of the few layered materials whose band gap lies in the high energy side of the visible spectrum and can potentially reach the ultraviolet region. However, stability arises here as a major question to be addressed in next future. Possible encapsulation procedures by the use of different polymers are being currently investigated to solve such an issue [130].

3.2 Indium Selenide

3.2.1 Introduction

InSe was obtained as a III-VI 2D semiconductor after GaSe [125, 208, 334]. Similar to other members in the III - VI semiconductors, an InSe ML shares a D_{3h} point group symmetry, consisting in two atomic In layers embebed between two atomic Se layers, bonded covalently forming tetrahedra. This basic layered structure is determined by the hexagonal lattice parameters $a = b = 0.4002nm$ [169]. Due to vdW forces this ML are weakly bonded to consitute the bulk material, but different stacking sequences define different polytypes: β, γ, δ and ε, as can be observed in Figure 3.5. In this thesis, γ-InSe has been used (see Appendix A), with a non-primitive unit cell in the hexagonal description formed by three basic layers stacked in a ABC sequence ($c = 24.946$Å) [169].

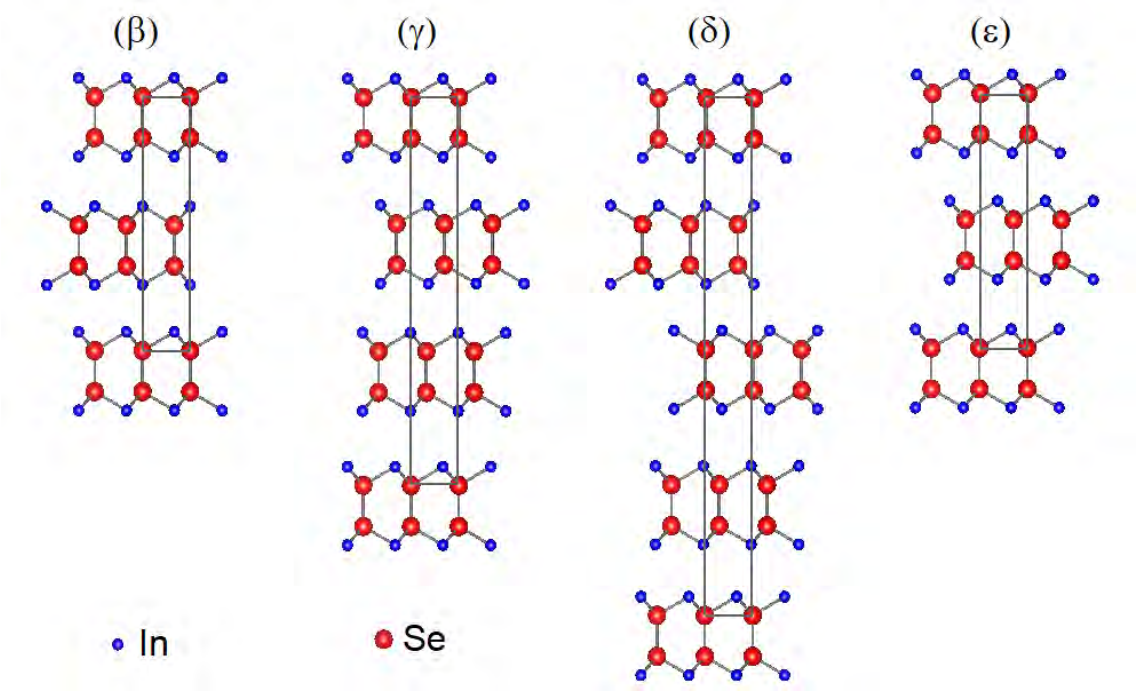

Figure 3.5: Structural polytypes in bulk InSe. From left to right, β, γ, δ and ε with an AB, AB, ABC and ABCD stacking sequences, respectively.

The band-structure analysis in bulk γ-InSe was studied in the 90's [163, 164, 151], with a well-known correction of ~0.8 eV from ab-initio calculations to be compared with the experimentally measured direct band gap at RT of 1.25 eV [156]. Besides,

due to the mechanical anisotropy between the c direction and the layer plane, a different effective mass for electrons and holes have been found when these directions are compared ($m^*_{e,\perp c} = 0.138m_0$, $m^*_{e,\parallel c} = 0.081m_0$, $m^*_{h,\perp c} = 0.73m_0$, $m^*_{h,\parallel c} = 0.17m_0$) [158, 154]. Also, transport properties in bulk InSe highlight due to its high doping versatility, from n - type (e.g., using Sn and Si impurities [150, 160]) to p - type (e.g., with Zn or Pt [162, 172]), reaching experimentally reported values up to $10^3 cm^2/Vs$ [155].

Bulk InSe gained interest in the past specially due to its non-linear optics properties [131, 147], specially in the infrared range for second-harmonic applications [176]. This fact, the stability in air compared with other III - VI, besides its direct band gap (unlike TMDs) offering a RT PL emission due to band-to-band transitions and its great mobility aimed for a versatile material in optoelectronic applications, starting its study in its 2D form.

When this material is exfoliated, due to quantum confinement effects, one of the largest band gap tunability ranges appear in InSe nanosheets, from 1.25 eV in bulk to 2.1 eV in the ML state [334]. This result contrast with TMDs, where due to the indirect to direct transition in their band structure [333] from few-layer to ML, the tunability is reduced to its ML form. That is the reason why procedures like strain [199], chemical doping [217] or the transfer onto different refractive index substrates have been used to acquire some tunability, needed in some applications. In the case of InSe, similar techniques can be used, such as nanotexturing effects to add more tunability [334].

Besides, its recently discovered out-of-plane (OP) dipolar behavior [297] hampers their reduced absorption coefficient and therefore, their quite low PL intensity in a vertical excitation – vertical collection approach, compared with the in-plane (IP) dipole observed in TMDs, which will be a key element in future chapters.

3.2.2 Electrical properties

As previously highlighted, InSe mobility in its bulk state aimed for its application in optoelectronic devices in its 2D form. Devices based on few-layer InSe have shown promising results as field-effect transistors with mobilities comparable to its bulk-form [258], large current on−off ratios [226], as high performance photodetectors [375] and as sensors [206].

In this subsection, the electrical properties of InSe nanosheets will be explored.

3.2.2.1 I - V characterisation of defect-free n - n^+ heterojunctions in InSe different-layered nanosheets

The most straightforward optoelectronic devices, such as photodetectors, photodiodes, phototransistors, for instance, are based in p - n heterojunctions, where two different materials (one n - doped and the other p - doped, i.e., with electron and hole in excess, respectively) are in physical contact, increasing in the material barrier the carrier recombination processes. Therefore, this barrier (which nature will be studied later), based in the different band gap between both materials, is the key element in these devices. However, due to the necessity of two different materials in contact to form these structures, an unavoidable mechanical contact will appear, hampering the final performance due to the intrinsic defects [161, 167, 171].

This problematic can be found in any heterojunction made until the appearance of 2D semiconductors. Due to quantum confinement it is possible to obtain different band gap energies within the same material, e.g., in layered 2D materials, in which each different-thickness area came from the same bulk material, maintaining its structural quality. As a example, a planar heterojunction based in this premise has been demonstrated in MoS_2 [173] despite the non-ideality of partly-indirect TMD BL band gap. In this project, defect-free n - n^+ heterojunctions in InSe exfoliated nanosheets have been performed taking advantage of the always-direct different band gap due to the different thicknesses in the samples. Using a band structure model are theoretically understood and physically explained the I - V curves that has been characterised obtaining as a result the behavior expected in p - n heterojunctions, proving that this kind of structures work as a photodetector when illuminated.

Prior to the study of multiterraced nanosheets, for comparison, Figure 3.6 shows the I - V characteristics in InSe homogeneous nanosheets transferred on Au contacts (see Subsections 2.1.1 and 2.1.3.1). The Au microgap contacts have been prepared by Dr. Alberto Maulu by photolithography (see Subsection 2.3.1). The contacted nanosheets have been completely iluminated with a halogen white light source, using different power excitation values. In homogeneus nanosheets, where no different thicknesses appear and, therefore, no different band gap energies are present between contacted areas, a symmetrical behavior in the I - V characteristics applying positive and negative voltage biases is obtained. This behavior is similar to the expected

where no barrier is found between the contacts due to the symmetry on the system.

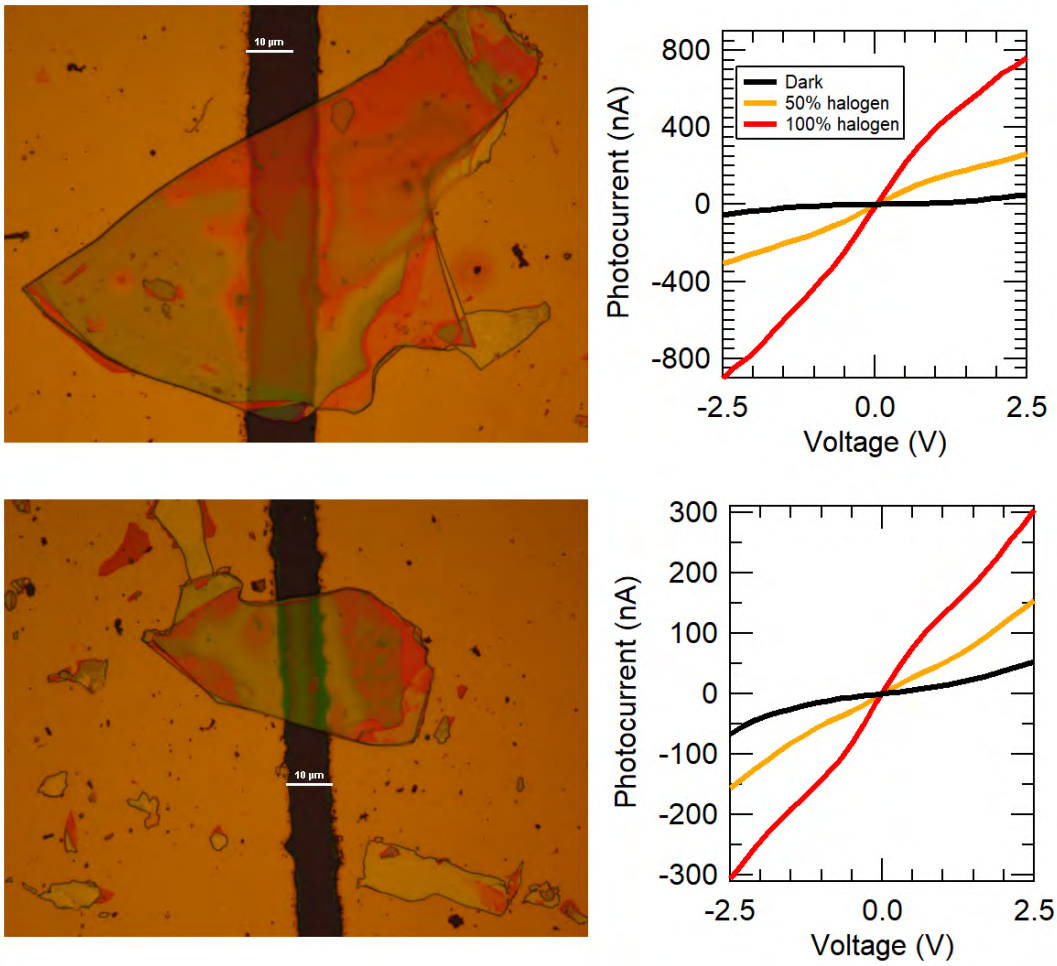

Figure 3.6: I - V characteristics in homogeneus InSe nanosheets. On the left, optical images of homogeneous volumic InSe nanosheets transfered onto a gold microgap. On the right, photocurrent generated applying different ilumination power, obtaining a simetric behaviour with positive and negative bias.

In contrast with these homogeneus nanosheets behavior, multiterraced InSe nanosheets have been analysed in Figure 3.7, observing an asymmetrical behavior in positive and negative voltage bias, similar to p - n heterojunctions [177, 157, 166, 179]. In Figure 3.7a, a similar transfer method as previous samples have been used, locating the thickness barrier between both contacts that can be seen via OC. RT PL measurements have been taken in each thickness to determine the band gap difference (see Subsection 2.2.3 [334]), obtaining 1.2467eV to 1.2704eV in the thicker sample and 1.60eV to 1.36eV in the thinner one. In Figure 3.7c, due to the thinner

nanosheet thicknesses, on top of exfoliated samples, e-beam lithography has been performed by Dr. Josep Canet-Ferrer, to prevent sample physical hampering due to the transfer on microgaps.

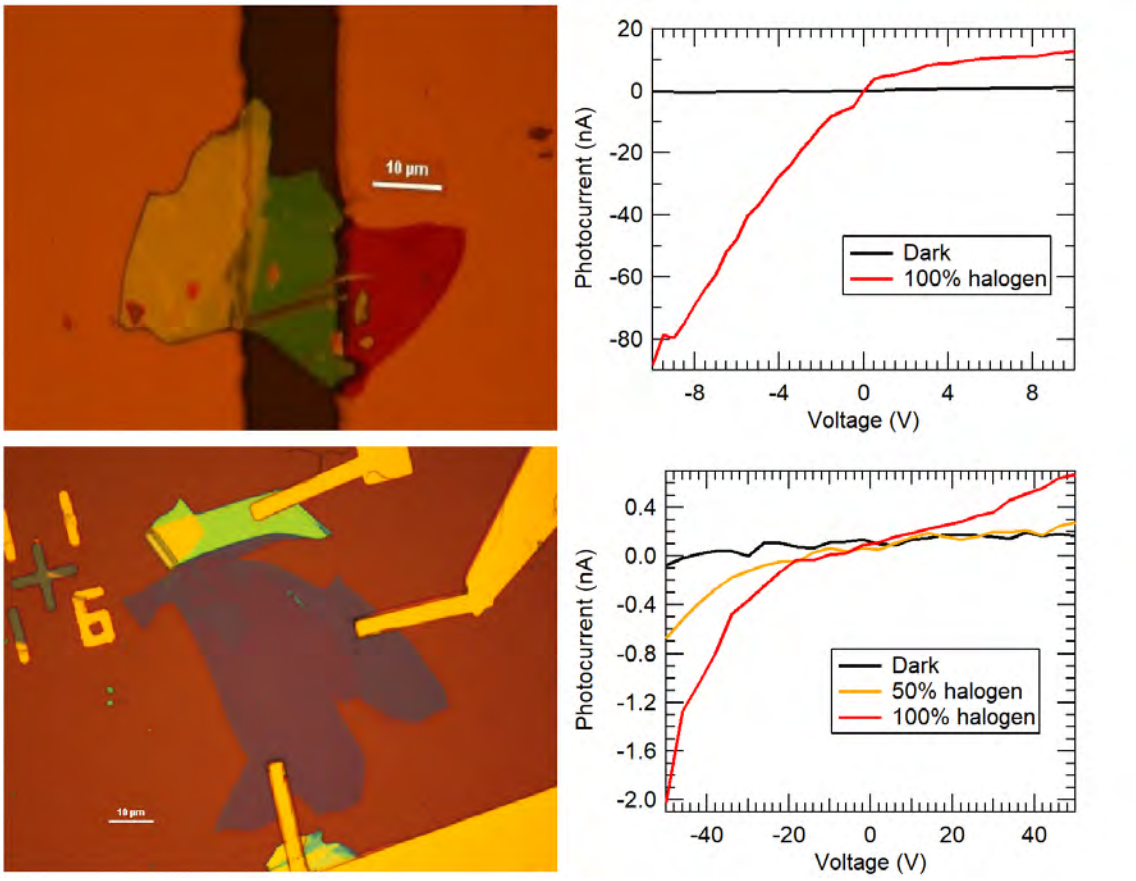

Figure 3.7: I - V characteristics in multiterraced InSe nanosheets. On the left, optical images of layered InSe nanosheets transfered onto a gold microgap (up) or contacted with e-beam (down). On the right, photocurrent generated applying different ilumination power, obtaining an asymmetric behaviour with positive and negative bias.

The asymmetry in the I - V curves in layered nanosheets applying positive and negative voltage biases, unlike homogeneous ones, must be produced by an intrinsic inner barrier in the layered samples. In the barrier surroundings, due to the different energy band gap between both thicknesses, a different carrier density (in this case, electrons due to the n - doped original material, Appendix A) is expected. Some carriers from one thickness will pass to the other, enhancing a n^+ doping of the thicker terrace [170, 152, 180, 178], due to the higher number of electrons in comparison. Therefore, a n - n^+ heterojunction is expected in the inner edge between

thicknesses. This fact has been studied in Figure 3.8.

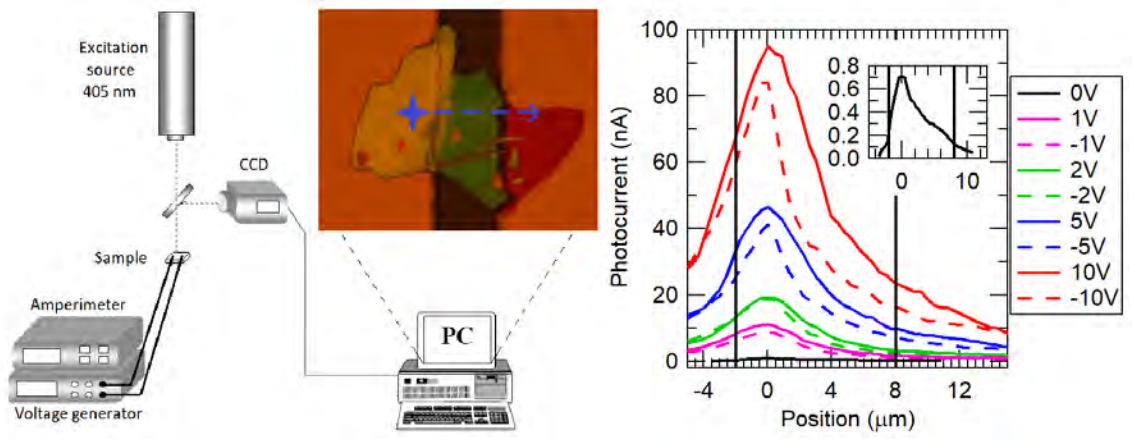

Figure 3.8: Excitation position impact in photocurrent generation. On the left, schematic setup used to measure. On the right, the photocurrent generated in a layered InSe nanosheet exciting the sample along the change of thickness with a 1mm^2-spot 405nm laser applying different voltajes. The 0 position has been set in the edge location between thicknesses of the sample along the line measured.

Figure 3.8 shows the photocurrent generated in the layered nanosheet when the sample is excited in different points. In this case, instead of an halogen white light source iluminating the whole nanosheet, a 405nm laser has been used, with a spot around 1mm^2 with a constant ~70μW excitation power to have control in the position excited, observing an enhancement in the photocurrent generated closer to the barrier edge. A line-scan in different positions perpendicular to the microgap direction have been taken. This enhancement in the photocurrent generated in the barrier surroundings is explained due to the higher density of accumulated carriers, where the recombination is enhanced in this n - n$^+$ heterojunction, being reduced exciting further from this location. Besides, similar to previous measurements, an asymmetrical behavior in the photocurrent generated is observed applying negative or positive voltage bias due to the inner band gap barrier (the asymmetry is less visible due to the fact that the excitation is now in one precise wavelength instead of the whole visible spectra, adding its contribution and effect). Finally, when no bias is applied, photocurrent is generated following the same behavior, proving the intrinsic barrier due to the different thicknesses.

This behavior is understood considering the band alignment shown in Figure 3.9 between two materials with different band gaps using two assumptions:

- Even though the band gap is different, the electronic affinity (χ) will be the same for both thicknesses (being InSe both of them, contrary when different materials are used).
- The electronic difference between thicknesses will be produced by the different band gaps due to the change by quantum confinement, added to the fact that the thinner area (higher band gap) will sustract carriers to the thicker one (smaller band gap). However, this carrier difference consideration is no specially relevant for the qualitative explanation due to its lesser contribution.

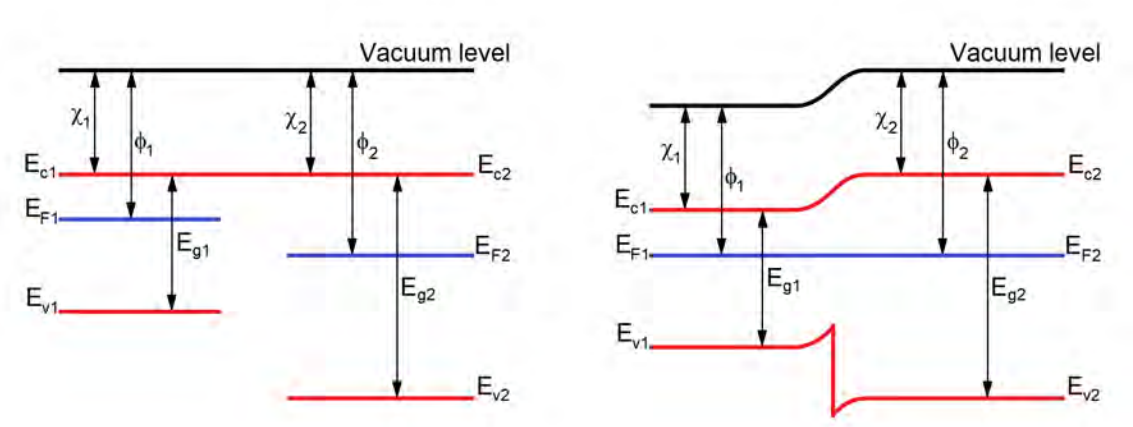

Figure 3.9: Band structure alignment of different InSe thickness nanosheets.

After the Fermi level alignment the electrons do not observe a difference between positive and negative bias (having, therefore, a carrier current J_e equal for both biases), but in the valence band a barrier appears, having holes accumulation for positive bias ($J_h = 0$) and free-pass for negative bias ($J_h \neq 0$). This qualitative behavior matches the measurements previously described.

3.2.2.2 Kelvin Probe microscopy on ITO

In the previous subsection, multiterraced InSe nanosheets have been proved to behave as a planar electrical n - n^+ heterojunction due to the band structure alignment of different InSe thicknesses and the inner-barrier between them. However, in order to theoretically explain this band alignment, χ, directly related with the work function (ϕ), has been considered equal regardless the thickness. This assumption, although valid for thicker samples, is not expected to remain in thinner nanosheets.

Just as a change in the band structure has been demonstrated by quantum confinement, theoretically [184, 181] and experimentally, e.g., via PL measurements [125, 208, 334], a change in ϕ is expected by reducing the thickness of the samples for the same reasons. Density functional theory (DFT) calculations have been presented about the dependance with thickness in β-InSe [183], but no experimental nor theoretical dependance study has been found in the bibliography about γ-InSe and the thickness of the nanosheets.

In order to modelise prior to develop optoelectronic devices where the electrical contacts between different materials is involved this is a necessary value to consider. From the behavior with the metalic contacts [190, 188] or to simulate the carrier transport between materials in contact, ϕ is the value which determine the junction type to expect [189, 98].

In this subsection, the electrical properties, specifically ϕ, for different InSe thicknesses will be measured via Kelvin Prove microscopy and compared with DFT calculations for γ-InSe different thicknesses.

InSe nanosheets have been exfoliated on ITO substrates (see Subsections 2.1.1 and 2.1.2) and topography and KP measurements have been taken (Subsection 2.3.2 for more details) in collaboration with Dra. Ana Cros-Stotter. RT PL measurements have been measured for every nanosheet to confirm AFM topography measurement thicknesses [334].

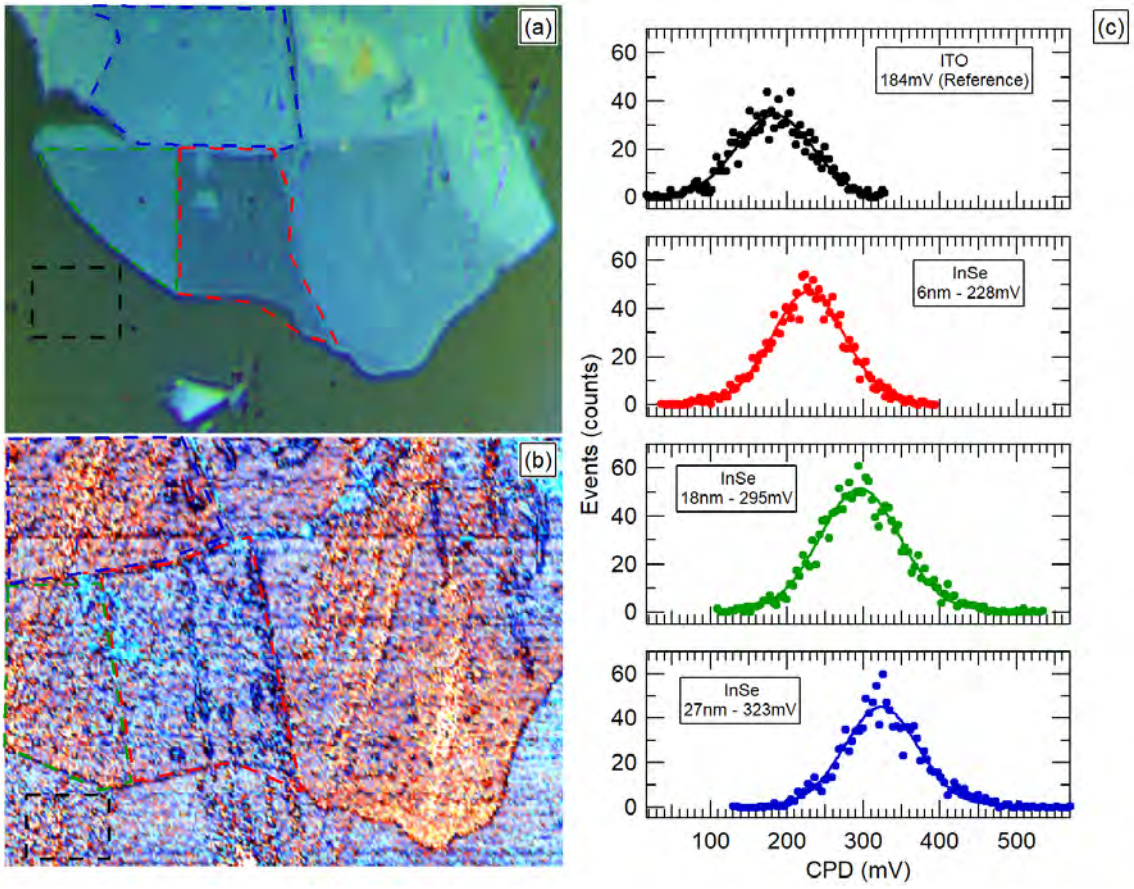

Figure 3.10: KPFM measurements in semibulk InSe nanosheet: optical image (a) and KPFM map (b), highlighting with different dashed lines the averaged areas shown on the right CPD curves for every different thickness.

Figure 3.10 and 3.11 show the KP results on different InSe thicknesses. Optical images (Figures 3.10a and 3.11a) can be compared with KP maps (Figures 3.10b and 3.11b), observing different behavior due to the multiterraced thicknesses. In every area (marked with dashed lines), average contact potencial difference (CPD) between the sample and the tip is shown on the right in both figures (for more details, see Subsection 2.3.2), observing a shift to lower CPD when the thickness is reduced.

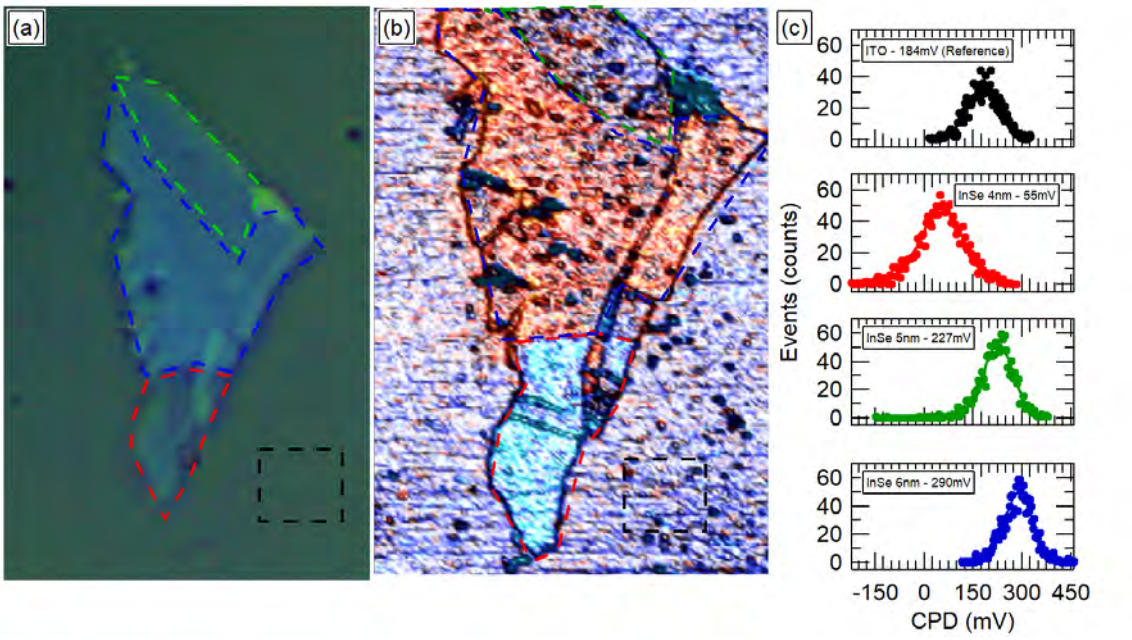

Figure 3.11: KPFM measurements in a thinner InSe nanosheet: optical image (a) and KPFM map (b), highlighting with different dashed lines the averaged areas shown on the right CPD curves for every different thickness.

By using the CPD signal of ITO and taking the ϕ of ITO as a value of reference (4.65 eV) [191, 193, 192] we have obtained the thickness dependence of the InSe ϕ shown in Figure 3.12. These results reveal that the ϕ value of 2D InSe as thin as 6-7 layers is that of bulk InSe. For thinner layers, the ϕ tends to increase. To understand these results, we have calculated the thickness dependence of the electron affinity and bandgap of InSe. These calculations have been performed by Dr. Alejandro Molina using Quantum Expresso [187]. The local density approximation including spin-orbit interaction with spinorial wave functions was used, with norm-conserving full relativistic pseudopotentials [186]. A slab model with a 20 Å vacuum thickness has been used to avoid interactions between periodic images. Ab-initio calculations have been corrected taking into account the well-known underestimation from DFT calculations in semiconductor band gaps, using the $\chi = 4.55$ InSe bulk value measured as reference to locate the conduction band reported for volumic InSe [212, 185, 175, 174].

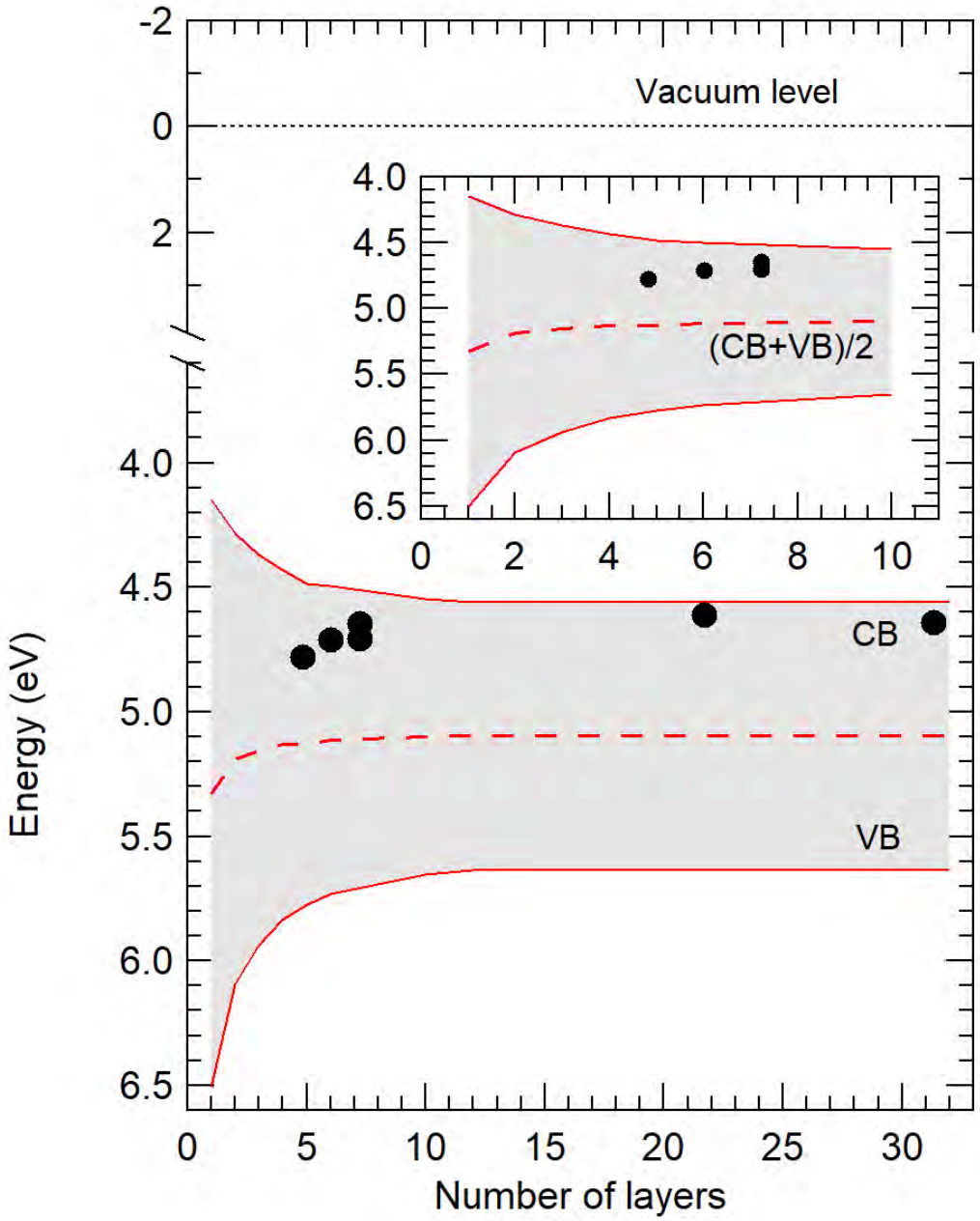

Figure 3.12: Work function (ϕ) in different InSe thicknesses measured via KPFM compared with DFT calculations for the valence band (VB) and the conduction band (CB).

From these results, one can estimate the thickness dependence of the ϕ of InSe, that may be approximated by $(E_c+E_v)/2$, as would correspond to intrinsic InSe. From this analysis, it seems that the ϕ of 2D InSe tends to remain practically unaltered in the range of thicknesses explored here, altough at the lower thicknesses explored,

the blueshift of the InSe bandgap tends to start to increase the ϕ of InSe, although the electron affinity appeared to decrease.

3.2.3 Application in sensing

Once the electrical properties of InSe have been studied, in this subsection an application will be presented using this material, in this case, using its change in its optical properties. 2D semiconductors are great candidates to be applied in gas sensing. The surface - to - volume ratio in this materials [101, 349, 100, 98], due to their laminar morphology, is ideal in order to react with particles suspended in air, which will change drastically the properties of the semiconductor [102, 110, 109]. Comparing the properties before and after the exposure to the gas could be a method to identify presence and conditions of different gases.

Due to the high reactivity in air of the Se radicals [105] and its always direct band gap (which makes all nanosheets thicknesses appliable), InSe is a promising candidate for these purposes, taking into account that the radicals S and N, similar in structure with Se radicals present in InSe, are quite present in different situations, such as batteries malfunction [106], organic decomposition [97, 103] or bombs detection [96]. In this subchapter different 2D thicknesses of InSe will be exposed to different concentrations, times and different gases and the PL intensity change will be studied.

Three different solutions (prepared by Dr. Rafael Abargues-Lopez and Eduardo Aznar-Gadea) will be analysed:

1. Pure 2-mercaptoethanol (2-MET $>$ 99%, Sigma Aldrich).
2. Pure 3-nitrotoluene (3-NT 99%, Sigma Aldrich).
3. 2-MET 0.1M solution in water (using 0.7813 g of pure 2-MET adding 100 mL of water).

2-MET has been chosen due to the presence of a S radical, quite common in the descomposition of organic matter (aiming for applications, e.g., in food industry [97, 103]) as one of the most reactive gases in this family. 3-NT, on the other hand, represents a N radical, being 3-NT interesting, for instance, in safety applications to detect traces of bombs in air [96].

Although InSe is stable in air [99], in order to prevent as many exposition with air as possible, the whole experimental process for every sample will be performed in

the same day. First, InSe nanosheets will be exfoliated in Si/SiO_2 (285nm) and identified via OC (see Subsections 2.1.1 and 2.1.2). After that, μ-PL measurements will be taken to caracterise every sample before and after the gas exposition in a Horiba Xplora setup, described in Subsection 2.2.3 with a micrometric 532nm laser excitation.

The exposition to the gas will be performed attaching the substrate bottom-up to the bottom of the lid covering the solution to be studied, leaving the substrate faced-down exposed directly to the previously over-exposed solution for the desired time. Figure 3.13 collects the results after several samples in different conditions, gases and exposition times, showing the average in any case.

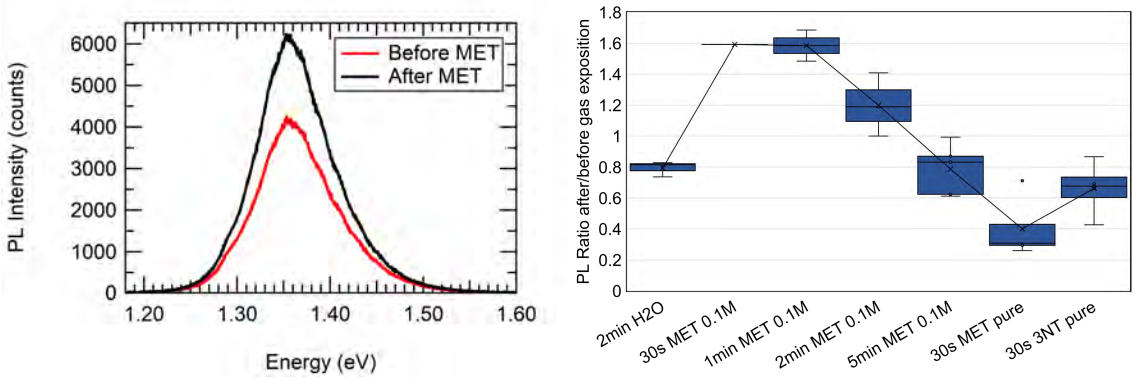

Figure 3.13: Gas sensing with InSe. (a) Example in a PL spectra before and after the exposition to 2-MET after 30s, (b) Ratio PL intensity after / before exposition to a gas. Error bars due to the different samples measured in the same conditions.

In Figure 3.13b two different situations can be observed: at the beginning, the PL intensity increases due to the fact that the gas is going to localise the Se defects in the InSe surface [108, 104, 107], promoting electron-hole interaction and therefore, the PL emission. However, increasing that exposition (more time or concentration), the gas will be forced to penetrate inside the material, hampering that PL.

Also can be observed that longer exposition times for the low-concentration gases produce the same effect as smaller times for the pure gas. Besides, 2-MET solutions are more reactive than 3-NT. Finally, it has been analysed the effect of highly saturated H_2O enviroments, producing a slight decrease in PL, which should be taken into account for longer exposition times.

The different behavior between semi-bulk samples and thinner ones will be shown in Figure 3.14. Due to the surface - to - volume ratio difference, in thinner samples

the reactivity will be larger compared with their volumic counterparts, as the effect in their PL will increase. For this Figure, it has been chosen as a limit between thin and semi-volumic samples a PL peak emission in 1.35eV. When the ratio drops to zero, no sample has been measured for that specific range of thicknesses, gas concentration and time.

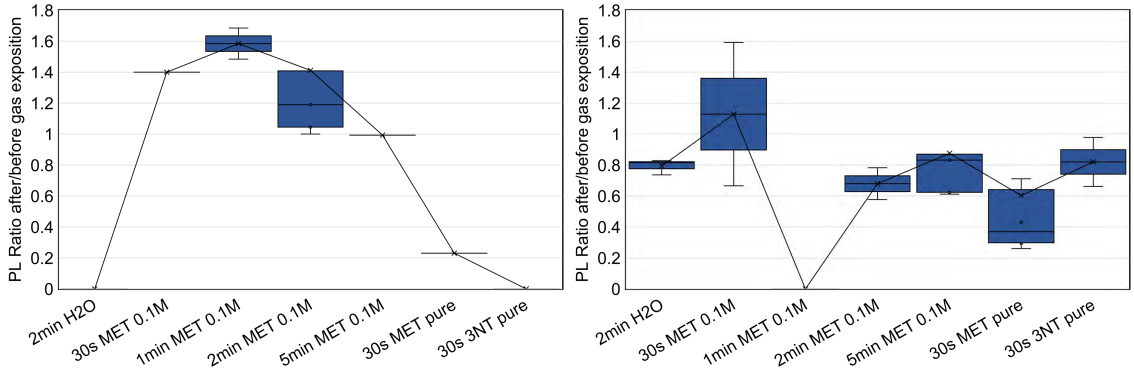

Figure 3.14: Gas sensing with InSe. Ratio PL intensity after / before exposition to a gas for semi-volumic samples (a) and for thinner nanosheets (b).

Finally, in some of the samples exposed, it has been observed a shift in the PL emission after the exposition to the gas. This fact can be explained because due to the reactivity of the surface to the molecules in air, with high concentrations or exposition times, the effective thickness of the sample could be reduced in one layer, considering the top layer completely bonded to the molecules in air, obtaining a shift in the PL emission of the resulting nanosheet. More measurements and samples are needed to corroborate this fact.

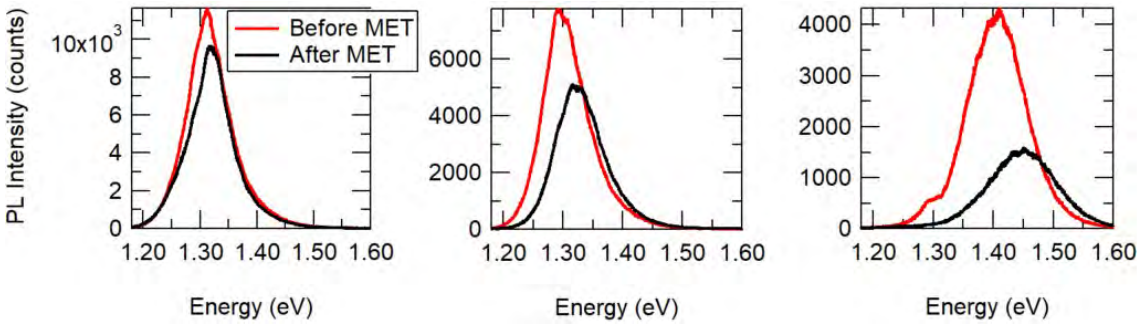

Figure 3.15: Gas sensing with InSe. Shift produced after the exposition to the gas in three different samples.

3.3 Conclusions

In this Chapter, the potential of III - VI semiconductors for optoelectronic applications have been shown. However, in both cases, GaSe and InSe, some of their properties are hampered due to its nature.

In GaSe, experimental results reported here and in the literature demonstrated the wide optical band gap can be tuned due to quantum confinement effects up to the ultraviolet. However, GaSe nanosheets are unstable in air, and the oxidation processes and its behavior is explored. This issue can be solved via encapsulation of the freshly-exfoliated GaSe nanosheets, as demonstrated in literature.

In InSe, the relatively unknown electrical properties in its bidimensional state have been explored. However, the reported OP dipole, contrary to the usual vertical excitation - vertical collection scientific approach hampers its usage, which will be studied in the following Chapters.

Concerning the electrical properties in InSe nanosheets, the I - V characteristic curves have been measured in homogeneous and layered InSe exfoliated samples obtaining a different behavior using positive and negative bias: symmetric in homogeneous ones and asymmetric in layered samples. This asymmetry is similar to the obtained in p - n heterojunction photodiode behavior, matching the n - n^+ heterojunction produced in multiterraced nanosheets due to the difference in its band gap. With a more detailed excitation system several conclusions have been obtained that point to the existence of an intrinsic inner-barrier in the layered samples due to the thickness (and, therefore, band gap) difference. This barrier is theoretically understood taking into account some assumptions, where the result is the appearance of a barrier in the valence band, explaining all the conclusions obtained in the previous measurements. Therefore, the usage of multiterraced InSe nanosheets have been demonstrated as heterojunction, adding the absence of defects in the junction.

However, one of the previous assumptions concerns a constant χ when the thickness change, assumption valid for semibulk thicknesses, but not expected in thinner ones. A related magnitude, ϕ, has been studied varying the thickness in different InSe nanosheets, obtaining a dependance with thickness following the trend calculated via DFT. Further analysis is needed to relate cuantitatively these two magnitudes with the carrier concentration in each nanosheet, which influence the location of the Fermi energy in each case.

Finally, an application using the optical properties of InSe has been presented. A change in the PL in exfoliated InSe nanosheets has been observed in presence of different gases due to the reactivity of surface exfoliated Se free radicals in InSe. 3-MET and 3NT as a S and N radical example, respectively, have been exposed to freshly exfoliated nanosheets. At lower concentrations and exposition times, the gas bonds and localise Se defects on the surface of the nanosheets, enhancing its PL. However, at higher concentration or exposition times, this molecules get embedded in the material, hampering its PL.

This effect is enhanced in thinner nanosheets due to its surface - to - volume ratio, more important compared with thicker ones. Lastly, in a few samples, a PL shift has been detected after the exposition to the gas, matching the shift expected when a layer is reduced due to quantum confinement. Further measurements must be performed to verify this effect. The data presented demonstrate InSe nanosheets as thin film gas detectors, which can be measured directly with its PL change.

Bibliography

[95] Joel I.Jan Wang, Yafang Yang, Yu An Chen, Kenji Watanabe, Takashi Taniguchi, Hugh O.H. Churchill, and Pablo Jarillo-Herrero. Electronic transport of encapsulated graphene and WSe2 devices fabricated by pick-up of prepatterned hBN. *Nano Letters*, 15(3):1898–1903, 2015.

[96] Joel B. Miller and Geoffrey A. Barrall. Explosives detection with nuclear quadrupole resonance: An emerging technology will help to uncover land mines and terrorist bombs. *American Scientist*, 93(1):50–57, 2005.

[97] William F. Taylor and Thomas J. Wallace. Kinetics of deposit formation from hydrocarbons: Effect of Trace Sulfur Compounds. *Industrial and Engineering Chemistry Product Research and Development*, 7(3):198–202, 1968.

[98] Chenhao Jin, Jonghwan Kim, Joonki Suh, Zhiwen Shi, Bin Chen, Xi Fan, Matthew Kam, Kenji Watanabe, Takashi Taniguchi, Sefaattin Tongay, Alex Zettl, Junqiao Wu, and Feng Wang. Interlayer electron-phonon coupling in WSe2/hBN heterostructures. *Nature Physics*, 13(2):127–131, 2017.

[99] O. Del Pozo-Zamudio, S. Schwarz, J. Klein, R. C. Schofield, E. a. Chekhovich, O. Ceylan, E. Margapoti, a. I. Dmitriev, G. V. Lashkarev, D. N. Borisenko, N. N. Kolesnikov, J. J. Finley, and a. I. Tartakovskii. Photoluminescence and Raman investigation of stability of InSe and GaSe thin films. *arXiv*, pages 1–6, 2015.

[100] L. C. Gomes, S. S. Alexandre, H. Chacham, and R. W. Nunes. Stability of edges and extended defects on boron nitride and graphene monolayers: The role of chemical environment. *Journal of Physical Chemistry C*, 117(22):11770–11779, 2013.

[101] Ying ying Wang, Zhen hua Ni, Ting Yu, Ze Xiang Shen, Hao min Wang, Yi hong Wu, Wei Chen, and Andrew Thye Shen Wee. Raman Studies of Monolayer Graphene: The Substrate Effect. *Journal of Physical Chemistry C*, 112(29):10637–10640, 2008.

[102] Kian Ping Loh, Qiaoliang Bao, Goki Eda, and Manish Chhowalla. Graphene oxide as a chemically tunable platform for optical applications. *Nature Publishing Group*, 2(12):1015–1024, 2010.

[103] William E. Haines, Glenn L. Cook, and John S. Ball. Gaseous Decomposi-

tion Products Formed by the Action of Light on Organic Sulfur Compounds. *Journal of the American Chemical Society*, 78(20):5213–5215, 1956.

[104] K. J. Xiao, A. Carvalho, and A. H. Castro Neto. Defects and oxidation resilience in InSe. *Physical Review B*, 96(5):1–8, 2017.

[105] Claude Paulmier. *Selenium Reagents and Intermediates in Organic Synthesis.* 1986.

[106] Qiang Wang, Jianming Zheng, Eric Walter, Huilin Pan, Dongping Lv, Pengjian Zuo, Honghao Chen, Z. Daniel Deng, Bor Yann Liaw, Xiqian Yu, Xiaoqing Yang, Ji Guang Zhang, Jun Liu, and Jie Xiao. Direct observation of sulfur radicals as reaction media in Lithium sulfur batteries. *Journal of the Electrochemical Society*, 162(3):A474–A478, 2015.

[107] O. A. Balitskii, R. V. Lutsiv, V. P. Savchyn, and J. M. Stakhira. Thermal oxidation of cleft surface of InSe single crystal. *Materials Science and Engineering B*, 56 B56(1):5–10, 1998.

[108] A. Politano, G. Chiarello, R. Samnakay, G. Liu, B. Gürbulak, S. Duman, A. A. Balandin, and D. W. Boukhvalov. The influence of chemical reactivity of surface defects on ambient-stable InSe-based nanodevices. *Nanoscale*, 8(16):8474–8479, 2016.

[109] Beibei Zhan, Chen Li, Jun Yang, Gareth Jenkins, Wei Huang, and Xiaochen Dong. Graphene Field-Effect Transistor and Its Application for Electronic Sensing. *Small*, (20):4042–4065, 2014.

[110] Ming Zhou, Yueming Zhai, and Shaojun Dong. Electrochemical Sensing and Biosensing Platform Based on Chemically Reduced Graphene Oxide. *Anal. Chem.*, 81(14):5603–5613, 2009.

[111] Chengzhou Zhu and Shaojun Dong. Energetic Graphene-Based Electrochemical Analytical Devices in Nucleic Acid , Protein and Cancer Diagnostics and Detection. *Electroanalysis Review*, pages 14–29, 2014.

[112] Mauro Brotons-Gisbert, Raphaël Proux, Raphaël Picard, Daniel Andres-Penares, Artur Branny, Alejandro Molina-Sánchez, Juan F. Sánchez-Royo, and Brian D. Gerardot. Out-of-plane orientation of luminescent excitons in atomically thin indium selenide flakes. *Nature Communications*, (2019):1–10, 2019.

[113] S. Schwarz, S. Dufferwiel, P. M. Walker, F. Withers, A. A P Trichet, M. Sich, F. Li, E. A. Chekhovich, D. N. Borisenko, N. N. Kolesnikov, K. S. Novoselov, M. S. Skolnick, J. M. Smith, D. N. Krizhanovskii, and A. I. Tartakovskii. Two-dimensional metal-chalcogenide films in tunable optical microcavities. *Nano Letters*, 14(12):7003–7008, 2014.

[114] Kin Fai Mak, Changgu Lee, James Hone, Jie Shan, and Tony F. Heinz. Atomically thin MoS2: A new direct-gap semiconductor. *Physical Review Letters*, 105(13):2–5, 2010.

[115] Wonjae Kim, Changfeng Li, Ferney A. Chaves, David Jiménez, Raul D. Rodriguez, Jannatul Susoma, Matthias A. Fenner, Harri Lipsanen, and Juha Riikonen. Tunable Graphene-GaSe Dual Heterojunction Device. *Advanced Materials*, 28(9):1845–1852, 2016.

[116] T. Siciliano, M. Tepore, A. Genga, G. Micocci, M. Siciliano, and A. Tepore. Thermal oxidation of amorphous GaSe thin films. *Vacuum*, 92:65–69, 2013.

[117] Rongtao Lu, Jianwei Liu, Hongfu Luo, Viktor Chikan, and Judy Z Wu. Graphene / GaSe-Nanosheet Hybrid: Towards High Gain and Fast Photoresponse. *Nature Publishing Group*, pages 1–7, 2016.

[118] Thomas E. Beechem, Brian M. Kowalski, Michael T. Brumbach, E Anthony, Catalin D. Spataru, Stephen W. Howell, Taisuke Ohta, Jesse A. Pask, Nikolai G. Kalugin, Anthony E. McDonald, Catalin D. Spataru, Stephen W. Howell, Taisuke Ohta, Jesse A. Pask, Nikolai G. Kalugin, E Anthony, Catalin D. Spataru, Stephen W. Howell, Taisuke Ohta, Jesse A. Pask, Nikolai G. Kalugin, Anthony E. McDonald, Catalin D. Spataru, Stephen W. Howell, Taisuke Ohta, Jesse A. Pask, and Nikolai G. Kalugin. Oxidation of ultrathin GaSe. *Applied Physics Letters*, 107(17):1–5, 2015.

[119] Wei Feng, Wei Zheng, Wenwu Cao, and PingAn Hu. Back Gated Multilayer InSe Transistors with Enhanced Carrier Mobilities via the Suppression of Carrier Scattering from a Dielectric Interface. *Advanced Materials*, 26(38):6587–6593, 2014.

[120] Pengke Li. Spin-Polarization Control in a Two-Dimensional Semiconductor. *Physical Review Applied*, 054007:1–7, 2016.

[121] Youbao Ni, Haixin Wu, Changbao Huang, Mingsheng Mao, Zhenyou Wang,

and Xudong Cheng. Growth and quality of gallium selenide (GaSe) crystals. *Journal of Crystal Growth*, 381:10–14, 2013.

[122] Yang Li, Xin Zhao, He Zhang, and Mingxin Li. GaSe saturable absorber for mode-locked Er-doped fiber laser. *Infrared Physics and Technology*, 2019.

[123] A. Castellanos-Gomez, N. Agrat, and G. Rubio-Bollinger. Optical identification of atomically thin dichalcogenide crystals. *Applied Physics Letters*, 96(21):2010–2012, 2010.

[124] Oriol Lopez-Sanchez, Dominik Lembke, Metin Kayci, Aleksandra Radenovic, and Andras Kis. Ultrasensitive photodetectors based on monolayer MoS2. *Nature Nanotechnology*, 8(7):497–501, 2013.

[125] Garry W. Mudd, Simon A. Svatek, Tianhang Ren, Amalia Patanè, Oleg Makarovsky, Laurence Eaves, Peter H. Beton, Zakhar D. Kovalyuk, George V. Lashkarev, Zakhar R. Kudrynskyi, and Alexandr I. Dmitriev. Tuning the bandgap of exfoliated InSe nanosheets by quantum confinement. *Advanced Materials*, 25(40):5714–5718, 2013.

[126] H. Ahmad, S. A. Reduan, A. S. Sharbirin, M. F. Ismail, and M. Z. Zulkifli. Q-switched thulium/holmium fiber laser with gallium selenide. *Optik*, 2018.

[127] Xu Zhou, Jingxin Cheng, Yubing Zhou, Ting Cao, Hao Hong, Zhimin Liao, Shiwei Wu, Hailin Peng, Kaihui Liu, and Dapeng Yu. Strong Second-Harmonic Generation in Atomic Layered GaSe. *Journal of the American Chemical Society*, 137(25):7994–7997, 2015.

[128] Sivacarendran Balendhran. Devices and systems based on two dimensional MoO3 and MoS2. *RMIT University*, 2013.

[129] Xufan Li, Ming-Wei Lin, Alexander Puretzky, Juan C Idrobo, Cheng Ma, Miaofang Chi, Mina Yoon, Christopher M Rouleau, Ivan I Kravchenko, David B Geohegan, and Kai Xiao. Controlled Vapor Phase Growth of Single Crystalline, Two-Dimensional GaSe Crystals with High Photoresponse. *Sci. Rep.*, 4:5497, 2014.

[130] Qinghua Zhao, Riccardo Frisenda, Patricia Gant, David Perez de Lara, Carmen Munuera, Mar Garcia-Hernandez, Yue Niu, Tao Wang, Wanqi Jie, and Andres Castellanos-Gomez. Toward Air Stability of Thin GaSe Devices: Avoiding Environmental and Laser-Induced Degradation by Encapsulation. *Advanced Functional Materials*, 2018.

[131] A. Segura, J. Bouvier, M.V. Andres, F.J. Manjon, and V. Munoz. Strong optical nonlinearities in gallium and indium selenides related to inter-valence-band transitions induced by light pulses. *Physical Review B*, 55(7):6981–4084, 1997.

[132] Sidong Lei, Fangfang Wen, Liehui Ge, Sina Najmaei, Antony George, Yongji Gong, Weilu Gao, Zehua Jin, Bo Li, Jun Lou, Junichiro Kono, Robert Vajtai, Pulickel Ajayan, and Naomi J. Halas. An atomically layered InSe avalanche photodetector. *Nano Letters*, 15(5):3048–3055, 2015.

[133] M. Brotons-Gisbert, J. F. Sánchez-Royo, and J. P. Martínez-Pastor. Thickness identification of atomically thin InSe nanoflakes on SiO2/Si substrates by optical contrast analysis. *Applied Surface Science*, 354(April):453–458, 2015.

[134] Andrea Splendiani, Liang Sun, Yuanbo Zhang, Tianshu Li, Jonghwan Kim, Chi Yung Chim, Giulia Galli, and Feng Wang. Emerging photoluminescence in monolayer MoS2. *Nano Letters*, 10(4):1271–1275, 2010.

[135] V. L. Cardetta, A. M. Mancini, and A. Rizzo. Melt growth of single crystal ingots of GaSe by Bridgman-Stockbarger's method. *Journal of Crystal Growth*, 16(2):183–185, 1972.

[136] B. Radisavljevic, A. Radenovic, J. Brivio, V. Giacometti, and A. Kis. Single-layer MoS2 transistors. *Nature nanotechnology*, 6(3):147–50, 2011.

[137] Juan F. Sánchez-Royo, Guillermo Muñoz-Matutano, Mauro Brotons-Gisbert, Juan P. Martínez-Pastor, Alfredo Segura, Andrés Cantarero, Rafael Mata, Josep Canet-Ferrer, Gerard Tobias, Enric Canadell, Jose Marqués-Hueso, and Brian D. Gerardot. Electronic structure, optical properties, and lattice dynamics in atomically thin indium selenide flakes. *Nano Research*, 7(10):1556–1568, 2014.

[138] Sukrit Sucharitakul, Nicholas J. Goble, U. Rajesh Kumar, Raman Sankar, Zachary A. Bogorad, Fang Cheng Chou, Yit Tsong Chen, and Xuan P A Gao. Intrinsic Electron Mobility Exceeding 10ˆ3 cmˆ2/(V s) in Multilayer InSe FETs. *Nano Letters*, 15(6):3815–3819, 2015.

[139] O A Balitskii, V P Savchyn, and V O Yukhymchuk. Raman investigation of InSe and GaSe single-crystals oxidation. *Semiconductor Science and Technology*, 17(2):L1–L4, 2002.

[140] Pingan Hu, Zhenzhong Wen, Lifeng Wang, Pingheng Tan, and Kai Xiao. Synthesis of few-layer GaSe nanosheets for high performance photodetectors. *ACS nano*, 6(7):5988–94, jul 2012.

[141] K.S. S Novoselov, A.K. K Geim, S.V. V Morozov, D Jiang, Y Zhang, S.V. V Dubonos, I.V. V Grigorieva, and A. A Firsov. Electric Field Effect in Atomically Thin Carbon Films. *Science*, 306(5696):666–669, 2004.

[142] Ch. Ferrer-Roca, J. Bouvier, A. Segura, M. V. Andres, and V. Munoz. Light-induced transmission nonlinearities in gallium selenide. *Journal of Applied Physics*, 85(7):3780, 1999.

[143] Daniel J. Terry, Viktor Zólyomi, Matthew Hamer, Anastasia V. Tyurnina, David G. Hopkinson, Alexander M. Rakowski, Samuel J. Magorrian, Nick Clark, Yuri M. Andreev, Olga Kazakova, Konstantin Novoselov, Sarah J. Haigh, Vladimir I. Fal'Ko, and Roman Gorbachev. Infrared-to-violet tunable optical activity in atomic films of GaSe, InSe, and their heterostructures. *2D Materials*, 2018.

[144] Wengang Luo, Yufei Cao, Pingan Hu, Kaiming Cai, Qi Feng, Faguang Yan, Tengfei Yan, Xinhui Zhang, and Kaiyou Wang. Gate Tuning of High-Performance InSe-Based Photodetectors Using Graphene Electrodes. *Advanced Optical Materials*, 3(10):1418–1423, 2015.

[145] Dattatray J. Late, Bin Liu, Jiajun Luo, Aiming Yan, H. S S Ramakrishna Matte, Matthew Grayson, C. N R Rao, and Vinayak P. Dravid. GaS and GaSe ultrathin layer transistors. *Advanced Materials*, 24(26):3549–3554, 2012.

[146] André K Geim and I V Grigorieva. Van der Waals heterostructures. *Nature*, 499(7459):419–25, 2013.

[147] E. Bringuier, A. Bourdon, N. Piccioli, and A. Chevy. Optical second-harmonic generation in lossy media: Application to GaSe and InSe. *Physical Review B*, 49(24):16971–16982, 1994.

[148] Mahito Yamamoto, Sudipta Dutta, Shinya Aikawa, and Shu Nakaharai. Self-Limiting Layer-by-Layer Oxidation of Atomically Thin WSe2. *Nano Letters*, 2015.

[149] Mauro Brotons-Gisbert, Daniel Andres-Penares, Joonki Suh, Francisco Hidalgo, Rafael Abargues, Pedro J. Rodríguez-Cantó, Alfredo Segura, Ana Cros,

Gerard Tobias, Enric Canadell, Pablo Ordejón, Junqiao Wu, Juan P. Martínez-Pastor, and Juan F. Sánchez-Royo. Nanotexturing To Enhance Photoluminescent Response of Atomically Thin Indium Selenide with Highly Tunable Band Gap. *Nano Letters*, 16(5):3221–3229, 2016.

[150] J. Riera, A. Segura, and A. Chevy. Photoluminescence in silicon-doped n-indium selenide. *physica status solidi (a)*, 1994.

[151] P. Gomes Da Costa, R. G. Dandrea, R. F. Wallis, and M. Balkanski. First-principles study of the electronic structure of gamma-InSe and beta-InSe. *Physical Review B*, 1993.

[152] H. Kressel and H. F. Lockwood. Lasing transitions in p+-n-n+(AlGa) assingle bond signGa As heterojunction lasers. *Applied Physics Letters*, 20(4):175–177, 1972.

[153] Shinichiro Mouri, Yuhei Miyauchi, and Kazunari Matsuda. Tunable photoluminescence of monolayer MoS2 via chemical doping. *Nano Letters*, 13(12):5944–5948, 2013.

[154] E. Kress-Rogers, R. J. Nicholas, J. C. Portal, and A. Chevy. Cyclotron resonance studies on bulk and two-dimensional conduction electrons in InSe. *Solid State Communications*, 1982.

[155] A. Segura, F. Pomer, A. Cantarero, W. Krause, and A. Chevy. Electron scattering mechanisms in n-type indium selenide. *Physical Review B*, 1984.

[156] J. Camassel, P. Merle, H. Mathieu, and A. Chevy. Excitonic absorption edge of indium selenide. *Physical Review B*, 1978.

[157] Hiromichi Ohta, Masahiro Hirano, Ken Nakahara, Hideaki Maruta, Tetsuhiro Tanabe, Masao Kamiya, Toshio Kamiya, and Hideo Hosono. Fabrication and photoresponse of a pn-heterojunction diode composed of transparent oxide semiconductors, p-NiO and n-ZnO. *Applied Physics Letters*, 83(5):1029–1031, 2003.

[158] Ch Ferrer-Roca, A. Segura, M. Andrés, J. Pellicer, and V. Muñoz. Investigation of nitrogen-related acceptor centers in indium selenide by means of photoluminescence: Determination of the hole effective mass. *Physical Review B - Condensed Matter and Materials Physics*, 1997.

[159] S. Kumar, A. Kaczmarczyk, and B. D. Gerardot. Strain-Induced Spatial and

Spectral Isolation of Quantum Emitters in Mono- and Bilayer WSe2. *Nano Letters*, 15(11):7567–7573, 2015.

[160] S. Shigetomi and T. Ikari. Electrical and optical properties of n- and p-InSe doped with Sn and As. *Journal of Applied Physics*, 2003.

[161] Masanobu Izaki, Tsutomu Shinagawa, Ko Taro Mizuno, Yuya Ida, Minoru Inaba, and Akimasa Tasaka. Electrochemically constructed p-Cu2O/n-ZnO heterojunction diode for photovoltaic device. *Journal of Physics D: Applied Physics*, 2007.

[162] G. Micocci, A. Tepore, R. Rella, and P. Siciliano. Investigation of deep levels in Zn-doped InSe single crystals. *Journal of Applied Physics*, 1992.

[163] D. Olguín, A. Cantarero, C. Ulrich, and K. Syassen. Effect of pressure on structural properties and energy band gaps of γ-InSe. In *Physica Status Solidi (B) Basic Research*, 2003.

[164] C. Ulrich, D. Olguin, A. Cantarero, A. R. Goñi, K. Syassen, and A. Chevy. Effect of pressure on direct optical transitions of γ-InSe. *Physica Status Solidi (B) Basic Research*, 2000.

[165] Philipp Tonndorf, Robert Schmidt, Philipp Böttger, Xiao Zhang, Janna Börner, Andreas Liebig, Manfred Albrecht, Christian Kloc, Ovidiu Gordan, Dietrich R. T. Zahn, Steffen Michaelis de Vasconcellos, and Rudolf Bratschitsch. Photoluminescence emission and Raman response of monolayer MoS2, MoSe2, and WSe2. *Advanced Materials*, 29(33):4908–4916, 2017.

[166] Deep Jariwala, Vinod K. Sangwan, Chung Chiang Wu, Pradyumna L. Prabhumirashi, Michael L. Geier, Tobin J. Marks, Lincoln J. Lauhon, and Mark C. Hersam. Gate-tunable carbon nanotube-MoS2 heterojunction p-n diode. *Proceedings of the National Academy of Sciences of the United States of America*, 110(45):18076–18080, 2013.

[167] Sang Woon Lee, Yun Seog Lee, Jaeyeong Heo, Sin Cheng Siah, Danny Chua, Riley E. Brandt, Sang Bok Kim, Jonathan P. Mailoa, Tonio Buonassisi, and Roy G. Gordon. Improved Cu2O-based solar cells using atomic layer deposition to control the Cu oxidation state at the p-n junction. *Advanced Energy Materials*, 2014.

[168] Robert Schmidt, Iris Niehues, Robert Schneider, Matthias Drüppel, Thorsten Deilmann, Michael Rohlfing, Steffen Michaelis De Vasconcellos, Andres

Castellanos-Gomez, and Rudolf Bratschitsch. Reversible uniaxial strain tuning in atomically thin WSe2. *2D Materials*, 3(2):2–9, 2016.

[169] J. Rigoult, A. Rimsky, and A. Kuhn. Refinement of the 3R gamma-indium monoselenide structure type. *Acta Crystallographica Section B Structural Crystallography and Crystal Chemistry*, 1980.

[170] R. People, K. W. Wecht, K. Alavi, and A. Y. Cho. Measurement of the conduction-band discontinuity of molecular beam epitaxial grown In0.52Al0.48As/In0.53Ga0.47As, N-n heterojunction by C-V profiling. *Applied Physics Letters*, 43(1):118–120, 1983.

[171] Rui Cheng, Dehui Li, Hailong Zhou, Chen Wang, Anxiang Yin, Shan Jiang, Yuan Liu, Yu Chen, Yu Huang, and Xiangfeng Duan. Electroluminescence and photocurrent generation from atomically sharp WSe2/MoS2 heterojunction p-n diodes. *Nano Letters*, 2014.

[172] J. F. Sánchez-Royo, J. Pellicer-Porres, A. Segura, S. J. Gilliland, J. Avila, M. C. Asensio, O. Safonova, M. Izquierdo, and A. Chevy. Buildup and structure of the InSe Pt interface studied by angle-resolved photoemission and x-ray absorption spectroscopy. *Physical Review B - Condensed Matter and Materials Physics*, 2006.

[173] Mahmut Tosun, Deyi Fu, Sujay B. Desai, Changhyun Ko, Jeong Seuk Kang, Der Hsien Lien, Mohammad Najmzadeh, Sefaattin Tongay, Junqiao Wu, and Ali Javey. MoS2 heterojunctions by thickness modulation. *Scientific Reports*, 2015.

[174] O. Lang, C. Pettenkofer, J. F. Sánchez-Royo, A. Segura, A. Klein, and W. Jaegermann. Thin film growth and band lineup of In2O3 on the layered semiconductor InSe. *Journal of Applied Physics*, 1999.

[175] O. Lang, A. Klein, C. Pettenkofer, W. Jaegermann, and A. Chevy. Band lineup of lattice mismatched InSe/GaSe quantum well structures prepared by van der Waals epitaxy: Absence of interfacial dipoles. *Journal of Applied Physics*, 1996.

[176] I. M. Catalano, A. Cingolani, C. Calí, and S. Riva-Sanseverino. Second harmonic generation in InSe. *Solid State Communications*, 1979.

[177] J P Donnelly, D Ph, A G Milnes, D Sc, and C Eng. Current / voltage

characteristics of p-n Ge-Si and Ge-GaAs heterojunctions. *Proc. IEE*, 113(9), 1966.

[178] K Tomizawa, Y Awano, N Hashizume, and F Suzuki. Monte carlo simulation of GaAs submicron n+-n-n+ diode with GaAlAs heterojunction cathode. *Electronics Letters*, 18(25):17–19, 1982.

[179] S. S. Perlman and D. L. Feucht. P-N Heterojunctions. *Solid State Electronics*, 7(12):911–923, 1964.

[180] Shailendra Kumar, Tapas Ganguli, Pijush Bhattacharya, U. N. Roy, S. S. Chandvankar, and B. M. Arora. Surface photovoltage spectroscopy of n-n+ and p-n+ AlGaAs/GaAs heterojunctions. *Applied Physics Letters*, 72(23):3020–3022, 1998.

[181] Zeyuan Ni, Emi Minamitani, Yasunobu Ando, and Satoshi Watanabe. The electronic structure of quasi-free-standing germanene on monolayer MX (M = Ga, In; X = S, Se, Te). *Physical Chemistry Chemical Physics*, 2015.

[182] Garry W. Mudd, Simon A. Svatek, Lee Hague, Oleg Makarovsky, Zakhar R. Kudrynskyi, Christopher J. Mellor, Peter H. Beton, Laurence Eaves, Kostya S. Novoselov, Zakhar D. Kovalyuk, Evgeny E. Vdovin, Alex J. Marsden, Neil R. Wilson, and Amalia Patanè. High Broad-Band Photoresponsivity of Mechanically Formed InSe-Graphene van der Waals Heterostructures. *Advanced Materials*, 2015.

[183] David K. Sang, Huide Wang, Meng Qiu, Rui Cao, Zhinan Guo, Jinlai Zhao, Yu Li, Quanlan Xiao, Dianyuan Fan, and Han Zhang. Two dimensional beta-InSe with layer-dependent properties: Band alignment, work function and optical properties. *Nanomaterials*, 9(1), 2019.

[184] Daniel Olguín, Alberto Rubio-Ponce, and Andrés Cantarero. Ab initio electronic band structure study of III-VI layered semiconductors. *European Physical Journal B*, 2013.

[185] Yuzheng Guo and John Robertson. Band structure, band offsets, substitutional doping, and Schottky barriers of bulk and monolayer InSe. *Physical Review Materials*, 2017.

[186] D. R. Hamann. Optimized norm-conserving Vanderbilt pseudopotentials. *Physical Review B - Condensed Matter and Materials Physics*, 2013.

[187] Paolo Giannozzi, Stefano Baroni, Nicola Bonini, Matteo Calandra, Roberto Car, Carlo Cavazzoni, Davide Ceresoli, Guido L. Chiarotti, Matteo Cococcioni, Ismaila Dabo, Andrea Dal Corso, Stefano De Gironcoli, Stefano Fabris, Guido Fratesi, Ralph Gebauer, Uwe Gerstmann, Christos Gougoussis, Anton Kokalj, Michele Lazzeri, Layla Martin-Samos, Nicola Marzari, Francesco Mauri, Riccardo Mazzarello, Stefano Paolini, Alfredo Pasquarello, Lorenzo Paulatto, Carlo Sbraccia, Sandro Scandolo, Gabriele Sclauzero, Ari P. Seitsonen, Alexander Smogunov, Paolo Umari, and Renata M. Wentzcovitch. QUANTUM ESPRESSO: A modular and open-source software project for quantum simulations of materials. *Journal of Physics Condensed Matter*, 2009.

[188] R Mamy, X Zaoui, J Barrau, A Chevy, R Mamy, X Zaoui, J Barrau, A Chevy Au, and Inse Schottky. Au / InSe Schottky barrier height determination To cite this version : Au / InSe Schottky. *Revue de physique appliquee*, 25(9):947–950, 1990.

[189] Juan P. Martínez-Pastor, A Segura, J L Valdés, and A Chevy. Electrical and photovoltaic properties of indium tin oxide / p-InSe / Au solar cells. *Journal of Applied Physics*, 1477(1987):1477–1483, 2013.

[190] X Zaoui and A Mamy, RChevy. Au/InSe Interface formation: a photoemission study. *Surface Science*, 204, 1988.

[191] Y. Park, V. Choong, Y. Gao, B. R. Hsieh, and C. W. Tang. Work function of indium tin oxide transparent conductor measured by photoelectron spectroscopy. *Applied Physics Letters*, 68(19):2699–2701, 1996.

[192] M. M. Beerbom, B. Lägel, A. J. Cascio, B. V. Doran, and R. Schlaf. Direct comparison of photoemission spectroscopy and in situ Kelvin probe work function measurements on indium tin oxide films. *Journal of Electron Spectroscopy and Related Phenomena*, 152(1-2):12–17, 2006.

[193] J.S. Kim, B. Lagel, E. Moons, N. Johansson, I.D. Baikie, W.R. Salaneck, R.H. Friend, and F. Cacialli. Kelvin probe and ultraviolet photoemission measurements of indium tin oxide work function: a comparison. *Synthetic Metals*, 111:311–314, 2000.

4 Microspherical resonators and two-dimensional semiconductors

PL emission and light emission management in 2D semiconductors is a major matter for the implementation of optoelectronic and photonic applications. In this sense, several strategies have been considered in order to enhance and tune light emission of 2D semiconductors for a specific device. In this chapter, SiO_2 microspheres deposited on top of exfoliated 2D nanosheets have been used to enhance the PL of III - VI 2D semiconductors by means of the whispering gallery modes (WGM) in the microspheres as well as to obtain a fine-tuning of the PL peak wavelength in TMDs, as another degree of freedom for photonic applications, by varying the microsphere diameter. Besides these advantages, microspheres produce an effective lensing effect of the incident laser beam that increases the excitation power density and hence PL intensity on the observation area of the 2D semiconductor, without any change in the laser setup used in the experiment added to a reverse lensing in collection. More relevant is the coupling between the microspheres and the dipole of the 2D semiconductor. Particularly, the OP dipolar behavior in InSe is clearly revealed by its PL enhancement effect, as compared to the case of TMDs where neutral and charged exciton to are characterised by IP and OP dipoles, respectively.

4.1 Introduction

2D materials have attracted the scientific community attention since the appearance of graphene [322]. Several physical properties such as mechanical strength and flexibility [228], on/off current ratio, high mobility [220] and a band gap tunability [227] due to quantum confinement make them excellent candidates for next generation applications in many fields, highlighting optoelectronics [201, 203, 238, 223], spintronics [231, 194, 202] and valleytronics [221, 213], among others. These properties

have been the focus for the growing interest in recent years on 2D materials. The zero band gap in graphene hampers its applications in optoelectronic and photonic devices and this was what motivated the study of other 2D materials with finite energy band gap, i.e., 2D semiconductors.

On one hand, semiconducting TMDs such as MoS_2, WS_2, $MoSe_2$ and WSe_2 proved themselves as the first suitable candidates overcoming that issue [234, 326, 225, 232]. Due to the indirect to direct transition in their band structure [333] from few-layer to the monolayer, TMDs have demonstrated high absorption coefficient and emission efficiency, especially under vertical excitation – vertical collection (backscattering) configuration, due to their excitonic IP dipolar behavior [297], the optimal dipole orientation for a vertical excitation. However, in optoelectronic applications, only ML is used, with a fixed PL wavelength emission. That is the reason why procedures like strain [195, 199], chemical doping [217] or the transfer onto different refractive index substrates have been used to provide for some tunability of the PL spectrum, needed in some applications. Multilayered substrates such as distributed Bragg reflectors (DBR) [200] or photonic nanocavities [229, 235, 300] have been demonstrated to optimize the PL intensity for different TMD MLs.

On the other hand, III - VI layered materials such as InSe and GaSe also show potential applications for next generation electronics and optoelectronics due to their suitable band gap tunability [208, 334, 410, 198] (see Chapter 3). However, the recently demonstrated excitonic out-of-plane (OP) dipolar behavior of InSe [297] is the origin of the reduced absorption coefficient of monochalcogenides and therefore, their quite low PL intensity in the vertical excitation – vertical collection configuration, as compared to 2D TMDs.

In this chapter, SiO_2 microspheres have been deposited on top of exfoliated 2D or near-2D nanosheets semiconductors, WSe_2 and InSe, respectively, to overcome both issues: whispering gallery modes (WGM) in the microspheres can be used to enhance PL emission of III-VI semiconductors due to the coupling of these modes to their OP dipole and to obtain a fine-tuning in the emission of TMDs as another degree of freedom varying the microsphere diameter. Besides, an effective excitation and collection lensing effect appeared in both of them, increasing the excitation power to the sample and, therefore, the final PL emission. Finally, the dipolar behavior in InSe is demonstrated as OP, where an IP nature in the neutral exciton X^0 and an OP behavior for the charged exciton X^+ is demonstrated for WSe_2 ML due to the

different coupling and resonance intensity with the tangential propagation nature of the WGMs in the microspheres.

4.2 Applications in III-VI for enhancement

InSe and WSe_2 2D nanosheets have been micromechanically exfoliated using the well-known scotch-tape technique (see Subsection 2.1.1 and Appendix A). SiO_2 microspheres solved in H_2O (from Sigma – Aldrich) have been used, with a nominal 5μm diameter (4.83 ± 0.19 μm). In order to have a sparse concentration of these microspheres in solution, different aliquots in ethanol were prepared, and dropped onto the exfoliated substrates via spin coating, after which high vacuum is applied to force evaporation and avoid H_2O residues. In the case of WSe_2 ML nanosheets, microspheres in their surroundings were shoved until precisely placed on top of the nanosheets, by using a tip probe attached to the transfer setup micromanipulators.

μ-PL measurements have been performed in a Horiba Scientific Xplora micro-Raman system (as described in Subsection 2.2.3). It is interesting to note here that we have maintained the same focal distance for PL spectra acquired in the 2D semiconductor without and with microspheres on top of them, in order to be able to perform a more direct quantitative comparison.

The global enhancement effect by placing SiO_2 microspheres on top of InSe nanosheets can be nicely observed in their PL spectra (Figure 4.1). An enhancement factor of 50 is measured if the microsphere resonance is very close to the PL peak energy, whereas the enhancement reduces to 5 – 8 times when it is detuned.

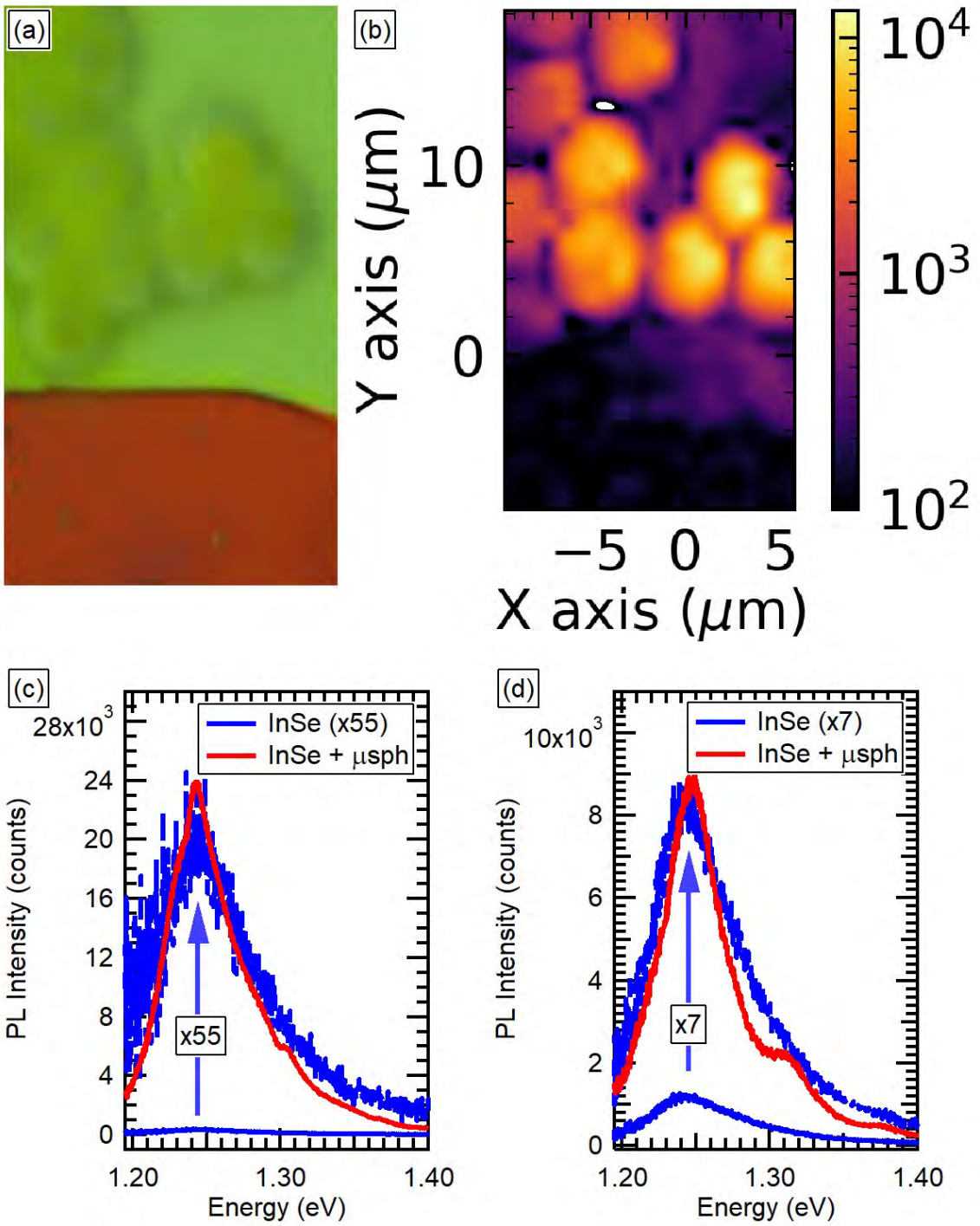

Figure 4.1: PL enhancement in semibulk-InSe exfoliated nanoflakes in the presence of microspheres: (a) Optical microscope image of the sample with microspheres on top; (b) μ-PL intensity map; (c) and (d) μ-PL spectra of the same InSe nanosheet before (blue curves) and after (red curves) placing SiO_2 microspheres on top.

Due to the presence of microspheres on top of the InSe nanosheets we should consider

two effects. First of all, from the excitation point of view, the difference between air and the microsphere refractive index will produce a lensing effect [211, 230, 209], i.e., an extra focusing effect of the excitation beam on the sample surface that increases the excitation power density on the sample, which will be reproduced in the collection step, lensing the emission of the nanosheet to our collection, adding emission that would otherwise have been outside the numerical aperture of our setup (NA = 0.9 in this case). The second effect is related to the internal spherical modes of the microsphere or WGMs. The PL emission from InSe nanosheets, due to the proximity to the microsphere, will couple to the WGMs producing almost equi-spaced resonances in PL intensity [239, 233, 204]. The spectral position of the WGMs will depend mostly on the precise diameter of the microsphere on top of the 2D-sample that is being considered, which produces small variations of the WGM wavelengths. In fact, when a WGM is located precisely at the PL peak energy the enhancement factor raised up to 50 (Figure 4.1c), as compared to factors 5 to 8 (Figure 4.1d) when the WGM is detuned with the PL peak. This low enhancement factor (5 to 8) is hence moslty attributed to the effective lensing in collection effect. A similar behavior can be observed in other semibulk and thinner InSe samples, which is the case of a 6.5nm-thick InSe nanosheet (Figure 4.2a) whose RT µ-PL is centered at 1.4 eV (blue curve in Figure 4.2b) [334]. For this nanosheet we observe two clearer resonances in its µ-PL spectrum (red curve in Figure 4.2b), due to the SiO_2 microspheres on top (Figure 4.2a).

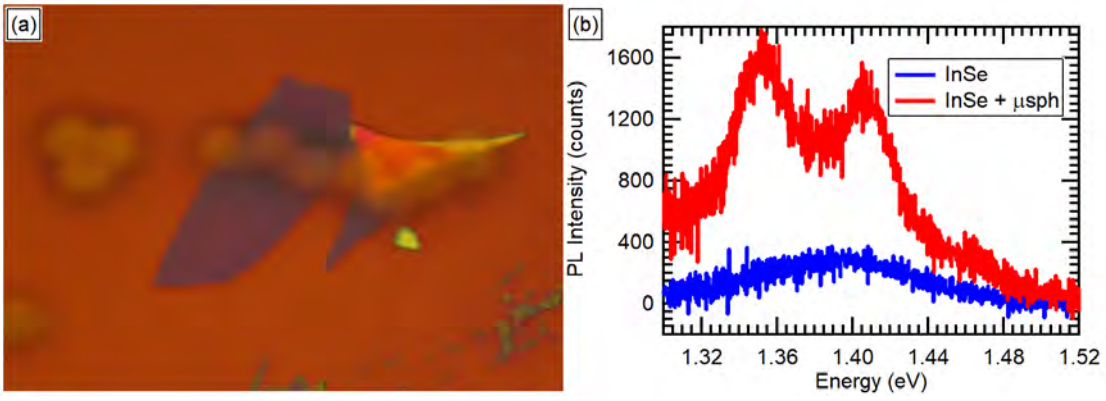

Figure 4.2: PL enhancement in thin InSe exfoliated nanoflakes in the presence of microspheres: (a) Optical image of a thin sample with SiO_2 microspheres on top; (b) µ-PL spectra comparing the emission of the thin InSe nanoflake before (blue curve) and after placing the microspheres (red curve).

4.3 Applications in two-dimensional transition metal dichalcogenides for fine-tuning

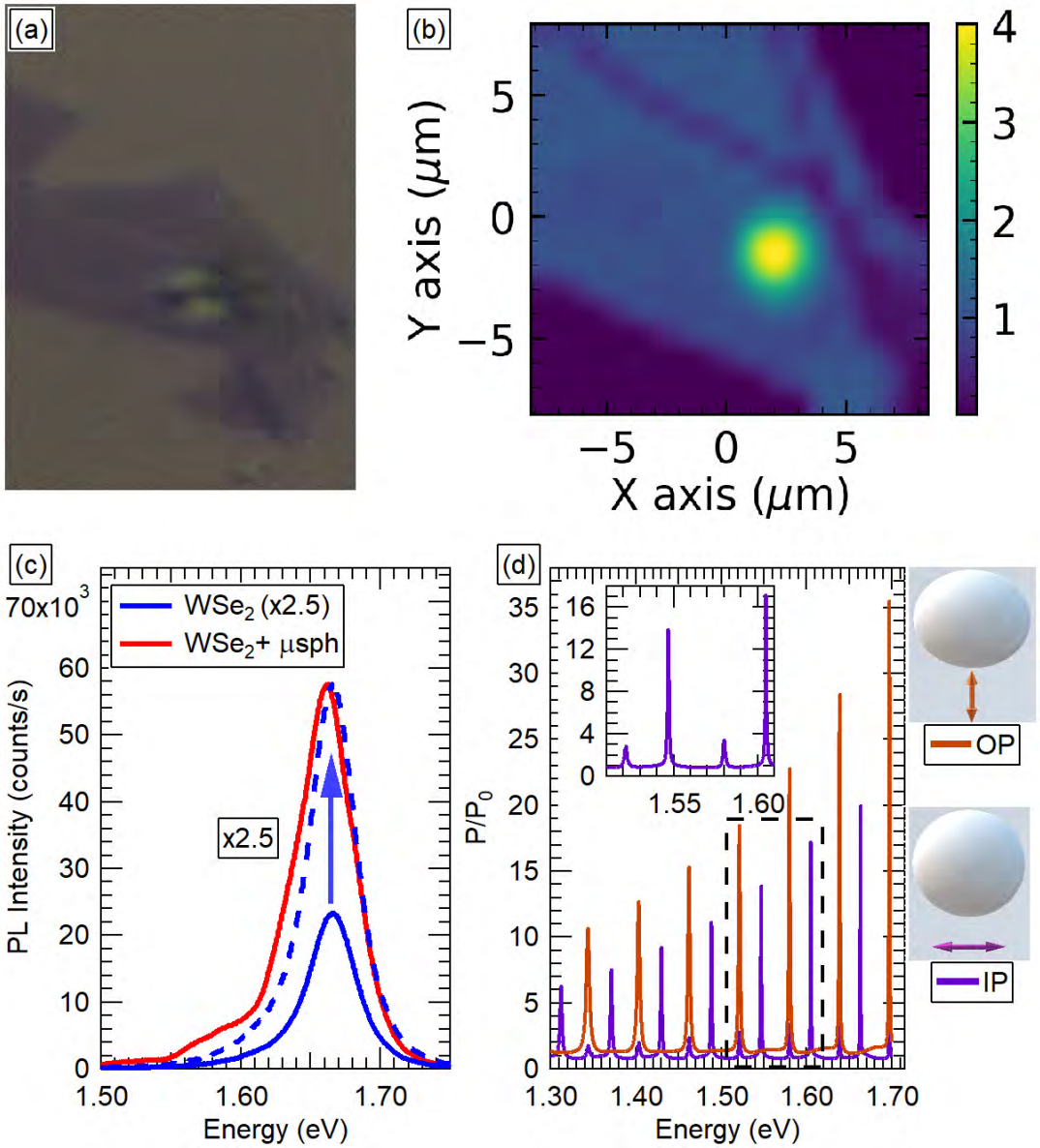

Figure 4.3: PL enhancement and fine tuning in WSe_2 ML exfoliated nanoflakes in presence of microspheres: (a) Optical image of a sample with a microsphere on top; (b) PL enhancement map using the ML emission as intensity reference; (c) μ-PL spectra of the ML nanosheet without (blue curves) and with a microsphere on top (red curve); (d) Power of the scattered light by the WGMs in a 5μm microsphere from a point electric dipole normalized to its power P_0 in vacuum, which is separated 3nm from the microsphere surface, as simulated by using the Mie theory under resonant conditions, and IP scattering in the inset.

The spectral dependence of the WGMs due to the precise diameter of the microsphere can be also used as a tool to produce a fine-tuning of the light emission in TMDs. If a WGM does not match the PL peak energy of the TMD, a certain spectral shift will be typically observed in the PL line due to the differential enhancement at the detuned WGM wavelengths as compared to the surroundings. This is the case of the WSe_2 ML (Figures 4.3a), where the SiO_2 microsphere on top produces a μ-PL enhancement of around a 2.5-to-4 factor (Figures 4.3b-c), other than a clear redshift of the spectrum in the order of 6-7 meV (red curve in Figure 4.3c). In both cases, for InSe and WSe_2, the size of the SiO_2 microsphere can be precisely calculated to produce the appropriate spectral position of the WGMs, which are simulated theoretically in Figure 4.3d. In one case the matching between a WGM and the PL peak energy for a given III - VI semiconductor nanosheet, in order to enhance its PL peak intensity, is targeted. In the other case, the TMD semiconductors, the interest resides in defining the desired PL (blue/red) shift.

In Figure 4.3d, the power P emitted by a point electric dipole, normalised to its power P_0 in vacuum, separated 3 nm from the dielectric microsphere (n = 1.4607; [196, 218] 5μm diameter), has been simulated using the well-known Mie theory [222] and imposing the resonance condition over their associated scattering coefficients by Dr. Carlos Zapata-Rodriguez. For instance, the resonant frequencies of the TE modes can be estimated to an excellent approximation by solving the equation $nj_l^{'}(nx)/j_l(nx) = n_l^{'}(x)/n_l(x)$ in terms of the normalised variable $x = kR$, where j_l and n_l are the spherical Bessel and Neumann functions of order l, respectively, n and R are the refractive index and the radius of the spherical microresonator, respectively, and k the light wavenumber in vacuum [215]. Once we have estimated the spectral positions of the WGM resonances for a given microsphere diameter (5 μm in Figure 4.3d), the spectral position dependence for other diameters can be estimated by using the relation $\omega_1 d_1 = \omega_2 d_2$, where ω_1 (ω_2) is the known (unknown) frequency of a WGM for the microsphere of diameter d_1 (d_2). This relation is valid as long as the chromatic dispersion of the sphere is neglected, useful to calculate the diameter needed for a specific application in short optical ranges, as the case evaluated in this work.

The Quality factors (Q) in our theoretical simulations are reaching values in the range 10^3 - 10^4, which are far from our experimental Q-factors, in the range 30 – 100. This difference can be perfectly understood, because of the use of commercial SiO_2 microspheres deposited on a Si/SiO_2 substrate, instead of perfect microspheres

in vacuum. Of course, the Q-factor of the microresonators can be eventually optimised for a specific application, for example by using shell-coated polymer dielectric microspheres [236] or different shaped high-Q microresonators [219], with higher refractive index than the substrate.

However, apart from the observed enhancement 2.5-to-4 factor for the PL intensity in WSe_2 MLs, it is worth to highlight the important difference with respect to the 7-to-50 enhancement factors measured in the case of InSe nanosheets. We attribute such a difference to the dipolar orientation of the optical excitonic transition in the two studied semiconductor nanosheets due to the different collection areas in presence of the microspheres.

A first common effect between the two experimentally studied cases is the effective lensing effect in excitation and collection (green shadowed areas in Figure 4.4), which gives the same enhancement factor ~2 in the PL intensity. This extra focusing through the microsphere of the excitation laser is the same in both cases, similar to the emitted light that can be collected in presence of the microsphere, hence independent of the nanosheet material. The difference is clearly observed for higher enhancement factors, as explained below by considering the dipolar nature of excitons in both materials.

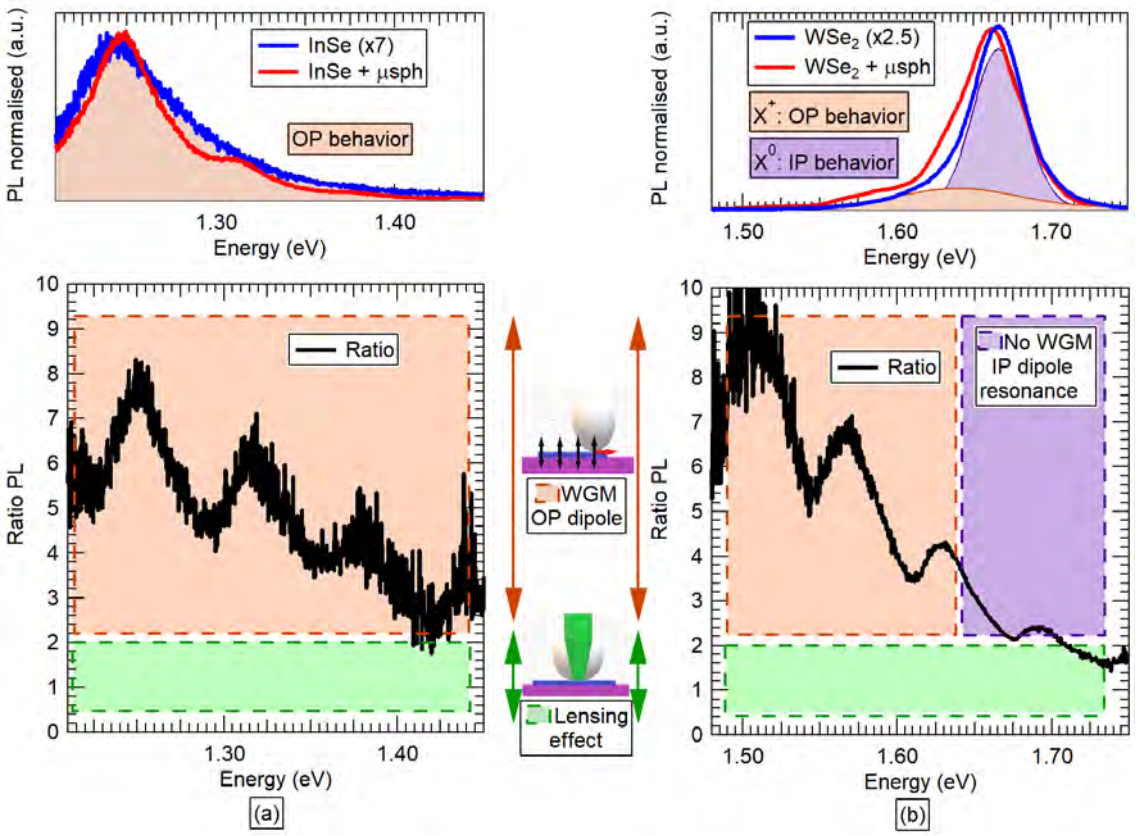

Figure 4.4: On top of a microsphere – nanosheet photoluminescence ratio in InSe nanosheet (a) and WSe_2 monolayer (b). Different enhancement contributions in the materials have been highlighted with shadowed areas in green, orange and purple as effective lensing effect, OP dipole contribution and IP non-contribution, respectively.

InSe thin films have been recently demonstrated to exhibit excitonic OP dipoles [297]. In fact, we observe a similar PL lineshape (top panel of Figure 4.4a) and hence an oscillatory behavior for the PL intensity (enhancement) ratio of the nanosheet with/without microsphere (black curve in bottom panel of Figure 4.4a) through the whole PL band energy region (this region has been highlighted in Figure 4.4 by using orange shadowed areas). This behavior nicely agrees with the coupling between the excitonic OP dipole and the tangential propagation direction in the WGM in the microspheres, giving rise to the observed maxima in the oscillatory PL ratio curve, as calculated previously, observing only 4 resonances in the range measured (assigned to the OP modes in Figure 4.3d) instead of 7 - 8 modes (as expected with IP modes). Due to the similar shape on the ratio in the whole range, we conclude that the OP behavior is homogeneous in this emission.

However, two different situations appear in WSe_2 ML, as observed in Figure 4.4b. In this case, at energies above its PL peak (top panel of Figure 4.4b), where the neutral exciton X^0 emission dominates [317], the PL intensity ratio (black curve in bottom panel of Figure 4.4b) drops to the background ~2 enhancement ratio very fast (shadowed violet region in Figure 4.4b). Simultaneously, at energies below its PL peak, we observe resonances in the PL intensity ratio (orange shadowed ratio in Figure 4.4b), similarly to InSe, i.e., consistent with an excitonic OP dipolar behavior in WSe_2, and reaching comparable enhancement factor values ~8. The energy region of the μ-PL spectrum in the WSe_2 ML where this effect is observed coincides with the expected contribution from charged exciton X^+ recombination (WSe_2 is unintentionally p-doped and higher hole concentrations are accumulated on the nanosheet edges and defects, which is the origin of a certain proportion of positively charged trions contributing to the PL of this material [317]). This dipolar behavior can be also observed in the previous simulations (Figure 4.3d). When the dipole is oriented radially to the microsphere (OP), only TM modes are excited, with more intense resonances. However, when it is set tangentially (IP), both TE and TM modes are excited at lower intensities, being TE excitation dominant. This fact, added to the low Q-factor values measured, explain the different coupling between an IP and OP dipole in the WGM on the microsphere, producing the different behavior in their resonances.

Besides, let's consider two different areas in our nanosheets: the area in contact with the microsphere and the proximities, slighly distanced, but with emission collected by the microsphere. The coupling to the WGMs is hampered drastically when the distance to the microsphere increases, e.g., in the surroundings to the contact position. In the area in contact, both IP and OP contributions will resonate in the WGM. However, due to the localised-nature of the charged excitons in TMDs, recombinations in the area will effectively produce the WGMs, in comparison with the IP contribution in TMDs, assigned to neutral excitons, with higher recombination distances. In the areas close to this contact position, no WGMs will be produced due to the increased distance to the microsphere. However, IP contribution, due to its dominant nature, will be collected, masking the resonances produced in the contact area, opposite to the OP contribution due to charged excitons, where its localised nature hampers spacially distanced recombinations.

4.4 Conclusions

In summary, here we present a new and simple technical approach to enhance the optical properties in 2D semiconductors, overcoming some of their basic limitations. For TMDs it is shown how can be matched their photoluminescent emission for a specific known wavelength. Firstly, after knowing the wavelength needed for a particular application, the microsphere diameter required can be calculated prior to locate it on top of a ML to be able to use the WGMs inside the microsphere to tune the emission to the desired wavelength. For the III-VI semiconductors, the same method should be used to identify first the diameter wanted to match the WGM with the PL peak emission of the III-VI semiconductor thickness used. In this chapter the usage of microspheres to enhance PL emission is presented, opening the possibility for specific applications to optimise the conditions proposed, such as better resonators for higher Q-factors, aiming for lasing effect in these materials, for instance.

Besides, this approach gives more understanding about the dipolar nature in both materials. For InSe, an OP dipole behavior is found when simulated scattered light from a point electric OP dipole is compared with the experimental results, demonstrating its recent OP reported nature. This fact focuses this material on its use in optoelectronics and integrated photonics. On the other hand, for WSe_2 MLs, two different components have been obtained: an IP dipolar behavior at higher energies, where the neutral X^0 exciton is located, and an OP dipolar nature at lower energies, where the charged excitons X^+ take place.

Bibliography

[194] Stephan Roche, Johan Åkerman, Bernd Beschoten, Jean Christophe Charlier, Mairbek Chshiev, Saroj Prasad Dash, Bruno Dlubak, Jaroslav Fabian, Albert Fert, Marcos Guimarães, Francisco Guinea, Irina Grigorieva, Christian Schönenberger, Pierre Seneor, Christoph Stampfer, Sergio O. Valenzuela, Xavier Waintal, and Bart Van Wees. Graphene spintronics: The European Flagship perspective. *2D Materials*, 2(3), 2015.

[195] Robert Schmidt, Iris Niehues, Robert Schneider, Matthias Drüppel, Thorsten Deilmann, Michael Rohlfing, Steffen Michaelis De Vasconcellos, Andres Castellanos-Gomez, and Rudolf Bratschitsch. Reversible uniaxial strain tuning in atomically thin WSe2. *2D Materials*, 3(2):2–9, 2016.

[196] C Z Tan. Determination of refractive index of silica glass for infrared wavelengths by IR spectroscopy. *Non-Crystaline Solids*, 1998.

[197] Oriol Lopez-Sanchez, Dominik Lembke, Metin Kayci, Aleksandra Radenovic, and Andras Kis. Ultrasensitive photodetectors based on monolayer MoS2. *Nature Nanotechnology*, 8(7):497–501, 2013.

[198] Daniel Andres-Penares, Ana Cros, Juan P. Martínez-Pastor, Juan F Sánchez-Royo, and Juan F. Sá Nchez-Royo. Quantum size confinement in gallium selenide nanosheets: Band gap tunability versus stability limitation. *Nanotechnology*, 28(17), 2017.

[199] S. Kumar, A. Kaczmarczyk, and B. D. Gerardot. Strain-Induced Spatial and Spectral Isolation of Quantum Emitters in Mono- and Bilayer WSe2. *Nano Letters*, 15(11):7567–7573, 2015.

[200] Mauro Brotons-Gisbert, Juan P. Martínez-Pastor, Guillem C. Ballesteros, Brian D. Gerardot, and Juan F. Sánchez-Royo. Engineering light emission of two-dimensional materials in both the weak and strong coupling regimes. *Nanophotonics*, 7(1):253–267, 2018.

[201] Jian Hao Chen, Chaun Jang, Shudong Xiao, Masa Ishigami, and Michael S. Fuhrer. Intrinsic and extrinsic performance limits of graphene devices on SiO2. *Actual Problems of Economics*, 3(12):200–209, 2009.

[202] Konstantina Iordanidou, Michel J.C. Houssa, Joseph Kioseoglou, Valeri V Afanas'ev, Andre Stesmans, and Clas Persson. Hole-doped 2D InSe for spintronic applications. *ACS Applied Nano Materials*, page acsanm.8b01476, 2018.

[203] Di Xiao, Gui Bin Liu, Wanxiang Feng, Xiaodong Xu, and Wang Yao. Coupled spin and valley physics in monolayers of MoS 2 and other group-VI dichalcogenides. *Physical Review Letters*, 108(19):1–5, 2012.

[204] Alessandro Chiasera, Yannick Dumeige, Patrice Féron, Maurizio Ferrari, Yoann Jestin, Gualtiero Nunzi Conti, Stefano Pelli, Silvia Soria, and Giancarlo C. Righini. Spherical whispering-gallery-mode microresonators. *Laser and Photonics Reviews*, 4(3):457–482, 2010.

[205] Xingli Wang, Yongji Gong, Gang Shi, Wai Leong Chow, Kunttal Keyshar, Gonglan Ye, Robert Vajtai, Jun Lou, Zheng Liu, Emilie Ringe, Beng Kang Tay, and Pulickel M. Ajayan. Chemical vapor deposition growth of crystalline monolayer MoSe2. *ACS Nano*, 8(5):5125–5131, 2014.

[206] Sidong Lei, Fangfang Wen, Liehui Ge, Sina Najmaei, Antony George, Yongji Gong, Weilu Gao, Zehua Jin, Bo Li, Jun Lou, Junichiro Kono, Robert Vajtai, Pulickel Ajayan, and Naomi J. Halas. An atomically layered InSe avalanche photodetector. *Nano Letters*, 15(5):3048–3055, 2015.

[207] Daniel J Terry, Viktor Zólyomi, Matthew Hamer, Anastasia V Tyurnina, David G Hopkinson, Alexander M Rakowski, Samuel J Magorrian, Nick Clark, Yuri M Andreev, Olga Kazakova, Konstantin Novoselov, Sarah J Haigh, Vladimir I Fal'ko, and Roman Gorbachev. Infrared-to-violet tunable optical activity in atomic films of GaSe, InSe, and their heterostructures. *2D Materials*, 5(4):041009, 2018.

[208] Juan F. Sánchez-Royo, Guillermo Muñoz-Matutano, Mauro Brotons-Gisbert, Juan P. Martínez-Pastor, Alfredo Segura, Andrés Cantarero, Rafael Mata, Josep Canet-Ferrer, Gerard Tobias, Enric Canadell, Jose Marqués-Hueso, and Brian D. Gerardot. Electronic structure, optical properties, and lattice dynamics in atomically thin indium selenide flakes. *Nano Research*, 7(10):1556–1568, 2014.

[209] Seoungjun Lee, Lin Li, Yacob Ben-Aryeh, Zengbo Wang, and Wei Guo. Overcoming the diffraction limit induced by microsphere optical nanoscopy. *Journal of Optics (United Kingdom)*, 15(12), 2013.

[210] K.S. S Novoselov, A.K. K Geim, S.V. V Morozov, D Jiang, Y Zhang, S.V. V Dubonos, I.V. V Grigorieva, and A. A Firsov. Electric Field Effect in Atomically Thin Carbon Films. *Science*, 306(5696):666–669, 2004.

[211] Pin-Yi Li, Yang Tsao, Yun-Ju Liu, Zong-Xing Lou, Wei-Li Lee, Shi-Wei Chu, and Chih-Wei Chang. Unusual imaging properties of superresolution microspheres. *Optics Express*, 24(15):16479, 2016.

[212] Garry W. Mudd, Simon A. Svatek, Lee Hague, Oleg Makarovsky, Zakhar R. Kudrynskyi, Christopher J. Mellor, Peter H. Beton, Laurence Eaves, Kostya S. Novoselov, Zakhar D. Kovalyuk, Evgeny E. Vdovin, Alex J. Marsden, Neil R. Wilson, and Amalia Patanè. High Broad-Band Photoresponsivity of Mechanically Formed InSe-Graphene van der Waals Heterostructures. *Advanced Materials*, 27(25):3760–3766, 2015.

[213] Yunqiu Kelly Luo, Jinsong Xu, Tiancong Zhu, Guanzhong Wu, Elizabeth J. McCormick, Wenbo Zhan, Mahesh R. Neupane, and Roland K. Kawakami. Opto-valleytronic spin injection in monolayer MoS2/few-layer graphene hybrid spin valves. *Nano Letters*, 17(6):3877–3883, 2017.

[214] Likai Li, Yijun Yu, Guo Jun Ye, Qingqin Ge, Xuedong Ou, Hua Wu, Donglai Feng, Xian Hui Chen, and Yuanbo Zhang. Black phosphorus field-effect transistors. *Nature Nanotechnology*, 9(5):372–377, 2014.

[215] C. C. Lam, P. T. Leung, and K. Young. Explicit asymptotic formulas for the positions, widths, and strengths of resonances in Mie scattering. *Journal of the Optical Society of America B*, 9(9):1585, 1992.

[216] Xuetao Gan, Yuanda Gao, Kin Fai Mak, Xinwen Yao, Ren Jye Shiue, Arend Van Der Zande, Matthew E. Trusheim, Fariba Hatami, Tony F. Heinz, James Hone, and Dirk Englund. Controlling the spontaneous emission rate of monolayer MoS2 in a photonic crystal nanocavity. *Applied Physics Letters*, 103(18):1–5, 2013.

[217] Shinichiro Mouri, Yuhei Miyauchi, and Kazunari Matsuda. Tunable photoluminescence of monolayer MoS2 via chemical doping. *Nano Letters*, 13(12):5944–5948, 2013.

[218] I. H. Malitson. Interspecimen Comparison of the Refractive Index of Fused Silica. *Journal of the Optical Society of America*, 1965.

[219] Mohammad Soltani, Siva Yegnanarayanan, and Ali Adibi. Ultra-high Q planar silicon microdisk resonators for chip-scale silicon photonics. *Optics Express*, 15(8):4694, 2007.

[220] Branimir Radisavljevic and Andras Kis. Mobility engineering and a metal-insulator transition in monolayer MoS2. *Nature Materials*, 12(9):815–820, 2013.

[221] John R. Schaibley, Hongyi Yu, Genevieve Clark, Pasqual Rivera, Jason S. Ross, Kyle L. Seyler, Wang Yao, and Xiaodong Xu. Valleytronics in 2D materials. *Nature Reviews Materials*, 1(11), 2016.

[222] P J Dobson. Absorption and Scattering of Light by Small Particles. *Physics Bulletin*, 1984.

[223] Zongyou Yin, Hai Li, Hong Li, Lin Jiang, Yumeng Shi, Yinghui Sun, Gang Lu, Qing Zhang, Xiaodong Chen, and Hua Zhang. Single-layer MoS2 phototransistors. *ACS Nano*, 6(1):74–80, 2012.

[224] Denis A. Bandurin, Anastasia V. Tyurnina, Geliang L. Yu, Artem Mishchenko, Viktor Zólyomi, Sergey V. Morozov, Roshan Krishna Kumar, Roman V. Gorbachev, Zakhar R. Kudrynskyi, Sergio Pezzini, Zakhar D. Kovalyuk, Uli Zeitler, Konstantin S. Novoselov, Amalia Patanè, Laurence Eaves, Irina V. Grigorieva, Vladimir I. Fal'Ko, Andre K. Geim, and Yang Cao. High electron mobility, quantum Hall effect and anomalous optical response in atomically thin InSe. *Nature Nanotechnology*, 12(3):223–227, 2017.

[225] Sina Najmaei, Zheng Liu, Wu Zhou, Xiaolong Zou, Gang Shi, Sidong Lei, Boris I. Yakobson, Juan Carlos Idrobo, Pulickel M. Ajayan, and Jun Lou. Vapour phase growth and grain boundary structure of molybdenum disulphide atomic layers. *Nature Materials*, 12(8):754–759, 2013.

[226] Wei Feng, Wei Zheng, Wenwu Cao, and PingAn Hu. Back Gated Multilayer InSe Transistors with Enhanced Carrier Mobilities via the Suppression of Carrier Scattering from a Dielectric Interface. *Advanced Materials*, 26(38):6587–6593, 2014.

[227] Likai Li, Yijun Yu, Guo Jun Ye, Qingqin Ge, Xuedong Ou, Hua Wu, Donglai Feng, Xian Hui Chen, and Yuanbo Zhang. Black phosphorus field-effect transistors. *Nature Nanotechnology*, 9(5):372–377, 2014.

[228] Changgu Lee, Xiaoding Wei, Jeffrey W. Kysar, and James Hone. Measurement of the Elastic Properties and Intrinsic Strength of Monolayer Graphene. *Science*, 321(July):385–388, 2008.

[229] Corey Janisch, Haomin Song, Chanjing Zhou, Zhong Lin, Ana Laura Elías, Dengxin Ji, Mauricio Terrones, Qiaoqiang Gan, and Zhiwen Liu. MoS2 monolayers on nanocavities: Enhancement in light-matter interaction. *2D Materials*, 3(2):1–7, 2016.

[230] Dylan Lu and Zhaowei Liu. Hyperlenses and metalenses for far-field superresolution imaging. *Nature Communications*, 3:1–9, 2012.

[231] Alberto F. Morpurgo. Spintronics: Gate control of spin-valley coupling. *Nature Physics*, 9(9):532–533, 2013.

[232] Jing Kai Huang, Jiang Pu, Chang Lung Hsu, Ming Hui Chiu, Zhen Yu Juang, Yung Huang Chang, Wen Hao Chang, Yoshihiro Iwasa, Taishi Takenobu, and Lain Jong Li. Large-area synthesis of highly crystalline WSe2 monolayers and device applications. *ACS Nano*, 8(1):923–930, 2014.

[233] Xavier Roselló-Mechó, Daniele Farnesi, Gabriele Frigenti, Andrea Barucci, Alberto Fernández-Bienes, Tupak García-Fernández, Fulvio Ratto, Martina Delgado-Pinar, Miguel V. Andrés, Gualtiero Nunzi Conti, and Silvia Soria. Parametrical Optomechanical Oscillations in PhoXonic Whispering Gallery Mode Resonators. *Scientific Reports*, 9(1):1–7, 2019.

[234] Chunxiao Cong, Jingzhi Shang, Xing Wu, Bingchen Cao, Namphung Peimyoo, Caiyu Qiu, Litao Sun, and Ting Yu. Synthesis and optical properties of large-area single-crystalline 2D semiconductor WS2 monolayer from chemical vapor deposition. *Advanced Optical Materials*, 2(2):131–136, 2014.

[235] Yang Chun Lee, Yi Chuan Tseng, and Hsuen Li Chen. Single type of nanocavity structure enhances light outcouplings from various two-dimensional materials by over 100-fold. *ACS Photonics*, 4(1):93–105, 2017.

[236] S. Soria, F. Baldini, S. Berneschi, F. Cosi, A. Giannetti, G. Nunzi Conti, S. Pelli, G. C. Righini, and B. Tiribilli. High-Q polymer-coated microspheres for immunosensing applications. *Optics Express*, 17(17):14694, 2009.

[237] Philipp Tonndorf, Robert Schmidt, Philipp Böttger, Xiao Zhang, Janna Börner, Andreas Liebig, Manfred Albrecht, Christian Kloc, Ovidiu Gordan, Dietrich R. T. Zahn, Steffen Michaelis de Vasconcellos, and Rudolf Bratschitsch. Photoluminescence emission and Raman response of monolayer MoS2, MoSe2, and WSe2. *Advanced Materials*, 29(33):4908–4916, 2017.

[238] K S Novoselov, D Jiang, F Schedin, T J Booth, V V Khotkevich, S V Morozov, and A K Geim. Two-dimensional atomic crystals. *PNAS*, 102(30):10451–10453, 2005.

[239] Motoki Asano, Yuki Takeuchi, Weijian Chen, Sahin Kaya Ozdemir, Rikizo Ikuta, Nobuyuki Imoto, Lan Yang, and Takashi Yamamoto. Observation of optomechanical coupling in a microbottle resonator. *Laser and Photonics Reviews*, 10(4):603–611, 2016.

[240] Mauro Brotons-Gisbert, Raphaël Proux, Raphaël Picard, Daniel Andres-Penares, Artur Branny, Alejandro Molina-Sánchez, Juan F. Sánchez-Royo, and Brian D. Gerardot. Out-of-plane orientation of luminescent excitons in atomically thin indium selenide flakes. *Nature Communications*, (2019):1–10, 2019.

[241] Mauro Brotons-Gisbert, Daniel Andres-Penares, Joonki Suh, Francisco Hidalgo, Rafael Abargues, Pedro J. Rodríguez-Cantó, Alfredo Segura, Ana Cros, Gerard Tobias, Enric Canadell, Pablo Ordejón, Junqiao Wu, Juan P. Martínez-Pastor, and Juan F. Sánchez-Royo. Nanotexturing To Enhance Photoluminescent Response of Atomically Thin Indium Selenide with Highly Tunable Band Gap. *Nano Letters*, 16(5):3221–3229, 2016.

5 Perovskites and two-dimensional semiconductors

Shortly after the isolation of the first 2D materials, it was conceived the stacking of different 2D materials with the aim of forming new nanomaterials with tailored properties. First, similar to how it was discovered, graphene was implemented alongside other structures to take advantage of its properties in existing elements. From decorated-graphene nanosheets with CdS-clusters for photocathalysis [245], with ZnO as a gas sensor [257], with DNA for chemical sensors [286], or Ca and Li for hydrogen storage [270] and superconductivity properties [263], respectively. Usually, graphene were used due to its surface - to - volume ratio and its great conductivity to cover that issue in other nanomaterials.

Soon, 2D TMDs were incorporated to this race. In this case, aiming for optoelectronic applications due to its semiconductor nature. PbS quantum dots for phototransistors [272, 278] and photodetectors [255, 259] or Fe_3O_4 nanoparticles for battery applications [285], for instance. The usage of this materials combined with nanoparticles (e.g., Pt [291, 276], Pd [293], MoS_2 [277]) as electrocatalysts for hydrogen evolution reaction and water splitting has been specially studied by the scientific community.

On the other hand, 2D materials and perovskites have been two of the main explored topics in the last years [279, 246, 294]. Their ease of fabrication, combined with their strong solar absorption [248, 256, 265] and low non-radiative carrier recombination rates [252] make them interesting in solar cells [262, 284, 281, 252, 271], achieving up to a 20% in its external quantum eficiency [253]. Among all their optical properties, for this chapter, it is worth noticing their multi-oriented photoluminescent emission [247, 254, 273], as shown in Figure 5.1.

These perovskites have been also exploited to complement (or be complemented) by 2D materials. With graphene, among others, they have been implemented in

photodetectors [411, 282] and phototransistors [274, 260], to act as solar cells [60] or, as described previously, as oxygen reduction reaction electrocatalyst [283]. Similar optoelectronic-oriented devices can be found in literature using TMDs [387, 251, 244, 266, 269, 288, 280]. These are examples of different nanomaterials which combined offer enhanced properties, complementing them for specific applications and devices.

The multi-directionallity previously highlighted in perovskites emission contrast with the OP dipolar behavior in InSe [297], which hampers its absorption and emission in a classical vertical excitation - vertical collection configuration, as described in previous chapters.

In this chapter, PL of InSe nanosheets with and without presence of perovskites will be compared, obtaining an enhancement in its emission due to the reabsorption between the perovskites multi-oriented photoluminescent emission and the OP dipole in InSe, presenting its joint use as a way to increase its absorption. For comparison, two different synthesised perovskites will be utilised, and in order to demonstrate the OP dipolar relevance for the reabsorption, $MoSe_2$, known for its IP dipole as a TMD, will be compared.

5.1 Theoretical background

The structure that will be studied in this project is defined in Figure 5.1. On a Si/SiO_2 substrate with a 285 nm thick SiO_2 layer, a 2D material will be exfoliated and, on top of it, perovskite agglomerates will be transferred. The comparison between areas with and without the presence of perovskites will be the focus of the later measurements. In the case of InSe, due to the OP dipole orientation [297], a vertical excitation in the z-direction is not ideal for its absorption (Figure 5.1a), compared with other 2D materials like the TMDs, which IP dipole orientation optimise the z-direction absorption (Figure 5.1b).

In presence of the perovskites, two contrary effects will occur. First, due to its presence on top of the 2D material, the direct excitation power that can excite the 2D material will be partially blocked by the perovskites on top, absorbing most of the excitation that without the perovskites it would have arrived directly to the 2D material. This first effect will be highly hampering for the TMDs due to their optimal absorption in this direction.

However, opposed to this effect, the perovskites will have its own emission, in all directions due to its nature [247, 254, 273], being this excitation another source that could be absorbed by the 2D material underneath. In the case of InSe, due to its OP dipole, the reabsorption will be relevant compared with the not ideal absorption in the z-direction, as opposite with a TMD, where the absorption was already optimal without the perovskites, so the reabsorption in this case will be the main source for the InSe and not harnessed by the TMD (Figures 5.1c and 5.1d, respectivelly). These two contraposed effects will be the main difference that will be analysed in the following lines.

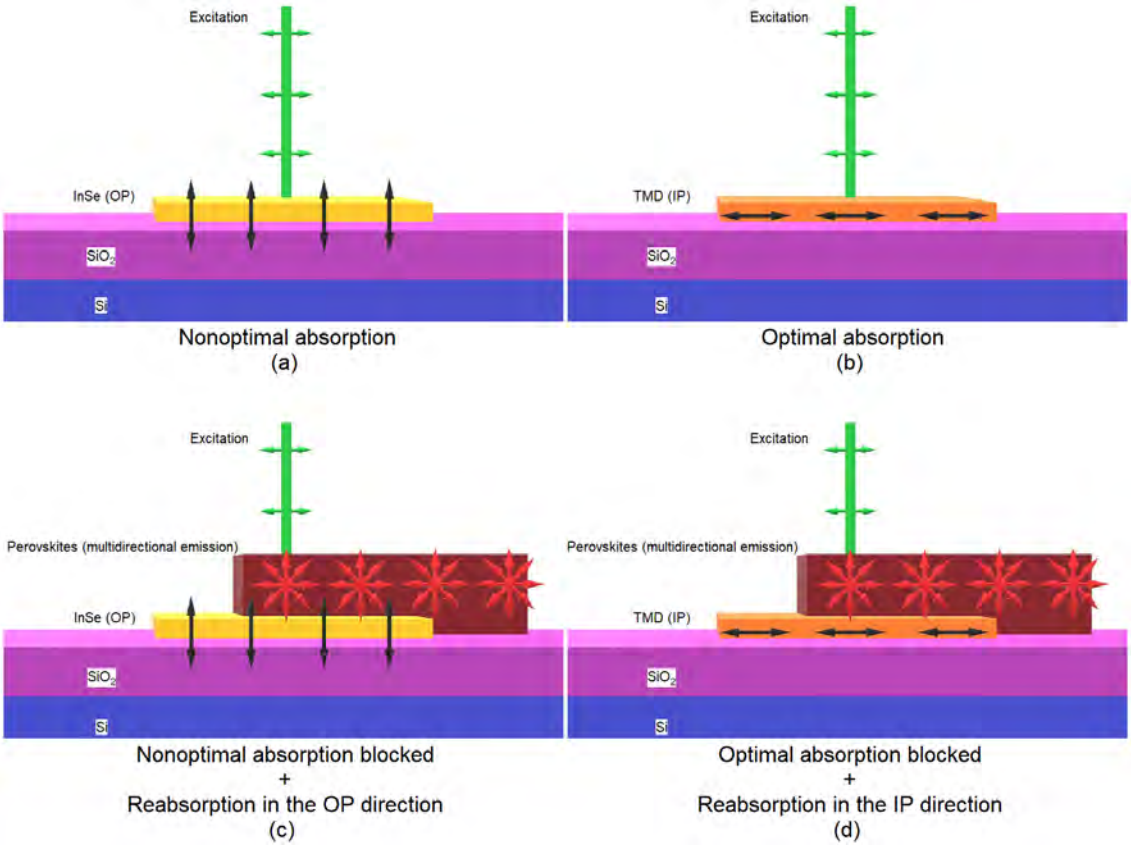

Figure 5.1: Sample diagram of the absorption and dipoles orientation with the effects expected exciting in the vertical direction to (a) an InSe sample, (b) a TMD sample, (c) an InSe sample with perovskites on top and (d) a TMD sample with perovskites on top.

5.2 InSe and perovskites

InSe and $MoSe_2$ 2D nanosheets have been prepared through the well-known scotch-tape micromechanically exfoliation technique (see Subsection 2.1.1 and Appendix A). InSe samples have been then directly transferred onto Si substrates coated with 285nm of SiO_2, as described in Subsection 2.1.2. Bulk $MoSe_2$ (Appendix A) has been used here to obtain $MoSe_2$ nanosheets. ML were exfoliated using the same scotch-tape technique to a PDMS stamp. ML identification has been done using their known PL emission at RT [333], and then through the all-dry viscoelastic technique transferred onto Si/SiO_2 (285nm) cleaned substrates similar as used for InSe. The samples have been identified via OC using a Zeiss Axio Scope.a1 microscope with an Axiocam ERc 5s camera (for more details, see Subsection 2.2.1).

The synthesis of the perovskites used and their purification have been carried out by Juan Navarro-Arenas. Perovskite nanocrystals (PNCs) of $CsPbI_3$ (red perovskites) and $CsPbBr_3$ (green perovskites) were synthetised following the hot-injection method [292]. A reprecipitation method was used for the purification of the PNCs; two solvent/antisolvent (hexane/ethyl acetate) washing cycles were applied to archieve high purity PNCs. This washing procedure was key to allow the isolation of the PNCs for the further processing into heterostructures by the 2D-transfer techniques. For both kind of perovskites, after the synthesis, a PDMS stamp was used to pluck areas with high perovskite agglomerates concentration, identified by their back-scattering emission under a 404 nm laser excitation and detected with a Pixelink camera with a longpass edge 450nm filter in the collection, to transfer these localised areas on top of the nanosheet previously exfoliated through the all-dry viscoelastic technique (Subsection 2.1.3.1), adapted to the perovskites transfer.

A Horiba Scientific Xplora μ-Raman system using a 532nm CW excitation laser have been used to perform the μ-PL measurements, not exceeding 60μW of power in InSe and 10μW in $MoSe_2$ to prevent overheating in the samples (Subsection 2.2.3). The optical beams in the excitation and collection spot have been focused to less than $1\mu m^2$. It has been took into account the same focal distance during the PL spectra mapping in each sample in order to being able to compare intensities in areas with perovskites with areas without them.

First, green perovskites agglomerates have been used to excite InSe samples through reabsorption. Perovskites with emission centred in the green-range in the wavelength spectra have been chosen due to the quasi-resonant excitation using a 532 nm CW

laser, increasing to optimise the distance between InSe and the perovskites absorption to enhance it.

Although the perovskites and the 2D exfoliated materials will be in contact in the vertical heterostructure, a relevant charge transfer between them is not expected due to the transfer method, in which the contact surfaces have been exposed to air and perovskites nature: organic ligands surrounding the agglomerates hamper the carrier transfer to and from the 2D underneath [289, 275, 268]. For that reason, in this project only reabsorption will be considered as re-excitation mechanism between these two materials.

In Figure 5.2a can be seen the optical image, being able to determine optically the areas corresponding exclusively with InSe, areas with the only presence of perovskites and areas with perovskites on top of the InSe nanosheet (highlighted, respectively, with dashed black, red and green bounds). These are the areas to compare, the bare InSe against InSe with perovskites, comparing an average using different points in Figure 5.2b, observing that in the areas presenting perovskites (as shown optically and in the inset spectra at higher energies, observing the tail of their emission) the InSe PL is enhanced. This can be observed in Figure 5.2c, where a PL map is shown integrating the collection between 1.23 and 1.36 eV, the range of energies where the InSe has its PL emission.

Finally, in order to re-determine the areas with perovskites a PL map integrating the collection intensity between 1.95 and 2.15 eV has been shown in Figure 5.2d, matching this area with the area with enhanced InSe emission.

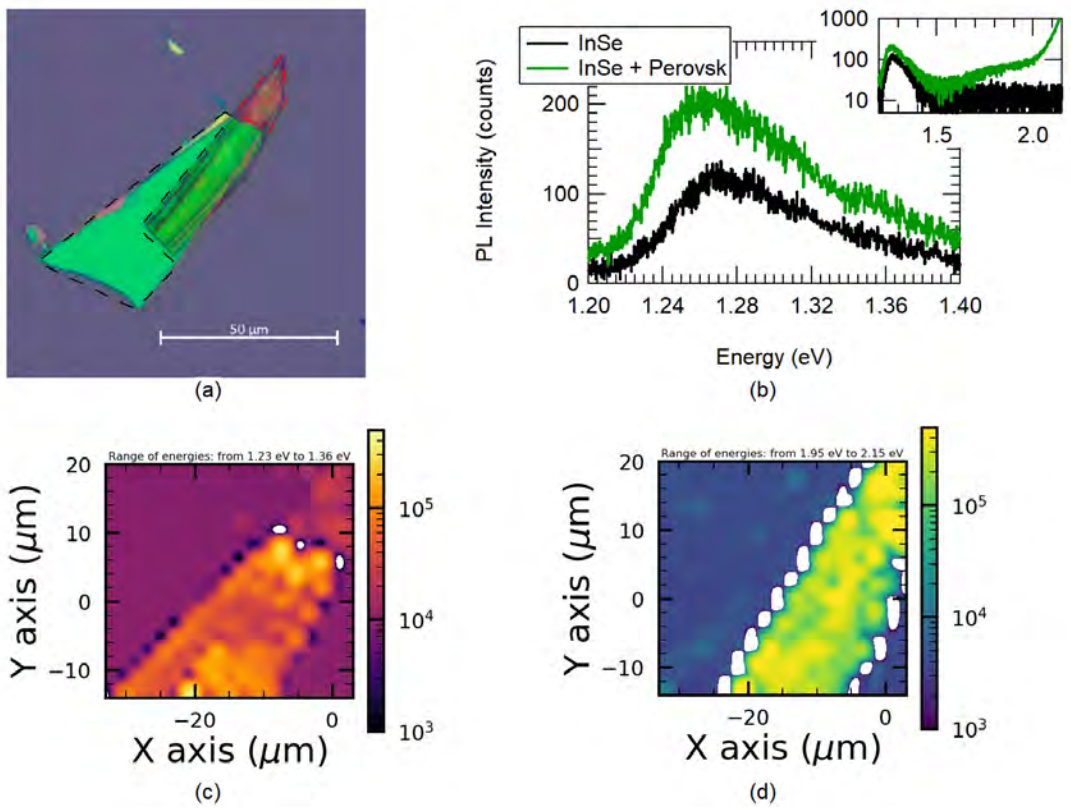

Figure 5.2: (a) Optical image of an InSe nanosheet with green perovskites on top, defining three different areas: exclusively with InSe (black), exclusively with perovskites (red) and with InSe and perovskites on top (green), (b) PL spectra showing the average emission in different points in the InSe area and in the InSe with perovskites area, (c) PL map integrating the InSe emission (1.23 – 1.36 eV), (d) PL map integrated in the green perovskites emission (1.95 – 2.15 eV).

Reabsorption effects have been observed in 2D InSe/perovskites systems when different perovskites have been used, which have their PL emission centred in the red-range wavelength spectra. In this case the agglomerates obtained, due to the nature of the synthesis, are smaller, but still can be observed optically (Figure 5.3a) and, in order to support this localisation, in the PL map integrated between 1.70 and 2.00 eV, where the perovskites have their emission (Figure 5.3d).

With these comparison between the map shown in the Figure 5.3d (the location of the perovskites agglomerates) and the PL map in the Figure 5.3c (integrating the emission spectra between 1.23 and 1.36 eV, the InSe emission) can be observed the same effect: that in the areas where the perovskites are located, the intensity in the InSe emission is enhanced. Averaged PL spectra are shown in Figure 5.3b. In this

case, due to the high difference between the emission of the perovskites compared with the InSe nanosheets two different maps have been taken, one for each energy range, in order to avoid saturating the collection.

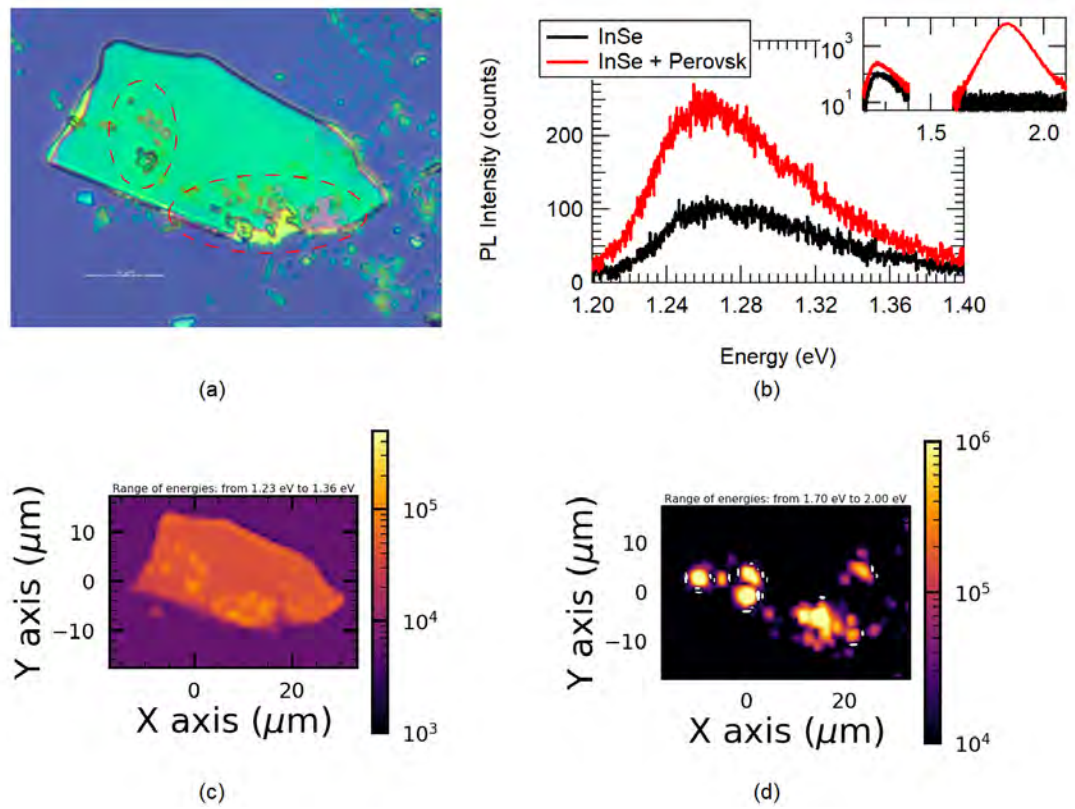

Figure 5.3: (a) Optical image of an InSe nanosheet with red perovskites on top (in this case, small agglomerates can be seen on top of the InSe nanosheet, marked with dashed red bounds), (b) PL spectra showing the average emission in different points in the InSe area and in the InSe with perovskites area, (c) PL map integrating the InSe emission (1.23 – 1.36 eV), (d) PL map integrated in the red perovskites emission (1.70 – 2.00 eV).

In both cases, using green or red perovskites, it is shown that in the areas where the perovskites are located, which can be seen optically (Figures 5.2a and 5.3a respectively) or in the PL map (Figures 5.2d and 5.3d respectively), the InSe PL emission is enhanced (Figures 5.2c and 5.3c respectively) compared with the areas without perovskites on top (Figures 5.2b and 5.3b respectively shows both PL spectra for comparison). The fact that the InSe samples, due to its OP dipole, absorbs the emission in all directions of the perovskites exceeds the blocking of vertical excitation that the perovskites absorb and do not reach the InSe, which would not be

properly absorbed by that dipole.

5.3 $MoSe_2$ and perovskites

Finally, a different exfoliated material will be used in order to demonstrate the relevance of the OP dipole in the reabsorption that enhance the InSe emission. $MoSe_2$ has been used as an example of the TMDs, all of them with IP dipole, due to its minor absorption energy compared with WSe_2, MoS_2 or WS_2 in order to optimise the reabsorption between perovskites and material, separating them. Red perovskites have been transferred on top and the same measurements have been taken to compare with the InSe samples.

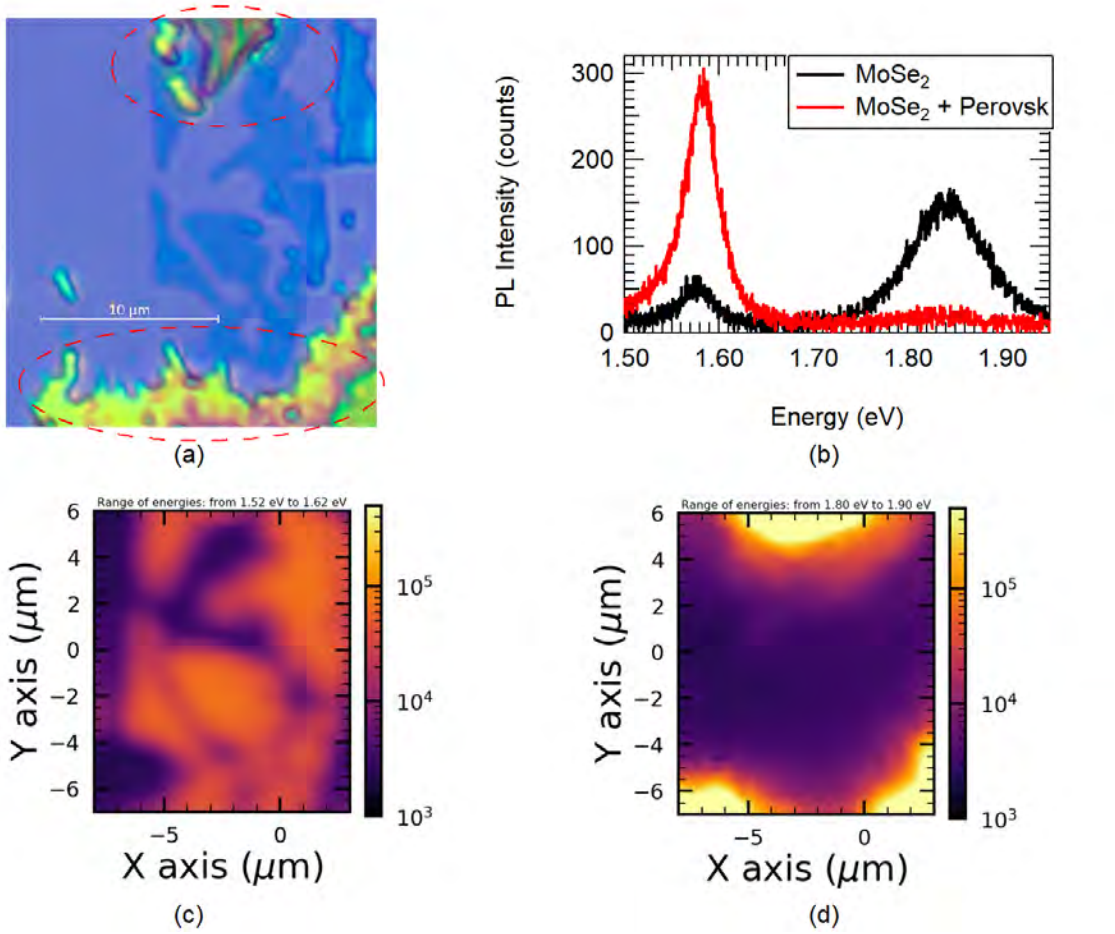

Figure 5.4: (a) Optical image of an $MoSe_2$ nanosheet with red perovskites on top (in this case, two big agglomerates can be seen on top of the $MoSe_2$ nanosheet, marked with dashed red bounds), (b) PL spectra showing the average emission in different points in the $MoSe_2$ area and in the $MoSe_2$ with perovskites area, (c) PL map integrating the $MoSe_2$ emission (1.52 – 1.62 eV), (d) PL map integrated in the red perovskites emission (1.80 – 1.90 eV).

In this case, contrary with the InSe nanosheets, we observe a decrease of PL emission in presence of the perovskites (Figure 5.4b, where PL spectras taken only in presence of $MoSe_2$ monolayer and in areas with red perovskites on top of $MoSe_2$ are compared, as can be seen in the PL maps in Figures 5.4c and 5.4d of optically from Figure 5.4a). Due to the IP dipole orientation in $MoSe_2$ ML the absorption of the excitation source was optimal without the perovskites, so the perovskites on top only block it, and the multi-oriented perovskites emission is not harnessed.

This result contrast with a recent publication [250], where instead of transferring the perovskite on top of the TMD, is the TMD that is above, not being blocked

and, therefore, obtaining greater emission from the substrate.

5.4 Conclusions

The perovskites and 2D materials interaction due to reabsorption mechanisms has been studied in this chapter. First, using perovskites on top of InSe exfoliated nanosheets, the PL enhancement in the areas with perovskites has been proved due to the reabsorption of the multi-directional perovskites emission by the OP InSe dipole, which in the absence of perovskites was not ideal for vertical excitation.

This effect has been demonstrated using different perovskites, with photoluminescent emission in the green-range and the red-range wavelength spectra. In order to demonstrate that the dipole orientation was the main reabsorption mechanism, a $MoSe_2$ ML sample has been studied, this case with an IP dipole. In this case the presence of perovskites, instead of enhancing the PL emission, hampers it due to the blocking of the optimal vertical excitation source.

With this study we present two messages: first, the implementation of perovskites in order to enhance the optical properties for OP materials and second, an experimental demonstration of the OP dipole nature in InSe, compared with the IP nature in TMDs, with $MoSe_2$ as example. These two materials together open the door to devices for large-range light absorption with the usage of different perovskites which will be absorbed by the InSe underneath for optical applications.

Even more, combining the enhanced optical properties in InSe due to the presence of perovskites (as demonstrated in this project) with the InSe electrical properties (high mobility [242, 258] compared with the perovskites, which organic ligands diminish [264, 287, 261]) could be explored in future projects optimising the carrier transport between the surfaces in both materials.

Bibliography

[242] Denis A. Bandurin, Anastasia V. Tyurnina, Geliang L. Yu, Artem Mishchenko, Viktor Zólyomi, Sergey V. Morozov, Roshan Krishna Kumar, Roman V. Gorbachev, Zakhar R. Kudrynskyi, Sergio Pezzini, Zakhar D. Kovalyuk, Uli Zeitler, Konstantin S. Novoselov, Amalia Patanè, Laurence Eaves, Irina V. Grigorieva, Vladimir I. Fal'Ko, Andre K. Geim, and Yang Cao. High electron mobility, quantum Hall effect and anomalous optical response in atomically thin InSe. *Nature Nanotechnology*, 12(3):223–227, 2017.

[243] Philipp Tonndorf, Robert Schmidt, Philipp Böttger, Xiao Zhang, Janna Börner, Andreas Liebig, Manfred Albrecht, Christian Kloc, Ovidiu Gordan, Dietrich R. T. Zahn, Steffen Michaelis de Vasconcellos, and Rudolf Bratschitsch. Photoluminescence emission and Raman response of monolayer MoS2, MoSe2, and WSe2. *Advanced Materials*, 29(33):4908–4916, 2017.

[244] Dong Ho Kang, Seong Ryul Pae, Jaewoo Shim, Gwangwe Yoo, Jaeho Jeon, Jung Woo Leem, Jae Su Yu, Sungjoo Lee, Byungha Shin, and Jin Hong Park. An Ultrahigh-Performance Photodetector based on a Perovskite - Transition-Metal-Dichalcogenide Hybrid Structure. *Advanced Materials*, 28(35):7799–7806, 2016.

[245] Qin Li, Beidou Guo, Jiaguo Yu, Jingrun Ran, Baohong Zhang, Huijuan Yan, and Jian Ru Gong. Highly efficient visible-light-driven photocatalytic hydrogen production of CdS-cluster-decorated graphene nanosheets. *Journal of the American Chemical Society*, 133(28):10878–10884, 2011.

[246] Yaoguang Rong, Yue Hu, Anyi Mei, Hairen Tan, Makhsud I. Saidaminov, Sang Il Seok, Michael D. McGehee, Edward H. Sargent, and Hongwei Han. Challenges for commercializing perovskite solar cells. *Science*, 361(6408), 2018.

[247] Yu Cao, Nana Wang, He Tian, Jingshu Guo, Yingqiang Wei, Hong Chen, Yanfeng Miao, Wei Zou, Kang Pan, Yarong He, Hui Cao, You Ke, Mengmeng Xu, Ying Wang, Ming Yang, Kai Du, Zewu Fu, Decheng Kong, Daoxin Dai, Yizheng Jin, Gongqiang Li, Hai Li, Qiming Peng, Jianpu Wang, and Wei Huang. Perovskite light-emitting diodes based on spontaneously formed submicrometre-scale structures. *Nature*, 562(7726):249–253, 2018.

[248] Yifei Shi, Wen Wu, Hua Dong, Guangru Li, Kai Xi, Giorgio Divitini, Chenxin Ran, Fang Yuan, Min Zhang, Bo Jiao, Xun Hou, and Zhaoxin Wu. A Strategy

for Architecture Design of Crystalline Perovskite Light-Emitting Diodes with High Performance. *Advanced Materials*, 30(25):1–10, 2018.

[249] Qipeng Lu, Yifu Yu, Qinglang Ma, Bo Chen, and Hua Zhang. 2D Transition-Metal-Dichalcogenide-Nanosheet-Based Composites for Photocatalytic and Electrocatalytic Hydrogen Evolution Reactions. *Advanced Materials*, 28(10):1917–1933, 2016.

[250] Arky Yang, Jean-Christophe Blancon, Wei Jiang, Hao Zhang, Joeson Wong, Ellen Yan, Yi-Rung Lin, Jared Crochet, Mercouri G. Kanatzidis, Deep Jariwala, Tony Low, Aditya D. Mohite, and Harry A. Atwater. Giant Enhancement of Photoluminescence Emission in WS2 -Two-Dimensional Perovskite Heterostructures. *Nano Letters*, 2019.

[251] Andrea Capasso, Fabio Matteocci, Leyla Najafi, Mirko Prato, Joka Buha, Lucio Cinà, Vittorio Pellegrini, Aldo Di Carlo, and Francesco Bonaccorso. Few-Layer MoS2 Flakes as Active Buffer Layer for Stable Perovskite Solar Cells. *Advanced Energy Materials*, 6(16):1–12, 2016.

[252] Deying Luo, Wenqiang Yang, Zhiping Wang, Aditya Sadhanala, Qin Hu, Rui Su, Ravichandran Shivanna, Gustavo F. Trindade, John F. Watts, Zhaojian Xu, Tanghao Liu, Ke Chen, Fengjun Ye, Pan Wu, Lichen Zhao, Jiang Wu, Yongguang Tu, Yifei Zhang, Xiaoyu Yang, Wei Zhang, Richard H. Friend, Qihuang Gong, Henry J. Snaith, and Rui Zhu. Enhanced photovoltage for inverted planar heterojunction perovskite solar cells. *Science*, 360(6396):1442–1446, 2018.

[253] Kebin Lin, Jun Xing, Li Na Quan, F. Pelayo García de Arquer, Xiwen Gong, Jianxun Lu, Liqiang Xie, Weijie Zhao, Di Zhang, Chuanzhong Yan, Wenqiang Li, Xinyi Liu, Yan Lu, Jeffrey Kirman, Edward H. Sargent, Qihua Xiong, and Zhanhua Wei. Perovskite light-emitting diodes with external quantum efficiency exceeding 20 per cent. *Nature*, 562(7726):245–248, 2018.

[254] Zhi Kuang Tan, Reza Saberi Moghaddam, May Ling Lai, Pablo Docampo, Ruben Higler, Felix Deschler, Michael Price, Aditya Sadhanala, Luis M. Pazos, Dan Credgington, Fabian Hanusch, Thomas Bein, Henry J. Snaith, and Richard H. Friend. Bright light-emitting diodes based on organometal halide perovskite. *Nature Nanotechnology*, 9(9):687–692, 2014.

[255] Zhenhua Sun, Zhike Liu, Jinhua Li, Guo An Tai, Shu Ping Lau, and Feng Yan.

Infrared photodetectors based on CVD-grown graphene and PbS quantum dots with ultrahigh responsivity. *Advanced Materials*, 24(43):5878–5883, 2012.

[256] Fei Yan, Jun Xing, Guichuan Xing, Lina Quan, Swee Tiam Tan, Jiaxin Zhao, Rui Su, Lulu Zhang, Shi Chen, Yawen Zhao, Alfred Huan, Edward H. Sargent, Qihua Xiong, and Hilmi Volkan Demir. Highly Efficient Visible Colloidal Lead-Halide Perovskite Nanocrystal Light-Emitting Diodes. *Nano Letters*, 18(5):3157–3164, 2018.

[257] Gaurav Singh, Anshul Choudhary, D. Haranath, Amish G. Joshi, Nahar Singh, Sukhvir Singh, and Renu Pasricha. ZnO decorated luminescent graphene as a potential gas sensor at room temperature. *Carbon*, 50(2):385–394, 2012.

[258] Sukrit Sucharitakul, Nicholas J. Goble, U. Rajesh Kumar, Raman Sankar, Zachary A. Bogorad, Fang Cheng Chou, Yit Tsong Chen, and Xuan P A Gao. Intrinsic Electron Mobility Exceeding 10ˆ3 cmˆ2/(V s) in Multilayer InSe FETs. *Nano Letters*, 15(6):3815–3819, 2015.

[259] Dominik Kufer, Ivan Nikitskiy, Tania Lasanta, Gabriele Navickaite, Frank H L Koppens, and Gerasimos Konstantatos. Hybrid 2D-0D MoS2 -PbS quantum dot photodetectors. *Advanced materials (Deerfield Beach, Fla.)*, 27(1):176–180, 2015.

[260] Yusheng Wang, Yupeng Zhang, Yao Lu, Weidong Xu, Haoran Mu, Caiyun Chen, Hong Qiao, Jingchao Song, Shaojuan Li, Baoquan Sun, Yi Bing Cheng, and Qiaoliang Bao. Hybrid Graphene-Perovskite Phototransistors with Ultrahigh Responsivity and Gain. *Advanced Optical Materials*, 3(10):1389–1396, 2015.

[261] Laraib Sarfraz Khanzada, Ievgen Levchuk, Yi Hou, Hamed Azimi, Andres Osvet, Rameez Ahmad, Marco Brandl, Patrick Herre, Monica Distaso, Rainer Hock, Wolfgang Peukert, Miroslaw Batentschuk, and Christoph J. Brabec. Effective Ligand Engineering of the Cu2ZnSnS4 Nanocrystal Surface for Increasing Hole Transport Efficiency in Perovskite Solar Cells. *Advanced Functional Materials*, 26(45):8300–8306, 2016.

[262] Mingzhen Liu, Michael B. Johnston, and Henry J. Snaith. Efficient planar heterojunction perovskite solar cells by vapour deposition. *Nature*, 501(7467):395–398, 2013.

[263] B. M. Ludbrook, G. Levy, P. Nigge, M. Zonno, M. Schneider, D. J. Dvorak,

C. N. Veenstra, S. Zhdanovich, D. Wong, P. Dosanjh, C. Straßer, A. Stöhr, S. Forti, C. R. Ast, U. Starke, A. Damascelli, and J. C. Séamus Davis. Evidence for superconductivity in Li-decorated monolayer graphene. *Proceedings of the National Academy of Sciences of the United States of America*, 112(38):11795–11799, 2015.

[264] Yao Liu, Markelle Gibbs, James Puthussery, Steven Gaik, Rachelle Ihly, Hugh W. Hillhouse, and Matt Law. Dependence of carrier mobility on nanocrystal size and ligand length in pbse nanocrystal solids. *Nano Letters*, 10(5):1960–1969, 2010.

[265] Matthew D. Smith and Hemamala I. Karunadasa. White-Light Emission from Layered Halide Perovskites. *Accounts of Chemical Research*, 51(3):619–627, 2018.

[266] Uttiya Dasgupta, Soumyo Chatterjee, and Amlan J. Pal. Thin-film formation of 2D MoS2 and its application as a hole-transport layer in planar perovskite solar cells. *Solar Energy Materials and Solar Cells*, 172(August):353–360, 2017.

[267] Zhenhua Sun, Lionel Aigouy, and Zhuoying Chen. Plasmonic-enhanced perovskite-graphene hybrid photodetectors. *Nanoscale*, 8(14):7377–7383, 2016.

[268] R. J. Stead, M. A. Barradas, D. P. Mikhailidis, M. E. Hodson, J. C. Batten, and P. Dandona. *Platelet function in patients with cystic fibrosis*, volume 25. 1986.

[269] Hung Chieh Cheng, Gongming Wang, Dehui Li, Qiyuan He, Anxiang Yin, Yuan Liu, Hao Wu, Mengning Ding, Yu Huang, and Xiangfeng Duan. Van der Waals Heterojunction Devices Based on Organohalide Perovskites and Two-Dimensional Materials. *Nano Letters*, 16(1):367–373, 2016.

[270] Hoonkyung Lee, Jisoon Ihm, Marvin L. Cohen, and Steven G. Louie. Calcium-decorated graphene-based nanostructures for hydrogen storage. *Nano Letters*, 10(3):793–798, 2010.

[271] Quinten A. Akkerman, Gabriele Rainò, Maksym V. Kovalenko, and Liberato Manna. Genesis, challenges and opportunities for colloidal lead halide perovskite nanocrystals. *Nature Materials*, 17(5):394–405, 2018.

[272] Chao Hu, Dongdong Dong, Xiaokun Yang, Keke Qiao, Dun Yang, Hui Deng, Shengjie Yuan, Jahangeer Khan, Yang Lan, Haisheng Song, and Jiang Tang. Synergistic Effect of Hybrid PbS Quantum Dots/2D-WSe2 Toward High Performance and Broadband Phototransistors. *Advanced Functional Materials*, 27(2):1603605, 2017.

[273] Matthew J. Jurow, Thomas Lampe, Erika Penzo, Jun Kang, Matthew A. Koc, Thomas Zechel, Zachary Nett, Michael Brady, Lin Wang Wang, A. Paul Alivisatos, Stefano Cabrini, Wolfgang Brütting, and Yi Liu. Tunable Anisotropic Photon Emission from Self-Organized CsPbBr3 Perovskite Nanocrystals. *Nano Letters*, 17(7):4534–4540, 2017.

[274] Vinh Quang Dang, Gill Sang Han, Tran Quang Trung, Le Thai Duy, Young Un Jin, Byeong Ung Hwang, Hyun Suk Jung, and Nae Eung Lee. Methylammonium lead iodide perovskite-graphene hybrid channels in flexible broadband phototransistors. *Carbon*, 105:353–361, 2016.

[275] Vikash Kumar Ravi, Pralay K. Santra, Niharika Joshi, Jeetender Chugh, Sachin Kumar Singh, Håkan Rensmo, Prasenjit Ghosh, and Angshuman Nag. Origin of the Substitution Mechanism for the Binding of Organic Ligands on the Surface of CsPbBr 3 Perovskite Nanocubes. *Journal of Physical Chemistry Letters*, 8(20):4988–4994, 2017.

[276] Jiaguo Yu, Lifang Qi, and Mietek Jaroniec. Hydrogen production by photocatalytic water splitting over Pt/TiO 2 nanosheets with exposed (001) facets. *Journal of Physical Chemistry C*, 114(30):13118–13125, 2010.

[277] Yanguang Li, Hailiang Wang, Liming Xie, Yongye Liang, Guosong Hong, and Hongjie Dai. MoS2 nanoparticles grown on graphene: An advanced catalyst for the hydrogen evolution reaction. *Journal of the American Chemical Society*, 133(19):7296–7299, 2011.

[278] Yu Yu, Yating Zhang, Xiaoxian Song, Haiting Zhang, Mingxuan Cao, Yongli Che, Haitao Dai, Junbo Yang, Heng Zhang, and Jianquan Yao. PbS-Decorated WS2 Phototransistors with Fast Response. *ACS Photonics*, 4(4):950–956, 2017.

[279] Martin A. Green, Anita Ho-Baillie, and Henry J. Snaith. The emergence of perovskite solar cells. *Nature Photonics*, 8(7):506–514, 2014.

[280] Shan Chen and Gaoquan Shi. Two-Dimensional Materials for Halide

Perovskite-Based Optoelectronic Devices. *Advanced Materials*, 29(24):1–31, 2017.

[281] Hsinhan Tsai, Reza Asadpour, Jean Christophe Blancon, Constantinos C. Stoumpos, Olivier Durand, Joseph W. Strzalka, Bo Chen, Rafael Verduzco, Pulickel M. Ajayan, Sergei Tretiak, Jacky Even, Muhammad Ashraf Alam, Mercouri G. Kanatzidis, Wanyi Nie, and Aditya D. Mohite. Light-induced lattice expansion leads to high-efficiency perovskite solar cells. *Science*, 360(6384):67–70, 2018.

[282] Youngbin Lee, Jeong Kwon, Euyheon Hwang, Chang Ho Ra, Won Jong Yoo, Jong Hyun Ahn, Jong Hyeok Park, and Jeong Ho Cho. High-performance perovskite-graphene hybrid photodetector. *Advanced Materials*, 27(1):41–46, 2015.

[283] Jie Hu, Lina Wang, Lina Shi, and Hao Huang. Preparation of La 1-x Ca x MnO 3 perovskite-graphene composites as oxygen reduction reaction electrocatalyst in alkaline medium. *Journal of Power Sources*, 269:144–151, 2014.

[284] Nam Joong Jeon, Hyejin Na, Eui Hyuk Jung, Tae Youl Yang, Yong Guk Lee, Geunjin Kim, Hee Won Shin, Sang Il Seok, Jaemin Lee, and Jangwon Seo. A fluorene-terminated hole-transporting material for highly efficient and stable perovskite solar cells. *Nature Energy*, 3(8):682–689, 2018.

[285] Yu Chen, Bohang Song, Xiaosheng Tang, Li Lu, and Junmin Xue. Ultrasmall Fe3O4 nanoparticle/MoS2 nanosheet composites with superior performances for lithium ion batteries. *Small*, 10(8):1536–1543, 2014.

[286] Ye Lu, B. R. Goldsmith, N. J. Kybert, and A. T.C. Johnson. DNA-decorated graphene chemical sensors. *Applied Physics Letters*, 97(8):8–11, 2010.

[287] Jinfei Dai, Jun Xi, Lu Li, Jing Feng Zhao, Yifei Shi, Wenwen Zhang, Chenxin Ran, Bo Jiao, Xun Hou, Xinhua Duan, and Zhaoxin Wu. Charge Transport between Coupling Colloidal Perovskite Quantum Dots Assisted by Functional Conjugated Ligands. *Angewandte Chemie - International Edition*, 57(20):5754–5758, 2018.

[288] Junpeng Lu, Alexandra Carvalho, Hongwei Liu, Sharon Xiaodai Lim, Antonio H. Castro Neto, and Chorng Haur Sow. Hybrid Bilayer WSe2 - CH3NH3PbI3 Organolead Halide Perovskite as a High-Performance Photodetector. *Angewandte Chemie - International Edition*, 55(39):11945–11949, 2016.

[289] Aizhao Pan, Bo He, Xiaoyun Fan, Zeke Liu, Jeffrey J. Urban, A. Paul Alivisatos, Ling He, and Yi Liu. Insight into the Ligand-Mediated Synthesis of Colloidal CsPbBr3 Perovskite Nanocrystals: The Role of Organic Acid, Base, and Cesium Precursors. *ACS Nano*, 10(8):7943–7954, 2016.

[290] Yan Wang, Raymond Fullon, Muharrem Acerce, Christopher E. Petoukhoff, Jieun Yang, Chenggan Chen, Songnan Du, Sin Ki Lai, Shu Ping Lau, Damien Voiry, Deirdre O'Carroll, Gautam Gupta, Aditya D. Mohite, Shengdong Zhang, Hang Zhou, and Manish Chhowalla. Solution-Processed MoS2 /Organolead Trihalide Perovskite Photodetectors. *Advanced Materials*, 29(4):1–7, 2017.

[291] Dongman Hou, Weijia Zhou, Xiaojun Liu, Kai Zhou, Jian Xie, Guoqiang Li, and Shaowei Chen. Pt nanoparticles/MoS 2 nanosheets/carbon fibers as efficient catalyst for the hydrogen evolution reaction. *Electrochimica Acta*, 166:26–31, 2015.

[292] Loredana Protesescu, Sergii Yakunin, Maryna I. Bodnarchuk, Franziska Krieg, Riccarda Caputo, Christopher H. Hendon, Ruo Xi Yang, Aron Walsh, and Maksym V. Kovalenko. Nanocrystals of Cesium Lead Halide Perovskites (CsPbX3, X = Cl, Br, and I): Novel Optoelectronic Materials Showing Bright Emission with Wide Color Gamut. *Nano Letters*, 15(6):3692–3696, 2015.

[293] Vinayan Bhagavathi Parambhath, Rupali Nagar, K. Sethupathi, and S. Ramaprabhu. Investigation of spillover mechanism in palladium decorated hydrogen exfoliated functionalized graphene. *Journal of Physical Chemistry C*, 115(31):15679–15685, 2011.

[294] Henry J. Snaith. Present status and future prospects of perovskite photovoltaics. *Nature Materials*, 17(5):372–376, 2018.

[295] Mauro Brotons-Gisbert, Raphaël Proux, Raphaël Picard, Daniel Andres-Penares, Artur Branny, Alejandro Molina-Sánchez, Juan F. Sánchez-Royo, and Brian D. Gerardot. Out-of-plane orientation of luminescent excitons in atomically thin indium selenide flakes. *Nature Communications*, (2019):1–10, 2019.

6 Light-matter interaction in two-dimensional materials on waveguides

In this chapter, the optical measurements of 2D nanosheets on waveguides will be analysed. This project has been developed in collaboration with Dr. Isaac Suárez-Álvarez (waveguide preparation and measurements), Rodolfo Canet-Albiach (preparation of samples and measurements), Dr. Mauro Brotons-Gisbert and Dr. Alejandro Molina-Sanchez (theoretical discussion).

6.1 Introduction

In previous chapters, several optoelectronic properties of 2D materials have been studied, showing promising results for its implementation for specific applications. As in most publications on the field, the properties to be studied on a material and its potential use as a photodiode, photodetector, solar cell, for instance, is demonstrated using the air as path for transporting the photons involved. These types of devices, although perfectly useful and valid to demonstrate this purpose, are very sensitive and unstable to calibration, where any mechanical disturbance, however minimal, completely cancels the detection and usability of the effect pursued. In order to do so in photonic devices, the excitation source and the photoluminescent emission must be collected and contained in every step through the whole process.

Generally speaking, in photonic applications, where the wavelengths involved in the processes in the devices lying in the visible and near infrared spectra (400 nm - 1100 nm), optical waveguides are the channel of choice for light transportation. Due to the internal optical modes in the waveguides and effects such as total internal reflexion due to the difference between refractive indexes, light is confined in the

device, avoiding losses due to multidireccional emission on the materials involved or mechanical disaligning on the elements. Usually, optical materials (i.e., they do not absorb propagating photons) are used, such as polymers (PDMS [305, 303] or PMMA [306, 304, 299], for instance) and Si-compounds (SiN_x [307, 308, 311] or SiO_2 in fibre optics, like the project developed in Chapter 7) in most cases.

The relevance of photon confinement and guiding of waveguides is highlighted in some projects specially, from using a TMD as a saturable absorber for lasing [309], an experiment showing a two-particle bosonic-fermionic quantum walk [337], surface plasmons using these materials [301] or any photonic-device oriented for a foldable usage [314].

Another advantage of the integration of waveguides into devices is their complete compatibility and integration with the Si and CMOS optoelectronic industry developed in the last years [315, 393, 312, 313, 339], optimising the cicle of basic research - device implementation - development into commercial devices.

Due to the recent birth of the 2D materials field (2004 with the discovery of graphene [322] and its rise in 2010 with the Nobel prize [310]), most publications aimed for the basic properties, leaving a proper photonic implementation for future projects. Although in the electrical part some publications obtained flexible and reliable contacts [300, 298], in the optical or photonic part not so many articles focus on this topic. Note the usage of Black Phosphorus as a photodetector integrated in a Si waveguide [336] (aiming for a more optoelectronic device), the waveguide collection for WSe_2 quantum emitters [320] and second-harmonic generation in $MoSe_2$ [319], a polarization-dependent study in MoS2 on a waveguide [325] and, specially, the encapsulation of a MoS_2 ML in a waveguide [317], where the excitation is in the horizontal direction and its collection in the vertical direction, project aiming for similar objectives as this chapter attemps. However, these processes need further study for its proper implementation in large scale devices [302].

This directionality effect on the excitation and collection is expected to be specially relevant in InSe. As commented in previous chapters (Chapters 4 and 5), the usual scientific vertical excitation - vertical collection approach hampers InSe due to its OP dipolar behavior [297], deminishing its absorption and emission. This problematic could be fixed with different configurations involving the horizontal direction, highly unexplored in general, which take advantages from this OP orientation.

In this chapter, starting with InSe and, for comparison, WSe_2 and $MoSe_2$ as TMDs

examples, will be integrated on an optical waveguide for its further study. To do so, every excitation - collection configuration possible has been explored, as shown in Figure 6.1.

The waveguides used for this chapter have been prepared by Dr. Isaac Suárez-Álvarez, and a $MoSe_2$ sample whose measurements will be presented in this chapter, has been prepared by Rodolfo Canet-Albiach.

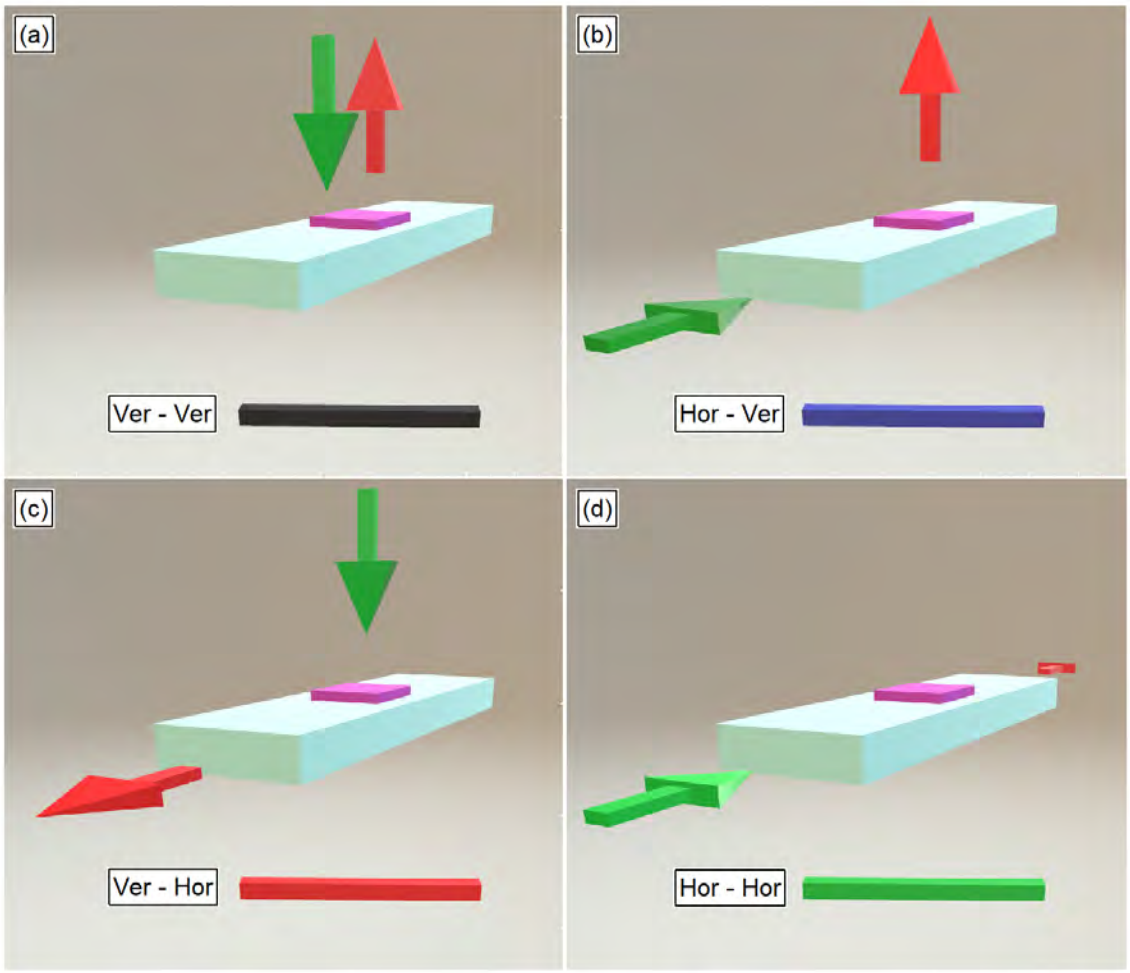

Figure 6.1: Schematic waveguide and sample measurements configurations, labeled, in this order, as the "excitation - collection" directions.

6.2 Guiding InSe photoluminescence

In order to measure through this approach the OP dipolar behavior in InSe, an exfoliated sample with a shift in its RT PL emission, proving therefore quantum

confinement (with a thickness of 4 nm due to its emission at 1.45 eV [334]), was transferred via all-dry viscoelastic transfer (see Subsections 2.1.1 and 2.1.3.1) on a 1D waveguide prepared using photolitography in SU-8 photoresist resin. The PL measurements performed in a horizontal excitation - vertical collection, vertical excitation - horizontal collection and horizontal excitation - horizontal collection have been taken using the hand-made setup showed in Subsection 2.2.3 (Figure 2.8b), where the directions for excitation and collection can be freely chosen between horizontal and vertical in any configuration possible (Figure 6.1), while the vertical excitation - vertical collection measurements have been performed in the Horiba Xplora μ-Raman setup described in Subsection 2.2.3 (Figure 2.8a).

In spite of all essays performed, no data in any guiding configuration, in which the horizontal direction is involved, was obtained due to the low PL of InSe compared with the intrinsic waveguide resin emission. As an example of the results obtained, Figure 6.2 shows the PL response of an InSe flake on a waveguide measured in a confocal vertical excitation and collection configuration, where the confocal resolution allow its detection.

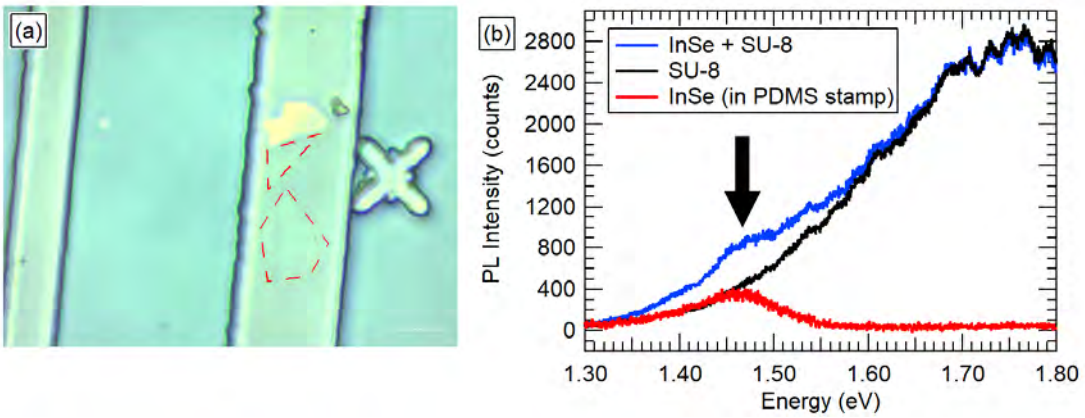

Figure 6.2: PL measurements in InSe on SU-8 waveguide: on the left (a), optical image of the sample transferred (highlighted with dashed red areas) and, on the right (b), RT PL measured in a confocal vertical excitation and collection of the InSe nanosheet (red) and the SU-8 waveguide (black) before the transfer and the PL measured after the sample was transferred (blue).

Due to this experimental unavoidable emission, hampering every measurement taken in InSe, the following waveguide devices were prepared using TMDs MLs, with higher RT PL emission [335, 333, 338, 321], instead of InSe in order to optimise the techniques and experimental setup prior to start studying this material. Besides, 2D

Poly(methyl methacrylate) (PMMA) waveguides, will be employed (if not indicated otherwise) instead of the SU-8 1D ones to avoid its resin fluorescence.

6.3 Guiding transition metal dichalcogenides photoluminescence

The 2D PMMA waveguides have been prepared via spin coating on a Si wafer, obtaining thicknesses of ~1 μm on top of Si substrate to have confinement in the vertical direction (instead of a confinement in 2 directions, vertical and horizontal, in the 1D waveguides). After several monolayered TMD samples transferred onto 2D PMMA waveguides it can be observed the following common summary experimental results, as these sumarised in Figure 6.3:

- Horizontal excitation - vertical collection: double narrower separated peak emission.
- Vertical excitation - horizontal collection: wide emission with an apparent shoulder at lower energies.
- Horizontal excitation - horizontal collection: wide emission with an apparent shoulder at lower energies.
- Vertical excitation - vertical collection: unlike the previous configurations, the μ-PL Horiba Xplora confocal setup (described in Subsection 2.2.3) has been used, with a collection spot around ~1 μm^2, allowing a micrometric-resolution mapping study. A wide emission was observed in any point, but in edges, cracks or folded areas a clearer shoulder, even as a second peak can be observed, but never isolated or separated from the other peak as in the horizontal excitation - vertical collection configuration.

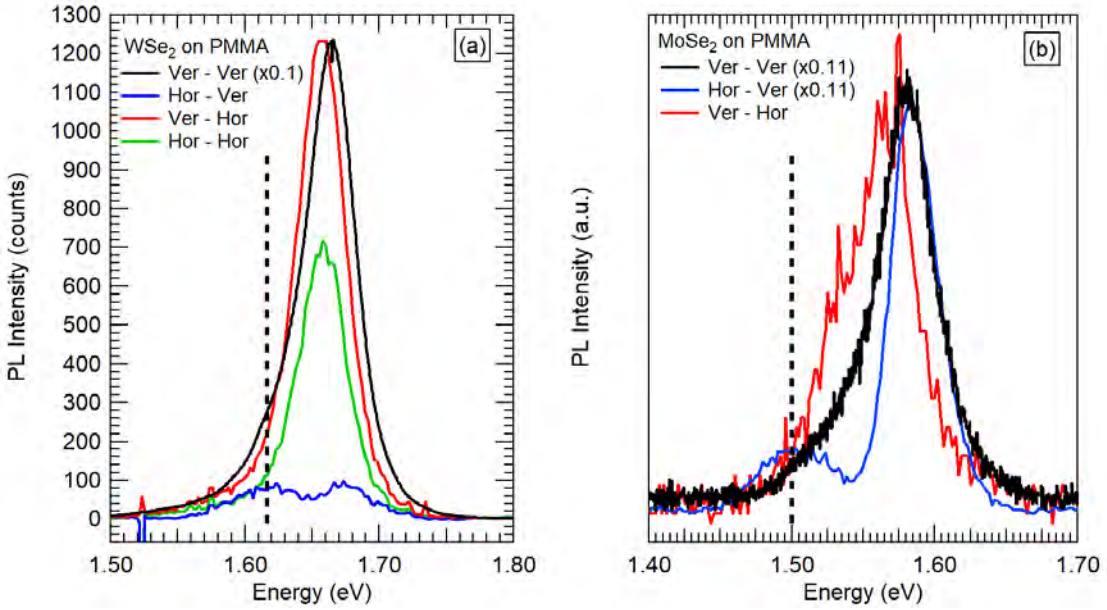

Figure 6.3: PL emission measured in WSe_2 (a) and $MoSe_2$ (b) on 2D PMMA waveguides in different configurations. WSe_2 measurements have not been normalised (except vertical - vertical configuration) to show intensities comparison. $MoSe_2$ measurements have been normalised according to the factors on the legend

In the first set of measurements, these shown in Figure 6.3, it can be observed different emission detected just varying the configuration of the measurement. Two different emission components can be observed depending on the excitation and collection direction. In both materials, a weak feature can be observed in the low-energy side of PL peak attributable to the X^+ exciton appearing around 1.61 eV for WSe_2 and 1.50 eV for $MoSe_2$ [329, 328, 327, 324, 326], which has been marked by dotted lines. The relative intensity of this feature, as compared to that of the X^0 exciton, strongly depends on the excitation/collection modes. These facts have been observed in all samples studied, resulting independent of the following parameters:

- Traversed waveguide distance, this fact allows discarding reabsorption in the waveguide (as observed in Figure 6.4a, where the same sample, transferred in an area close to an edge of a 2D PMMA waveguide, has been measured in horizontal excitation and vertical collection, but rotating the sample in both sides, exciting through the longer and the shorter guiding side, with qualitatively no change in the measurements but an intensity change due to the losses in collection in the longer guiding direction).
- Size of the sample in the guiding direction, this fact allows discarding reabsorp-

tion in the own TMD (after measuring several samples with different WSe_2 MLs of different sizes, no qualitatively effect has been observed apart from having an enhancement in intensity detected in larger samples).

- Excitation laser, as observed in Figure 6.4b, where 532nm and 633nm have been used as excitation source.
- Waveguide material or configuration, discarding different waveguide material influence or effect in 1D or 2D confinement (as observed in Figure 6.4c, obtaining similar behavior in WSe_2 MLs in 1D SU-8 considering its own fluorescence, 2D PMMA or 1D PMMA waveguides).
- TMD monolayer used, obtaining the same behavior in WSe_2 and $MoSe_2$ (each of them in its own RT emission range [333]), this fact allows discarding a possible dark exciton as the low energy peak, since in $MoSe_2$ this peak should appear at higher energies [332, 429, 330]).

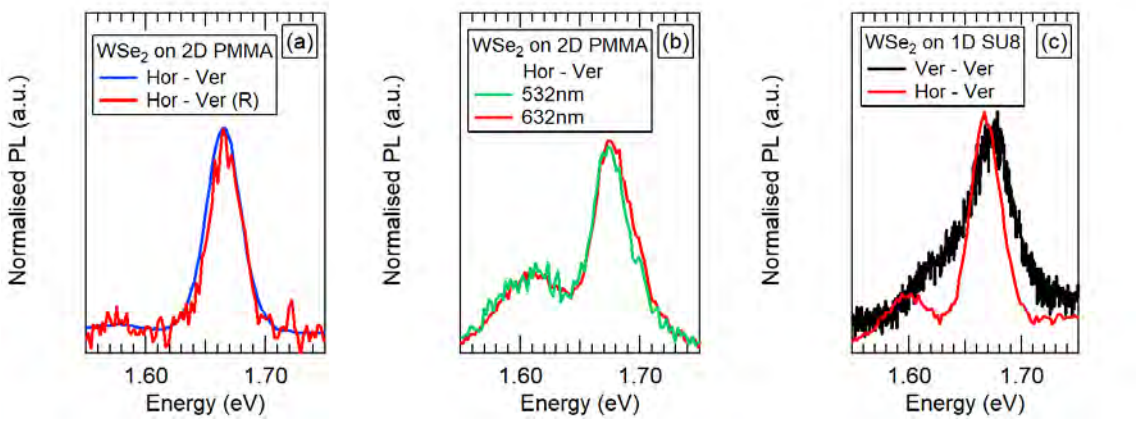

Figure 6.4: PL measurements in WSe_2 on waveguides, changing the propagation distance in the excitation direction (a), the excitation laser wavelength (b) and material and confinement directions in the waveguide (c).

In all measurements, it is present the emission expected at RT attributable to the exciton X^0 in the transferred material at higher energies (1.66 eV in WSe_2 and 1.59 eV in $MoSe_2$ [333]). However, the lower energy peak/shoulder, after discarding dark exciton or reabsorptions in the active material or waveguide, can be atributed to the bounded exciton or charged exciton X^+ (due to the p-doping in our bulk material, see Appendix A), coherent with reported energy position [329, 328, 327, 324, 326]. This is demonstrated in the confocal vertical excitation and collection PL maps,

where this contribution, although present in every point in the tail of the emission, is clearly enhanced in the borders, edges or raised parts [323]. In these areas the localised defects increase the density of electrons, recombining in bounded excitons in that areas, as observed in Figure 6.5.

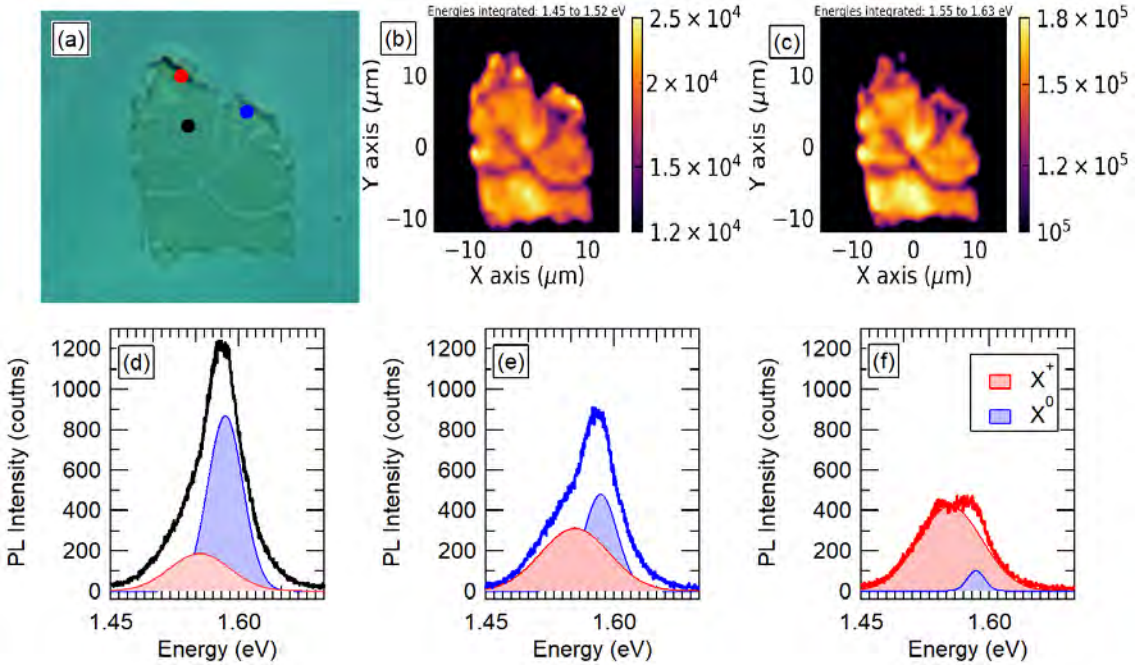

Figure 6.5: Confocal vertical excitation and collection PL map in a $MoSe_2$ monolayer on a 2D PMMA waveguide. In the optical image in (a) has been marked different coloured points, which spectras are shown in (d) as an example of an average point, and (e) and (f) points on the edges where the bounded exciton contribution is enhanced. In (b) and (c), the PL maps integrating in the bounded exciton energies (b) and the X^0 exciton (c), respectively. In the PL spectras, it has been highlighted two different contributions X^+ and X^0, fitting with two separated gaussian components.

However, this two-contribution emission in the RT PL in TMDs monolayers, where the exciton X^0 and the charged exciton X^+ are the responsible of the effects before described does not explain the following experimental observations:

- Comparing measurements taken in the same sample, the peak position of both contributions is not constant changing the configuration. This fact is clearly shown in Figure 6.3a, where the double peak observed in horizontal excitation - vertical collection does not match with the other measurements,

nor the charged exciton with the shoulders observed nor the X^0 with the peak maximum position.

- Even though the localised exciton does not have a specific energy position (the fact that it is created dominantly in localised defects like borders or tilted edges differs one from the others, producing a wide band emission) it has been observed that it shifts to higher energies when the localised exciton is enhanced, reducing the X^0 exciton intensity (Figures 6.5d, e and f).
- It does not explain why in horizontal excitation - vertical collection the contributions are clearly separated. Such an intense narrowing due exclusively to the configuration measurement is not expected.

A polarisation study has been realised, as shown in Figure 6.6, where the horizontal collection is filtered through a linear polariser, obtaining more intensity when the polariser matches the reported IP X^0 directionality, variance not seen in the energy ranges where the X^+ is expected.

On the left in Figure 6.6, what has been polarised is the excitation arriving to the ML, observing, therefore, its absorption behavior. After renormalising, no qualitatively change is observed in the X^0 exciton nor in the X^+. Independently of the polarisation in the excitation, the propagation $\overrightarrow{k}$ vector is perpendicular to the IP or OP dipole, agreeing with the absorption expected behavior.

On the right, the collection has been filtered through a polariser, collecting the emission of the sample depending on the polarisation. In this case, after renormalising, exciton X^0 is unaffected (besides having an increased intensity in TE polarisation due to the natural IP TMD behavior), but at lower energies the emission is reduced when the IP component is blocked (polariser in TM mode, vertical). This situation affects the low-energy shoulder where the exciton X^+ is located, showing OP behavior, opposite to X^0, due to the preference in the waveguide to TE modes.

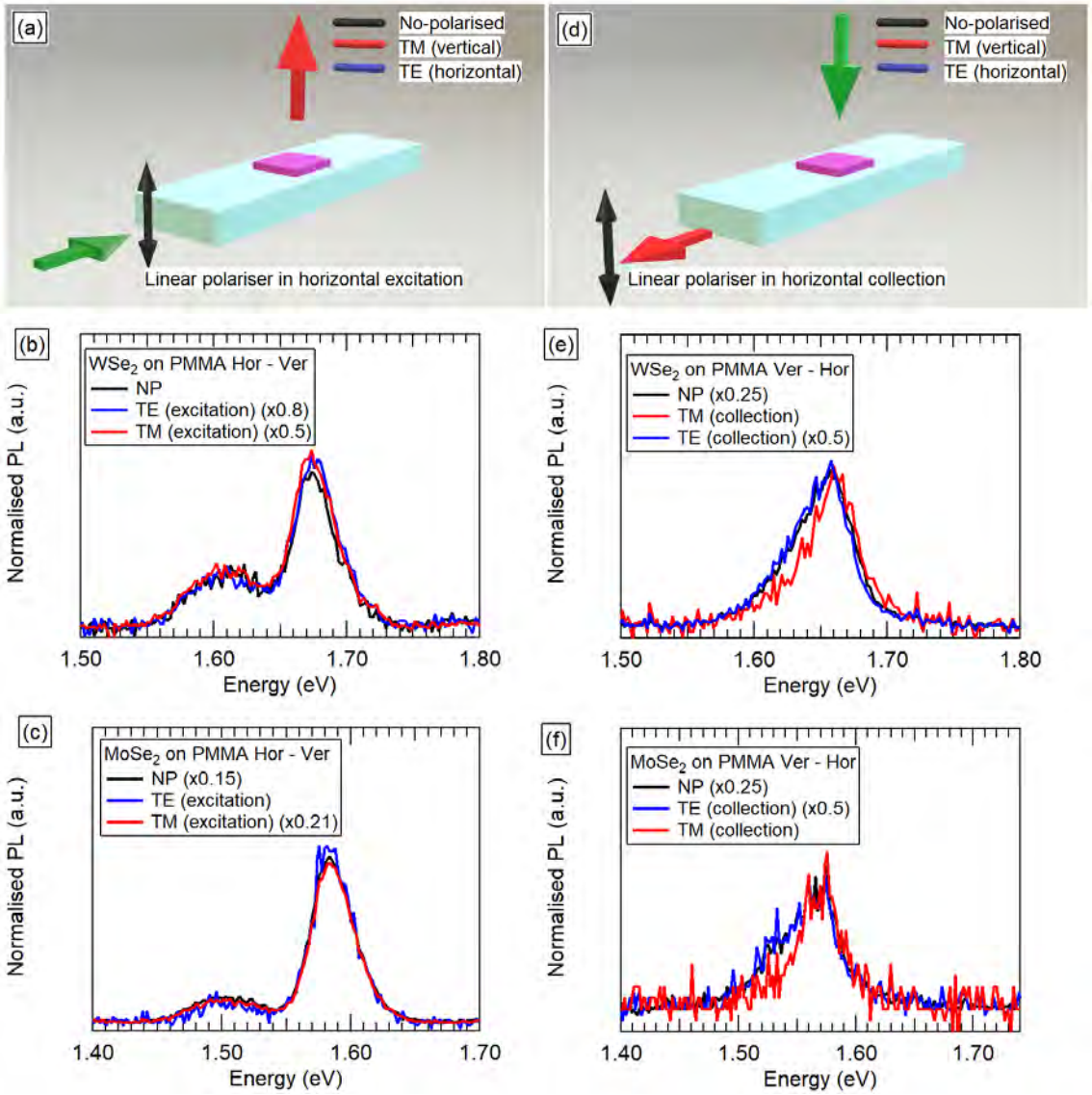

Figure 6.6: Polarisation study in PL in waveguides. On the left, horizontal polarised excitation and vertical collection and on the right vertical excitation and horizontal polarised collection. (a) and (d) show the experimental diagram, while (b), (e) and (c), (f) show the measurements in WSe_2 and $MoSe_2$, respectively.

With this concept in mind it is easy to understand some previous concerns about the experimental results. At RT, in normal conditions, X^0 is the dominant contribution in TMDs ML PL. Besides, due to the IP carrier confinement in the nanosheet, the nature of this contribution behaves as an IP dipole, as observed in the collection polarisation measurements, agreeing with the IP dipolar behavior reported in TMDs MLs [297] due to its dominant behavior.

Finally, as observed in Figure 6.5, X^0 contribution is reduced in the edges and tilted nanosheet borders, where the bounded exciton formation is enhanced and the X^0 emission is hampered. In our measurements involving the horizontal direction, these contributions are detected clearly due to the fact that all the sample is excited and its emission collected, adding up all localised defect contributions to become a relevant emission. At LT, the lifetime of these two contributions increase, narrowing its emission, being able to separate the isolated contribution of X^0 and X^+, as observed in literature [329, 328, 327, 324, 326].

However, the double peak nature in horizontal excitation - vertical collection measurements remains undetermined. This bounded exciton localisation cannot be explained due to Fabry-Perot resonances (Figure 6.7) nor polaritonic effects (Figure 6.8). Figure 6.7a and b show a colorplot of reflectivity, as a function of the emission angle and the emission energy, calculated for a WSe_2 and $MoSe_2$ ML on a PMMA/SiO_2/Si substrate as that used in this work. Taking into account that the numerical aperture of the objective used in our experiments (22º), it would be expected that emission at 1.65 eV, that corresponds to that of WSe_2, was strongly suppresed. This may explain results shown in Figure 6.6b. However, similar calculations would predict an enhancement of emission at 1.55 eV, that contrasts to the minimum of emission observed in $MoSe_2$ at this energy. Refractive indexes for WSe_2 and $MoSe_2$ MLs used for the calculations have been obtained from [296].

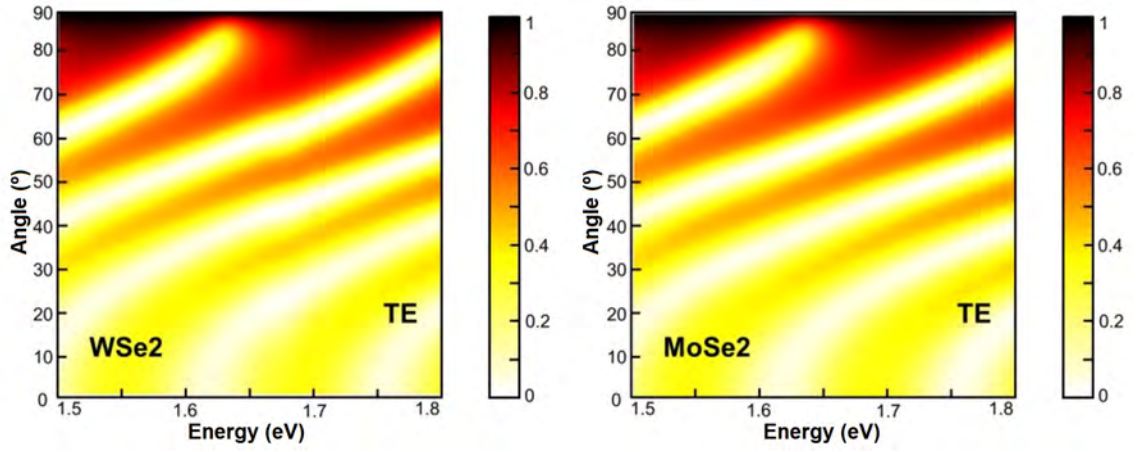

Figure 6.7: Reflectivity calculations considering the multilayered structure Si / SiO_2 (1 μm) / PMMA (1 μm) / TMD ML (1 nm) / air as a Fabry-Perot cavity for WSe_2 (left) and $MoSe_2$ (right) as TMD ML.

Regarding a polaritonic influence in the separation of both peaks, in Figure 6.8 can

be observed similar PL when the collection angle is changed. The directionality of polaritonic effects should vary drastically when the angle is changed, this fact allows discarding this explanation.

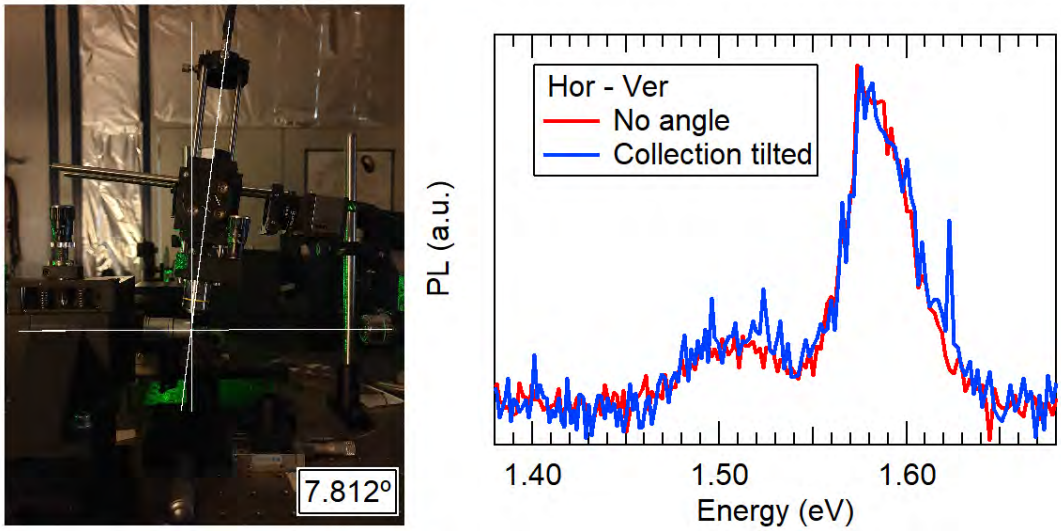

Figure 6.8: PL collection in the vertical direction exciting in the horizontal direction with (blue) and without (red) a slight change in the collection angle.

6.4 Conclusions

In this chapter, 2D WSe_2 and $MoSe_2$ ML have been implemented in waveguides, exploring not only horizontal excitation - vertical collection [317], but all different configurations possible. This waveguide implementation, specially in the horizontal excitation - horizontal collection, highlights due to its clear compatibility with integrated optoelectronic devices, as well as current Si integrated technologies. These results, therefore, show the compatibility of this materials with a more tecnological and commercial appliability, withholding the fabrication techniques already developed and standarised.

Besides, for TMDs, at RT, two different contributions in their PL emission have been observed: the neutral exciton X^0 and the charged exciton X^+, showing a dipolar nature as reported or already studied in other chapters. These results matches recent publications [317, 329, 326]. However, our results show that in a horizontal excitation - vertical collection, these contributions are clearly separated. This fact, on one hand, leaves these components narrower to its usage for a specific application,

allowing the interaction separately in each of them and, on the other hand, separate them for its further study without complex conditions such as low temperatures [326, 327] or magnetic fields [330].

Even though this chapter started aiming to the study of the OP dipolar InSe nature and its implementation, it has resulted in a study on other semiconductors like the TMDs. Therefore the next step, after optimising the techniques used using TMDs, InSe nanosheets will be studied in future projects.

Bibliography

[296] Chunwei Hsu, Riccardo Frisenda, Robert Schmidt, Ashish Arora, Steffen Michaelis de Vasconcellos, Rudolf Bratschitsch, Herre S.J. van der Zant, and Andres Castellanos-Gomez. Thickness-Dependent Refractive Index of 1L, 2L, and 3L MoS2, MoSe2, WS2, and WSe2. *Advanced Optical Materials*, 7(13), 2019.

[297] Mauro Brotons-Gisbert, Raphaël Proux, Raphaël Picard, Daniel Andres-Penares, Artur Branny, Alejandro Molina-Sánchez, Juan F. Sánchez-Royo, and Brian D. Gerardot. Out-of-plane orientation of luminescent excitons in atomically thin indium selenide flakes. *Nature Communications*, (2019):1–10, 2019.

[298] Denis A. Areshkin and Carter T. White. Building blocks for integrated graphene circuits. *Nano Letters*, 7(11):3253–3259, 2007.

[299] F Bender, R W Cernosek, and F Josse. Love-wave biosensors using cross-linked polymer waveguides on LiTaO3 substrates. *Electronics Letters*, 35(9):698–699, 1995.

[300] Xuetao Gan, Ren Jye Shiue, Yuanda Gao, Inanc Meric, Tony F. Heinz, Kenneth Shepard, James Hone, Solomon Assefa, and Dirk Englund. Chip-integrated ultrafast graphene photodetector with high responsivity. *Nature Photonics*, 7(11):883–887, 2013.

[301] Xiaoyong He, Feng Liu, Fangting Lin, Guina Xiao, and Wangzhou Shi. Tunable MoS2 modified hybrid surface plasmon waveguides. *Nanotechnology*, 30(12), 2019.

[302] Brent E. Little and Sai T. Chu. Toward Very Large-Scale Integrated Photonics. *Optics and Photonics News*, 11(11):24, 2000.

[303] Stefan Kopetz, Dengke Cai, Erik Rabe, and Andreas Neyer. PDMS-based optical waveguide layer for integration in electrical-optical circuit boards. *AEU - International Journal of Electronics and Communications*, 61(3):163–167, 2007.

[304] Antonio Bueno, Isaac Suárez, Rafael Abargues, Salvador Sales, and Juan P Martínez Pastor. Temperature sensor based on colloidal quantum dots-PMMA nanocomposite waveguides. *IEEE Sensors Journal*, 12(10):3069–3074, 2012.

[305] Ziliang Cai, Weiping Qiu, Guocheng Shao, and Wanjun Wang. A new fabrication method for all-PDMS waveguides. *Sensors and Actuators, A: Physical*, 204:44–47, 2013.

[306] Anadi Mukherjee. Two-photon pumped upconverted lasing in dye doped polymer waveguides. *Applied Physics Letters*, 62(26):3423–3425, 1993.

[307] Daryl T. Spencer, Tara Drake, Travis C. Briles, Jordan Stone, Laura C. Sinclair, Connor Fredrick, Qing Li, Daron Westly, B. Robert Ilic, Aaron Bluestone, Nicolas Volet, Tin Komljenovic, Lin Chang, Seung Hoon Lee, Dong Yoon Oh, Myoung Gyun Suh, Ki Youl Yang, Martin H.P. Pfeiffer, Tobias J. Kippenberg, Erik Norberg, Luke Theogarajan, Kerry Vahala, Nathan R. Newbury, Kartik Srinivasan, John E. Bowers, Scott A. Diddams, and Scott B. Papp. An optical-frequency synthesizer using integrated photonics. *Nature*, 557(7703):81–85, 2018.

[308] Saeed Khan, Jeff Chiles, Jichi Ma, and Sasan Fathpour. Silicon-on-nitride optical waveguides for mid- and near-infrared integrated photonics. *2013 Conference on Lasers and Electro-Optics, CLEO 2013*, 121104:1–4, 2013.

[309] Chen Cheng, Hongliang Liu, Zhen Shang, Weijie Nie, Yang Tan, Blanca del Rosal Rabes, Javier R. Vázquez de Aldana, Daniel Jaque, and Feng Chen. Femtosecond laser written waveguides with MoS2 as satuable absorber for passively Q-switched lasing. *Optical Materials Express*, 6(2):367, 2016.

[310] Ed Gerstner. Nobel Prize 2010: Andre Geim & Konstantin Novoselov. *Nature Physics*, 6(11):836–836, 2010.

[311] Ehsan Shah Hosseini, Siva Yegnanarayanan, Mohammad Soltani, and Ali Adibi. Ultra-high quality factor silicon nitride planar microdisk resonators for integrated photonics in the visible range. *Optics InfoBase Conference Papers*, 17(17):2487–2489, 2008.

[312] G. Cocorullo, C. Minarini, A. Rubino, F. G. Della Corte, I. Rendina, and E. Terzini. Amorphous silicon waveguides and light modulators for integrated photonics realized by low-temperature plasma-enhanced chemical-vapor deposition. *Optics Letters*, 21(24):2002, 1996.

[313] Pavel Cheben, Robert Halir, Jens H. Schmid, Harry A. Atwater, and David R. Smith. Subwavelength integrated photonics. *Nature*, 560(7720):565–572, 2018.

[314] Juejun Hu, Lan Li, Hongtao Lin, Ping Zhang, Weidong Zhou, and Zhenqiang Ma. Flexible integrated photonics: where materials, mechanics and optics meet [Invited]. *Optical Materials Express*, 3(9):1313, 2013.

[315] Ming Liu and Xiang Zhang. Graphene benefits. *Nature Photonics*, 7(11):851–852, 2013.

[316] Kin Fai Mak, Changgu Lee, James Hone, Jie Shan, and Tony F. Heinz. Atomically thin MoS2: A new direct-gap semiconductor. *Physical Review Letters*, 105(13):2–5, 2010.

[317] Filip Auksztol, Daniele Vella, Ivan Verzhbitskiy, Kian Fong Ng, Yi Wei Ho, James A. Grieve, José Viana-Gomes, Goki Eda, and Alexander Ling. Elastomeric Waveguide on-Chip Coupling of an Encapsulated MoS2 Monolayer. *ACS Photonics*, 6(3):595–599, 2019.

[318] Linghai Liu, Ke Xu, Xi Wan, Jianbin Xu, Chi Yan Wong, and Hon Ki Tsang. Enhanced optical Kerr nonlinearity of MoS2 on silicon waveguides. *Photonics Research*, 3(5):206, 2015.

[319] Haitao Chen, Vincent Corboliou, Alexander S Solntsev, Duk-Yong Choi, Maria A Vincenti, Domenico de Ceglia, Costantino de Angelis, Yuerui Lu, and Dragomir N Neshev. Enhanced second-harmonic generation from two-dimensional MoSe2 on a silicon waveguide. *Light: Science & Applications*, 6(10):e17060–e17060, 2017.

[320] Subhojit Dutta, Tao Cai, Mustafa Atabey Buyukkaya, Sabyasachi Barik, Shahriar Aghaeimeibodi, and Edo Waks. Coupling quantum emitters in WSe2 monolayers to a metal-insulator-metal waveguide. *Applied Physics Letters*, 113(19), 2018.

[321] Xingli Wang, Yongji Gong, Gang Shi, Wai Leong Chow, Kunttal Keyshar, Gonglan Ye, Robert Vajtai, Jun Lou, Zheng Liu, Emilie Ringe, Beng Kang Tay, and Pulickel M. Ajayan. Chemical vapor deposition growth of crystalline monolayer MoSe2. *ACS Nano*, 8(5):5125–5131, 2014.

[322] K.S. Novoselov, A.K. Geim, S.V. Morozov, D. Jiang, Y. Zhang, S.V. Dubonos, I.V. Grigorieva, and A.A. Firsov. Electric Field Effect in Atomically Thin Carbon Films. *Science Reports*, 306(October):666–670, 2004.

[323] Yifei Yu, Yiling Yu, Chao Xu, Yong Qing Cai, Liqin Su, Yong Zhang, Yong Wei Zhang, Kenan Gundogdu, and Linyou Cao. Engineering Substrate Interactions

for High Luminescence Efficiency of Transition-Metal Dichalcogenide Monolayers. *Advanced Functional Materials*, 26(26):4733–4739, 2016.

[324] Matteo Barbone, Alejandro R.P. Montblanch, Dhiren M. Kara, Carmen Palacios-Berraquero, Alisson R. Cadore, Domenico De Fazio, Benjamin Pingault, Elaheh Mostaani, Han Li, Bin Chen, Kenji Watanabe, Takashi Taniguchi, Sefaattin Tongay, Gang Wang, Andrea C. Ferrari, and Mete Atatüre. Charge-tuneable biexciton complexes in monolayer WSe2. *Nature Communications*, 9(1), 2018.

[325] Yang Tan, Ruiyun He, Chen Cheng, Dong Wang, Yanxue Chen, and Feng Chen. Polarization-dependent optical absorption of MoS 2 for refractive index sensing. *Scientific Reports*, 4:1–6, 2014.

[326] G. Wang, L. Bouet, D. Lagarde, M. Vidal, A. Balocchi, T. Amand, X. Marie, and B. Urbaszek. Valley dynamics probed through charged and neutral exciton emission in monolayer WSe2. *Physical Review B - Condensed Matter and Materials Physics*, 90(7):1–6, 2014.

[327] Ke Wei, Yu Liu, Hang Yang, Xiangai Cheng, and Tian Jiang. Large range modification of exciton species in monolayer WS_2. *Applied Optics*, 55(23):6251, 2016.

[328] Jiani Huang, Thang B. Hoang, and Maiken H. Mikkelsen. Probing the origin of excitonic states in monolayer WSe2. *Scientific Reports*, 6(August 2015):1–7, 2016.

[329] Jason W. Christopher, Bennett B. Goldberg, and Anna K. Swan. Long tailed trions in monolayer MoS2: Temperature dependent asymmetry and resulting red-shift of trion photoluminescence spectra. *Scientific Reports*, 7(1):1–8, 2017.

[330] Xiao Xiao Zhang, Ting Cao, Zhengguang Lu, Yu Chuan Lin, Fan Zhang, Ying Wang, Zhiqiang Li, James C. Hone, Joshua A. Robinson, Dmitry Smirnov, Steven G. Louie, and Tony F. Heinz. Magnetic brightening and control of dark excitons in monolayer WSe2. *Nature Nanotechnology*, 12(9):883–888, 2017.

[331] Xiao Xiao Zhang, Yumeng You, Shu Yang Frank Zhao, and Tony F. Heinz. Experimental Evidence for Dark Excitons in Monolayer WSe2. *Physical Review Letters*, 115(25):1–6, 2015.

[332] J. P. Echeverry, B. Urbaszek, T. Amand, X. Marie, and I. C. Gerber. Splitting between bright and dark excitons in transition metal dichalcogenide monolayers. *Physical Review B*, 93(12):1–5, 2016.

[333] Philipp Tonndorf, Robert Schmidt, Philipp Böttger, Xiao Zhang, Janna Börner, Andreas Liebig, Manfred Albrecht, Christian Kloc, Ovidiu Gordan, Dietrich R. T. Zahn, Steffen Michaelis de Vasconcellos, and Rudolf Bratschitsch. Photoluminescence emission and Raman response of monolayer MoS2, MoSe2, and WSe2. *Advanced Materials*, 29(33):4908–4916, 2017.

[334] Mauro Brotons-Gisbert, Daniel Andres-Penares, Joonki Suh, Francisco Hidalgo, Rafael Abargues, Pedro J. Rodríguez-Cantó, Alfredo Segura, Ana Cros, Gerard Tobias, Enric Canadell, Pablo Ordejón, Junqiao Wu, Juan P. Martínez-Pastor, and Juan F. Sánchez-Royo. Nanotexturing to Enhance Photoluminescent Response of Atomically Thin Indium Selenide with Highly Tunable Band Gap. *Nano Letters*, 16(5):3221–3229, 2016.

[335] B. Radisavljevic, A. Radenovic, J. Brivio, V. Giacometti, and A. Kis. Single-layer MoS2 transistors. *Nature nanotechnology*, 6(3):147–50, 2011.

[336] Nathan Youngblood, Che Chen, Steven J. Koester, and Mo Li. Waveguide-integrated black phosphorus photodetector with high responsivity and low dark current. *Nature Photonics*, 9(4):247–252, 2015.

[337] Linda Sansoni, Fabio Sciarrino, Giuseppe Vallone, Paolo Mataloni, Andrea Crespi, Roberta Ramponi, and Roberto Osellame. Two-particle bosonic-fermionic quantum walk via integrated photonics. *Physical Review Letters*, 108(1):1–5, 2012.

[338] Andrea Splendiani, Liang Sun, Yuanbo Zhang, Tianshu Li, Jonghwan Kim, Chi Yung Chim, Giulia Galli, and Feng Wang. Emerging photoluminescence in monolayer MoS2. *Nano Letters*, 10(4):1271–1275, 2010.

[339] Sebastian Romero-García, Florian Merget, Frank Zhong, Hod Finkelstein, and Jeremy Witzens. Silicon nitride CMOS-compatible platform for integrated photonics applications at visible wavelengths. *Optics Express*, 21(12):14036, 2013.

7 Bismuth Sulphide

In this chapter, the anisotropy in exfoliated Bismuth Sulphide nanoflakes will be explored, from its optical properties to its implementation in fibre optics.

7.1 Introduction

In the previous chapters, the anisotropy between the exfoliation direction (z) and the exfoliation plane (x - y plane) concerning the IP or OP dipolar behavior of the 2D nanosheets studied fundamented the approach to each project. Even more, this laminar structure, from its mere concept, implies and is built from a characteristic anisotropy, at least in the mechanical properties, when these directions are compared. The mechanical properties in the x – y exfoliation plane compared with the vertical z direction diverse hugely, reason why these 2D materials even exist. However, this laminar structure does not pigeonhole these materials just among the biaxial symmetrical materials.

Different materials have shown not only anisotropy in the z direction (like every 2D exfoliable material), but also within the layer plane. This anisotropy in the exfoliation plane is increasing its amount of interest in order to fabricate nanodevices taking into advantage these anisotropic planar properties. In this context, black phosphorus [381, 363, 364, 384, 371, 354] is the most studied anisotropic material. This material differs from other well-known 2D materials, like graphene [372, 361] or the TMDs [197, 113, 370, 377], in which two different non-equivalent in-plane crystallographic directions are present (usually called armchair and zigzag directions) [373, 379]. Not only its mechanical [384], electrical [363] or thermal properties [375] have been demonstrated to be anisotropic, but optical properties such as its photoluminescence [373, 349, 376, 380], Raman scattering [380, 368, 362, 387, 383, 385], optical contrast [356], absorption [356] or optical phase [347] have shown anisotropic behaviour too.

Using these properties, different applications and possibilities have been proposed, from polarisation-sensitive broadband photodetectors [376, 380, 368, 362, 387, 383, 356, 385, 347, 351], linearly polarised ultrafast lasers [343] or optical waveplates [379]. Black phosphorus is not the only example among the 2D materials, e.g., Rhenium Sulphide (ReS_2) [348, 378, 367, 340, 382, 365], Rhenium Selenide ($ReSe_2$) [346] or Titanium Sulphide (TiS_2) [344, 374], among others, have shown different anisotropic properties in the exfoliation plane.

In this project we will study the optical properties in Bi_2S_3 exfoliated nanosheets, demonstrating anisotropy in the layer plane. Finally, we will propose an application in fibre optics using this anisotropy.

Although basic properties of Bi_2S_3 were studied in the past in different configurations, from nanoparticles, nanoribbons, nanorods, bulk or thin films preparation [404, 391, 396, 450, 392, 397, 400, 394], not many aim for its anisotropic nature [395, 401]. In the last years, a few publications can be found about this material, most of them aiming for its synthesis [398, 403, 399, 451, 402] or some applications in batteries [393] and photodetectors [448] in its solved and nanoparticle nature. The lack of studies in exfoliated samples motivated this project.

7.2 Theory and crystallographic structure

In normal conditions, the most stable and common crystallographic structure for Bi_2S_3 is orthorhombic, with a Pnma (62) Hermann Maugin space group [403], as shown in Figure 7.1.

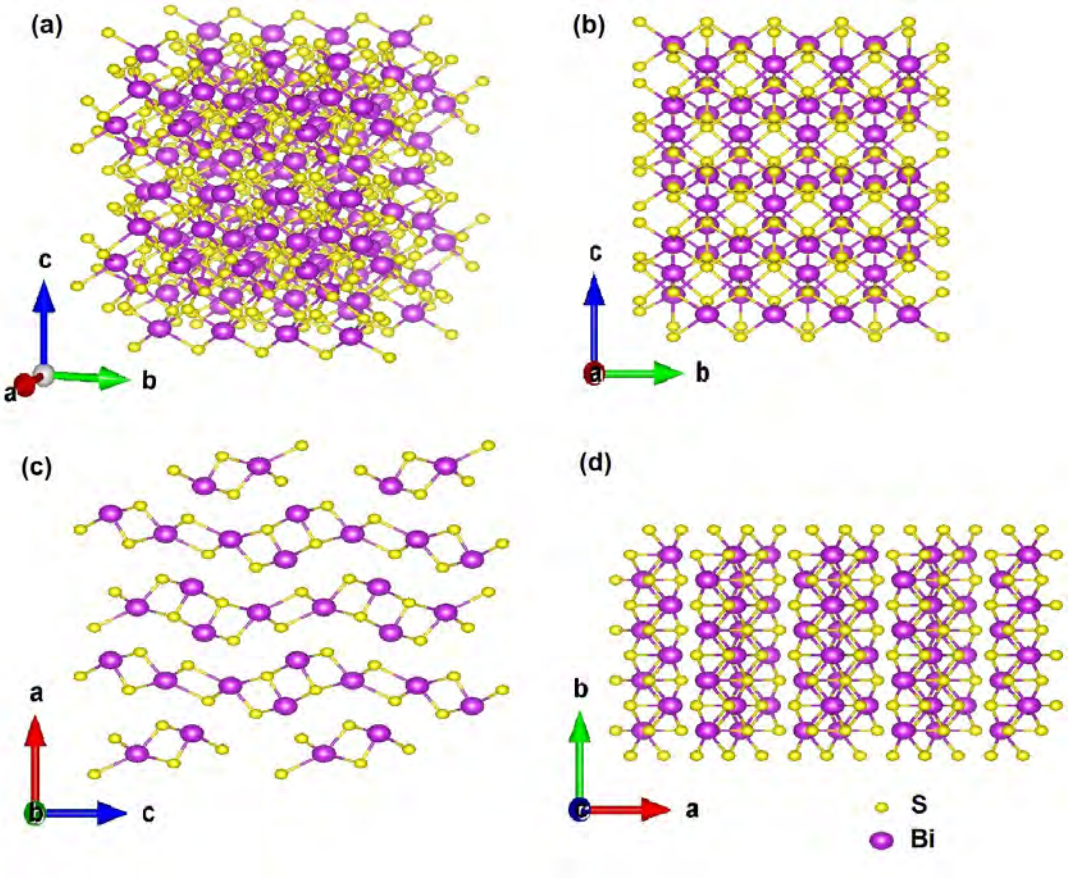

Figure 7.1: Crystallographic structure of Bi_2S_3: (a) 3D representation and view from the a, b and c axes, (b), (c), and (d) respectively.

A layered structure with vdW bonds in the a-direction can be observed. However, when the remaining two directions are compared, the difference between the bond density in the b-axis is higher compared with the c-axis (Figure 7.1c). This fact helped in the past to easily identify these directions [395], comparing the fracturing in one dimension with a bending in the other, due to the different bonding strength between c and b axis, respectively.

In micromechanically exfoliated samples (Figure 7.2a) can be observed typically rectangles, where due to this crystallographic difference ease the recognition of this directions, coinciding the shorter side with the c-axis (weaker density in covalent bonds) and the b-axis with the longer one (due to the stronger covalent bonds density in comparison). In order to confirm this fact, Raman measurements have been taken in exfoliated samples from bulk Bi_2S_3 monocrystals (for more details, see Subsection 2.1.1 and Appendix A).

7.3 Optical properties: anisotropy in-plane

7.3.1 Photoluminescence and Raman spectroscopy

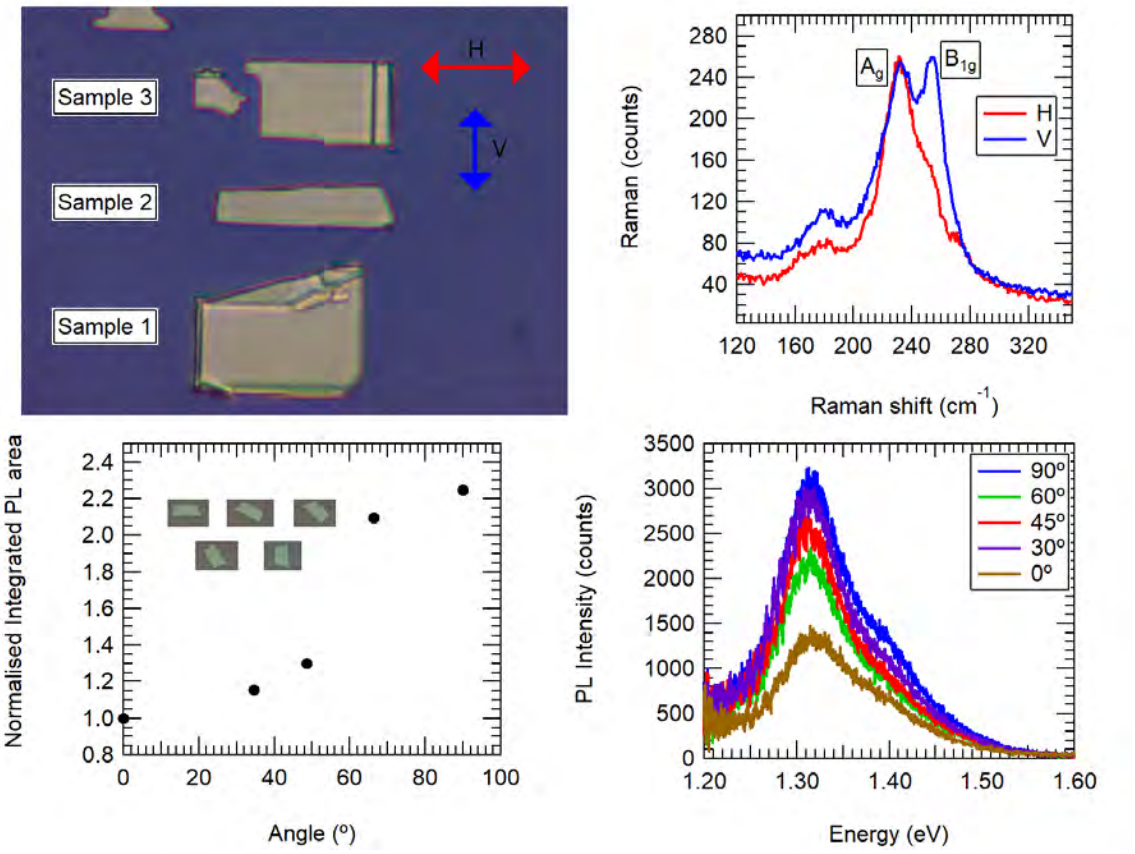

Figure 7.2: Raman and PL measurements in Bi_2S_3 nanosheets: optical image (a) and Raman spectra detected when excitation polarisation source is parallel to the b-axis (blue) and to the c-axis (red), showing a difference in the B_{1g} peak. In PL measurements, different intensity detected rotating the sample measured.

In easily recognizable rectangular-shaped samples (Figure 7.2a), Raman spectroscopy has been studied (Subsection 2.2.4). The laser has been lineally polarised for the measurements in one of the rectangular sides defining the crystallographic directions of the exfoliated nanosheets. Raman peaks correspond with the peaks reported for Bi_2S_3 [403], but B_{1g} peak appears just as a shoulder with one polarization and as a proper peak in the other. B_{1g} is a longitudinal optical mode, so it is observed that in the direction where the bonds are weaker (short side of the rectangle, c-axis) the mode is enhanced due to the vibrational freedom compared with the other direction

(longer side, b-axis), where the bonds are stronger.

These nanosheet orientation and crystallographic axes correspondence has been verified studying the same Raman polarised measurements in a volumic material in which its crystalographic orientations were identified via XRD spectroscopy by Dra. María del Carmen Martínez Tomás. Raman spectroscopy is a fast and reliable technique to characterise the crystallographic orientation of the samples for non-rectangular shaped Bi_2S_3 samples, but usually the optical picture is enough to identify them due to their rectangular shape.

This anisotropy in the b and c axes can be observed in different optical properties. Using the same Horiba Xplora Raman setup, a different intensity in PL spectra has been found rotating the sample due to the polarised excitation and the difference in absorption between the two directions [401], observing less intensity when the excitation polarisation is parallel with the b-axis.

The samples showed in Figure 7.2a have been measured via AFM (see Subsection 2.10), obtaining thicknesses of 540 ± 1 nm, 203 ± 1 nm and 216 ± 1 nm, respectively, discarding quantum effects due to confinement in this nanosheets.

7.3.2 Optical Contrast anisotropy

OC measurements (see Subsection 2.2.1 for more details) behave similarly to PL when a polariser is fixed and the sample is rotated. In this case, due to the difference between the absorption between the two axes, OC follows the rectangular directions of the nanosheet, as shown in Figure 7.3, where using bandwidth filters in 450, 550 and 650 nm can be observed an angular dependence as the sample is rotated.

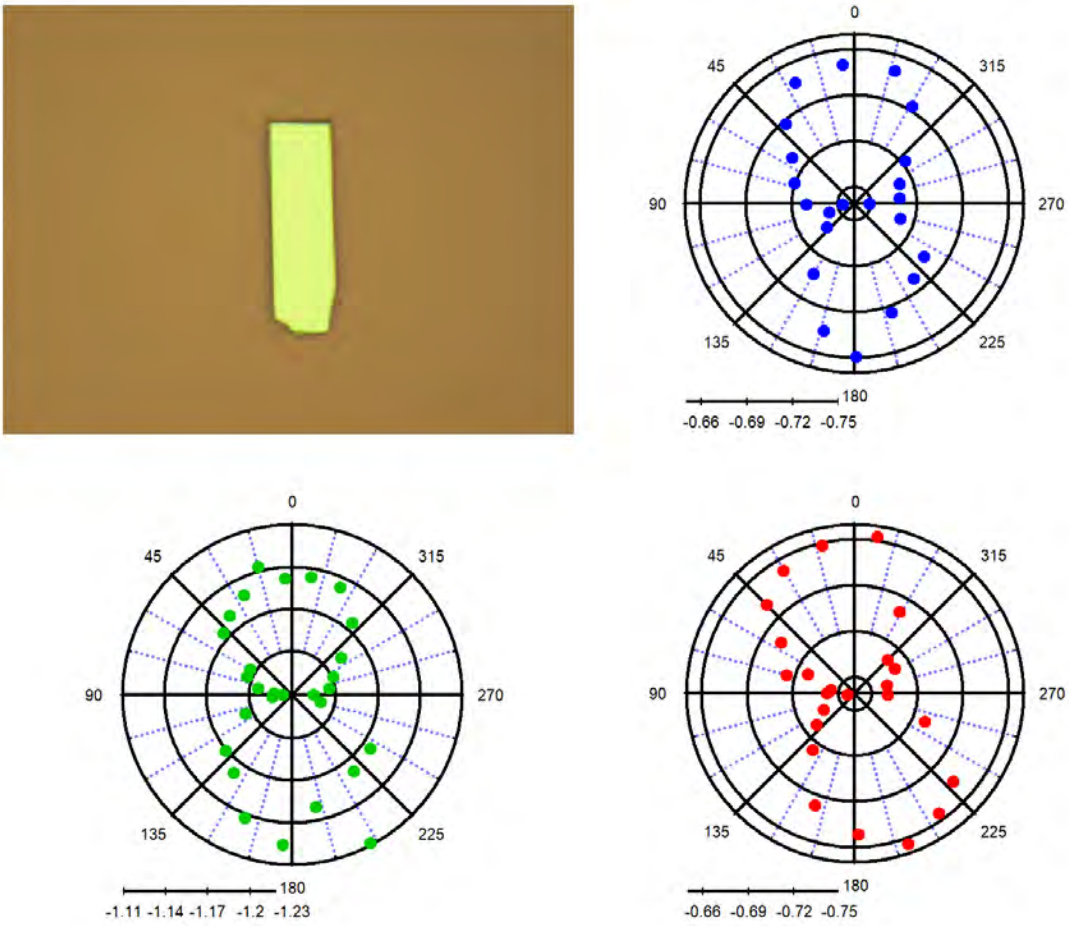

Figure 7.3: OC measurements when a linear polarised is fixed after the white light source and the Bi_2S_3 nanosheet is rotated: optical image without wavelength filter (a) and OC using a 450, 550 and 650 nm filter, respectively.

7.3.3 Differential Reflectivity anisotropy

DR has been measured (see details in Subsection 2.2.1) in the samples in Figure 7.2a where can be observed different peak intensities when the sample is rotated alongside polarisation direction. Since DR and absorption are highly related, this behaviour is explained coinciding the maximum DR peak intensities when the polarisation matches the c-axis direction in the samples.

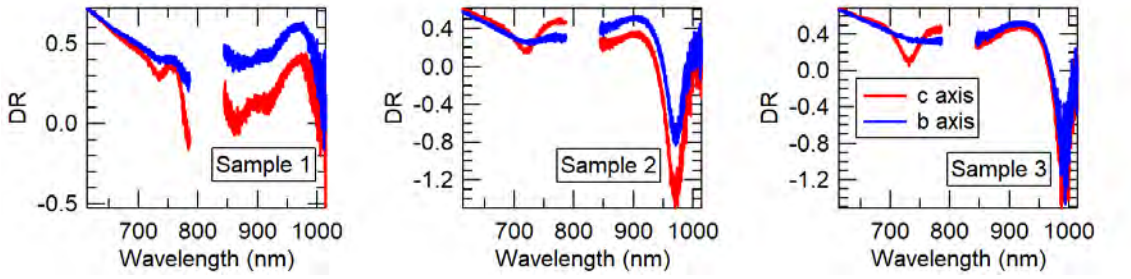

Figure 7.4: Maximum and minimum DR spectra rotating Bi_2S_3 nanosheets from Figure 7.2a, matching the c and b crystallographic directions, respectively.

7.3.4 Transmission measurements

On Bi_2S_3 nanosheets exfoliated on SiO_2 transparent substrates (see Subsections 2.1.1, 2.1.2 and 2.2.2), transmission measurements were taken, as shown in Figure 7.5. Even though the collection and illumination spot is larger than the sample measured area, an effect in the global transmittance measured when the Bi_2S_3 nanosheet is rotated along and against the polarisation direction can be observed. Further measurements will be taken using an illumination and collection spot completely within the sample.

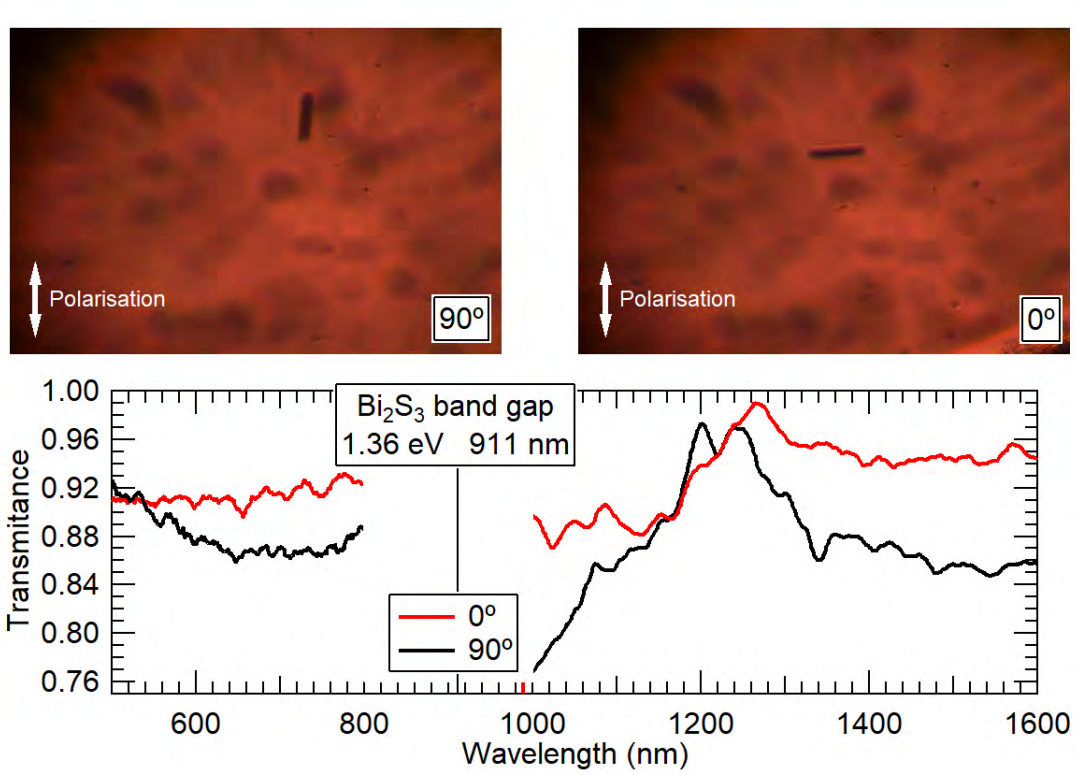

Figure 7.5: Transmission measurements rotating a Bi_2S_3 nanosheet through a polarised white source.

7.3.5 Optical properties conclusion

In previous subsections the anisotropy in the exfoliation x - y plane of Bi_2S_3 nanosheets has been demonstrated. Raman spectroscopy, PL, OC, DR and transmission measurements prove this anisotropy due to the different vibrational freedom in its atoms because its mechanical anisotropy in the b and c bonds direction (Raman) and to the anisotropy in the absorption between both directions (PL, OC, DR and transmission). However, due to its huge absorption in both directions, in the wavelengths close to the Bi_2S_3 band gap (1.36 eV, 911 nm) no counts have been detected in DR or transmission.

Measurements via ellipsometry (see Subsection 2.4.1) have been taken in the Institute of Photonics and Quantum Sciences from the Heriot-Watt University (Edinburgh, United Kingdom) to obtain the refractive indexes in the three directions to finally characterise the optical properties of this material, which will be analised by Dr. Mauro Brotons-Gisbert to complete an optical analysis of this material.

7.4 Application in fiber optics

Finally, once the IP anisotropy has been demonstrated (through Raman, PL, OC, DR and transmission measurements), it will be explored an application in fibre optics devices. In concrete, different exfoliated Bi_2S_3 nanosheet have been transferred (details in Subsection 2.1.3.1) capping the core of a fibre in order to act as a plane-parallel sheet to the light transmited through its core, with interferences below the material band gap.

The transmission measurements in fibres have been taken in collaboration with Dra. Martina Delgado Pinar and Dr. Miguel Vicente Andrés Bou. These interferences or resonances (acting the nanosheet as a Fabry-Perot cavity) can be tuned rotating the sample, as can be seen in Figure 7.6 as an example of the samples prepared. This rotation, due to the refractive index change between the b and c axes, will create small windows of transmittance that could be tuned for a specific application.

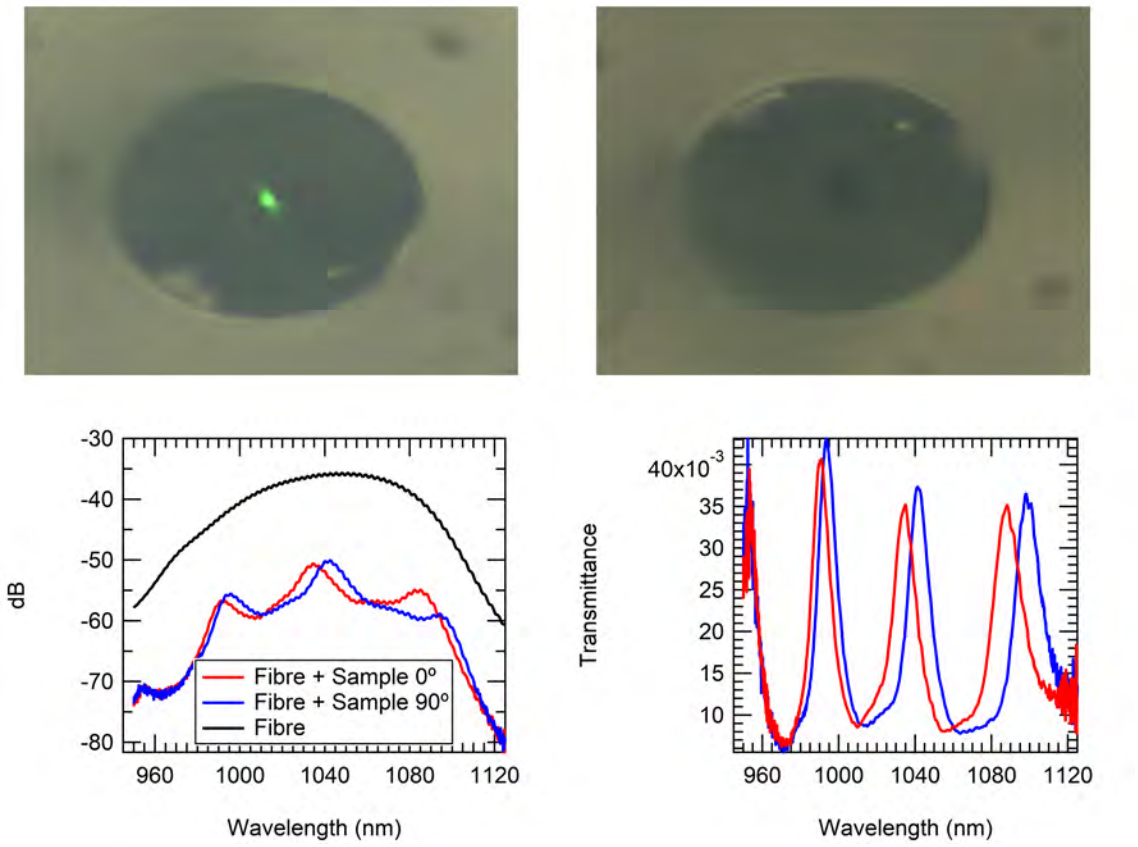

Figure 7.6: 980nm fibre before (a) and after (b) the nanosheet deposition. (c) Transmission spectra detected through the sample rotating the polarisation (red and blue) and reference without sample (black). (d) Transmittance through the sample in both directions.

In Figure 7.6d, 4 resonant peaks can be observed in each curve, being the first peak at the same wavelength in both anisotropy directions, coinciding with the zero-order of resonance in a Fabry-Perot interferometer, as the nanosheet can be compared with two parallel-reflective sheets.

Resonances will occur at wavelengths at which light exhibit a constructive interference after the reflections inside the nanosheet, which will be quantified with an integer mode index q, relating wavelengths with resonances as $2\,n\,d = q\,\lambda_q$, being n, d and λ_q the refractive index in a specific direction, the thickness of the sample and the q-mode wavelength resonance, respectively.

Therefore, the dependence between the refractive index change (or birrefringence, Δn) can be obtained as $d\,\Delta n(\lambda) = \frac{1}{2}\,q(\lambda)\,\Delta\lambda(\lambda)$ comparing the difference in wavelength between same modes. Despite not having measured the thickness d of the

precise sample, an estimate can be approximated using the thicknesses obtained in the samples from Figure 7.2a, measured via AFM, between 200 and 500nm.

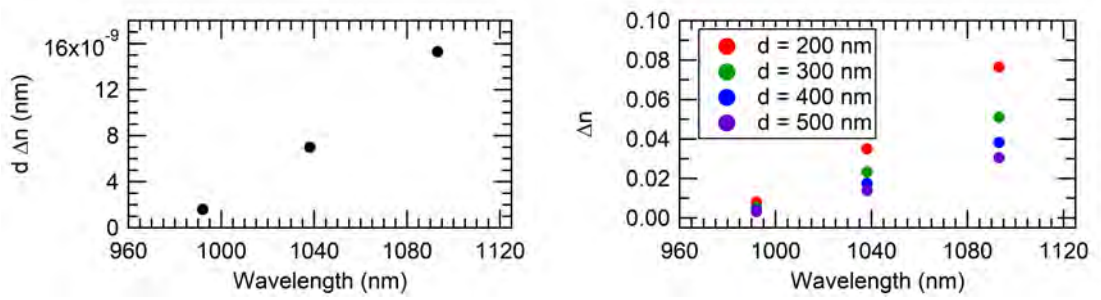

Figure 7.7: Birrefringence between the b and c axes in Bi_2S_3 nanosheets. On the left, depending on the thickness and on the right, different thicknesses have been used to estimate the actual value.

Using thicknesses from 200nm to 500nm, birrefringence values up to 0.08 can be obtained in this material, comparable with the obtained in ReS_2 and $ReSe_2$ [379].

7.5 Conclusions

In this chapter, the IP optical anisotropy of Bi_2S_3 nanosheets has been studied. From a crystallographical point of view, the material aimed for a structural anisotropy between the b and c axes in the exfoliation plane, which has been verified through several techniques such as Raman spectroscopy, PL, OC, DR and transmission.

These techniques show an anisotropy in the refractive index, more important in the absorption. Finally, this anisotropy in its optical properties has been implemented as a plane-parallel sheet in a fibre to act in the transmitted light through its core.

From a transferred nanosheet on the core of a fibre, transmittance measurements have been obtained, obtaining resonance windows as a Fabry-Perot inferometer. A birrefringence up to 0.08 has been obtained in this sample estimating its thickness, comparable with other birrefringent laminar materials such as ReS_2 and $ReSe_2$.

Bibliography

[340] Yung Chang Lin, Hannu Pekka Komsa, Chao Hui Yeh, Torbjörn Björkman, Zheng Yong Liang, Ching Hwa Ho, Ying Sheng Huang, Po Wen Chiu, Arkady V. Krasheninnikov, and Kazu Suenaga. Single-Layer ReS2: Two-Dimensional Semiconductor with Tunable In-Plane Anisotropy. *ACS Nano*, 9(11):11249–11257, 2015.

[341] Changhui Ye, Guowen Meng, Zhi Jiang, Yinhai Wang, Guozhong Wang, and Lide Zhang. Rational growth of Bi2S3 nanotubes from quasi-two-dimensional precursors. *Journal of the American Chemical Society*, 124(51):15180–15181, 2002.

[342] N Benramdane, M Latreche, H Tabet, M Boukhalfa, Z Kebbab, and a Bouzidi. Structural and optical properties of spray-pyrolysed Bi2S3 thin films. *Materials Science and Engineering: B*, 64(2):84–87, 1999.

[343] Diao Li, Henri Jussila, Lasse Karvonen, Guojun Ye, Harri Lipsanen, Xianhui Chen, and Zhipei Sun. Polarization and thickness dependent absorption properties of black phosphorus: New saturable absorber for ultrafast pulse generation. *Scientific Reports*, 5(August):1–9, 2015.

[344] E. Guilmeau, T. Barbier, A. Maignan, and D. Chateigner. Thermoelectric anisotropy and texture of intercalated TiS2. *Applied Physics Letters*, 111(13), 2017.

[345] Tingting Liu, Yang Zhao, Lijun Gao, and Jiangfeng Ni. Engineering Bi2O3-Bi2S3 heterostructure for superior lithium storage. *Scientific reports*, 5:9307, 2015.

[346] Huan Zhao, Jiangbin Wu, Hongxia Zhong, Qiushi Guo, Xiaomu Wang, Fengnian Xia, Li Yang, Pingheng Tan, and Han Wang. Interlayer interactions in anisotropic atomically thin rhenium diselenide. *Nano Research*, 8(11):3651–3661, 2015.

[347] Shoufeng Lan, Sean Rodrigues, Lei Kang, and Wenshan Cai. Visualizing Optical Phase Anisotropy in Black Phosphorus. *ACS Photonics*, 3(7):1176–1181, 2016.

[348] Ozgur Burak Aslan, Daniel A. Chenet, Arend M. Van Der Zande, James C. Hone, and Tony F. Heinz. Linearly Polarized Excitons in Single- and Few-Layer ReS2 Crystals. *ACS Photonics*, 3(1):96–101, 2016.

[349] Xiaomu Wang, Aaron M. Jones, Kyle L. Seyler, Vy Tran, Yichen Jia, Huan Zhao, Han Wang, Li Yang, Xiaodong Xu, and Fengnian Xia. Highly anisotropic and robust excitons in monolayer black phosphorus. *Nature Nanotechnology*, 10(6):517–521, 2015.

[350] W Jaegermann, a Klein, and C Pettenkofer. *Physics and Chemistry of Materials with Low-Dimensional Structures*, volume 24. 2000.

[351] Michele Buscema, Dirk J. Groenendijk, Sofya I. Blanter, Gary A. Steele, Herre S J Van Der Zant, and Andres Castellanos-Gomez. Fast and broadband photoresponse of few-layer black phosphorus field-effect transistors. *Nano Letters*, 14(6):3347–3352, 2014.

[352] A. Cantarero, J. P. Martínez, A. Seguba, and A. Chevy. Refractive index of bismuth sulfide in the infrared region. *Physica Status Solidi (a)*, 101(2):603–609, 1987.

[353] Jing Tang and A. Paul Alivisatos. Crystal splitting in the growth of Bi2S3. *Nano Letters*, 6(12):2701–2706, 2006.

[354] Vy Tran, Ryan Soklaski, Yufeng Liang, and Li Yang. Layer-controlled band gap and anisotropic excitons in few-layer black phosphorus. *Physical Review B - Condensed Matter and Materials Physics*, 89(23):1–6, 2014.

[355] Raul Suarez, P. K. Nair, and Prashant V. Kamat. Photoelectrochemical Behavior of Bi2S3 Nanoclusters and Nanostructured Thin Films. *Langmuir*, 14(12):3236–3241, 2002.

[356] Nannan Mao, Jingyi Tang, Liming Xie, Juanxia Wu, Bowen Han, Jingjing Lin, Shibin Deng, Wei Ji, Hua Xu, Kaihui Liu, Lianming Tong, and Jin Zhang. Optical Anisotropy of Black Phosphorus in the Visible Regime. *Journal of the American Chemical Society*, 138(1):300–305, 2016.

[357] Neha Mahuli, Debabrata Saha, and Shaibal K. Sarkar. Atomic Layer Deposition of p-Type Bi2S3. *Journal of Physical Chemistry C*, 121(14):8136–8144, 2017.

[358] Hua Zhang, Jing Huang, Xinggui Zhou, and Xinhua Zhong. Single-crystal Bi2S3 nanosheets growing via attachment-recrystallization of nanorods. *Inorganic Chemistry*, 50(16):7729–7734, 2011.

[359] Michael B. Sigman and Brian A. Korgel. Solventless synthesis of Bi2S3 (bis-

muthinite) nanorods, nanowires, and nanofabric. *Chemistry of Materials*, 17(7):1655–1660, 2005.

[360] A. Cantarero, J. Martinez-Pastor, A. Segura, and A. Chevy. Excitonic absorption and Urbach's tail in bismuth sulfide single crystals. *Applied Physics A: Solids and Surface*, 45(2):125–132, 1988.

[361] Andrea C. Ferrari, Francesco Bonaccorso, Vladimir Fal'ko, Konstantin S. Novoselov, Stephan Roche, Peter Bøggild, Stefano Borini, Frank H.L. Koppens, Vincenzo Palermo, Nicola Pugno, José A. Garrido, Roman Sordan, Alberto Bianco, Laura Ballerini, Maurizio Prato, Elefterios Lidorikis, Jani Kivioja, Claudio Marinelli, Tapani Ryhänen, Alberto Morpurgo, Jonathan N. Coleman, Valeria Nicolosi, Luigi Colombo, Albert Fert, Mar Garcia-Hernandez, Adrian Bachtold, Grégory F. Schneider, Francisco Guinea, Cees Dekker, Matteo Barbone, Zhipei Sun, Costas Galiotis, Alexander N. Grigorenko, Gerasimos Konstantatos, Andras Kis, Mikhail Katsnelson, Lieven Vandersypen, Annick Loiseau, Vittorio Morandi, Daniel Neumaier, Emanuele Treossi, Vittorio Pellegrini, Marco Polini, Alessandro Tredicucci, Gareth M. Williams, Byung Hee Hong, Jong Hyun Ahn, Jong Min Kim, Herbert Zirath, Bart J. Van Wees, Herre Van Der Zant, Luigi Occhipinti, Andrea Di Matteo, Ian A. Kinloch, Thomas Seyller, Etienne Quesnel, Xinliang Feng, Ken Teo, Nalin Rupesinghe, Pertti Hakonen, Simon R.T. Neil, Quentin Tannock, Tomas Löfwander, and Jari Kinaret. Science and technology roadmap for graphene, related two-dimensional crystals, and hybrid systems. *Nanoscale*, 7(11):4598–4810, 2015.

[362] Jungcheol Kim, Jae Ung Lee, Jinhwan Lee, Hyo Ju Park, Zonghoon Lee, Changgu Lee, and Hyeonsik Cheong. Anomalous polarization dependence of Raman scattering and crystallographic orientation of black phosphorus. *Nanoscale*, 7(44):18708–18715, 2015.

[363] Han Liu, Adam T. Neal, Zhen Zhu, Zhe Luo, Xianfan Xu, David Tománek, and Peide D. Ye. Phosphorene: An unexplored 2D semiconductor with a high hole mobility. *ACS Nano*, 8(4):4033–4041, 2014.

[364] Likai Li, Jonghwan Kim, Chenhao Jin, Guo Jun Ye, Diana Y. Qiu, Felipe H. Da Jornada, Zhiwen Shi, Long Chen, Zuocheng Zhang, Fangyuan Yang, Kenji Watanabe, Takashi Taniguchi, Wencai Ren, Steven G. Louie, Xian Hui Chen, Yuanbo Zhang, and Feng Wang. Direct observation of the layer-dependent

electronic structure in phosphorene. *Nature Nanotechnology*, 12(1):21–25, 2017.

[365] Daniel A. Chenet, O. Burak Aslan, Pinshane Y. Huang, Chris Fan, Arend M. Van Der Zande, Tony F. Heinz, and James C. Hone. In-Plane Anisotropy in Mono- and Few-Layer ReS2 Probed by Raman Spectroscopy and Scanning Transmission Electron Microscopy. *Nano Letters*, 15(9):5667–5672, 2015.

[366] Yixuan Zhou, Qiyi Zhao, Keyu Si, Zehan Yao, Xinlong Xu, and Yaohui Guo. Efficient mixed-solvent exfoliation of few-quintuple layer Bi2S3 and its photoelectric response. *Nanotechnology*, 28(33):335602, 2017.

[367] Qiannan Cui, Jiaqi He, Matthew Z. Bellus, Mirzojamshed Mirzokarimov, Tino Hofmann, Hsin Ying Chiu, Matthew Antonik, Dawei He, Yongsheng Wang, and Hui Zhao. Transient Absorption Measurements on Anisotropic Monolayer ReS2. *Small*, 11(41):5565–5571, 2015.

[368] Henrique B. Ribeiro, Marcos A. Pimenta, Christiano J.S. De Matos, Roberto Luiz Moreira, Aleksandr S. Rodin, Juan D. Zapata, Eunézio A.T. De Souza, and Antonio H. Castro Neto. Unusual angular dependence of the Raman response in black phosphorus. *ACS Nano*, 9(4):4270–4276, 2015.

[369] Rhiannon M. Clark, Jimmy C. Kotsakidis, Bent Weber, Kyle J. Berean, Benjamin J. Carey, Matthew R. Field, Hareem Khan, Jian Zhen Ou, Taimur Ahmed, Christopher J. Harrison, Ivan S. Cole, Kay Latham, Kourosh Kalantar-Zadeh, and Torben Daeneke. Exfoliation of Quasi-Stratified Bi2S3 Crystals into Micron-Scale Ultrathin Corrugated Nanosheets. *Chemistry of Materials*, 28(24):8942–8950, 2016.

[370] Der Hsien Lien, Jeong Seuk Kang, Matin Amani, Kevin Chen, Mahmut Tosun, Hsin Ping Wang, Tania Roy, Michael S. Eggleston, Ming C. Wu, Madan Dubey, Si Chen Lee, Jr Hau He, and Ali Javey. Engineering light outcoupling in 2D materials. *Nano Letters*, 15(2):1356–1361, 2015.

[371] Xiaomu Wang and Shoufeng Lan. Optical properties of black phosphorus. *Advances in Optics and Photonics*, 8(4):618, 2016.

[372] Diao Li, Hui Xue, Mei Qi, Yadong Wang, Sinan Aksimsek, Nikolai Chekurov, Wonjae Kim, Changfeng Li, Juha Riikonen, Fangwei Ye, Qing Dai, Zhaoyu Ren, Jintao Bai, Tawfique Hasan, Harri Lipsanen, and Zhipei Sun. Graphene actively Q-switched lasers. *2D Materials*, 4(2), 2017.

[373] Jingsi Qiao, Xianghua Kong, Zhi Xin Hu, Feng Yang, and Wei Ji. High-mobility transport anisotropy and linear dichroism in few-layer black phosphorus. *Nature Communications*, 5:1–7, 2014.

[374] Daniel Rossi, Luis E. Camacho Forero, Guadalupe Ramos Sánchez, Jae Hyo Han, Jinwoo Cheon, Perla Balbuena, and Dong Hee Son. Anisotropic electron phonon coupling in colloidal layered TiS2 nanodiscs observed via coherent acoustic phonons. *Journal of Physical Chemistry C*, 119(13):7436–7442, 2015.

[375] Zhe Luo, Jesse Maassen, Yexin Deng, Yuchen Du, Richard P. Garrelts, Mark S. Lundstrom, Peide D. Ye, and Xianfan Xu. Anisotropic in-plane thermal conductivity observed in few-layer black phosphorus. *Nature Communications*, 6:1–8, 2015.

[376] Hongtao Yuan, Xiaoge Liu, Farzaneh Afshinmanesh, Wei Li, Gang Xu, Jie Sun, Biao Lian, Alberto G. Curto, Guojun Ye, Yasuyuki Hikita, Zhixun Shen, Shou Cheng Zhang, Xianhui Chen, Mark Brongersma, Harold Y. Hwang, and Yi Cui. Polarization-sensitive broadband photodetector using a black phosphorus vertical p-n junction. *Nature Nanotechnology*, 10(8):707–713, 2015.

[377] Tengfei Yan, Xiaofen Qiao, Xiaona Liu, Pingheng Tan, and Xinhui Zhang. Photoluminescence properties and exciton dynamics in monolayer WSe2. *Applied Physics Letters*, 105(10):101901, 2014.

[378] Sangwan Sim, Doeon Lee, Minji Noh, Soonyoung Cha, Chan Ho Soh, Ji Ho Sung, Moon Ho Jo, and Hyunyong Choi. Selectively tunable optical Stark effect of anisotropic excitons in atomically thin ReS2. *Nature Communications*, 7(May):1–6, 2016.

[379] He Yang, Henri Jussila, Anton Autere, Hannu Pekka Komsa, Guojun Ye, Xianhui Chen, Tawfique Hasan, and Zhipei Sun. Optical Waveplates Based on Birefringence of Anisotropic Two-Dimensional Layered Materials. *ACS Photonics*, 4(12):3023–3030, 2017.

[380] Shuang Zhang, Jiong Yang, Renjing Xu, Fan Wang, Weifeng Li, Muhammad Ghufran, Yong Wei Zhang, Zongfu Yu, Gang Zhang, Qinghua Qin, and Yuerui Lu. Extraordinary photoluminescence and strong temperature/angle-dependent raman responses in few-layer phosphorene. *ACS Nano*, 8(9):9590–9596, 2014.

[381] Fengnian Xia, Han Wang, and Yichen Jia. Rediscovering black phosphorus

as an anisotropic layered material for optoelectronics and electronics. *Nature Communications*, 5:1–6, 2014.

[382] Qiannan Cui, Rodrigo A. Muniz, J. E. Sipe, and Hui Zhao. Strong and anisotropic third-harmonic generation in monolayer and multilayer ReS2. *Physical Review B*, 95(16):2–7, 2017.

[383] Xi Ling, Shengxi Huang, Eddwi H. Hasdeo, Liangbo Liang, William M. Parkin, Yuki Tatsumi, Ahmad R.T. Nugraha, Alexander A. Puretzky, Paul Masih Das, Bobby G. Sumpter, David B. Geohegan, Jing Kong, Riichiro Saito, Marija Drndic, Vincent Meunier, and Mildred S. Dresselhaus. Anisotropic Electron-Photon and Electron-Phonon Interactions in Black Phosphorus. *Nano Letters*, 16(4):2260–2267, 2016.

[384] Qun Wei and Xihong Peng. Superior mechanical flexibility of phosphorene and few-layer black phosphorus. *Applied Physics Letters*, 104(25):251915, 2014.

[385] Nannan Mao, Juanxia Wu, Bowen Han, Jingjing Lin, Lianming Tong, and Jin Zhang. Birefringence-Directed Raman Selection Rules in 2D Black Phosphorus Crystals. *Small*, 12(19):2627–2633, 2016.

[386] O. C. Monteiro and T. Trindade. Preparation of Bi2S3 nanofibers using a single-source method. *Journal of Materials Science Letters*, 19(10):859–861, 2000.

[387] Tianyu Wang, Jing Liu, Biao Xu, Ridong Wang, Pengyu Yuan, Meng Han, Shen Xu, Yangsu Xie, Yue Wu, and Xinwei Wang. Identifying the Crystalline Orientation of Black Phosphorus by Using Optothermal Raman Spectroscopy. *ChemPhysChem*, 18(20):2828–2834, 2017.

[388] Gerasimos Konstantatos, Larissa Levina, Jiang Tang and Edward H. Sargent*. Sensitive Solution-Processed Bi2S3 Nanocrystalline Photodetectors. *Nanoletters*, 8(May):1–4, 2010.

[389] L. M. Peter. The photoelectrochemical properties of anodic Bi2S3 films. *Journal of Electroanalytical Chemistry*, 98(1):49–58, 1979.

[390] Husnu Koc, Haci Ozisik, Engin Deligoz, Amirullah M. Mamedov, and Ekmel Ozbay. Mechanical, electronic, and optical properties of Bi2S3 and Bi2Se3 compounds: First principle investigations. *Journal of Molecular Modeling*, 20(4), 2014.

8 Molybdenum Trioxide

Even though the main focus of this thesis aims to the 2D semiconductors, their properties and their implementation in optoelectronic devices, in this chapter MoO_3, a new clean zero nuclear spin 2D insulator will be presented to fulfil the absence in the 2D material framework of substitutes to hBN as insulator. This project have been developed under the supervision of Prof. Dr. Brian D. Gerardot in the Institute of Photonics and Quantum Sciences (IPaQS) in the Heriot-Watt University (Edinburgh, United Kingdom) during a 5-months research stay.

8.1 Introduction

In order to develop optoelectronic devices for any application needed, from a simplistic point of view, there are mostly three main components to work with: conductors, semiconductors and insulators. With these three basic "blocks", every imaginable device like transistors, photodetectors, LEDs, capacitors... can be structured by the combination of this different elements and their properties.

Among the 2D materials, only hBN is known as an insulator for these applications [415, 427, 410, 408, 442, 432, 411]. During the last years, this material has been vastly studied and employed in basically every 2D project where a 2D insulator is involved. It has been, therefore, the only option since no other common 2D insulator is known.

However, hBN has its own disadvantages. First, the hBN that can be obtained in the market is plenty of defects at LT, observing PL emission due these defects, hampering its usage in optoelectronic applications [416, 405]. To fulfil that issue, T. Taniguchi and K. Watanabe developed a method to synthesise hBN with an outstanding quality, without defects to compromise the result [443]. Nevertheless, not every research group has access to it.

Second, hBN presents serious disadvantages for the development of 2D related devices with potential applications in spintronics. Boron and Nitrogen have an intrinsic nuclear spin [438, 449], which would mask any spin signal coming from the active elements of any eventual 2D device incorporating hBN.

In this chapter, a new material to replace hBN as a 2D transparent insulator in the situations where the disadvantages already exposed would determine the behavior of the final application will be proposed.

The looked-for properties will be the following:

- It must behave as an insulator compared with the rest of the materials among the most known 2D semiconductors, so its band gap should be as high as possible. For the usually employed materials in the 2D semiconductors list (TMDs, III-VI semiconductors, BP...), a semiconductor with a band gap over 3 eV could be considered enough for an insulator in comparison.
- In order to obtain 2D samples it must have a laminar crystallographic structure, either experimentally mechanically exfoliated or theoretically.
- A zero nuclear spin is needed. For that purpose, every atom in its atomic configuration should have a nuclear spin number I = 0. To fulfil that condition their atomic numbers Z and A must be even. This condition, atomically speaking, will be dependent of the natural abundance percentage of the isotopes possible, so the less frequent with a non-zero nuclear spin, the better.

Before start looking for possible alternatives, the previously listed properties of hBN will be commented in order to compare them. hBN has a band gap of approx. 5.955 eV at RT [440], behaving as an insulator among the usual 2D materials, and it has already used as a 2D layered material in many publications [415, 427, 410, 408, 442, 432, 411]. In order to check the nuclear spin behaviour, its nuclear spin numbers will be analysed.

Table 8.1: Nuclear spin number and abundance in nature of Boron and Nitrogen [438, 449].

	Element	Z	A	I	% in nature
B	Boron	5	10	3	19.9
			11	1.5	80.01
N	Nitrogen	7	14	1	99.632
			15	0.5	0.368

In Table 8.1 it can be observed that in case of Boron, with an 80.1% a nuclear spin number of 1.5 is found, reaching a value of 3 in the remaining 19.9% in nature. In case of Nitrogen, with a 99.632%, a value of 1 in the nuclear spin number is expected, being 0.5 in the remaining 0.368%. These values and percentages are extremely damnific for hBN as a 2D insulator for any nuclear spin application involved.

Table 8.2 contains all the theoretical exfoliable materials considered as possible candidates with band gap over 3 eV [412], which nuclear spin value have been tested. For every material, abundance percentage and value has been analysed compared with hBN, and for simplicity and trying to avoid excessive numerical data, a numeric code has been assigned considering these factors to define a nuclear spin ideality (NSI), from 4 to 1 in order of increasing ideality, closer to zero, as an orientative value to compare materials in this context.

Table 8.2: Theoretically exfoliable 2D materials [412] with band gap higher than 3 eV, analysing the nuclear spin ideality.

Formula	Band gap (eV)	NSI	Formula	Band gap (eV)	NSI
$LiBH_4$	6.4	4	SrI_2	3.8	4
$MgCl_2$	6.0	4	$Ca(OH)_2$	3.7	2
AlOCl	5.8	4	CaHI	3.7	4
SrBrF	5.3	4	MgI_2	3.6	4
$MgBr_2$	4.8	3	TlF	3.6	4
NaCN	4.8	4	PbClF	3.5	3
BN	4.7	3	BaHI	3.4	4
RbCl	4.6	4	LaOI	3.4	4
$ZnCl_2$	4.5	3	$ZnBr_2$	3.4	3
OLuBr	4.4	4	$Mg(OH)_2$	3.3	2
SrHBr	4.4	3	OLuI	3.3	4
YOCl	4.4	3	ZrNCl	3.3	3
CaHBr	4.2	3	$CdBr_2$	3.2	3
LaOBr	4.0	4	ScOBr	3.2	4
$CdCl_2$	3.9	3	PbBrF	3.1	3
SnF_4	3.9	3	MnO_2	3.1	4
SrHI	3.9	4	MoO_3	3.1	1
CaI_2	3.8	4	Sb_2OS_2	3.0	4

Among this list the three best candidates will be $Mg(OH)_2$, $Ca(OH)_2$ and MoO_3, which as example of the methodology employed to assign a nuclear spin ideality, will be studied separately.

Table 8.3: Nuclear spin number and abundance in nature of Hydrogen, Oxygen, Magnesium and Calcium [438, 449].

	Element	Z	A	I	% in nature
H	Hydrogen	1	1	0.5	99.9885
			2	1	0.0115
			3	0.5	0.0
O	Oxygen	8	16	0	99.757
			17	2.5	0.038
			18	0	0.205
Mg	Magnesium	12	24	0	78.99
			25	2.5	10.00
			26	0	11.01
Ca	Calcium	20	40	0	96.941
			41	3.5	0.0
			42	0	0.647
			43	3.5	0.135
			44	0	2.086
			46	0	0.004
			48	0	0.187

In case of $Ca(OH)_2$ and $Mg(OH)_2$, both having the OH radical, Hydrogen, with a 99% of the atoms will have a nuclear spin number of 0.5, hampering its usage. In case of Oxygen, only a 0.038% of the atoms will have a nuclear spin number of 2.5, so after seeing the percentages in the rest of materials could be considered negligible. In Magnesium, a relevant 10.00% will have a nuclear spin number of 2.5, being 3.5 in case of Calcium only in a 0.135%. Compared with hBN the improvement is enormous and could be enough for some applications involving nuclear spin, but MoO_3 will be studied looking for the purest zero spin insulator.

In next Table the nuclear spin numbers in MoO_3 will be analysed.

Table 8.4: Nuclear spin number and abundance in nature of Oxygen and Molybdenum [438, 449].

	Element	Z	A	I	% in nature
O	Oxygen	8	16	0	99.757
			17	2.5	0.038
			18	0	0.205
Mo	Molybdenum	42	92	0	14.84
			94	0	9.25
			95	2.5	15.92
			96	0	16.68
			97	2.5	9.55
			98	0	24.13
			100	0	9.63

Concerning the Oxygen, as before, only a 0.038% of the atoms in nature will have a nuclear spin number of 2.5, being negligible. However, in Molybdenum, due to the natural percentage abundance isotopes there is a relevant probability to have non-zero nuclear spin in 25.47% of the Mo atoms in nature. The probability to have two of this Mo atoms with non-zero nuclear spin next to each other is 6.487%. This is not the ideal scenario, but and after looking the probabilities of the other materials, it is clearly the best compared with any other candidate considered. Therefore, MoO_3 will be the chosen to study in this project as a zero nuclear spin insulator.

The thermically stable phase is the α-MoO_3, with a Pnma (62) structure [425, 418], as define in Figure 8.1.

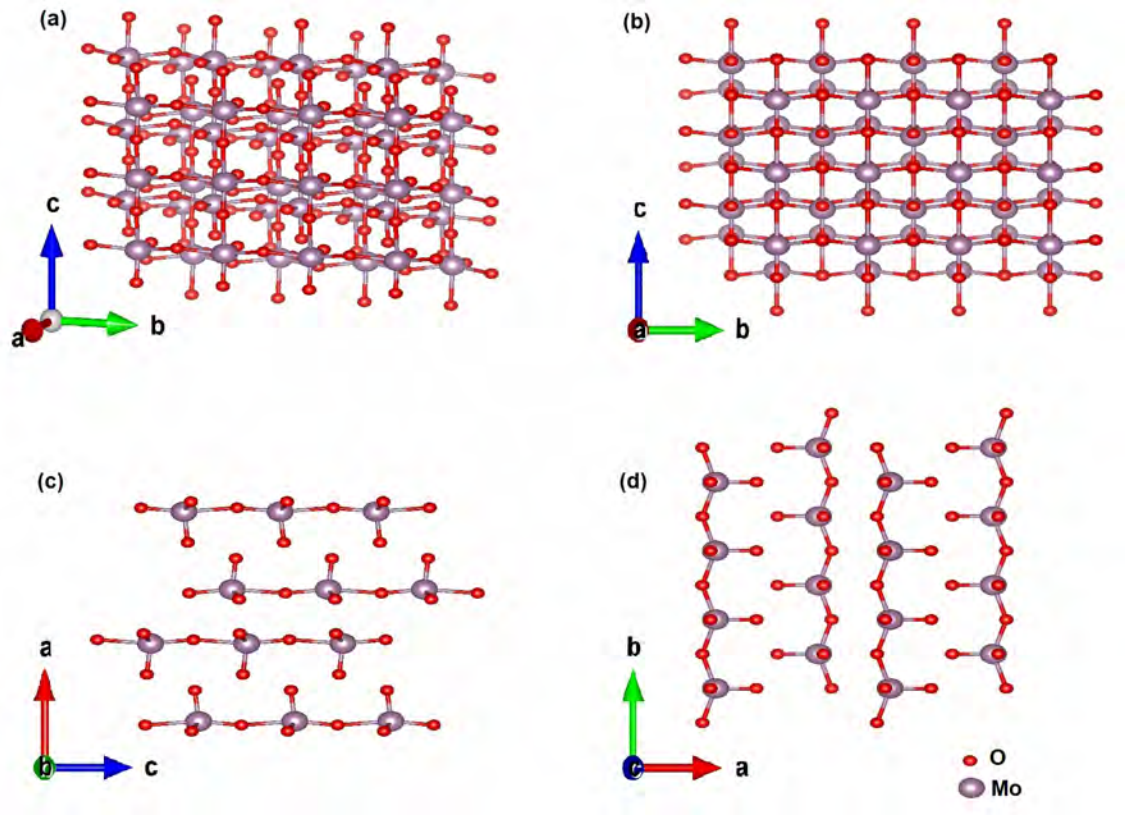

Figure 8.1: Orthorrombic α-MoO_3 Pnma (62) structure: (a) standart orientation of the crystal shape and views along the a, b and c axis, (b), (c), and (d) respectively.

This material has a laminar structure (Figure 8.1d). Mo-O bonding within each layer has a covalent behavior, whereas bonding between layers is of vdW type.

Although some articles about MoO_3 have been found in the bibliography, from synthesis methods and basic properties [439, 423, 434, 431, 436, 441, 413, 409, 422, 430, 426, 407, 406, 417, 445, 437, 444, 428, 447, 435] to devices aiming to different purposes [414, 429, 419, 421, 433], none of them properly studies its behaviour and propose it as an insulator for exfoliable 2D optoelectronic devices.

8.2 Optical properties and cleanness at low temperature

MoO_3 bulk samples (Appendix A) have been used for the next experiments. Exfoliated samples were prepared using the usual scotch-tape method using Nitto tape

(Subsections 2.1.1 and 2.1.2), proving its layered structure, with similar nanosheet shapes compared to Bi_2S_3 in Chapter 7 (Figures 7.2 and 7.3), as can be observed in Figure 8.2, aiming at a possible anisotropy in the layer plane, which will be explored later in this chapter (Section 8.4).

The material obtained was transferred to Si/SiO_2(90nm) common substrates and after that, cooled down up to 4 K in an attoDry 1000 Cryostat to study its PL emission at LT (see details in Subsections 2.1.1, 2.1.2, 2.2.1 and 2.2.3).

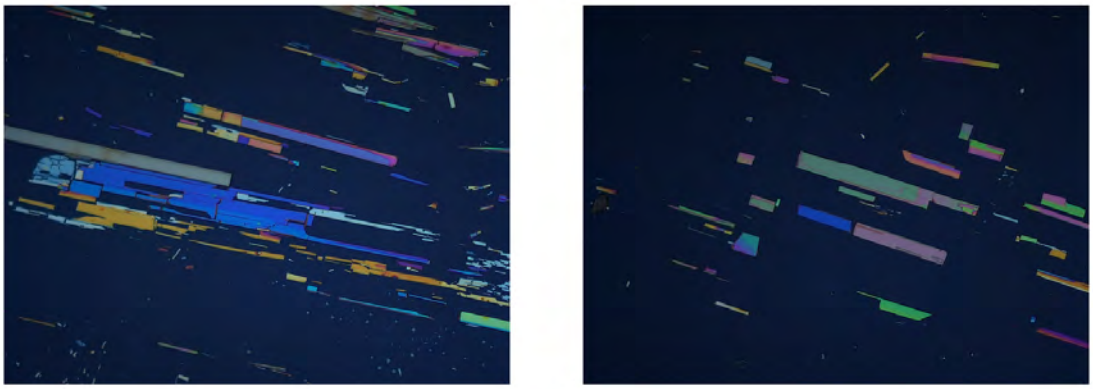

Figure 8.2: Optical images of exfoliated MoO_3 samples.

20 s acquisitions (longer than usual) were measured, at high excitation power (50μW) in a Cobolt 532nm laser as excitation source to measure different PL maps to check if MoO_3 has defects at LT. As seen in Figure 8.3, no PL is detected due to the MoO_3 nanosheet, only the PL emission already present in Si/SiO_2, that appears due to the high-power long acquisition measurements, has been amplified due to the cavity behavior of the nanosheet on top.

Similar measurements measurements have been performed in different samples with different conditions (acquisition time or power) at LT, proving in all of them the absence of defects in MoO_3 with emission at LT.

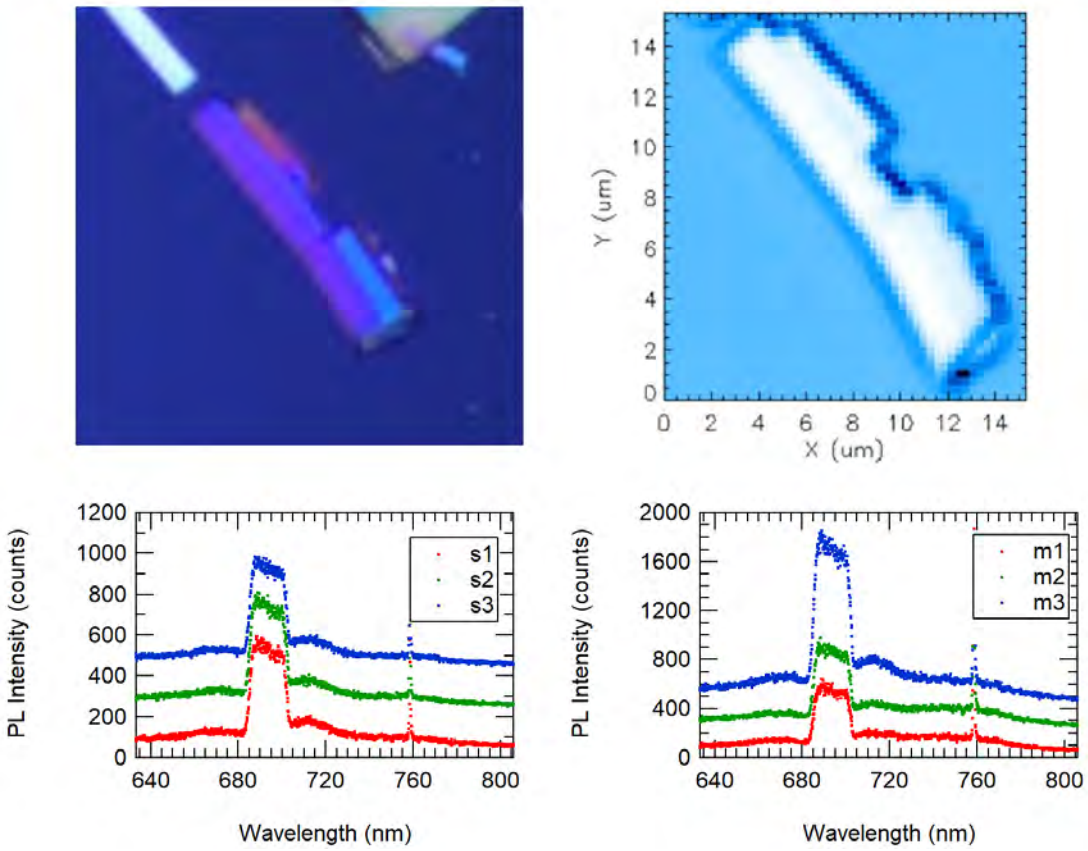

Figure 8.3: μ-PL map and spectra at low temperature in MoO_3 samples: reflectivity at 780nm map, optical image and PL spectra in different substrate points and sample points (bottom left and bottom right, respectively).

8.3 Applications as encapsulation materials

Finally, once demonstrated MoO_3 as a great candidate as a zero-nuclear spin 2D insulator and its absence of defects at LT, a prototypical device will be prepared using MoO_3 as insulator. A WSe_2 ML (mechanically exfoliated, see Appendix A and Subsections 2.1.1 and 2.1.2 for more details) has been fully encapsulated using this material using the hot pick-up transfer technique (see Subsection 2.1.3.2) in an Ar environment (glovebox GP Campus Jacomex) to prevent the appearance of impurities related to H_2O or Oxygen among the nanosheets contact lattices.

First, DR at LT (which behaves qualitatively in a similar way compared to absorption, for more details, see Subsection 2.2.1) will be presented in three different situations: on the WSe_2 ML, on the ML on top of a bottom MoO_3 and in the ML

completely encapsulated, top and bottom:

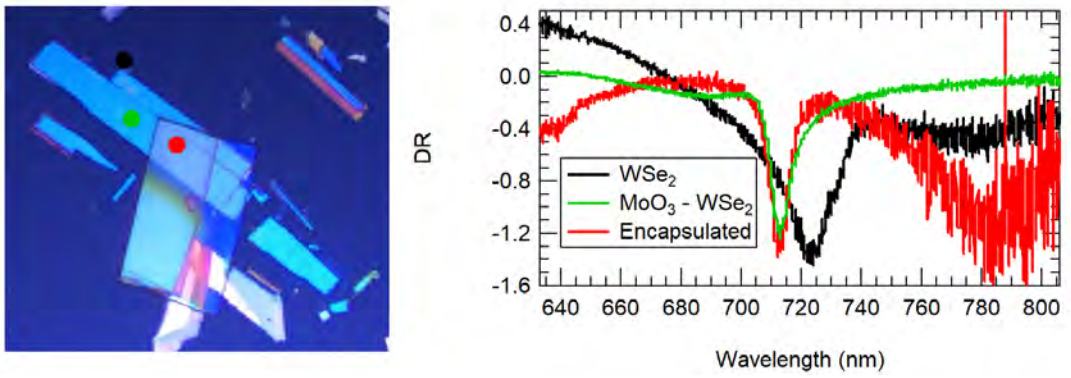

Figure 8.4: On the left, optical image of WSe_2 ML encapsulated in MoO_3. On the right, DR comparing the WSe_2 ML on Si/SiO_2 substrate (black), on $Si/SiO_2/MoO_3$ (green) and covered with MoO_3 on top (red).

A shift (from 723 nm to 712 nm) and a line narrowing (from 47.45 meV to 26.79 meV in width) in the DR is observed when the WSe_2 ML is on $Si/SiO_2/MoO_3$, compared to that directly on Si/SiO_2. Such a peak blueshift can be attributable to dielectric effects due to changes in the refractive index underneath. Line narrowing can be attributable to the decrease of roughness in the WSe_2 ML when it is on MoO_3 and its isolation from the SiO_2 substrate. A slight further line narrowing (from 26.79 meV to 21.98 meV in width) is obtained when encapsulated adding a MoO_3 on top for the same reason. These qualitative results are comparable with the reported WSe_2 ML encapsulated in hBN [424].

Secondly, μ-PL measurements have been taken at LT on the device. Only PL emission due to the defect band is measured at LT in WSe_2 due to the thermal behaviour of the X^0 free exciton at LT, which intensity is reduced in these conditions in favour of the localised excitons [377]. Some localised emitters in the WSe_2 defect band were found, with usual crossed-polarized fine structure splitting (FSS) and usual power dependence between both peaks as compared with the behaviour found when encapsulated with hBN [420].

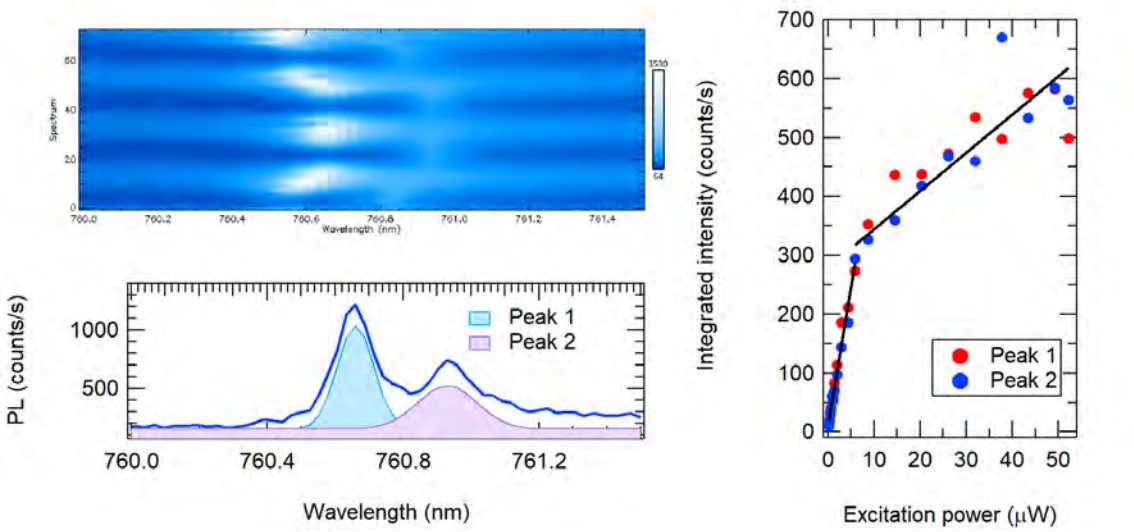

Figure 8.5: Fine structure splitting in LT emitters in WSe_2 encapsulated monolayer on MoO_3. Crossed-polarized behaviour rotating polarization and power dependence between both peaks.

Therefore, these results demonstrate the main objective of the project: present MoO_3 as a new clean 2D insulator, with close to zero-nuclear spin capabilities for 2D spintronic devices and similar insulator behavior in 2D devices. However, one of the devices prepared presented a set of surprising characteristics and properties that deserves to be highlighted, which will be analysed in the following lines.

The same procedure has been used to prepare the device, in this case with a WSe_2 BL encapsulated in MoO_3, in the same Ar environment via hot pick-up transfer (see Subsection 2.1.3.2). Unlike in the previous cases, a huge shift in the PL (in both direct and indirect band in the WSe_2 BL) and DR has been obtained when comparing the BL on Si/SiO_2 and encapsulated in MoO_3 (Figure 8.6). μ-PL at RT has been measured using the same setup, with 1.88 μW of power excitation and 60 s acquisition time. For the DR, at room and low temperature, it has been used the previous white light source from Mightex.

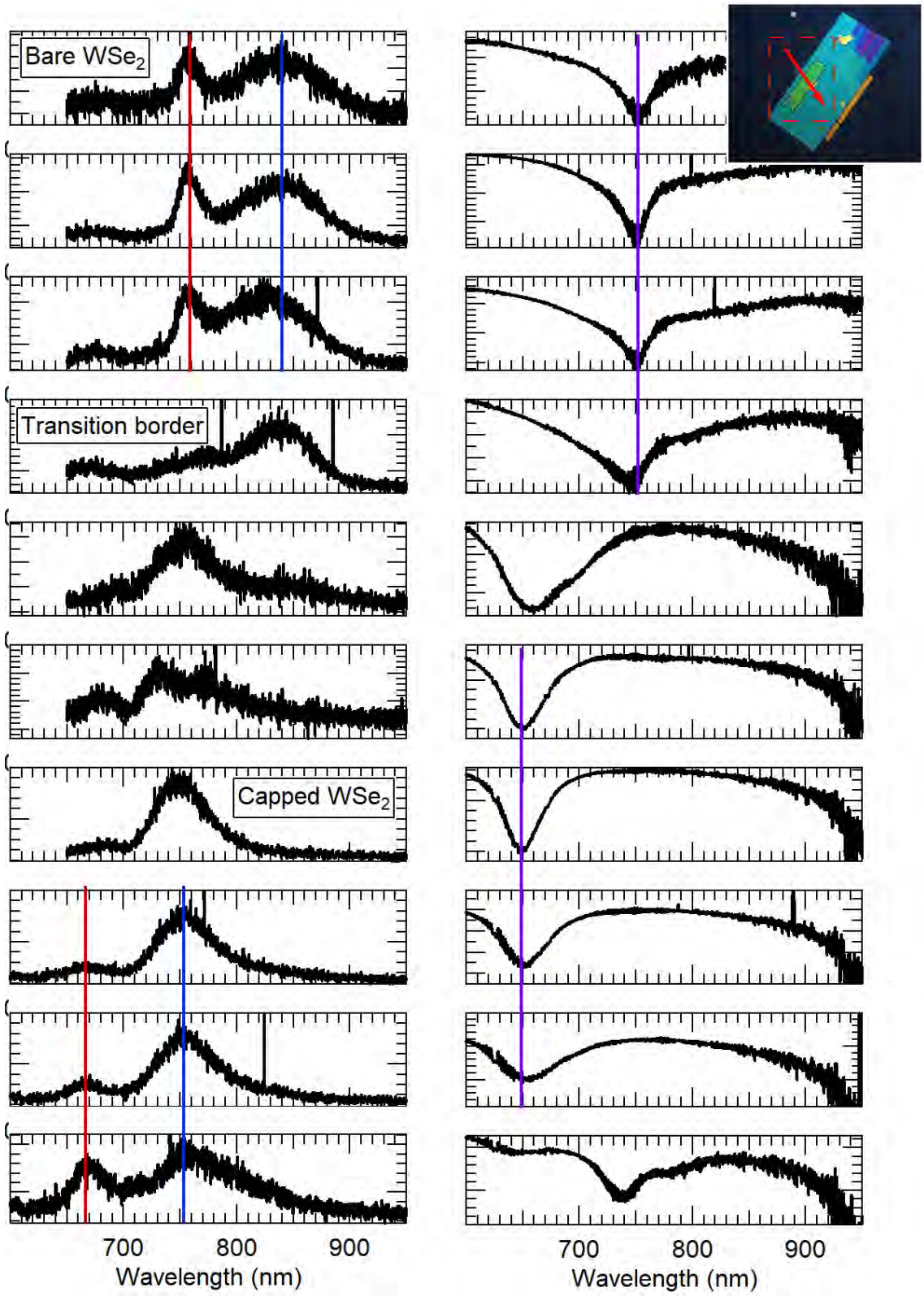

Figure 8.6: μ-PL (in counts, on the left) and DR (on the right) spectra at RT on different points in a WSe_2 BL encapsulated by MoO_3, starting in the WSe_2 BL on Si/SiO_2 taking measures towards the encapsulated area.

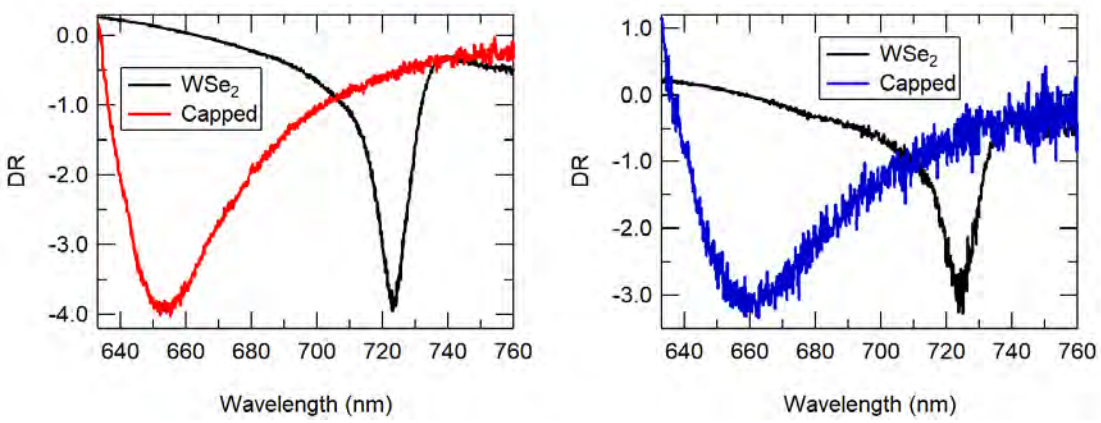

Figure 8.7: DR spectra at LT on different points in a WSe_2 BL encapsulated in MoO_3 (coloured) and on WSe_2 BL on Si/SiO_2 (black).

In case of PL measurements at RT, it has been obtained a shift in the direct band emission from 758 nm to 667 nm (91 nm, 0.22315 eV) and from 840 nm to 756 nm (84 nm, 0.164 eV) for the indirect band, over a factor 10 compared with the around 15 meV shift in reported publications encapsulated with hBN [424]. DR at RT matches this shift, from 750 nm to 650 nm.

Finally, the LT DR shows a huge shift too (from 725 nm to 655 nm), compatible with the RT measurements. It is worth noticing that in both cases, WSe_2 capped BL DR widens compared to DR in the bare WSe_2 BL. Further measurements must be taken concerning this topic to clarify these results, although these results have been verified and proved solid due to the different techniques and different temperatures measured. The main differences in this device presented are:

- WSe_2 BL encapsulated instead of a ML.
- Different orientation in the encapsulating MoO_3 material. In the encapsulated ML the crystallographic orientation of the encapsulating MoO_3 are almost perpendicular between each other, being parallel in the BL device (Figure 8.4 and Figure 8.6).

This second effect will be analysed considering the MoO_3 anisotropy in the layer plane.

8.4 Anisotropy in MoO_3

Even though there are some works studying the MoO_3 refractive index without considering or even mentioning possible anisotropy in this material [430, 446], other works point to its relevance [441]. This anisotropy could act as another degree of freedom for the final device application, being able to tune the conditions of the encapsulation due to the orientation, e.g., for different tuning in the final emission of a semiconductor encapsulated. In order to show this effect, DR has been measured for different angles in the layer plane in a MoO_3 sample, as seen in Figure 8.8, proving a relevant shift comparable with the shift observed in the BL device, showing anisotropic behavior.

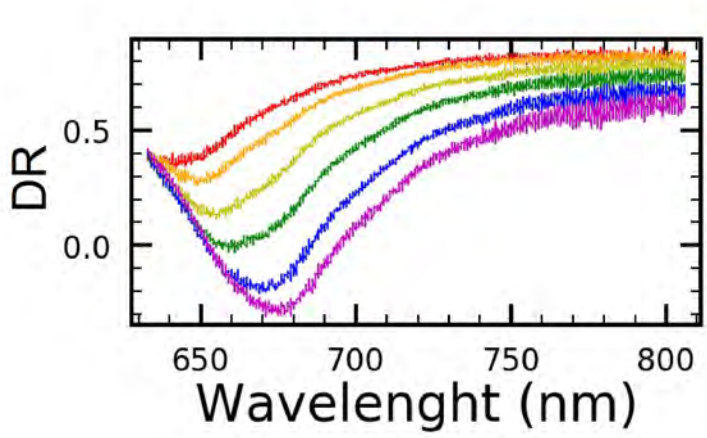

Figure 8.8: DR spectras rotating in the layer plane a MoO_3 nanosheet.

Ellipsometry measurements (see Subsection 2.4.1) have been taken to obtain the refractive index in both directions in nanosheets exfoliated to characterise and understand the anisotropy of this material. The refractive index modeling from the measurements taken by ellipsometry has been carried out by Dr. Mauro Brotons-Gisbert, whose results are shown in the Figure 8.9.

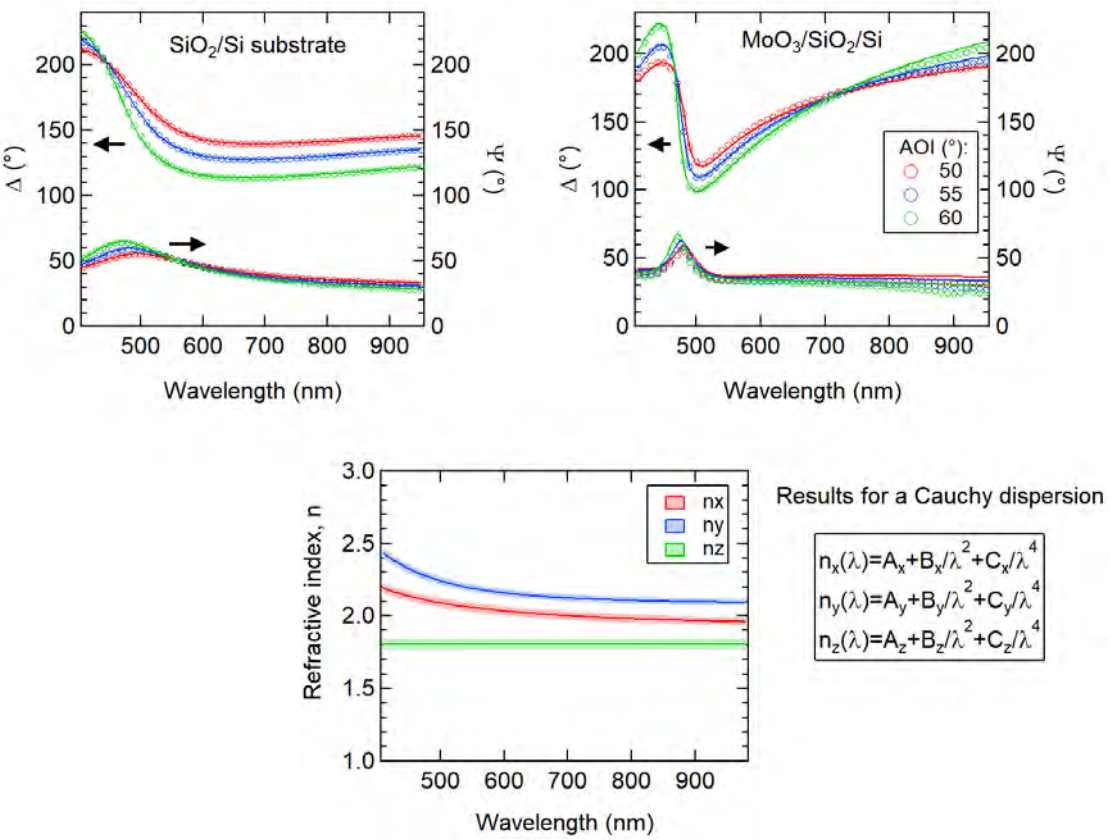

Figure 8.9: Ellipsometry measurements and refractive indexes in MoO_3 nanosheets.

8.5 Conclusions

To sum up, MoO_3 has been proved as a candidate to complement hBN as a 2D insulator. First, due to its zero nuclear spin for spintronic applications, a rare characteristic among the 2D exfoliable materials and second, due to its cleanness at LT, properties where clearly surpass hBN.

This proposal as a clean 2D insulator has been applied as a capping material for a WSe_2 ML, obtaining similar behavior as capped in hBN, proving its applicability for 2D optoelectronic devices, specially in spintronic applications. Finally, due to another device prepared with a WSe_2 BL encapsulated in MoO_3, obtaining a shift in PL at RT and in DR at both room and low temperature around 10 times larger as reported in any semiconductor encapsulated in hBN, the anisotropy of MoO_3 has been studied.

Shown in its DR and through an ellipsometry study, the refractive index along the three axis have been obtained, adding another degree of freedom to tune a final device emission for a specific application.

Bibliography

[391] Changhui Ye, Guowen Meng, Zhi Jiang, Yinhai Wang, Guozhong Wang, and Lide Zhang. Rational growth of Bi2S3 nanotubes from quasi-two-dimensional precursors. *Journal of the American Chemical Society*, 124(51):15180–15181, 2002.

[392] N Benramdane, M Latreche, H Tabet, M Boukhalfa, Z Kebbab, and a Bouzidi. Structural and optical properties of spray-pyrolysed Bi2S3 thin films. *Materials Science and Engineering: B*, 64(2):84–87, 1999.

[393] Tingting Liu, Yang Zhao, Lijun Gao, and Jiangfeng Ni. Engineering Bi2O3-Bi2S3 heterostructure for superior lithium storage. *Scientific reports*, 5:9307, 2015.

[394] W Jaegermann, a Klein, and C Pettenkofer. *Physics and Chemistry of Materials with Low-Dimensional Structures*, volume 24. 2000.

[395] A. Cantarero, J. P. Martínez, A. Seguba, and A. Chevy. Refractive index of bismuth sulfide in the infrared region. *Physica Status Solidi (a)*, 101(2):603–609, 1987.

[396] Jing Tang and A. Paul Alivisatos. Crystal splitting in the growth of Bi2S3. *Nano Letters*, 6(12):2701–2706, 2006.

[397] Raul Suarez, P. K. Nair, and Prashant V. Kamat. Photoelectrochemical Behavior of Bi2S3 Nanoclusters and Nanostructured Thin Films. *Langmuir*, 14(12):3236–3241, 2002.

[398] Neha Mahuli, Debabrata Saha, and Shaibal K. Sarkar. Atomic Layer Deposition of p-Type Bi2S3. *Journal of Physical Chemistry C*, 121(14):8136–8144, 2017.

[399] Hua Zhang, Jing Huang, Xinggui Zhou, and Xinhua Zhong. Single-crystal Bi2S3 nanosheets growing via attachment-recrystallization of nanorods. *Inorganic Chemistry*, 50(16):7729–7734, 2011.

[400] Michael B. Sigman and Brian A. Korgel. Solventless synthesis of Bi2S3 (bismuthinite) nanorods, nanowires, and nanofabric. *Chemistry of Materials*, 17(7):1655–1660, 2005.

[401] A. Cantarero, J. Martinez-Pastor, A. Segura, and A. Chevy. Excitonic ab-

sorption and Urbach's tail in bismuth sulfide single crystals. *Applied Physics A: Solids and Surface*, 45(2):125–132, 1988.

[402] Yixuan Zhou, Qiyi Zhao, Keyu Si, Zehan Yao, Xinlong Xu, and Yaohui Guo. Efficient mixed-solvent exfoliation of few-quintuple layer Bi2S3 and its photoelectric response. *Nanotechnology*, 28(33):335602, 2017.

[403] Rhiannon M. Clark, Jimmy C. Kotsakidis, Bent Weber, Kyle J. Berean, Benjamin J. Carey, Matthew R. Field, Hareem Khan, Jian Zhen Ou, Taimur Ahmed, Christopher J. Harrison, Ivan S. Cole, Kay Latham, Kourosh Kalantar-Zadeh, and Torben Daeneke. Exfoliation of Quasi-Stratified Bi2S3 Crystals into Micron-Scale Ultrathin Corrugated Nanosheets. *Chemistry of Materials*, 28(24):8942–8950, 2016.

[404] O. C. Monteiro and T. Trindade. Preparation of Bi2S3 nanofibers using a single-source method. *Journal of Materials Science Letters*, 19(10):859–861, 2000.

[405] Toan Trong Tran, Christopher Elbadawi, Daniel Totonjian, Charlene J. Lobo, Gabriele Grosso, Hyowon Moon, Dirk R. Englund, Michael J. Ford, Igor Aharonovich, and Milos Toth. Robust multicolor single photon emission from point defects in hexagonal boron nitride. *2017 Conference on Lasers and Electro-Optics, CLEO 2017 - Proceedings*, 2017-Janua:1–2, 2017.

[406] L. Boudaoud, N. Benramdane, R. Desfeux, B. Khelifa, and C. Mathieu. Structural and optical properties of MoO3 and V2O5 thin films prepared by Spray Pyrolysis. *Catalysis Today*, 113(3-4):230–234, 2006.

[407] H. Liu, Y. Cai, M. Han, S. Guo, M. Lin, M. Zhao, Y. Zhang, and D. Chi. Aqueous and mechanical exfoliation, unique properties, and theoretical understanding of MoO3 nanosheets made from free-standing alpha-MoO3 crystals: Raman mode softening and absorption edge blue shift. *Nano Research*, 11(3):1193–1203, 2017.

[408] Nilanthy Balakrishnan, Zakhar R Kudrynskyi, Emily F Smith, Michael W Fay, Oleg Makarovsky, Zakhar D Kovalyuk, Laurence Eaves, Peter H Beton, and Amalia Patanè. Engineering p - n junctions and bandgap tuning of InSe nanolayers by controlled oxidation. *2D Materials*, 4(2):025043, 2017.

[409] David O. Scanlon, Graeme W. Watson, D. J. Payne, G. R. Atkinson, R. G. Egdell, and D. S. L. Law. Theoretical and Experimental Study of the Elec-

tronic Structures of MoO3 and MoO2. *The Journal of Physical Chemistry C*, 114(10):4636–4645, 2010.

[410] Daniel J Terry, Viktor Zólyomi, Matthew Hamer, Anastasia V Tyurnina, David G Hopkinson, Alexander M Rakowski, Samuel J Magorrian, Nick Clark, Yuri M Andreev, Olga Kazakova, Konstantin Novoselov, Sarah J Haigh, Vladimir I Fal'ko, and Roman Gorbachev. Infrared-to-violet tunable optical activity in atomic films of GaSe, InSe, and their heterostructures. *2D Materials*, 5(4):041009, 2018.

[411] Zhipei Sun, Amos Martinez, and Feng Wang. Optical modulators with two-dimensional layered materials. *Nature Publishing Group*, 10(4):1–8, 2016.

[412] Nicolas Mounet, Marco Gibertini, Philippe Schwaller, Davide Campi, Andrius Merkys, Antimo Marrazzo, Thibault Sohier, Ivano Eligio Castelli, Andrea Cepellotti, Giovanni Pizzi, and Nicola Marzari. Two-dimensional materials from high-throughput computational exfoliation of experimentally known compounds. *Nature Nanotechnology*, 13(3):246–252, 2018.

[413] Aday J. Molina-Mendoza, José L. Lado, Joshua O. Island, Miguel Angel Niño, Lucía Aballe, Michael Foerster, Flavio Y. Bruno, Alejandro López-Moreno, Luis Vaquero-Garzon, Herre S.J. Van Der Zant, Gabino Rubio-Bollinger, Nicolás Agraït, Emilio M. Pérez, Joaquín Fernández-Rossier, and Andres Castellanos-Gomez. Centimeter-Scale Synthesis of Ultrathin Layered MoO3 by van der Waals Epitaxy. *Chemistry of Materials*, 28(11):4042–4051, 2016.

[414] Hiroshi Kanno, Russell J. Holmes, Yiru Sun, Stephane Kena-Cohen, and Stephen R. Forrest. White stacked electrophosphorescent organic light-emitting devices employing MoO3 as a charge-generation layer. *Advanced Materials*, 18(3):339–342, 2006.

[415] Y. Cao, A. Mishchenko, G. L. Yu, E. Khestanova, A. P. Rooney, E. Prestat, A. V. Kretinin, P. Blake, M. B. Shalom, C. Woods, J. Chapman, G. Balakrishnan, I. V. Grigorieva, K. S. Novoselov, B. A. Piot, M. Potemski, K. Watanabe, T. Taniguchi, S. J. Haigh, A. K. Geim, and R. V. Gorbachev. Quality Heterostructures from Two-Dimensional Crystals Unstable in Air by Their Assembly in Inert Atmosphere. *Nano Letters*, 15(8):4914–4921, 2015.

[416] Annemarie L. Exarhos, David A. Hopper, Richard R. Grote, Audrius Alkauskas, and Lee C. Bassett. Optical Signatures of Quantum Emitters in Suspended Hexagonal Boron Nitride. *ACS Nano*, 11(3):3328–3336, 2017.

[417] M. R. Tubbs. MoO3 layers - optical properties, colour centres, and holographic recording. *Physica Status Solidi (a)*, 21(1):253–260, 1974.

[418] David Di Yao, Jian Zhen Ou, Kay Latham, Serge Zhuiykov, Anthony P. O'Mullane, and Kourosh Kalantar-Zadeh. Electrodeposited alpha- And beta-phase MoO3 films and investigation of their gasochromic properties. *Crystal Growth and Design*, 12(4):1865–1870, 2012.

[419] Sivacarendran Balendhran, Sumeet Walia, Manal Alsaif, Emily P. Nguyen, Jian Zhen Ou, Serge Zhuiykov, Sharath Sriram, Madhu Bhaskaran, and Kourosh Kalantar-Zadeh. Field effect biosensing platform based on 2D alpha-MoO3. *ACS Nano*, 7(11):9753–9760, 2013.

[420] S. Schwarz, A. Kozikov, F. Withers, J. K. Maguire, A. P. Foster, S. Dufferwiel, L. Hague, M. N. Makhonin, L. R. Wilson, A. K. Geim, K. S. Novoselov, and A. I. Tartakovskii. Electrically pumped single-defect light emitters in WSe2. *2D Materials*, 3(2), 2016.

[421] Sivacarendran Balendhran. Devices and systems based on two dimensional MoO3 and MoS2. *RMIT University*, 2013.

[422] Sivacarendran Balendhran, Sumeet Walia, Hussein Nili, Jian Zhen Ou, Serge Zhuiykov, Richard B. Kaner, Sharath Sriram, Madhu Bhaskaran, and Kourosh Kalantar-Zadeh. Two-dimensional molybdenum trioxide and dichalcogenides. *Advanced Functional Materials*, 23(32):3952–3970, 2013.

[423] M. B. Sreedhara, H. S S Ramakrishna Matte, A. Govindaraj, and C. N R Rao. Synthesis, characterization, and properties of few-layer MoO3. *Chemistry - An Asian Journal*, 8(10):2430–2435, 2013.

[424] Iann C. Gerber and Xavier Marie. Dependence of band structure and exciton properties of encapsulated WSe2 monolayers on the hBN-layer thickness. *Physical Review B*, 98(24):28–31, 2018.

[425] Jong Hun Kim, Jatis Kumar Dash, Junyoung Kwon, Changbae Hyun, Hangyel Kim, Eunji Ji, and Gwan Hyoung Lee. Van der Waals epitaxial growth of single crystal alpha-MoO3 layers on layered materials growth templates. *2D Materials*, 6(1), 2019.

[426] Sivacarendran Balendhran, Junkai Deng, Jian Zhen Ou, Sumeet Walia, James Scott, Jianshi Tang, Kang L. Wang, Matthew R. Field, Salvy Russo, Serge Zhuiykov, Michael S. Strano, Nikhil Medhekar, Sharath Sriram, Madhu

Bhaskaran, and Kourosh Kalantar-Zadeh. Enhanced charge carrier mobility in two-dimensional high dielectric molybdenum oxide. *Advanced Materials*, 25(1):109–114, 2013.

[427] Deji Akinwande, Nicholas Petrone, and James Hone. Two-dimensional flexible nanoelectronics. *Nature communications*, 5:5678, 2014.

[428] Manal M Y A Alsaif, Sivacarendran Balendhran, Matthew R. Field, Kay Latham, Wojtek Wlodarski, Jian Zhen Ou, and Kourosh Kalantar-Zadeh. Two dimensional alpha-MoO3 nanoflakes obtained using solvent-assisted grinding and sonication method: Application for H2gas sensing. *Sensors and Actuators, B: Chemical*, 192:196–204, 2014.

[429] Huijuan Zhang, Lijun Gao, and Yongji Gong. Exfoliated MoO3 nanosheets for high-capacity lithium storage. *Electrochemistry Communications*, 52:67–70, 2015.

[430] Martijn F. J. Vos, Bart Macco, Nick F. W. Thissen, Ageeth A. Bol, and W. M. M. (Erwin) Kessels. Atomic layer deposition of molybdenum oxide from (NtBu)2(NMe2)2Mo and O2 plasma. *Journal of Vacuum Science & Technology A: Vacuum, Surfaces, and Films*, 34(1):01A103, 2016.

[431] Vipin Kumar, Afriyanti Sumboja, Jiangxin Wang, Venkateswarlu Bhavanasi, Viet Cuong Nguyen, and Pooi See Lee. Topotactic phase transformation of hexagonal MoO3 to layered MoO3-II and its two-dimensional (2D) nanosheets. *Chemistry of Materials*, 26(19):5533–5539, 2014.

[432] A. V. Kretinin, Y. Cao, J. S. Tu, G. L. Yu, R. Jalil, K. S. Novoselov, S. J. Haigh, A. Gholinia, A. Mishchenko, M. Lozada, T. Georgiou, C. R. Woods, F. Withers, P. Blake, G. Eda, A. Wirsig, C. Hucho, K. Watanabe, T. Taniguchi, A. K. Geim, and R. V. Gorbachev. Electronic properties of graphene encapsulated with different two-dimensional atomic crystals. *Nano Letters*, 14(6):3270–3276, 2014.

[433] Jian Chang, Meihua Jin, Fei Yao, Tae Hyung Kim, Viet Thong Le, Hongyan Yue, Fethullah Gunes, Bing Li, Arunabha Ghosh, Sishen Xie, and Young Hee Lee. Asymmetric supercapacitors based on graphene/MnO2 nanospheres and graphene/MoO3 nanosheets with high energy density. *Advanced Functional Materials*, 23(40):5074–5083, 2013.

[434] L. Seguin, M. Figlarz, R. Cavagnat, and J. C. Lassgues. Infrared and Ra-

man spectra of MoO3 molybdenum trioxides and MoO3xH2O molybdenum trioxide hydrates. *Spectrochimica Acta Part A: Molecular and Biomolecular Spectroscopy*, 51(8):1323–1344, 1995.

[435] M Anwar and C a Hogarth. Optical properties of amorphous thin films of MoO3 deposited by vacuum evaporation. *Physica Status Solidi (a)*, 109(2):469–478, 1988.

[436] R. Cárdenas, J. Torres, and J. E. Alfonso. Optical characterization of MoO3 thin films produced by continuous wave CO2 laser-assisted evaporation. *Thin Solid Films*, 478(1-2):146–151, 2005.

[437] Lili Cai, Connor J. McClellan, Ai Leen Koh, Hong Li, Eilam Yalon, Eric Pop, and Xiaolin Zheng. Rapid flame synthesis of atomically thin MoO3 down to monolayer thickness for effective hole doping of WSe2. *Nano Letters*, 17(6):3854–3861, 2017.

[438] J R Rumble. CRC Handbook of Chemistry and Physics. *Journal of Molecular Structure*, 1992.

[439] A. Abdellaoui, G. Lévêque, A. Donnadieu, A. Bath, and B. Bouchikhi. Iteratively derived optical constants of MoO3 polycrystalline thin films prepared by CVD. *Thin Solid Films*, 304(1-2):39–44, 1997.

[440] G. Cassabois, P. Valvin, and B. Gil. Hexagonal boron nitride is an indirect bandgap semiconductor. *Nature Photonics*, 10(4):262–266, 2016.

[441] L. Lajaunie, F. Boucher, R. Dessapt, and P. Moreau. Strong anisotropic influence of local-field effects on the dielectric response of alpha-MoO3. *Physical Review B - Condensed Matter and Materials Physics*, 88(11):1–9, 2013.

[442] Bevin Huang, Genevieve Clark, Dahlia R. Klein, David MacNeill, Efrén Navarro-Moratalla, Kyle L. Seyler, Nathan Wilson, Michael A. McGuire, David H. Cobden, Di Xiao, Wang Yao, Pablo Jarillo-Herrero, and Xiaodong Xu. Electrical control of 2D magnetism in bilayer CrI3. *Nature Nanotechnology*, pages 1–5, 2018.

[443] T. Taniguchi and K. Watanabe. Synthesis of high-purity boron nitride single crystals under high pressure by using Ba-BN solvent. *Journal of Crystal Growth*, 303(2):525–529, 2007.

[444] A. Boukhachem, O. Kamoun, C. Mrabet, C. Mannai, N. Zouaghi, A. Yumak, K. Boubaker, and M. Amlouk. Structural, optical, vibrational and photolu-

minescence studies of Sn-doped MoO3 sprayed thin films. *Materials Research Bulletin*, 72:252–263, 2015.

[445] Taka Aki Yano, Keisuke Yoshida, Yuhei Hayamizu, Tomohiro Hayashi, Fumio Ohuchi, and Masahiko Hara. Probing edge-activated resonant Raman scattering from mechanically exfoliated 2D MoO3nanolayers. *2D Materials*, 2(3), 2015.

[446] Christian Stelling, Chetan R. Singh, Matthias Karg, Tobias A.F. König, Mukundan Thelakkat, and Markus Retsch. Plasmonic nanomeshes: Their ambivalent role as transparent electrodes in organic solar cells. *Scientific Reports*, 7(February):1–13, 2017.

[447] Navas Illyaskutty, Sreeja Sreedhar, G. Sanal Kumar, Heinz Kohler, Matthias Schwotzer, Carsten Natzeck, and V. P Mahadevan Pillai. Alteration of architecture of MoO3 nanostructures on arbitrary substrates: Growth kinetics, spectroscopic and gas sensing properties. *Nanoscale*, 6(22):13882–13894, 2014.

[448] Gerasimos Konstantatos, Larissa Levina, Jiang Tang and Edward H. Sargent*. Sensitive Solution-Processed Bi2S3 Nanocrystalline Photodetectors. *Nanoletters*, 8(May):1–4, 2010.

[449] N J Stone. Table of nuclear magnetic dipole and electric quadrupole moments. *Nuclear Data Section*, (February):171, 2014.

[450] L. M. Peter. The photoelectrochemical properties of anodic Bi2S3 films. *Journal of Electroanalytical Chemistry*, 98(1):49–58, 1979.

[451] Husnu Koc, Haci Ozisik, Engin Deligoz, Amirullah M. Mamedov, and Ekmel Ozbay. Mechanical, electronic, and optical properties of Bi2S3 and Bi2Se3 compounds: First principle investigations. *Journal of Molecular Modeling*, 20(4), 2014.

9 Conclusions and future prospects

This thesis covers various two-dimensional semiconductors, from their preparation and study of basic properties to its implementation and characterisation in different optoelectronic devices. With a large experimental component, it brings together several micromanipulation and characterisation techniques in diverse elements such as microspheres, perovskites, waveguides, optical fibres... to be implemented together with the two-dimensional materials for that purposes.

In Chapter 3, the optical and electrical properties of the family of III - VI semiconductors have been studied. PL of exfoliated GaSe nanosheets have been measured, obtaining a shift in its luminescent emission of 120 meV when it reaches a thickness of 8 nm. This result contrasts with experimental publications previously reported, agreeing with first principle calculations reported before. However, no experimental results have been obtained in nanosheets thinner than 8 nm due to the hampering and deterioration of the samples in our experiments. The oxidation mechanism of this material on air has been also studied, which can be observed via OC and AFM as spots and spikes, respectively, formed in the surface of the nanosheets after exfoliation due to strong local structural relaxation processes that take place which are associated to the strain introduced by the nanosheet oxidation. Using XPS measurements, it is concluded that these oxidation reactions differ from these occurring in bulk or bulk-like GaSe nanosheets and have a deep effect on the structural, optical, and luminescent properties of GaSe nanosheets. Taking into account this deterioration and hampering, in Ar atmosphere or encapsulating the material, GaSe and its band gap tunability becomes relevant in optoelectronic devices with InSe or GaS, taking advantages of its similar structure and wide band gap tunability, from the infrared in case of InSe to ultraviolet in GaSe, that could cover the whole solar spectra for photodetection applications using this III - VI semiconductors family.

After this, electrical properties in InSe nanosheets have been studied. First, it is demonstrated the usage of multiterraced nanosheets of this material as heterojunc-

tions without defects in its junction that behave as p - n heterojunctions. Based on the change in its band structure when thickness is reduced, its behavior as a photodetector is understood through its I - V characteristics and a detailed study of the carrier recombination in the barrier generated by the change of band gap in the area where the thickness changes. The interest in these results resides not only in InSe, but in the possibility using different materials such as GaSe for different photodetector range, as explained before. Besides, these techniques exploit InSe great mobility for electric applications. In addition, for the modeling and design of electrical devices with this material, the dependance of the work function with the nanosheet thickness is studied by means of KPFM, accompanied by first principles calculations, obtaining a similar trend together with the experimental data. It is one of the first projects aiming for the characterisation of the electrical properties with dependance on thickness in literature in order to take advantage of the free-defect heterojunctions that can be developed. In future projects, due to the work function dependence on carrier concentration, obtaining the electronic affinity for each thickness can be a further step to better comprehension of this mechanisms. Finally, as an application of this material in its two-dimensional form, its usage for sensing of gases due to the change in the PL of the samples exposed to different concentrations, times and gases is proposed and demonstrated, taking advantage on its wide band gap tunability and, therefore, sensing range. In this case, the effect and usability is demonstrated, but further statistics to obtain sensibility, effect with other gases could be interesting to reach its full potential for its implementation.

After proposing III - VI semiconductors and some of their fundamental properties, next Chapters aimed for the enhancement or implementation of these properties in optoelectronic and photonic devices. Chapter 4 uses microspherical resonators to enhance and tune the effective photoluminescent emission in InSe and WSe_2 nanosheets by means of a lensing effect in excitation and collection and due to the resonances or WGM that these emissions create in the microspheres. It fullfills what it was sought: an enhancement in the RT PL emission in both materials (specially in InSe) and a tunability mechanism for WSe_2, adding understanding about its dipolar nature. In following projects, LT measurements in order to separate the contributions detected would help to a further fundamental study of the intrinsic IP and OP components in the materials analysed, due to the limitations in a micrometric range in the areas coupled to the WGMs.

In Chapter 5, perovskites have been analysed together with 2D semiconductors to

enhance its optical properties. In case of InSe, due to its OP dipolar nature, multidirectional perovskites on top enhances its emission, contrary to IP TMD MLs, where the vertical disposition were optimal. Here it is demonstrated the combination of properties: where the great absorption in perovskites enhance the optical properties in InSe, distinguishing the effect produced in InSe and TMDs. Further studies could aim on the opposite: a device where the outstanding mobility properties in InSe nanosheets enhance the electrical properties in perovskites, handicapped due to its nanoclusters nature, hampering carrier transport in the material. With these considerations and studies, a mixed optoelectronic device, where the optical absorption is given by the perovskites, and the optoelectronic behavior (wide range tunability and mobility) by InSe nanosheets is possible, with the better of both materials.

Chapter 6 demonstrates the implementation of 2D materials in integrated optics as photonic waveguides for further applications. First of all, an horizontal excitation - horizontal collection, i.e., a guiding configuration, has been achieved for the first time in literature using evanescent excitation and collection to do so. Besides, the double-peak detection when the TMD is excited in the horizontal direction and collected in vertical opens and enhances its usability for photonic devices due to the narrowing in the detection and the separation in its contributions. Even though these studies gave new understanding in TMD MLs fundamental behavior, the initial idea for this project remains unachieved: InSe implementation, which after the knowledge obtained in the measurements presented, will be the next material to analyse. Its OP nature, already demonstrated not only in the bibliography, but in Chapters 4 and 5, is ideal for these kind of horizontal techniques. Further studies must aim in this direction, once the techniques are optimised for other 2D materials. Besides, in order to maximise the comprehension we have on TMDs, LT measurements, where neutral exciton and charged exciton can be precisely located and isolated, would help this study.

Finally, in Chapters 7 and 8, two new 2D materials are presented: Bi_2S_3 and MoO_3, opening its usage among other semiconductors. Both count with an IP anisotropy that can be useful in some application, each one in its field, as demonstrated in each Chapter: as a semiconductor with an exceptional absorption and as an insulator, where only hBN takes its place. In the case of Bi_2S_3, due to its tunable absorption, can be envisioned, e.g, as a controlable saturable absorber using these two directions, a linear polariser or a waveplate. In the case of MoO_3, opens the door

to nuclear spintronic studies, field blocked using hBN due to its own nuclear spin, which applications for nuclear spintronic devices could follow the trend marked by other spintronic devices already studied at an atomic level.

In the last paragraphs of this thesis, instead of only aiming at the results and conclusions obtained in the gathered projects (which can be found in detail in their separated subsections per Chapter), it is worth noticing that for each result obtained, new projects can be envisioned by applying that results. These last paragraphs attemp to mirror and reproduce the first paragraphs of this thesis: that within material science, nanomaterials (and specially, 2D materials) constitute actually a field in its heyday, where research on different materials, different properties and different applications only grow everyday, which potential seems unreachable.

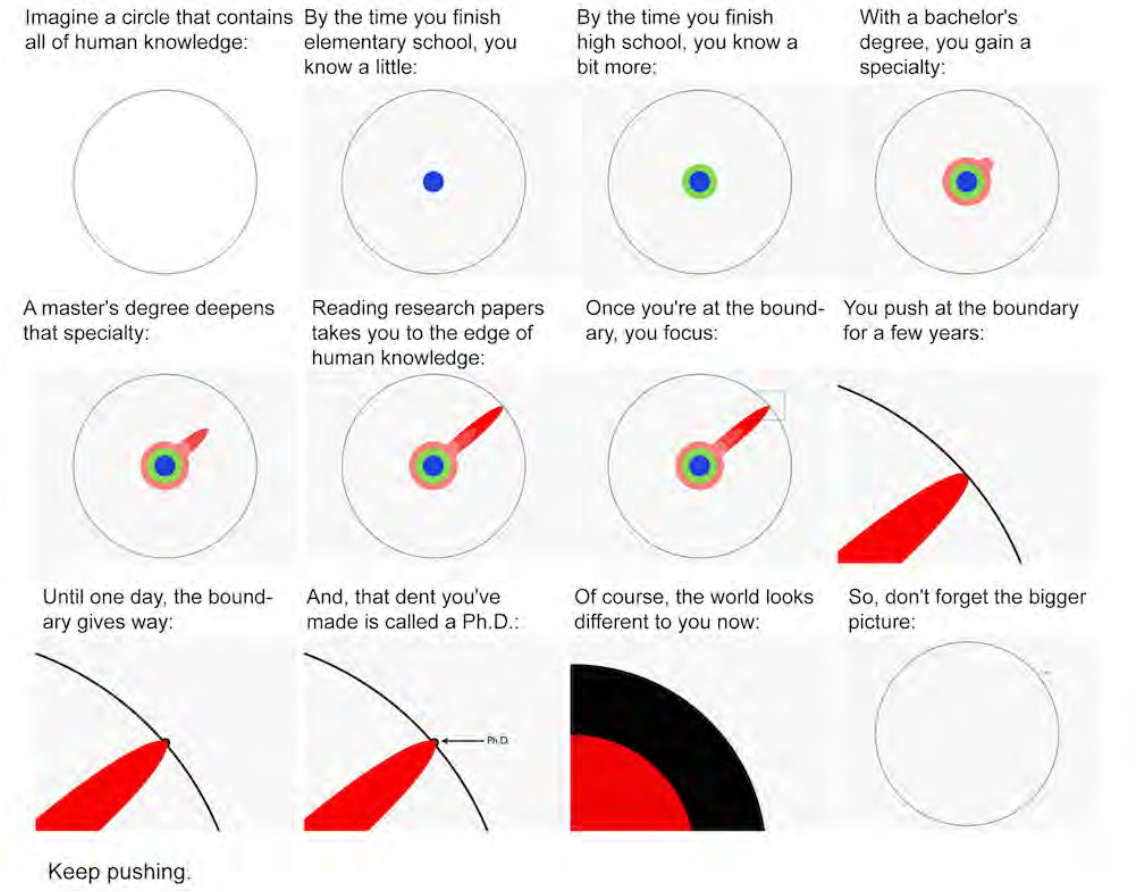

Figure 9.1: The Illustrated Guide to a Ph.D., original work from Matt Might, http://matt.might.net/articles/phd-school-in-pictures/

Appendix A. Materials used

- GaSe: GaSe monocrystals here used to prepare the nanosheets were cleaved perpendicular to the (001) direction from an ingot grown by the Bridgman-Stockbarger method [135, 121].
- InSe: InSe monocrystals used here to prepare the nanosheets were cleaved perpendicular to the (001) direction from an ingot grown by the Bridgman method from a nonstoichiometric $In_{1.05}Se_{0.95}$ melt. To act as n-dopant, tin, in a content 0.01%, was introduced previously to growth. From these ingots, thin n-doped InSe samples were cleaved and used to prepare atomically thin InSe nanosheets.
- 2-MET and 3-NT purchased from Sigma - Aldrich.
- Microspheres: purchased from Sigma - Aldrich.
- WSe_2: bulk WSe_2 used in this thesis were purchased from HQ Graphene.
- $MoSe_2$: synthesized by the flux zone technique, avoiding halides in its growth, from 2D Semiconductors.
- Perovskites: $CsPbI_3$ and the $CsPbBr_3$ nanocrystals were synthetized following the hot-injection method. A reprecipitation method was used for the purification of the PNCs; two solvent/antisolvent (hexane/ethyl acetate) washing cycles were applied to archieve high purity PNCs.
- Bi_2S_3: bulk Bi_2S_3 monocrystals grown by the Bridgman method from a stoichiometric polycrystalline material which was previously obtained by reaction of Bi and S (3N and 5N8 in purity, respectively).
- MoO_3: purchased from 2D Semiconductors.

Appendix B. List of Abreviations

0D, 1D, 2D, 3D	Zero-, One-, Two-, Three-dimensional
AFM, KPFM	Atomic, Kelvin-Probe Force Microscopy
Bi_2S_3	Bismuth Sulphide
GaSe	Gallium Selenide
hBN	Hexagonal Boron Nitride
I - V	Current - Voltage
InSe	Indium Selenide
IP, OP	In-plane, Out-of-plane
ITO	Indium Tin Oxide
LT, RT	Low, Room temperature
ML, BL, TL	Monolayer, Bilayer, Trilayer
MoO_3	Molybdenum Trioxide
MoS_2	Molybdenum Sulphide
$MoSe_2$	Molybdenum Selenide
OC, DR	Optical contrast, Differential reflectivity
PDMS, PMMA, PPC	Polydimethylsiloxane, Poly(methyl methacrylate)
ϕ, χ	Work function, Electronic affinity
PL	Photoluminescence
PPC	Polypropylene carbonate
SiO_2	Silicon Oxide
TMD	Transition Metal Dichalchogenides
vdW	van der Waals
WGM	Whispering gallery modes
WS_2	Tungsten Sulphide
WSe_2	Tungsten Selenide
XPS	X-ray photoemission spectroscopy
XRD	X-ray diffraction

Appendix C. Related publications

C.1 Already published, included in this thesis

- Quantum size confinement in gallium selenide nanosheets: band gap tunability versus stability limitation, Daniel Andres-Penares, Ana Cros, Juan P. Martínez-Pastor, Juan F. Sánchez-Royo, *Nanotechnology* **28** (17), 175701 (2017)

C.2 Already published, not included in this thesis

- Out-of-plane orientation of luminescent excitons in two-dimensional indium selenide, Mauro Brotons-Gisbert, Raphaël Proux, Raphaël Picard, Daniel Andres-Penares, Artur Branny, Alejandro Molina-Sánchez, Juan F. Sánchez-Royo, Brian D. Gerardot, *Nature Communications* **10** (1), 1-10 (2019)
- Optical Contrast and Raman Spectroscopy Techniques Applied to Few-Layer 2D Hexagonal Boron Nitride, Marie Krečmarová, Daniel Andres-Penares, Ladislav Fekete, Petr Ashcheulov, Alejandro Molina-Sánchez, Rodolfo Canet-Albiach, Ivan Gregora, Vincent Mortet, Juan P. Martínez-Pastor, Juan F. Sánchez-Royo, *Nanomaterials* **9** (7), 1047 (2019)
- Optical contrast of 2D InSe on SiO_2/Si and transparent substrates using band-pass filters, Mauro Brotons-Gisbert, Daniel Andres-Penares, Juan P. Martínez-Pastor, Ana Cros, Juan F. Sánchez-Royo, *Nanotechnology* **28** (11), 115706 (2017)
- Nanotexturing to enhance photoluminescent response of atomically thin indium selenide with highly tunable band gap, Mauro Brotons-Gisbert, Daniel Andres-Penares, Joonki Suh, Francisco Hidalgo, Rafael Abargues, Pedro J.

Rodríguez-Cantó, Alfredo Segura, Ana Cros, Gerard Tobias, Enric Canadell, Pablo Ordejón, Junqiao Wu, Juan P. Martínez-Pastor, Juan F. Sánchez-Royo, *Nano letters* **16** (5), 3221-3229 (2016)

C.3 To be published in the next months, included in this thesis

The following list gathers the separate publications that are intended to be sent in the coming months as these are understood as different projects. The final publication title, as well as the order and number of authors of each one is provisional with respect to what can finally be sent and accepted in the future.

- I - V characterisation of defect-free n - N heterojunctions in InSe different-layered nanosheets and work function analysis via Kelvin probe force microscopy, Daniel Andres-Penares, Alberto Maulu, Josep Canet-Ferrer, Ana Cros, Juan P. Martínez-Pascual, Juan F. Sánchez-Royo (Subsections 3.2.2.1 and 3.2.2.2)
- Photoluminescence effect in InSe exfoliated nanosheets for gas sensing applications, Daniel Andres-Penares, Rafael Abargues-Lopez, Eduardo Aznar-Gadea, Juan P. Martínez-Pastor, Juan F. Sánchez-Royo (Subsection 3.2.3)
- SiO_2-microsphere resonators for light emission management upon dipole orientation of 2D semiconductors, Daniel Andres-Penares, Juan P. Martínez-Pastor, Carlos J. Zapata-Rodriguez, Juan F. Sánchez-Royo (Chapter 4)
- Enhanced photoluminescence in exfoliated Indium Selenide nanosheets harnessing the out-of-plane dipole orientation through reabsorption from perovskites multi-directional emission, Daniel Andres-Penares, Juan Navarro-Arenas, Juan P. Martínez-Pastor and Juan F. Sánchez-Royo (Chapter 5)
- Waveguide implementation of WSe_2 and $MoSe_2$ exfoliated monolayers, Daniel Andres-Penares, Isaac Suarez-Álvarez, Rodolfo E. Canet-Albiach, Mauro Brotons-Gisbert, Alejandro Molina-Sanchez, Juan P. Martínez-Pastor, Juan F. Sánchez-Royo (Chapter 6)
- Anisotropy in exfoliated Bismuth Sulphide nanoflakes: optical properties and implementation in fibre optics, Daniel Andres-Penares, Mauro Brotons-Gisbert,

Martina Delgado-Pinar, Alejandro Molina-Sanchez, M. Carmen Martínez-Tomás, Miguel V. Andrés-Bou, Juan P. Martínez-Pastor, Juan F. Sánchez-Royo (Chapter 7)

- Molybdenum oxide: a new clean zero nuclear spin 2D insulator, Daniel Andres-Penares, Mauro Brotons-Gisbert, Juan F. Sánchez-Royo, Brian D. Gerardot (Chapter 8)

Appendix D. Resúmenes en distintas lenguas oficiales

D.1 Resumen amplio en castellano

Dentro del campo de la Ciencia de Materiales, los materiales bidimensionales han acaparado la atención de la comunidad científica en los últimos años. Desde la aparición del grafeno en 2004, el interés y estudio de éste y otros materiales similares han aumentado exponencialmente. El cambio y la aparición de nuevas propiedades cuando el espesor de éstos se ve reducido a escalas nanométricas tiene un especial interés para el estudio de sus propiedades fundamentales para, a partir de éstas, el diseño y su implementación en dispositivos de diversa índole. En cuanto al grafeno, sus sorprendentes propiedades mecánicas, como su dureza, flexibilidad y elasticidad, así como su alta conductividad térmica y eléctrica y el comportamiento como cuasipartículas sin masa (i.e., como fermiones de Dirac) de los electrones que se trasladan sobre el mismo, fomentaron el estudio de este material. Sin embargo, la dificultad para abrir en este material una banda prohibida en su estructura de bandas, que en condiciones normales se comporta como un conductor, promovió la investigación e interés en otros materiales laminares que intrínsecamente se comportaban en estado volúmico como semiconductores de forma natural, pero que pudieron ser obtenidos en su estado bidimensional con técnicas similares a las utilizadas para el grafeno.

La gran variedad de materiales con posibilidad de ser exfoliables a nivel bidimensional que han aparecido tras la estela del grafeno, así como las distintas propiedades que poseen, abren el campo a distintas aplicaciones, desde dispositivos optoelectrónicos, detección y sensado, almacenamiento de energía, catálisis, aplicaciones médicas y tecnologías de información cuántica, entre otras. El hecho de poder encontrar en estos materiales tanto aislantes, conductores y semiconductores, materiales flexibles, transparentes y de gran dureza, así como propiedades más exóticas como supercon-

ductividad, aislantes topológicos, entre otros.

En este contexto, la presente tesis está enfocada y recoge resultados considerando las siguientes premisas: (1) dentro de los diferentes métodos de preparación de materiales bidimensionales, cada uno con sus distintas ventajas y desventajas, se ha elegido la exfoliación micromecánica debido a la pureza y ordenación cristalográfica conservada de su precursor volúmico en las muestras obtenidas de cara a la obtención de dispositivos de mayor calidad; (2) se explorarán tanto desde un estudio a nivel de ciencia fundamental para el entendimiento de nuevas propiedades en distintos materiales bidimensionales poco explorados por la comunidad científica, así como su implementación en dispositivos optoelectrónicos enfocados a distintas aplicaciones mediante el uso de sus propiedades; (3) para comparar las propiedades estudiadas en los materiales bidimensionales tratados, los mayormente conocidos dicalcogenuros de metales de transición serán estudiados en las mismas condiciones, obteniendo mayor entendimiento en sus propiedades; (4) la presente tesis tiene una gran componente experimental, ya que todo el proceso para los distintos materiales será recogido y tratado, desde la preparación de distintos materiales bidimensionales, su manipulación y ordenación mediante distintas técnicas, así como su caracterización en distintos aspectos, desde el estudio de distintas propiedades ópticas, eléctricas y morfológicas a su implementación y caracterización en dispositivos orientados a aplicaciones específicas en diversos campos, desde sensado, a su implementación junto con microresonadores, perovskitas, guías ópticas fotónicas integradas o fibras ópticas, tanto para el estudio de las propiedades básicas de dichos materiales como para tener una visión global y general de su aplicación en distintos ámbitos y campos.

En una primera parte, se estudiarán las propiedades ópticas y eléctricas de la familia de los semiconductores III - VI, poco explorados y complementarios en muchas propiedades a los más conocidos dicalcogenuros de metales de transición. Se estudiará la fotoluminiscencia a temperatura ambiente de muestras exfoliadas de Seleniuro de Galio, donde experimentalmente se demuestra un corrimiento en su emisión luminiscente debido a efectos de confinamiento cuántico de 120 meV al llegar a 8 nm de espesor, resultado superior al reportado en el momento de estudio, y que sigue la tendencia a lo reportado teóricamente, con un corrimiento desde los 2.02 eV en su estado volúmico hasta 3.2 eV al llegar a la monocapa, llegando desde el visible al ultravioleta cercano según cálculos de primeros principios reportados. Sin embargo y pese al gran interés en este material debido al gran rango del espectro que barre al reducir su espesor, también se estudia el mecanismo de oxidación de este material

en condiciones normales, a tener en cuenta en este material, mediante técnicas como microscopía de fuerza atómica, contraste óptico y espectroscopía de fotoemisión de rayos X para comprender la evolución en su deterioro de cara a su implementación. Estas reacciones de oxidación difieren de las estudiadas en muestras volúmicas de Seleniuro de Galio y tienen un importante efecto en las propiedades ópticas, estructurales y luminiscentes de las muestras exfoliadas. Ópticamente, se demuestra que técnicas como el contraste óptico pierden precisión debido a la aparición de manchas de distinta coloración que, por tanto, perjudican su estudio analítico mediante esta técnica, debido a la aparición de nanopilares en la superficie de las muestras exfoliadas – reportados mediante microscopía de fuerza atómica - debido a una gran densidad de defectos que aparecen en muestras recién exfoliadas tras 24h que reducen su intensidad de fotoluminiscencia al aumentar el tiempo expuestas al aire. Este estudio experimental permite, por una parte, demostrar experimentalmente el gran potencial de las muestras exfoliadas de Seleniuro de Galio dado su amplio rango de tunabilidad con el espesor de las mismas y, por otro, ofrece entendimiento de los mecanismos de deterioro de cara a evitarlo previo su uso en dispositivos optoelectrónicos con este material.

Tras esto, se pasará al Seleniuro de Indio, material cuyas propiedades ópticas se conocen en mayor medida, pero cuyas propiedades eléctricas en su estado bidimensional no han sido apenas exploradas. Por ello, en esta tesis, aprovechando la gran movilidad reportada de las muestras exfoliadas de Seleniuro de Indio, comparables a su estado volúmico, se demuestra experimentalmente el uso de muestras multiescalonadas de este material (i.e., nanocopos que presentan distintos espesores dentro del mismo material) como heterouniones sin defectos en la interfase que se comportan como heterouniones p - n, elemento base de la optoelectrónica moderna en dispositivos como transistores, fotodetectores o fotoemisores. Basados en el cambio en su estructura de bandas al cambiar de espesor (por efectos de confinamiento cuántico, similar a lo anteriormente demostrado en muestras exfoliadas de Seleniuro de Galio, al reducir el espesor de este material a escalas nanométricas, la banda prohibida de los nanocopos se separa, produciendo diferentes bandas prohibidas dentro del mismo nanocopo) se estudia su funcionamiento como fotodetector mediante sus características I - V y un estudio detallado de la recombinación de portadores en la barrera generada por el cambio de banda prohibida en el cambio de espesor. Mediante técnicas de microfotoluminiscencia se obtiene fotocorriente generada por muestras multiescalonadas en ausencia de voltaje aplicado y un comportamiento asimétrico

al aplicar voltajes positivos y negativos, pruebas de la naturaleza de heterounión de las muestras multiescalonadas, teniendo un comportamiento simétrico en muestras con un solo espesor dada la ausencia de barrera interna. Además, de cara a la modelización y diseño de dispositivos eléctricos con este material, se estudia la variación de la función de trabajo de distintos espesores del material mediante microscopía de fuerza de sonda Kelvin, acompañado de cálculos de primeros principios, obteniendo una tendencia similar junto con los datos experimentales. Estos resultados demuestran, por tanto, la necesidad de caracterizar dichos valores para los diferentes espesores en este material de cara a su utilización en dispositivos optoelectrónicos dada su relevancia a la hora de formar distintos tipos de contactos eléctricos entre materiales que afectarían al desempleo final del dispositivo. Finalmente, como aplicación de este material, se propone y demuestra su uso para el sensado de gases debido al cambio en la fotoluminiscencia de las muestras expuestas a distintas concentraciones, tiempos y gases. Se usarán como gases tioles debido a su presencia del radical sulfuro, presente en distintos decaimientos orgánicos de alimentos y similares y trinitrotolueno como ejemplo de gas presente en la detección de explosivos, entre otros. Se observa que, a bajas concentraciones y tiempo de exposición frente a estos gases, la fotoluminiscencia de las muestras exfoliadas aumenta debido a la localización de los defectos de selenio superficiales en las nanocapas, para tras ello disminuir a mayores concentraciones y tiempos de exposición al embeberse dichos gases dentro de las nanocapas, provocando por ello defectos en las mismas que reducen su emisión. Además, se observa una mayor respuesta en muestras delgadas en comparación con muestras más volúmicas al tener una mayor ratio superficie – volumen. Estos tres resultados han sido demostrados para muestras de Seleniuro de Indio, apuntando por ello comportamientos similares en otro tipo de materiales como, por ejemplo, en muestras escalonadas de Seleniuro de Galio.

Tras la presentación de los semiconductores III - VI, una segunda parte de la tesis se centrará en su implementación experimental en dispositivos conceptuales para aprovechar u optimizar las propiedades antes descritas, comparando los resultados en cada caso con monocapas de dicalcogenuros de metales de transición como el Seleniuro de Tungsteno o el Seleniuro de Molibdeno, al ser materiales cuyas propiedades se conocen en mayor medida y en algunas de ellas presentan su contraparte en los semiconductores III - VI. En concreto, se intentará aprovechar la recientemente demostrada naturaleza dipolar del Seleniuro de Indio como perpendicular al plano de exfoliación, distinta a los dicalcogenuros de metales de transición y a la mayoría

de materiales bidimensionales reportados, hecho que perjudica su uso en la configuración de excitación vertical - colección vertical usual en los estudios científicos, pero que puede ser aprovechado en otras situaciones. Primero, mediante el uso de microesferas de óxido de silicio depositadas por goteo sobre las muestras exfoliadas de ambos materiales bidimensionales se optimizará la extracción y colección de su fotoluminescencia, tanto en el caso de Seleniuro de Indio como en el Seleniuro de Tungsteno, debido al aumento en la superficie excitada y, finalmente, un aumento en la colección global de la emisión de las muestras. Por la presencia de la microesfera y el desenfoque producido en comparación con la situación previamente enfocada en ausencia de la microesfera, hace que la cantidad de material excitado y, por tanto, donde se fomentará la recombinación de portadores, aumentará, aumentando consecuentemente su emisión fotoluminiscente. Tras ello, una vez los nanocopos han sido excitados, su emisión será re-enfocada por la microesfera, de forma que la colección total aumentará con respecto a la situación sin la misma debido a la apertura numérica del sistema de colección, que se verá aumentado de forma efectiva por dicho efecto lente en colección debido a la microesfera. Finalmente, se demostrará el comportamiento como dipolo perpendicular al plano en el caso de la emisión fotoluminiscente de los nanocopos de Seleniuro de Indio, así como de la componente de baja energía en la emisión fotoluminiscente de las monocapas de Seleniuro de Tungsteno, siendo estas asociadas al trión o excitón cargado. Esta naturaleza dipolar se ve reflejada como perpendicular al plano debido a las resonancias que presenta la emisión colectada, provocada por los modos de galería susurrante que se producen en las microesferas por la excitación emitida por el material bidimensional, actuando estas microesferas como elemento dispersante. La cantidad y forma cualitativa de estos modos resonantes observados en la emisión global colectada coinciden con las resonancias de un dipolo perpendicular al plano tras una microesfera dispersora, calculados tanto por métodos analíticos como numéricos, en comparación con los calculados para un dipolo paralelo al plano, donde la distancia entre modos se reduce claramente. El hecho de estudiar la emisión fotoluminiscente de las muestras bidimensionales junto con las microesferas depositadas sobre ellas ofrece un control adicional a la emisión fotoluminiscente de estos materiales en función del diámetro de dicha microesfera, cuyo valor puede ser modificado de cara a variar la posición de los modos de galería susurrantes en ella, tanto en aumento de intensidad como en posición del pico efectivo de emisión colectado de cara a su implementación para una aplicación en concreto al poder afinar la posición de dichas resonancias en función

de la finalidad deseada.

Cambiando de sistema para aprovechar la naturaleza dipolar antes descrita, estos materiales bidimensionales, tanto el Seleniuro de Indio como el Seleniuro de Molibdeno, se estudiarán en heteroestructuras verticales junto con nanocristales de perovskitas con emisión en el visible. Estas heteroestructuras verticales han sido preparadas tratando los cristales de perovskitas de forma similar a un material bidimensional mediante transferencia viscoelástica seca para cubrir zonas del material exfoliado con perovskitas y así poder comparar las zonas cubiertas con las zonas sin tratar. En presencia de las perovskitas sobre los nanocopos exfoliados, se observa un aumento de la fotoluminescencia colectada en el caso de los nanocopos de Seleniuro de Indio en comparación a lo obtenido junto con monocapas de Seleniuro de Molibdeno, donde la fotoluminescencia detectada se ve reducida al depositar un nanocristal de perovskitas sobre las muestras exfoliadas. El aumento de fotoluminiscencia en el caso del Seleniuro de Indio se ha verificado con dos tipos de perovskitas, con emisión en la zona del espectro visible en el rojo y en el verde, respectivamente. El motivo de dicho efecto es la reabsorción por parte del Seleniuro de Indio de lo emitido por la perovskita superior, que absorberá parcialmente la excitación que llega al conjunto y tendrá su propia emisión fotoluminiscente, debido a la disposición óptima del dipolo perpendicular al plano de los nanocopos de Seleniuro de Indio con respecto a la emisión multidireccional de las perovskitas, en comparación a la ausencia de perovskitas, donde el dipolo perpendicular al plano del Seleniuro de Indio perjudica la absorción de la excitación vertical. En contraposición a esta situación, el dipolo paralelo al plano de los dicalcogenuros de metales de transición, en este caso reflejado en las monocapas de Seleniuro de Molibdeno, que ya tenía una disposición óptima para la excitación y colección vertical, la presencia de las perovskitas sobre las mismas deteriora su emisión final al absorber parte de la excitación que no se consigue reabsorber por la emisión de la perovskita. Este estudio, junto con lo descrito anteriormente con las microesferas y lo previamente reportado, confirma la naturaleza dipolar en el Seleniuro de Indio como perpendicular al plano.

Finalmente, y para cerrar esta segunda parte de dispositivos enfocados a optimizar la extracción efectiva en los semiconductores III - VI, con vistas a la implementación de estos materiales bidimensionales en dispositivos fotónicos integrados, se estudia el comportamiento de nanocopos de Seleniuro de Indio y monocapas de Seleniuro de Tungsteno y Seleniuro de Molibdeno sobre guías de onda fotónicas, permitiendo así la excitación de las muestras y la colección de su emisión fotoluminiscente indistin-

tamente en las direcciones horizontal y vertical al plano de exfoliación, en todas las configuraciones posibles. Tras unos primeros pasos con el Seleniuro de Indio, se estudia en detalle la implementación de los dicalcogenuros de metales de transición en las mismas, Seleniuro de Tungsteno y Seleniuro de Molibdeno, obteniendo medidas experimentales en todas las configuraciones de guiado (es decir, tanto en excitación horizontal – colección vertical, excitación vertical – colección horizontal, excitación horizontal – colección horizontal y la ya ampliamente estudiada excitación vertical – colección vertical), así como su distinto comportamiento con respecto a la absorción y emisión frente a luz polarizada en la guía. En las muestras preparadas de ambos materiales, Seleniuro de Molibdeno y Seleniuro de Tungsteno, se observa emisión en todas las configuraciones, confirmando la posibilidad de guiado de los mismos, siendo esta configuración de excitación horizontal – colección horizontal la que presenta potenciales aplicaciones en óptica integrada. Sin embargo, en excitación horizontal – colección vertical, a diferencia del resto de configuraciones, donde cualitativamente es similar, se observa un doble pico con una disminución de la anchura de ambos picos. Estos resultados han sido verificados para guías de onda de distintos materiales, distintos láseres de excitación y diferente confinamiento en la guía, tanto en ondas planas como en guías en una dimensión, en diversas medidas, corroborando dichos resultados experimentales. Mediante medidas de microfotoluminiscencia se determina que en las monocapas de los dicalcogenuros de metales de transición se observan dos contribuciones en su emisión fotoluminiscente, causantes de los distintos resultados experimentales observados. En estas medidas se pueden observar la contribución del excitón neutro, dominante en la mayoría de las situaciones, y el trión a menores energías, que produce la asimetría en la emisión de estos materiales. La contribución debida al trión se puede observar con mayor intensidad en bordes o pliegues del material, donde se producen defectos y acumulación de portadores, aumentando la recombinación de excitones localizados o cargados. Siendo el trión una cuasipartícula formada por dos huecos y un electrón (en nuestro caso, dado el dopado p del material original volúmico del que se han obtenido las monocapas estudiadas), esta acumulación de portadores fomenta la formación de esta recombinación, produciendo emisión a menor energía a la del excitón neutro. De esta forma se observa el distinto peso de estas contribuciones en función del punto medido en la muestra. Esta separación de contribuciones tiene especial interés dado que permite la manipulación de ambas señales separadamente para aplicaciones, por ejemplo, de codificación de información. Con ello, y haciendo un estudio en las

guías fotónicas con respecto a la polarización de la luz emitida y colectada, se observa un distinto comportamiento dentro de las componentes que intervienen en la emisión fotoluminiscente de los dicalcogenuros de metales de transición con respecto a su naturaleza dipolar, donde se observa un comportamiento de emisión paralela al plano, coherente con lo esperado por su naturaleza dipolar en el plano, como se ha reportado para el excitón neutro en los dicalcogenuros de metales de transición. Estos resultados ayudan a su entendimiento y aprovechamiento de cara a dispositivos en el plano, donde especialmente los semiconductores III – VI antes estudiados tienen especial interés debido a su comportamiento dipolar perpendicular al plano, asentando las bases y técnicas experimentales para su futura implementación en fotónica integrada compatible con técnicas ya conocidas empleadas en la industria del silicio, donde a diferencia de los dicalcogenuros de metales de transición, en los semiconductores III – VI se espera un rendimiento similar al obtenido en los materiales con dipolo en el plano en la configuración de excitación vertical – colección vertical ampliamente estudiada.

En una tercera y última parte de la tesis se presentarán dos materiales bidimensionales no explorados en la literatura: el Sulfuro de Bismuto y el Trióxido de Molibdeno. En el caso del Sulfuro de Bismuto, se presenta un material semiconductor como los anteriormente estudiados dicalcogenuros de metales de transición y los semiconductores III – VI que, a diferencia de éstos y lo que le hace destacar es que, además de presentar anisotropía entre el plano de exfoliación y la vertical (anisotropía que todos los materiales bidimensionales presentan, al menos a nivel estructural y morfológico, lo que permite que sean exfoliables en capas), presenta una gran anisotropía óptica y estructural entre las direcciones x – y dentro del propio plano de exfoliación. Tras la exfoliación del material, mediante microscopía óptica se observan nanocapas claramente con forma rectangular en el plano x – y de exfoliación en comparación con lo distintos ángulas y formas observadas en otros materiales. Estas dos direcciones en las muestras rectangulares en el Sulfuro de Bismuto denotan dos ejes (determinados por ambos lados de los rectángulos que forman las muestras) como los ejes ópticos ordinario y extraordinario de dicha anisotropía, demostrado mediante espectroscopía Raman y difracción de rayos X. Esta anisotropía es experimentalmente demostrada por diversas técnicas ópticas como espectroscopía Raman tanto en muestras delgadas como volúmicas (donde un modo de vibración asociado a la dirección cristalográfica en una de las direcciones se ve claramente anulada al rotar la muestra con respecto a la polarización de excitación), fotoluminescencia (donde se observa una reducción de

intensidad de emisión fotoluminiscente colectada al rotar los nanocopos), contraste óptico y reflectividad diferencial (siendo el contraste óptico medido en tres rangos distintos en el visible, rojo, azul y verde y la reflectividad diferencial en todo el espectro visible, donde ambas propiedades siguen una dependencia lobular al rotar la muestra con respecto a un polarizador lineal en colección) y transmitancia, donde en todas ellas se observa un comportamiento dependiente de la orientación de las nanocapas con respecto a la dirección de polarización de la luz de excitación o la colección, dependiente de la distinta absorción entre ambos ejes en el material estudiado. Una vez la anisotropía de este material ha sido demostrada, se presenta la aplicación de dicha anisotropía al depositar muestras exfoliadas de este material en el núcleo de fibras ópticas, que actúan como cavidad de Fabry-Perot en el núcleo de las mismas. La aparición de bandas de transmitancia tras las múltiples reflexiones internas en el material es producida interferencias constructivas que, a determinadas longitudes de onda, cumplen que están en fase. Al rotar la polarización de la luz incidente en la muestra con respecto a los ejes cristalográficos es posible modificar la posición de dichas bandas, dando un grado de libertad como polarizador o filtro de banda estrecha. De los primeros órdenes de interferencia y la diferencia entre la posición entre picos entre ambas direcciones se obtienen resultados de la birrefringencia del sulfuro de bismuto al rotar polarización de la luz en el núcleo con respecto a las direcciones de la muestra depositada en comparación con otros materiales laminares reportados. Finalmente, a diferencia de los anteriores semiconductores laminares, se presenta el Trióxido de Molibdeno como material bidimensional aislante, propiedad poco frecuente en el campo de los materiales bidimensionales, donde el Nitruro de Boro hexagonal es el único utilizado para este cometido en dispositivos donde un aislante bidimensional es empleado. Se demuestra la exfoliabilidad del Trióxido de Molibdeno, obteniendo nanocapas rectangulares similares a las antes obtenidas en el Seleniuro de Bismuto, así como sus ventajas con respecto al Nitruro de Boro hexagonal como material laminar aislante: primero se presenta al material con un espín nuclear casi-nulo en comparación con el Nitruro de Boro hexagonal y otros posibles candidatos dentro de los teórica o experimentalmente exfoliados, hecho que impide el uso del nitruro de boro hexagonal en dispositivos orientados a la espintrónica atómica y tras esto, se demuestra experimentalmente la ausencia de defectos localizados emisores de fotoluminiscencia a baja temperatura, que actúen como puntos de emisión que afecten al resultado final del dispositivo diseñado, presente en la mayoría de nitruro de boro hexagonal crecido a día de hoy. El uso de este

nuevo material como aislante bidimensional se demuestra mediante dispositivos de dicalcogenuros de metales de transición encapsulados en este material y estudiando su comportamiento a baja temperatura. Primero, se obtiene un ligero corrimiento y un estrechamiento en la reflectividad diferencial de las monocapas de seleniuro de tungsteno encapsuladas en este material, resultado similar al obtenido al encapsularlo en nitruro de boro hexagonal y, además, se estudia el comportamiento de varios emisores de fotón único presentes en el semiconductor encapsulado mediante microfotoluminiscencia, observando desdoblamiento de estructura fina, un comportamiento de polarización cruzada en ambas contribuciones y una tendencia con la potencia de excitación similares a las reportadas, probando por tanto su uso como aislante en sustitución al nitruro de boro hexagonal. Sin embargo, otros resultados usando el trióxido de molibdeno, en este caso encapsulando una bicapa de seleniuro de tungsteno, destacan con diferencia con respecto a los anteriormente mencionados y los reportados con otros materiales en la literatura. Tanto en fotoluminiscencia y reflectividad a temperatura ambiente como en reflectividad diferencial a baja temperatura, se observan corrimientos en torno a diez veces superiores a los reportados en otros casos y materiales, tanto en la contribución del excitón directo y el indirecto en el caso de la fotoluminiscencia como en la absorción observada en la reflectividad diferencial. El hecho de que se haya producido en una bicapa de seleniuro de tungsteno en vez de en una monocapa y la distinta orientación relativa de los nanocopos de trióxido de molibdeno que encapsulan a la misma se proponen como causantes de dicho corrimiento inesperado, siendo demostrada tras esto la anisotropía de nanocopos exfoliados de trióxido de molibdeno mediante reflectividad diferencial al rotar la muestra con respecto a la polarización de colección, propiedad ya atisbada al comparar la forma rectangular de las muestras exfoliadas con las anteriores de sulfuro de bismuto. Finalmente, y de cara a caracterizar ópticamente dicha anisotropía en nanocapas de trióxido de molibdeno, se obtiene por elipsometría mediante el uso de tres ángulos de incidencia el índice de refracción en el espectro visible de este material, presentando diferente valor en las tres direcciones espaciales.

La presente tesis, por tanto, cerraría presentando las conclusiones antes expuestas y futuros proyectos que se abren tras los mismos.

D.2 Resumen breve en castellano

En el campo de la Ciencia de Materiales, los materiales bidimensionales han acaparado la atención de la comunidad científica en los últimos años. El cambio y la aparición de nuevas propiedades cuando su espesor se ve reducido a escalas nanométricas tiene un especial interés para el estudio de sus propiedades fundamentales para, a partir de éstas, el diseño y su implementación en dispositivos de diversa índole. La gran variedad de materiales con posibilidad de ser exfoliables a nivel bidimensional abre el campo a distintas aplicaciones, desde dispositivos optoelectrónicos, detección y sensado, almacenamiento de energía, catálisis, aplicaciones médicas y tecnologías de información cuántica, entre otras.

Esta tesis recoge resultados en ambos sentidos: un estudio a nivel de ciencia fundamental en materiales bidimensionales poco explorados por la comunidad científica y su implementación en dispositivos optoelectrónicos enfocados a distintas aplicaciones.

En una primera parte, se estudiarán las propiedades ópticas y eléctricas de la familia de los semiconductores III - VI, poco explorados y complementarios en muchas propiedades a los conocidos dicalcogenuros de metales de transición. Se estudiará la fotoluminiscencia del Seleniuro de Galio, donde experimentalmente se demuestra un corrimiento en su emisión luminiscente de 120 meV al llegar a 8 nm de espesor, resultado superior al reportado en el momento y que sigue la tendencia a lo reportado teóricamente, con un corrimiento de los 2.02 eV en su estado volúmico hasta 3.2 eV al llegar a la monocapa, llegando desde el visible al ultravioleta cercano según cálculos de primeros principios. También se estudia el mecanismo de oxidación de este material en condiciones normales mediante técnicas como microscopía de fuerza atómica, contraste óptico y espectroscopía de fotoemisión de rayos X para comprender la evolución en su deterioro de cara a su implementación en dispositivos. Tras esto, se pasará al Seleniuro de Indio, material cuyas propiedades ópticas se conocen en mayor medida, pero cuyas propiedades eléctricas en su estado bidimensional no han sido exploradas. Por ello, en esta tesis se demuestra el uso de muestras multiescalonadas de este material como heterouniones sin defectos que se comportan como heterouniones p - n, base de la optoelectrónica moderna en dispositivos como transistores, fotodetectores o fotoemisores. Basados en el cambio en su estructura de bandas al cambiar de espesor, se estudia su funcionamiento como fotodetector mediante sus características I - V y un estudio detallado de la recombinación de

portadores en la barrera generada por el cambio de banda prohibida en el cambio de espesor. Además, de cara a la modelización y diseño de dispositivos eléctricos con este material, se estudia la variación de la función de trabajo de distintos espesores del material mediante microscopía de fuerza de sonda Kelvin, acompañado de cálculos de primeros principios, obteniendo una tendencia similar junto con los datos experimentales. Finalmente, como aplicación de este material, se propone y demuestra su uso para el sensado de gases debido al cambio en la fotoluminiscencia de las muestras expuestas a distintas concentraciones, tiempos y gases. Se usarán como gases tioles debido a su presencia del radical sulfuro, presente en distintos decaimientos orgánicos de alimentos y similares y trinitrotolueno como ejemplo de gas presente en la detección de bombas, entre otros.

Tras la presentación de los semiconductores III - VI, una segunda parte de la tesis se centrará en su implementación experimental en dispositivos conceptuales para aprovechar u optimizar las propiedades antes descritas, comparando los resultados en cada caso con monocapas de dicalcogenuros de metales de transición como el Seleniuro de Tungsteno o el Seleniuro de Molibdeno. En concreto, se intentará aprovechar la recientemente demostrada orientación vertical al plano de exfoliación de los excitones en el Seleniuro de Indio que contrasta con orientación horizontal de éstos en los dicalcogenuros de metales de transición, hecho que perjudica su uso en la configuración de excitación vertical - colección vertical usual en los estudios científicos. Primero, mediante el uso de microesferas de óxido de silicio sobre las muestras bidimensionales se optimizará la extracción y colección de su fotoluminescencia, tanto en el caso de Seleniuro de Indio como en el Seleniuro de Tungsteno. Además, se demostrará el comportamiento como dipolo perpendicular al plano en el caso del Seleniuro de Indio y de la componente de baja energía del Seleniuro de Tungsteno asociada al trión o excitón cargado debido a las resonancias debidas a los modos de galería susurrante que se producen en las microesferas. Esta técnica ofrece un control adicional a la emisión fotoluminiscente de estos materiales en función del diámetro de dicha microesfera, tanto en aumento de intensidad como en posición del pico efectivo de emisión colectado de cara a su implementación para una aplicación en concreto.

Tras ello, estos materiales bidimensionales se estudiarán en heteroestructuras verticales junto con nanocristales de perovskitas con emisión en el visible, obteniendo un aumento de la fotoluminescencia colectada en el caso del Seleniuro de Indio en comparación a lo obtenido junto con Seleniuro de Molibdeno, donde la fotolumines-

cencia detectada se ve reducida al depositar un nanocristal de perovskitas sobre las muestras exfoliadas. El origen de dicho efecto es la reabsorción por parte del Seleniuro de Indio de lo emitido por la perovskita superior, debido a la disposición óptima de su dipolo perpendicular al plano con respecto a la emisión multidireccional de las perovskitas, en contraposición al dipolo paralelo al plano de los dicalcogenuros de metales de transición, ya óptimo para la excitación y colección vertical. Este estudio confirma la naturaleza dipolar en el Seleniuro de Indio como perpendicular al plano junto con el resultado anterior.

Finalmente, en esta segunda parte y con vistas a la implementación de estos materiales bidimensionales en dispositivos fotónicos integrados, se estudia el comportamiento del Seleniuro de Indio y monocapas de Seleniuro de Tungsteno y Seleniuro de Molibdeno sobre guías de onda fotónicas, permitiendo la excitación y colección indistintamente en las direcciones horizontal y vertical al plano de exfoliación, en todas las configuraciones posibles. Tras unos primeros pasos con el Seleniuro de Indio, se estudia en detalle la implementación de los dicalcogenuros de metales de transición en las mismas, obteniendo medidas experimentales en todas las configuraciones de guiado, así como su distinto comportamiento con respecto a la absorción y emisión frente a luz polarizada en la guía.

En una tercera parte de la tesis se presentarán dos materiales bidimensionales no explorados en la literatura: el Sulfuro de Bismuto y el Óxido de Molibdeno. En el caso del semiconductor Sulfuro de Bismuto, estudiaremos la anisotropía de sus propiedades ópticas en el plano de las capas, mediante diversas técnicas ópticas como espectroscopía Raman, fotoluminescencia, contraste óptico, reflectividad diferencial y transmitancia. Tras ello, se demuestra la aplicación de dicha anisotropía en fibras ópticas como cavidad de Fabry-Perot en el núcleo de las mismas, de donde se obtienen resultados de su birrefringencia en comparación con otros materiales laminares reportados. Finalmente, se presenta el Óxido de Molibdeno como material bidimensional aislante, poco frecuente en el campo de los materiales bidimensionales, donde el Nitruro de Boro hexagonal es el único utilizado. Se demuestra la exfoliabilidad del Óxido de Molibdeno y sus ventajas con respecto al Nitruro de Boro hexagonal: su ausencia de defectos a baja temperatura y su espín nuclear casinulo en comparación con el Nitruro de Boro hexagonal, hecho que impide su uso en dispositivos orientados a la espintrónica. El uso de este nuevo material como aislante bidimensional se demuestra mediante dispositivos de dicalcogenuros de metales de transición encapsulados en este material y estudiando su comportamiento a baja

temperatura, desde sus emisores de fotón único al estrechamiento en la emisión y absorción del semiconductor encapsulado, obtenido por fotoluminiscencia y reflectividad diferencial a baja temperatura, respectivamente.

D.3 Resum breu en valencià

En el camp de la Ciència de Materials, els materials bidimensionals han acaparat l'atenció de la comunitat científica en els últims anys. El canvi i l'aparició de noves propietats quan el seu gruix es veu reduït a escales nanomètriques té un especial interés per al estudi dels seu propietats fonamentals per a, a partir de les quals, el disseny i la seua implementació en dispositius de diversa índole. La gran varietat de materials amb possibilitat de ser exfoliables a nivell bidimensional obri el camp a distintes aplicacions, des de dispositius optoelectrònics, detecció i sensat, emmagatzemament d'energia, catàlisi, aplicacions mèdiques i tecnologies d'informació quàntica, entre altres.

Aquesta tesi recull resultats en ambdós sentits: un estudi a nivell de ciència fonamental en materials bidimensionals poc explorats per la comunitat científica i la seua implementació en dispositius optoelectrònics enfocats a distintes aplicacions.

En una primera part, s'estudiaran les propietats òptiques i elèctriques de la família dels semiconductors III - VI, poc explorats i complementaris en moltes propietats als coneguts dicalcogenurs de metalls de transició. S'estudiarà la fotoluminiscència del Selenur de Gal · li, on experimentalment es demostra un corriment en la seua emissió luminiscent de 120 meV a l'arribar a 8 nm de gruix, resultat superior al reportat en el moment i que seguix la tendència al reportat teòricament, amb un corriment dels 2.02 eV en el seu estat volúmic fins a 3.2 eV a l'arribar a la monocapa, arribant des del visible a l'ultravioleta pròxim segons càlculs de primers principis. També s'estudia el mecanisme d'oxidació d'aquest material en condicions normals mitjançant tècniques com microscòpia de força atòmica, contrast òptic i espectroscòpia de fotoemissió de raix X per comprendre l'evolució en el seu deteriorament de cara a la seua implementació. Després d'açò, es passarà al Selenur d'Indi, material del qual les propietats òptiques es coneixen en major grau, però les propietats elèctriques en el seu estat bidimensional no han estat explorades. Per això, en aquesta tesi es demostra l'ús de mostres multiescalonades d'aquest material com heterounions sense defectes que es comporten com heterounions p - n, base de l'optoelectrònica moderna en dispositius com a transistors, fotodetectors o fotoemissors. Basats en el canvi en la seua estructura de bandes al canviar de gruix, s'estudia el seu funcionament com fotodetector mitjançant les seues característiques I - V i un estudi detallat de la recombinació de portadors en la barrera generada pel canvi de banda prohibida en el canvi de gruix. A més, de cara a la modelització i

disseny de dispositius elèctrics amb aquest material, s'estudia la variació de la funció de treball amb differents gruixos del material mitjançant microscòpia de força de sonda Kelvin, acompanyat de càlculs de primers principis, obtenint una tendència semblant junt amb les dades experimentals. Finalment, com a aplicació d'aquest material, es proposa i demostra el seu ús per al sensat de gasos a causa del canvi en la fotoluminiscència de les mostres exposades a differents concentracions, temps i gasos. S'utilitzaran per això gasos com a tiols degut a la seua presència del radical sulfur, present en distints decaïments orgànics d'aliments i semblants, i trinitrotolué com a exemple de gas present en la detecció de bombes, entre altres.

Després de la presentació dels semiconductors III - VI, una segona part de la tesi es centrarà en la seua implementació experimental en dispositius conceptuals per tal de aprofitar o optimitzar les propietats abans descrites, comparant els resultats en cada cas amb monocapes de dicalcogenurs de metalls de transició com el Selenur de Tungstè o el Selenur de Molibdè. En concret, s'intentarà aprofitar la recentment demostrada naturalesa dipolar del Selenur d'Indi com a perpendicular al pla d'exfoliació, diferent dels dicalcogenurs de metalls de transició, fet que perjudica el seu ús en la configuració d'excitació vertical - col · lecció vertical usual en els estudis científics. Primer, mitjançant l'ús de microesferes d'òxid de silici sobre les mostres bidimensionals s'optimitzarà l'extracció i col · lecció de la seua fotoluminescència, tant en el cas de Selenur d'Indi com en el Selenur de Tungstè. A més, es demostrarà el comportament dipolar com a perpendicular al pla en el cas del Selenur d'Indi i de la component de baixa energia del Selenur de Tungstè associada al trió o excitó carregat a causa de les ressonàncies degudes als modes de galeria xiuxiuejants que es produïxen en les microesferes. Aquesta tècnica oferix un control addicional a l'emissió fotoluminiscent d'aquestos materials en funció del diàmetre de dita microesfera, tant en augment d'intensitat com en la posició del pic efectiu d'emissió col · lectat de cara a la seua implementació per a una aplicació en concret.

Després d'això, estos materials bidimensionals s'estudiaran en heteroestructures verticals junt amb nanocristalls de perovskites amb emissió en el visible, obtenint un augment de la fotoluminescència col · lectada en el cas del Selenur d'Indi en comparació a allò que s'ha obtingut junt amb Selenur de Molibdè, on la fotoluminescència detectada es veu reduïda al depositar un nanocristall de perovskites sobre les mostres exfoliades. El motiu d'aquest efecte és la reabsorció per part del Selenur d'Indi d'allò que s'ha emès per la perovskita superior, a causa de la disposició òptima del seu dipol perpendicular al pla respecte a l'emissió multidireccional de les perovskites,

en contraposició al dipol paral · lel al pla dels dicalcogenurs de metalls de transició, ja òptim per a l'excitació i col · lecció vertical. Aquest estudi confirma la naturalesa dipolar del Selenur d'Indi com a perpendicular al pla junt amb el resultat anterior.

Finalment en aquesta segona part, de cara a la implementació d'aquestos materials bidimensionals en dispositius fotònics integrats, s'estudia el comportament del Selenur d'Indi i monocapes de Selenur de Tungstè i Selenur de Molibdè sobre guies d'ones fotòniques, tot permetent l'excitació i col · lecció indistintament en les direccions horitzontal i vertical al pla d'exfoliació, en totes les configuracions possibles. Després d'uns primers passos amb el Selenur d'Indi, s'estudia en detall la implementació dels dicalcogenurs de metalls de transició en les mateixes, obtenint mesures experimentals en totes les configuracions de guiat, així com el seu distint comportament respecte a l'absorció i emissió enfront de llum polaritzada en la guia.

En una tercera part de la tesi es presentaran dos materials bidimensionals no explorats en la literatura: el Sulfur de Bismut i l'Òxid de Molibdè. En el cas del Sulfur de Bismut, es presenta un material semiconductor que, a més de presentar anisotropia entre el pla d'exfoliació i la vertical, presenta una gran anisotropia òptica i estructural dins del pla, demostrada per diverses tècniques òptiques com espectroscòpia Raman, fotoluminescència, contrast òptic, reflectivitat diferencial i transmitància. Després d'açò, es demostra l'aplicació d'aquesta anisotropia en fibres òptiques com a cavitat de Fabry-Perot en el nucli de les mateixes, d'on s'obtenen resultats de la seua birefringència en comparació amb altres materials laminars reportats. Finalment, es presenta l'Òxid de Molibdè com a material bidimensional aïllant, poc freqüent en el camp dels materials bidimensionals, on el Nitrur de Bor hexagonal és l'únic utilitzat. Es demostra l'exfoliabilitat de l'Òxid de Molibdè i els seus avantatges respecte al Nitrur de Bor hexagonal: la absència de defectes a baixa temperatura i el seu espín nuclear quasi-nul en comparació amb el Nitrur de Bor hexagonal, fet que impedix el seu ús en dispositius orientats a l'espintrònica. L'ús d'este nou material com a aïllant bidimensional es demostra mitjançant dispositius de dicalcogenurs de metalls de transició encapsulats en aquest material i estudiant el seu comportament a baixa temperatura, des dels seus emissors de fotó únic a l'estretiment en l'emissió i absorció del semiconductor encapsulat, obtingut per fotoluminiscència i reflectivitat diferencial a baixa temperatura, respectivament.